Universidade do Minho
Escola de Engenharia

Rafael Jorge Neto Ferreira

Fall Prevention Strategy for an Active Orthotic System

março de 2022

março de 2022

Universidade do Minho
Escola de Engenharia

Rafael Jorge Neto Ferreira

Fall Prevention Strategy for an Active Orthotic System

Dissertação de Mestrado

Mestrado Integrado em Engenharia Biomédica

Ramo Eletrónica Médica

Trabalho efetuado sob a orientação de

Professora Doutora Cristina P. Santos

Doutora Joana Figueiredo

março de 2022

Agradecimentos

Na realização da presente dissertação, que me permitiu crescer tanto a nível profissional como pessoal, contei com o apoio de várias pessoas. Dessa forma, quero expressar o meu sincero agradecimento a todos aqueles que contribuíram, de alguma forma, para a realização desta dissertação.

Em primeiro lugar, quero agradecer à minha orientadora, professora Doutora Cristina P. Santos pela oportunidade de trabalhar neste projeto, pela confiança, acompanhamento e valorização do trabalho elaborado, bem como por todos os conselhos. Quero, igualmente, agradecer à minha coorientadora Doutora Joana Figueiredo pela colaboração e apoio providenciado. Quero deixar ainda um especial agradecimento ao Nuno, pela ajuda incansável, pelo acompanhamento, disponibilidade e apoio que, sem dúvida, foram fundamentais para o resultado final alcançado. Deixo também um agradecimento aos meus colegas investigadores do BiRD Lab, pelo apoio, por estarem sempre dispostos a ajudar e por todos os momentos partilhados.

Quero também agradecer aos meus colegas de curso. Com especial destaque para três grandes amigos que me acompanharam durante a vida universitária. Ao Miguel, amigo de longa data, que sempre me apoiou e com o qual cresci, trabalhei, e vivi grandes momentos durante a vida escolar e académica. À Diana que é, sem dúvida, uma das melhores amizades que a universidade me deu e com a qual tive o prazer de trabalhar e partilhar muitos bons momentos. Ao André por todo o companheirismo e apoio mostrado durante a universidade.

Não poderia deixar de agradecer à minha família, nomeadamente à minha mãe, irmã, avó e avô que me proporcionaram todas as condições para conseguir dar o meu melhor, me acompanharam nos bons e nos maus momentos e mostraram sempre confiança e orgulho em mim e no meu trabalho. Quero ainda agradecer à minha namorada, a Alexandra, por ser, todos os dias, a minha maior força e por todo o carinho e confiança incondicional que deposita em mim.

Por fim, o meu muito obrigado a todos, mesmo que injustamente não mencionados, que contribuíram direta ou indiretamente para a concretização deste trabalho.

Statement of Integrity

I hereby declare having conducted this academic work with integrity. I confirm that I have not used plagiarism or any form of undue use of information or falsification of results along the process leading to its elaboration.

I further declare that I have fully acknowledged the Code of Ethical Conduct of the University of Minho.

Resumo

Todos os anos, são reportadas cerca de 684,000 quedas fatais e 37.3 milhões de quedas não fatais que requerem atenção médica, afetando principalmente a população idosa. Assim, é necessário identificar eficientemente indivíduos com alto risco de queda, a partir da população alvo idosa, e prepará-los para superar perturbações da marcha inesperadas. Uma estratégia de prevenção de queda capaz de eficientemente e atempadamente detetar e contrariar os eventos de perdas de equilíbrio (PDE) mais frequentes pode reduzir o risco de queda. Como slips foram identificados como a causa mais prevalente de quedas, estes eventos devem ser abordados como foco principal da estratégia. No entanto, há falta de estratégias de prevenção de quedas por slip.

Esta dissertação tem como objetivo o *design* de uma estratégia de prevenção de quedas de *slips* baseada na conceção das etapas de atuação e deteção. A estratégia de atuação foi delineada com base na resposta biomecânica humana a *slips*, onde o joelho da perna perturbada (*leading*) apresenta um papel proeminente para contrariar LOBs induzidas por *slips*. Quando uma *slip* é detetada, a estratégia destaca uma ortótese de joelho que providencia um torque assisstivo para prevenir a queda. A estratégia de deteção considerou as propriedades atrativas dos controladores Central Pattern Generator (CPG) para prever parâmetros da marcha. Algoritmos baseados em *threshold* monitorizam o erro de previsão do CPG, que aumenta após uma perturbação inesperada na marcha, para a deteção de *slips*. O ângulo do joelho e a velocidade angular da canela foram selecionados como os parâmetros de monitorização da marcha. Um protocolo experimental concebido para provocar perturbações de *slip* a sujeitos humanos permitiu a recolha de dados destas variáveis para posteriormente validar o algoritmo de deteção de perturbações.

Algoritmos CPG foram capazes de produzir aproximações aceitáveis dos sinais de marcha em estado estacionário do ângulo do joelho e da velocidade angular da canela com sucesso. Além disso, o algoritmo de threshold adaptativo detetou LOBs induzidas por *slips* eficientemente. A melhor *performance* global foi obtida usando este algoritmo para monitorizar o ângulo do joelho, que detetou quase 80% (78.261%) do total de perturbações com um tempo médio de deteção (TMD) de 250 ms. Além disso, uma média de 0.652 falsas perturbações foram detetadas por cada perturbação corretamente identificada. Estes resultados sugerem uma *performance* aceitável de deteção de perturbações do algoritmo, de acordo com os requisitos especificados para a deteção.

Palavras-Chave: quedas induzidas por *slips*, biomecânica do *slip,* prevenção de quedas, avaliação do risco de queda, *Central Pattern Generators*, deteção de perturbações na marcha

Abstract

Every year, an estimated 684,000 fatal falls and 37.3 million non-fatal falls requiring medical attention are reported, mostly affecting the older population. Thus, it is necessary to effectively screen high fall risk individuals from targeted elderly populations and prepare them to successfully overcome unexpected gait perturbations. A fall prevention strategy capable of effectively and timely detect and counteract the most frequent loss of balance (LOB) events may reduce the fall risk. Since slips were identified as the main contributors to falls, these events should be addressed as a main focus of the strategy. Nonetheless, there is a lack of slip-induced fall prevention strategies.

This dissertation aims the design of a slip-related fall prevention strategy based on the conception of an actuation and a detection stage. The actuation strategy was delineated based on the human biomechanical reactions to slips, where the perturbed (leading) leg's knee joint presents a prominent role to counteract slip-induced LOBs. Thereby, upon the detection of a slip, this strategy highlighted a knee orthotic device that provides an assistive torque to prevent the falls. The detection strategy considered the attractive properties of biological-inspired Central Pattern Generator (CPG) controllers to predict gait parameters. Threshold-based algorithms monitored the CPG's prediction error produced, which increases upon an unexpected gait perturbation, to perform slip detection. The knee angle and shank angular velocity were selected as the monitoring gait parameters. An experimental protocol designed to provoke slip perturbations to human subjects allowed to collect data from these variables to further validate the perturbation detection algorithm.

CPG algorithms were able to successfully produce acceptable estimations of the knee angle and shank angular velocity signals during steady-state walking. Furthermore, an adaptive threshold algorithm effectively detected slip-induced LOBs. The best overall performance was obtained using this algorithm to monitor the knee angle from the perturbed leg, which detected almost 80% (78.261%) of the total perturbations with a mean detection time (MDT) of 250 ms. In addition, a mean of 0.652 false perturbations were detected for each correct perturbation identified. These results suggest an acceptable perturbation detection performance of the algorithm implemented in light of the detection requirements specified.

Keywords:.slip-induced falls, slip biomechanics, fall prevention, fall risk assessment, Central Pattern Generators, gait perturbation detection

Table of Contents

List of Figures

List of Tables

Abbreviations

6MWT – 6-minute Walking Test

30SCS – 30-second Chair Stand

AFO – Adaptive Frequency Oscillator

ANN – Artificial Neural Networks

AP – Anterior-posterior

APO – Active Pelvis Orthosis

AI – Artificial Intelligence

BBS – Berg Balance Scale

BOS – Base of Support

CNN – Convolutional Neural Network

CNS – Central Nervous System

COF – Coefficient of friction

COM – Centre of Mass

CPG – Central Pattern Generator

CV – Cross-validation

DT – Detection Time

EMG – Electromyography

FFT – Fast Fourier Transform

FIMP – Fall Inducing Platform

FMFP – Fast Mode Fall Prediction

fMRI – functional Magnetic Ressonance Imaging

FPGA – Field-Programmable Gate Array

IMU – Inertial Measurement Unit

LOB – Loss of Balance

ML – Machine Learning

MLat – Medial-lateral

MDT – Mean Detection Time

MoCap – Motion Capture

PBT – Perturbation-based Balance Training

PKO – Powered Knee Orthosis

PRISMA – Preferred Reporting Items for Systematic Review and Meta-Analysis

PS – Patient Specific

PVC – Premature Ventricular Contractions

ROKAD – Robotic Knee Assistive Device

RQ – Research Questions

RT – Reverse time

SITUG – Smart Insole TUG

SMFD – Slow Mode Fall Detection

TUG – Timed Up and Go

WASP – Wearable Apparatus for Slipping Perturbations

1. Introduction

1.1. Motivation and Problem Statement

Falls are the second main cause of unintentional injury deaths worldwide [1]. It is estimated that about 684,000 fatal falls and an estimated 37.3 million non-fatal falls, which require medical attention, occur each year. The elderly aged 60 and over entail the highest fall risk due to their increasingly reduced cognitive, physical, and sensory status, which arise with the ageing process [1]. Thereby, the quality of life of the elderly is constantly threatened by the unpredictability of fall risk events that can take place in a wide range of scenarios during the everyday living. Since walking is the most common activity preceding fall-related events, there is the need to identify high fall risk individuals and prepare them to successfully overcome unexpected gait perturbations [2–4].

Successful fall prevention relies on the: i) effective screening of high fall risk individuals; and ii) the definition of a comprehensive fall prevention strategy to assist them upon loss of balance (LOB) events. The fall risk assessment of targeted aged populations allows to timely identify high fall risk individuals and suggest evidence-based treatment interventions to reduce their fall risk by promoting a safer gait. These interventions may include a fall prevention strategy designed to assist these individuals upon a LOB scenario. This strategy must include the detection of gait perturbations and the supply of the respective adequate assistive actuation. An effective fall prevention strategy must address the human biomechanical response to counteract the most common LOB events. Considering that previous literature has identified slip perturbations during level ground walking as the main contributors to falls, special focus must be given towards the prevention of these LOB events [5,6].

Furthermore, human motion data while dealing with gait perturbation exposure is required to test the effectiveness of the strategy conceived. However, recording real-world fall data emerges as a difficult challenge. While these meaningful data are necessary to reliably test gait perturbation detection algorithms, some constraints arise from real-world gait perturbation data collection [7]. Although the fall incidence in the elderly is higher, the number of falls experienced per year only ranges from 0.3 falls in community-dwelling older adults to 3 falls in high fall risk older adults [8]. Hence, this relatively low incidence of LOB events combined with the limited data collection periods hinder the real-world fall data collection. Klenk *et al.* [7] even mentioned that to capture 100 real-world falls, an estimated 100,000 days, i.e., 300 years, of physical activity recordings would be required. Therefore, researchers have extensively attempted to provoke artificial perturbations in laboratory conditions that mimic the characteristics of real gait disturbances in order to collect data from individuals during LOB events. Slip- [9,10] and trip-like [11,12] perturbations are the most highlighted.

Bio-inspired controllers have been used to track human motion variables and assist the early detection of LOB events [13]. The foundation of the cyclic patterns generated during human locomotion is attributed to the functional activity of the neuronal circuits located in the spinal cord, i.e., biological Central Pattern Generators (CPG) [14,15]. Thereby, the implementation of a biological-inspired CPG controller systems to monitor and control variables of human locomotion becomes attractive [16,17]. These controllers are based on adaptive frequency oscillators, each one adapting to one main frequency component of a human locomotion signal. The occurrence of an unexpected gait perturbation would introduce abnormal variations to the tracking motion variable and lead the oscillators to seek for new signal patterns associated with distinct frequencies. This would quickly deviate the actual variable signal from the trajectory expected by the CPG. The increase of the CPG prediction error induced by this deviation allows even simple threshold-based algorithms to early and effectively detect an unexpected gait perturbation [13].

Overall, there is a lack of studies that conceived fall prevention strategies based on an extensive study of the human biomechanical reactions to slip events. This issue must be tackled in order to effectively prevent the most common fall events and enhance elders' quality of life.

1.2. Goals

The ultimate goal of this dissertation was to conceive a fall prevention strategy, specifically designed to prevent slip-induced falls. The aim of the work herein developed was two-fold: i) conception of the actuation and detection strategies to prevent slip-induced falls; and ii) development and validation of a perturbation detection algorithm able to timely and effectively identify slip-induced LOB events.

The fall prevention strategy must include a comprehensive study of the human biomechanical responses to slip perturbations in order to define an appropriate actuation profile for a robotic assistive device able to help the subject recover balance upon the detection of a slip. Concerning this detection, biological-inspired CPG controllers are suitable to track and predict human motion parameters. Upon a perturbation, they highlight deviations between the actual and predicted motion signals, which allows simple threshold algorithms to perform the perturbation detection.

To achieve these main goals, it was necessary to attend to the following step-goals:

- **Goal 1**: To gather knowledge of the most recent fall risk assessment methods. This state-of-the-art analysis also aimed to identify the fall risk assessment system's most adopted:

i) sensors and their characteristics; ii) tasks performed during the experimental protocol for data acquisition; iii) algorithms to classify the fall risk; and iv) validation processes. The identification of trends for each fall risk assessment method identified allows to better understand standard system's requirements to effectively and accurately screen high fall risk individuals. This is addressed in Chapter 2.

- **Goal 2**: To gather knowledge of the different methods used in the scientific literature to provoke artificial slip and trip perturbations to healthy adults during treadmill and overground walking. Although the preliminary focus of the fall prevention strategy was to address slip perturbations, further plans to extend the strategy to also prevent trip perturbations are planned, according to their relevance. Hence, this state-of-art analysis aims to identify the key experimental aspects considered in the scientific literature to deliver slip- and trip-like perturbations. This is addressed in Chapter 3.
- **Goal 3**: To gather knowledge of the human biomechanical reactions to slip perturbations and the slip-related fall prevention systems already implemented. This study allows to highlight the most relevant biomechanical reactions to slip events surveyed in the scientific literature, acknowledge the already existing slip-related fall prevention systems, and to define requirements needed to fulfil towards an accurate fall prevention strategy. This is addressed in Chapter 4.
- **Goal 4**: To design, develop and propose a new slip-related fall prevention strategy based on the literature reviewed. This allows to concept the characteristics of both the actuation and the detection stages of the strategy. Moreover, are also defined the timings and requirements associated with each stage to timely detect a slip perturbation and effectively provide the respective assistive countermeasures. This is addressed in Chapter 4.
- **Goal 5**: To design an experimental protocol to collect slip-like perturbation data from healthy young participants using a wide range of sensor systems. The conception of this protocol allows to: i) mimic real unexpected slip perturbations in laboratory settings; and ii) build a dataset with vast and relevant kinematic and biosignal data collected during both normal and perturbed walking. The collected data allows to better understand the changes that slip perturbations introduce to the human motion. This is addressed in Chapter 5.
- **Goal 6**: To develop, implement and validate a threshold-based algorithm towards the detection of slip-like perturbation occurrence. The error signal produced between the actual motion signal and the motion signal predicted by a CPG controller was used by threshold

algorithms to perform the perturbation detection. The validation of the detection process must: i) assess the ability of the biological-inspired CPG algorithm to adapt to the motion variable's signal during steady-state walking; and ii) evaluate the effectiveness of threshold-based algorithms to detect slip-like perturbation. Data collected from the slip-like perturbation protocol was used to perform these validation steps. This is addressed in Chapter 6.

1.3. Research Questions

The following Research Questions (RQs) were identified and answered, so as to achieve the main goal:

- **RQ1:** What are the main fall risk assessment methods implemented in the scientific literature? The answer is included in Chapter 2.
- **RQ2:** What are the key experimental methods implemented in the scientific literature to provoke artificial slip and trip perturbations? The answer is included in Chapter 3.
- **RQ3:** Which are the main aspects that a fall prevention strategy should include in terms of detection of slip perturbations and actuation upon slip-induced LOB events? The answer is included in Chapter 4.
- **RQ4:** Are the biological-inspired CPG controllers and the threshold-based algorithms able to effectively track human motion variables and timely detect slip perturbation occurrences, respectively? The answer is included in Chapter 6.

1.4. Contribution to Knowledge

This dissertation had the following main contributions to knowledge:

- A review of the most adopted fall risk assessment methods in the scientific literature to screen high fall risk subjects;
- A review of the key experimental aspects adopted to provoke artificial slip and trip perturbation in the scientific literature;
- A review of the human biomechanical reactions to counteract slip events and the most recent slip-related fall prevention strategies implemented in the scientific literature;
- A dataset with extensive and relevant kinematic and biosignal information collected during normal and perturbed treadmill walking that allows to study the changes to the human motion induced by slip-like perturbations.

- Evidence highlighting the effectiveness of the CPG controllers to adapt to steady-state human locomotion variables;
- Evidence highlighting the effectiveness of threshold-based algorithms to timely detect the occurrence of slip-like perturbations provoked during steady-state human locomotion based on the error produced between the real motion signal and the signal predicted by the CPG controllers.

1.4.1. Publications

The work developed during this dissertation enabled the publication of the following journal review article, which resulted from the work performed in Chapter 2:

- **R. N. Ferreira**, N. F. Ribeiro, C. P. Santos, "Fall Risk Assessment Using Wearable Sensors: A Narrative Review", Sensors **2022**, 22, 984. doi.org/10.3390/s22030984

Moreover, the work performed during this dissertation also allowed the publication of the following conference paper, in which the author of the present dissertation contributed in the discussion of the article's structure:

- R. Durães, N. F. Ribeiro, **R. N. Ferreira**, E. Seabra and C. P. Santos, "Product Design and Mechanical Validation of a Cane-Type Robot for Fall Prevention", 2021 IEEE International Conference on Autonomous Robot Systems and Competitions (ICARSC), Santa Maria da Feira, Portugal, 28-29 April 2021, pp. 246-251, doi: 10.1109/ICARSC52212.2021.9429810.

Additionally, the literature review work performed in Chapter 3, was submitted as a narrative review article to the GeroScience journal.

1.5. Thesis structure

This dissertation is organised in the following chapters.

Chapter 2 presents the state of the art of the fall risk assessment methods performed in the scientific literature using wearable sensors. For each identified method, a comprehensive analysis has been carried out in order to find trends regarding the most used sensors and its characteristics, activities performed in the experimental protocol, and algorithms used to classify the fall risk. It was also verified how studies performed the validation process of the developed fall risk assessment systems.

Furthermore, Chapter 3 surveys the different methods used in the scientific literature to provoke slip- and trip-like perturbations to healthy adults during treadmill and overground walking and identify the key experimental aspects to consider in future related research. It was ascertained the methods used to maintain the participants' responses to the perturbations unbiased, which limb was generally used to provoke the perturbations, which was the participants' walking speed during the trials, and what were the most used sensor systems to collect data during perturbation-based protocols. In addition, it was found whether there were benefits to apply both slip- and trip-like perturbations within the same experiment and if it was preferable to: i) deliver perturbation during treadmill or overground walking; and ii) use a single-belt or a split-belt treadmill to perturb walking.

Moreover, Chapter 4 describes the slip-related fall prevention strategy proposed in this dissertation. The human biomechanical responses to slip perturbations and the slip-related fall prevention systems already implemented are herein investigated. Further, based on the literature evidence collected, this Chapter highlights the actuation and detection strategies conceived to provide effective assistive torque and timely detect the slip perturbations, respectively.

In Chapter 5 it is presented the experimental protocol conducted to obtain meaningful data regarding the individuals' reactions to slip-like perturbations. Information about the participants enrolled and the equipment used is also herein detailed.

Chapter 6 comprises the results obtained in this dissertation concerning the validation strategy proposed for slip-like perturbation detection using the data collected during the experimental protocol. Firstly, it was studied the most suitable number of oscillators within the CPG controller to track each monitoring variable. Secondly, it is described the Normal Walking Testing, which assesses the ability of the CPG controllers to learn and adapt to the signals of each monitoring variable. Lastly, it is reported the Perturbed Walking Testing, which evaluates the ability of the monitoring variables to detect the occurrence of slip-like perturbations. The performance results obtained are herein provided.

Finally, Chapter 7 addresses the main conclusions of this dissertation, answers to the RQs specified and points out to the future work.

2. Fall Risk Assessment Review

Recently, fall risk assessment has been a main focus in fall-related research. Wearable sensors have been used to increase the objectivity of this assessment, building on the traditional use of oversimplified questionnaires. However, it is necessary to define standard procedures that will us enable to acknowledge the multifactorial causes behind fall events while tackling the heterogeneity of the currently developed systems. Thus, it is necessary to identify the different specifications and demands of each fall risk assessment method. Hence, this state-of-art analysis provides a review on the fall risk assessment methods performed in the scientific literature using wearable sensors. For each identified method, a comprehensive analysis has been carried out in order to find trends regarding the most used sensors and its characteristics, activities performed in the experimental protocol, and algorithms used to classify the fall risk. It also verified how studies performed the validation process of the developed fall risk assessment systems. The identification of trends for each fall risk assessment method would help researchers in the design of standard innovative solutions and enhance the reliability of this assessment towards a homogeneous benchmark solution.

Recent reviews targeting fall risk assessment have presented and discussed the different approaches to analyse fall risk. For instance, Rucco *et al.* [18] reviewed the state of art of the fall risk assessment using wearable sensors investigating the most used sensor technologies, their number and location, as well as the number and type of tasks performed in the experimental protocol. Montesinos *et al.* [19] conducted a systematic review that studied the most significant and strong associations between combinations of feature categories, tasks performed and sensor locations to ascertain a subject fall status, as faller or non-faller. Rajagopalan *et al.* [20] performed a comprehensive review regarding the relationship between the different fall risk factors and highlighted current work and challenges on fall prediction systems. However, the analysis within these manuscripts was performed without specifying the different fall risk assessment methods, such as long-term or real-time fall risk assessment. Therefore, the identification of trends is less reliable than an individual analysis carried out for each fall risk assessment method identified. The assessment of the fall risk from both long-term and real-time perspectives requires different specifications and setups and, consequently, different and individual analysis. For instance, a specific type of sensor placed on a certain position of the body can be widely used for a specific fall risk assessment method and not for another. Furthermore, none of the previously mentioned reviews ascertained the validation processes carried out to validate the fall risk assessment systems found in the literature.

Thus, the aim of this work was to find evidence on the following topics: (i) “Which are the main types of fall risk assessment methods using wearable sensors in literature studies?”'; (ii) “What types, number, and location of wearable sensors were adopted in the literature studies?”; (iii) “Which tasks or clinical scales were performed during experimental protocols for data acquisition?”; (iv) “Which algorithms are used in the scientific literature for the classification of fall risk?”; and (v) “How was the validation of fall risk assessment systems performed using wearable sensors?”. The first, fourth, and fifth questions offer novel analysis regarding the reviews articles [18–20]. To the best of the author's knowledge, no previous study has addressed the first question. The third question offers a technological description of the sensors used in fall risk assessment systems. This allows the further comparison with previous review studies to ascertain if trends of sensor specifications are maintained or updated. The fourth question offers a review of the tasks or clinical scale protocols performed for data collection.

2.1. Methods

An electronic systematic search was accomplished in IEEE, Scopus, Web of Science, and PubMed databases on the topic of fall risk assessment of towards the elderly population using wearable sensors. The search was completed in the aforementioned databases on 3 November 2020. On IEEE the keywords used were: (aged OR elderly OR geriatric OR old) AND fall risk AND wearable sensor. The terms (aged OR elderly OR geriatric OR old) AND (wearable sensor OR wearable device) AND fall risk AND (gait OR posture OR walking) were used in the other 3 databases. In order to provide an overview of the most recent and emerging trends of fall risk assessment using wearable sensors, the search was conducted considering all articles that were published after 2015. A total of 332 articles were found and 223 remained after removing duplicates. Further, a careful reading of the title and the abstract of those articles enabled the exclusion of articles that clearly did not perform fall risk assessment or were a review. Reviews were excluded from the search results as the purpose of the search strategy was to find studies which developed a fall risk assessment system. Following this procedure, 48 articles remained for full text reading. In order to screen the most important ones, eligibility criteria were applied to the selected papers. Articles were excluded if: (i) the system described in the study presented any kind of non-wearable device; (ii) a fall risk assessment method was not applied or described; (iii) there was a lack of information on either the sensor system or its placement on the body; and (iv) the study was a previous version of a more recent one, being both in the 48 selected articles group. Regarding the application of these criteria, 16 articles were selected for further analysis. In Figure 1, it is depicted the Preferred Reporting Items for

Systematic Review and Meta-Analysis (PRISMA) flowchart regarding the previously described literature search.

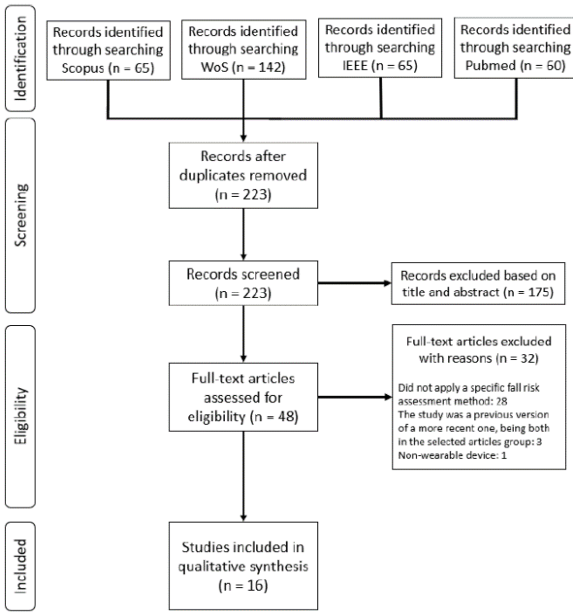

Figure 1. PRISMA flow diagram.

2.2. Fall Risk Assessment Methods

As suggested in Figure 2, the 16 selected manuscripts were divided into groups according to the method used to assess fall risk.

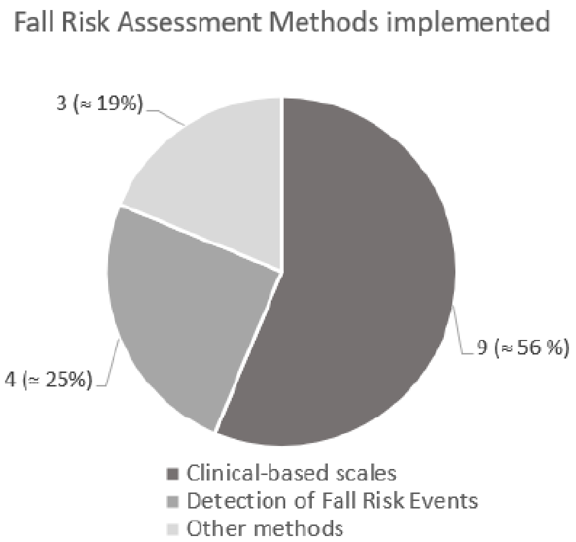

(a)

Author	Fall Risk Assessment Method
Saadeh (2019)	Detection of fall risk events
Leone (2019)	Detection of fall risk events
Rivolta (2015)	Clinical scales: Tinetti
Tang (2019)	Clinical scales: BBS and MiniBEST
Parvaneh (2016)	Other methods
Annese (2015)	Other methods
Rivolta (2019)	Clinical scales: Tinetti
Shahzad (2017)	Clinical scales: BBS
Saporito (2019)	Clinical scales: TUG
Rescio (2015)	Detection of fall risk events
Leone (2017)	Detection of fall risk events
Buisseret (2020)	Clinical scales: TUG and 6MWT
Yang (2019)	Clinical scales: TUG
Selvaraj (2018)	Other methods
Vieira (2015)	Clinical scales: BBS
Dzhagaryan (2015)	Clinical scales: TUG and 30SCS

(b)

Figure 2. (a) Number of studies from each fall risk assessment methods identified. (b) Fall risk assessment method adopted by each study. Saadeh [21], Leone [22], Rivolta [23], Tang [24], Parvaneh [25], Annese [26], Rivolta [27], Shahzad [28], Saporito [29], Rescio [30], Leone [31], Buisseret [32], Yang [33], Selvaraj [34], Vieira [35], and Dzhagaryan [36].

A group of 9 studies [23,24,27–29,32,33,35,36] assessed fall risk from a long-term perspective based on clinical established scales. This group comprised more than half of the manuscripts, i.e., 56%. In addition, 25% of the selected manuscripts [21,22,30,31] considered fall risk assessment from a short-term or real-time approach by developing a system and an algorithm able to identify pre-fall/unbalanced situations and consequently detect fall risk events. Lastly, 3 studies [25,26,34], i.e., 19%, which followed different approaches to assess fall risk, were identified and included in the "Other Methods" group.

2.2.1. Fall Risk Assessment Based on Clinical Scales

Vieira *et al.* [35] developed a gamified application for the elderly to independently measure the Berg Balance Scale (BBS) score at home by means of a custom-made sensor containing an accelerometer and a gyroscope. Shahzad *et al.* [28] estimated the BBS score from data acquired from a single accelerometer. Tang *et al.* [24] performed a study to obtain the BBS and MiniBEST test scores for each subject with a sensor apparatus composed by a SmartShoe, which comprised a pressure sensitive insole with 3 pressure sensors and an accelerometer, as well as an hip accelerometer. Yang *et al.* [33] conducted four environment-adapting TUGs in order to assess fall risk in a more comprehensive way than standard TUG by adapting gait in complex environments. During the trials, subjects wore a Smart Insole (SITUG) in each foot, with a sensing device composed by 16 pressure sensors array along with an Inertial Measurement Unit (IMU) including an accelerometer, gyroscope, and magnetometer. Saporito *et al.* [29] attempted to predict a remote TUG score based on data recorded from 3 days of free-living conditions by means of one accelerometer and one barometric sensor. Buisseret *et al.* [32] assessed subjects' fall risk based on the TUG test score and data acquired from an accelerometer, a gyroscope and a magnetometer during the 6-minute walking test (6MWT). Dzhagaryan *et al.* [36] developed a wearable system, the Smart Button, capable of providing an automated mobility assessment of TUG and 30-second Chair Stand (30SCS) tests from data collected by an IMU with an accelerometer, a gyroscope and magnetometer sensors. In both studies conducted by Rivolta *et al.* [23,27], the Tinetti test score was predicted for each of the test subjects by means of data collected from a single accelerometer. Further details about the sensor systems used are provided in Figure 3.

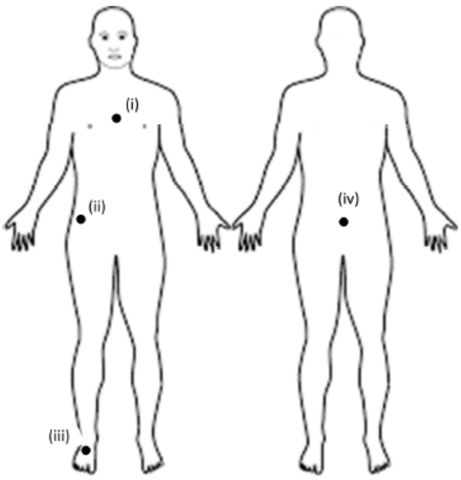

(a)

Author	Sensors	Number	fs (Hz)	Sensor location
Rivolta (2015)	Acc	1	50	chest
Tang (2019)	Acc Press	3 6	400	feet; right hip feet
Rivolta (2019)	Acc	1	50	chest
Shahzad (2017)	Acc	1	41	waist
Saporito (2019)	Acc Bar	1 1	50 25	chest
Buisseret (2020)	Acc Gyro Mag	1 1 1	100	waist
Yang (2019)	Acc Gyro Mag Press	2 2 2 32	100	feet
Vieira (2015)	Acc Gyro	1 1	N\A	chest
Dzhagaryan (2015)	Acc Gyro Mag	1 1 1	100	chest

(b)

Figure 3. Overview of the sensor characteristics from clinical scale-based fall risk assessment studies. (a) Anterior and posterior views of the human body depicting sensor location, where: (i) [23,27,29,35,36], (ii) [24], (iii) [24,33], and (iv) [28,32]. (b) Adopted sensor specifications, where: S = sensors, N = number, fs = sampling frequency, Acc = accelerometer, Gyro = gyroscope, Mag = magnetometer, Press = pressure sensors, Bar = barometer, Dist = distance sensors, $N\backslash A$ = Not Available. Rivolta [23], Tang [24], Rivolta [27], Shahzad [28], Saporito [29], Buisseret [32], Yang [33], Vieira [35], and Dzhagaryan [36].

2.2.1.1. Sensor System Characteristics

Figure 3 summarises the sensor characteristics from the studies that performed fall risk assessment based on clinical scales.

All the studies used at least one accelerometer, which underlines the importance of the use of acceleration data to characterise the score results from clinical standard scales. The use of gyroscope sensors was highlighted in 4 articles [32,33,35,36]. This search revealed that accelerometers and gyroscopes were the most widely used sensors for this fall risk assessment method. The magnetometer sensor is also included in the sensing device of 3 studies [32,33,36] and is used along with both accelerometer and gyroscope sensors. Beyond inertial sensors, pressure sensors were used in 2 studies [24,33]. Concerning the sensors' sampling frequency, all the studies acquired data from sensors at 100 Hz or less except Tang *et al.* [24], which used 400 Hz, and Vieira *et al.* [35] that did not mention the frequency adopted. However, in the data processing stage, Tang *et al.* [24] downsampled data from 400 Hz to 25 Hz.

Most of the studies used a small number of 3 sensors or less. However, Tang *et al.* [24]and Yang *et al.* [33] used 9 and 38 sensors, respectively. In their setup, Yang *et al.* [33] used 32 pressure sensors and 2 IMU's (with accelerometer, gyroscope, and magnetometer). Tang *et al.* [24] sensing apparatus consisted on 6 pressure sensors and 3 accelerometers. Within these manuscripts, almost all sensors were placed in the insole of the test subjects, thus the high number of sensors did not compromise the wearability of the system. All the single sensor solutions that assessed fall risk through clinical-based scales used accelerometers [23,27,28].

The most widely used two-sensor combination for fall risk assessment is accelerometer and gyroscope, which is line with the search results of Rucco *et al.* [18]. In addition, 4 articles used the accelerometer and gyroscope combination [32,33,35,36], with Buisseret *et al.* [32] and Vieira *et al.* [35] using only data from those two sensing modalities.

Furthermore, 5 studies described the sensor placement on the chest [23,27,29,35,36], 2 on the waist/lower back [28,32], 2 on the feet [24,33] and one on the right hip [24]. Both studies that considered the feet to place the sensors used pressure sensors [24,33]. Additionally, 8 studies [23,24,27–29,32,35,36] considered at least one upper body part to place the sensors, in which 7 of them only considered upper body parts [23,27–29,32,35,36]. The chest and the lower back were the most used upper body locations. Therefore, the upper body contains the preferred locations to place the wearable sensors in fall risk assessment based on clinical scales.

2.2.1.2. Clinical-based Scales Adopted

The variety of clinical-based scales adopted in the literature towards fall risk assessment is shown by the 6 different scales included in the group of 9 studies. TUG was the most selected scale [29,32,33,36] and BBS was the second most adopted [24,28,35]. The Tinetti test was implemented in both studies conducted by Rivolta *et al.* [23,27] and MiniBEST, 6MWT, and 30SCS were included in one study each [24,32,36]. In addition, 3 studies conducted 2 different clinical scales [24,32,36]. While the majority of the studies [23,24,27,32,33,35,36] collected data from activities performed during the clinical scales experimental protocols to assess fall risk, some collected data from activities outside the clinical scale protocols. For instance, Shahzad *et al.* [28] attempted to predict BBS score of test subjects by means of data collected during a routine which included a group of simple physical movement activities, namely the TUG test, five times sit-to-stand test, and alternate step test. Further, in Saporito *et al.* [29] data collected from subjects during 3 days of free-living conditions was used to predicted TUG time score.

2.2.1.3. Algorithms for the Classification of Fall Risk

In this fall risk assessment method, 4 studies implemented Machine Learning models [23,24,28,29], 2 considered a Deep Learning approach [27,32], 2 adopted threshold-based algorithms [32,35], and 2 studies did not perform this classification [33,36].

All 4 studies which applied Machine Learning used linear regression-based models to predict clinical scale scores. Shahzad *et al.* [28] used linear regression Machine Learning models to estimate the scores of the BBS test from the information provided by a single accelerometer positioned in the lower-back. In the same study, researchers opted to choose Machine Learning models that could be applied in small datasets and found that linear least square and LASSO regularised linear regression outperformed decision tree-based models, especially the LASSO one. Saporito *et al.* [29] also adopted a regularised linear model for the estimation of a TUG score, by means of signals collected from an accelerometer and a barometer in free living conditions for 3 days. Moreover, Rivolta *et al.* [23] applied a multiple linear regression model in order to predict the value of the Tinetti test scores assigned to the subjects by a clinician, using data obtained from a single sternum-mounted accelerometer. Tang *et al.* [24] applied a linear kernel support vector regression to predict clinical scores of BBS and MiniBEST from pressure and acceleration sensors data.

Some authors considered the use of Deep Learning [27,32]. Rivolta *et al.* [27] attempted to estimate the Tinetti test scores based on gait and balance features obtained from a single low-cost acceleration sensor, considering a two-fold problem: (i) a binary classification problem to dichotomize individuals at score 18 as High and Low Fall risk; and (ii) a regression problem in order to estimate the gold standard Tinetti score assigned to each subject. Based on the performance results, the Artificial Neural Networks (ANN) provided better classification outcomes than the linear model.

Buisseret *et al.* [32] implemented a Deep Learning model, as well as a threshold-based algorithm in order to predict the risk of falls based on the TUG and 6MWT. Therefore, a 6-month prediction of subjects' fall risk based on prospective fall occurrence as the start of the study was performed in three different classification ways: (i) a threshold-based approach considering only the time taken to complete standard TUG; (ii) another threshold-based approach (TUG+) considering the previously described time and kinematic parameters computed from IMU sensor data; and (iii) a Deep Learning Convolutional Neural Network (CNN) network that receives the raw IMU data only. The authors verified that both TUG+ and the Artificial Intelligence (AI) algorithm enhanced the performance in several classification metrics of the faller status of the subjects regarding the standard TUG alone. Vieira *et al.* [35] also implemented a threshold-based approach in order to assess the score of BBS through accelerometer and gyroscope measures. The researchers established reference values concerning each of the movements performed during the test in order to assign their respective classification. The works developed in [33,36] assessed the performance metrics of the features calculated by their systems against ground truth measures of video and optical motion capture system, respectively, rather than using algorithms to classify subject's fall risk.

2.2.2. Fall Risk Assessment Based on the Detection of Fall Risk Events

Besides the clinical scale-based approach, 4 manuscripts [21,22,30,31] addressed fall risk assessment from a real-time perspective, focusing on the detection of fall risk events during the performance of activities. The details about the sensor systems used are presented in Table 1. Saadeh *et al.* [21] used the data collected from an acceleration sensor to distinguish between ADLs and pre-fall events. Their system achieved a timely prediction of fall events, activating a fall risk alarm before the fall occurrence. Rescio *et al.* [30] described an electromyography (EMG) based system composed by 4 EMG sensors capable of detecting and recognising fall risk events. Leone *et al.* [31] also presented a 4 EMG sensor-based fall risk assessment system capable of recognising pre-fall events. Later, the authors developed a smart sock system, each one equipped with 2 EMG sensors, able to detect unbalance events associated with a potential fall risk [22]. More details about the performance metrics obtained by these systems are further provided in Table 2.

One important aspect analysed by each of the 4 studies was the lead-time. This time, which was used to study system's detection performance of fall risk events, was considered with two different meanings. Saadeh *et al.*'s investigation [21], as well as both studies conducted by Leone *et al.* [22,31], evaluated detection performance of the system considering the lead-time as the time between the detection of the unbalance event and the impact of the fall. Saadeh *et al.* [21] mentioned that their system could predict a fall event with a lead-time between 300 ms and 700 ms before the fall impact. Leone *et al.* [31] claimed a mean lead-time of 775 ms of their system and, in a later study performed by the same authors [22], a smart sock EMG system was able to detect unbalance conditions with 750 ms of mean lead-time. However, Rescio *et al.* [30] interpreted lead-time from a different perspective, by considering it to be the time delay between the onset of the perturbation and the instant when the perturbation was detected. The authors claimed that their system was able to detect a perturbation 200 ms, on average, after its onset.

2.2.2.1. Sensor System Characteristics

Table 1 depicts the sensor characteristics adopted in the studies that performed fall risk assessment based on the detection of fall risk events.

Table 1. Sensor characteristics from the fall risk assessment studies based on the detection of fall risk events, where: fs = Sampling Frequency, Acc = Accelerometer

Authors	Sensors	Number	fs (Hz)	Sensor Location	Mean Lead-Time (ms)	Lead-Time Meaning
Saadeh [21]	Acc	1	256	upper thigh	300-700	time between the detection of the unbalance event and the impact of the fall
Leone [22]	EMG	4	125	gastrocnemius and tibialis muscles	750	time between the detection of the unbalance event and the impact of the fall
Rescio [30]	EMG	4	1000	gastrocnemius and tibialis muscles	200	time difference between the perturbation onset and the detection of the perturbation
Leone [31]	EMG	4	1000	gastrocnemius and tibialis muscles	775	time between the detection of the unbalance event and the impact of the fall

EMG-based systems were used in 3 studies [22,30,31] to detect pre-fall scenarios or unstable situations associated with fall risk. On the other hand, Saadeh *et al.* [21] described the detection of fall risk events based on accelerometer data. All the studies collected data using sampling frequencies higher than 100 Hz. All sensor systems were composed of 4 wearable sensors or less. A single-sensor solution comprised by one accelerometer was used in [21], 2 EMG sensors were used for each smart sock in [22], and a system with 4 EMG sensors was presented both in [30,31]. Saadeh *et al.* [21] placed the accelerometer sensor in the upper thigh. The 3 other studies placed EMG sensors in the *gastronecmius* and *tibilias* muscle groups. Leone *et al.* [22,31] specified the use of these sensors in the *gastronecmius lateralis* and *tibialis anterior* muscles.

2.2.2.2. Types of Activities Performed

In order to collect data to identify fall risk events, the 4 studies performed ADL and fall events in the experimental protocol. Rescio *et al.* [30] instructed test subjects to simulate a series of events in a random order: (i) being at idle position or walking, both in either a normal context or presented with a deviant auditory stimuli; (ii) perform some common ADLs such as bending, lying down, standing up or sitting down; and (iii) unstable situations provoked by a tilting platform which simulated loss balance characteristic of fall events. Saadeh *et al.* [21] adopted an experimental protocol similar to the one performed to obtain the MobiFall dataset [37] and used the collected data along with the data from MobiFall dataset to train and test their system. A total of 6 different examples of falls and 11 ADL events were performed. ADLs included events that have a higher chance of being classified as false positives/falls such as: (i) jumping and jogging, as they are abrupt events that are alike to a fall event; (ii) stepping in a car or sitting on a seat; and (iii) performing standing or walking tasks and ascending or descending stairs. In addition, forward lying falls, back chair falls, front knees falls, and side falls were considered in the protocol. In [31], Leone and colleagues also developed a dataset consisting of ADLs and fall events to train and test their algorithm. Although the types of ADL performed were not specified in the study, the researchers mentioned that the falls were provoked through a movable platform to cause unstable events in the test subjects. In a later work performed by the same authors [22], simulated ADLs and fall events were conducted in order to acquire data to train and test their algorithm. Simulated ADLs included: (i) walking; (ii) sitting down on a chair; (iii) bending; and (iv) lying down on a mat. Additionally, forward, lateral, and backward falls were induced by the same movable platform described in [31].

2.2.2.3. Algorithms for the Classification of Fall Risk

Within the 4 studies that assessed fall risk from a real-time perspective based on the detection of fall risk events, 3 adopted Machine Learning models [21,22,31], whereas the remaining study used a threshold-based model [30].

Saadeh *et al.* [21] implemented a prototype system with two parallel real-time operating modes: slow mode fall detection (SMFD) and fast mode fall prediction (FMFP). In the FMFP mode, a nonlinear support vector machine classifier is used in order to predict fall events. This prediction is Patient Specific (PS) as, in the offline training stage of the classifier, PS parameters are computed and then uploaded to the system's repository. Once those parameters are uploaded, they are used in the classification phase of fall prediction, adapting this process for each subject. Leone *et al.* [31] also implemented Machine Learning in order to distinguish between pre-fall and non-pre-fall events. A linear discriminant analysis classifier was used to achieve a high generalisation capacity in the classification process while requiring low computational costs. Furthermore, in [22], Leone *et al.* used the same classifier to detect fall risk events using data collected from their developed smart EMG sock system. Rescio *et al.* [30] assessed the fall risk through a threshold-based approach as they had chosen the assurance of the system's real-time operation rather than its generalisation ability.

2.2.3. Other Fall Risk Assessment Methods

There were other approaches also identified to assess the risk of fall. Selvaraj *et al.* [34] highlighted the importance of analysing the foot clearance during stair negotiation, as reduced values of this metric have an explicit mechanism linked to falls by increasing the chance of tripping. Therefore, the authors developed a wearable system for the subject's shoe to determine the foot clearance during stair negotiation. The system was equipped with 2 distance sensors and an IMU sensor composed by an accelerometer, a gyroscope, and a magnetometer. Annese *et al.* [26] underlined the complexity of fall risk assessment and the need to perform it in a multifactorial approach in an everyday life monitoring scenario in order to accurately predict future falls. Hence, the same authors developed a cyber-physical system composed by EMG and EEG sensors interfaced to a Field-Programmable Gate Array (FPGA) responsible to perform an online processing of a subject's fall risk coefficient. This fall risk index is based on a multifactorial approach considering the partial sum of four indexes namely, a subject condition or baseline factor, an environmental factor, an EMG co-contraction factor, and an EEG signal factor. While the first two factors, which are PS, are constant, the latter two are re-calculated just after a new step is detected during gait. Parvaneh *et al.* [25] explored the relationship between fall risk and the number of Premature Ventricular Contractions (PVC) episodes per hour, by using an ECG sensor.

2.2.4. System's Validation

From the 16 selected studies, only 11 performed the validation of their fall risk assessment system [21,22,33,23,24,27–32]. As depicted in Table 2, the validation carried out on the fall risk assessment systems varied across these different studies. The fall risk outcome of the system was compared against reference measures in order to compute the system's performance metrics.

Table 2. Validation characteristics adopted by the 11 selected articles, where: ML = machine learning, Th = threshold-based, Accu = accuracy, Sens = sensitivity, Spec = specificity, CV = cross-validation, NLSVM = NonLinear Support Vector Machine classifier, LDA = Linear Discriminant Analysis classifier, SVR = Support Vector Regression, ANN = Artificial Neural Networks, LLS = Linear Least Square Regression, LASSO = Least Absolute Shrinkage and Selection Operator regression, and CNN = Convolutional Neural Network

Authors	Participants (Number/Age)	Model Used	Validation Method	Reference Measures for Classification	Results
Saadeh [21]	(77 / 20-70)	ML (NLSVM)	N\A	Type of event (pre-fall or normal ADL events)	Sens = 97.8%; Spec = 99.1%
Leone [22]	(5 / 28.7 ± 7.1)	ML (LDA)	Holdout (70% training; 30% testing)	Type of event (pre-fall or normal ADL events)	Accu = 82.3%; Sens = 86.4 %; Spec = 83.8%
Rivolta [23]	(13 / 69.7 ± 10.7)	ML (multiple linear regression model)	Leave-one-out CV	Clinical score (Tinetti)	Accu = 84.6% Sens = 85.7%; Spec = 83.3%
Tang [24]	(30 / 76.0 ± 10.5)	ML (Linear kernel SVR)	Leave-one-out CV	Clinical score (BBS and MiniBEST)	Mean error: 6.07 ± 3.76 (BBS); 5.45 ± 3.65 (MiniBEST)
Rivolta [27]	(90 / 69.3 ± 16.8)	ML (linear regression model); DL (single hidden layer ANN)	Holdout (60% training; 40% testing)	Clinical score (Tinetti)	Sens (ML) = 71% Spec (ML) = 81% Sens (DL) = 86%; Spec (DL) = 90%
Shahzad [28]	(23 / 72.87 ± 8)	ML (LLS and LASSO models)	10-fold CV	Clinical score (BBS)	Mean error: 1.9 ± 2.53 (LLS); 1.44 ± 1.98 (LASSO)
Saporito [29]	(239 / 75.2 ± 6.1)	ML (regularised linear model)	Leave-one-out CV	Clinical score (TUG)	Mean error: 2.1 ± 1.7s
Rescio [30]	(7 / 28.8 ± 7.6)	Th	10-fold CV	Type of event (pre-fall or normal ADL events)	Sens 70%; Spec 70%
Leone [31]	(15 / 32.6 ± 9.3)	ML (LDA)	10-fold CV	Type of event (pre-fall or normal ADL events)	Sens= 89.1%; Spec=87.1%
Buisseret [32]	(73 / 83.0 ± 8.3)	Th; DL (CNN)	Holdout (78% training; 22% testing)	Faller status based on prospective fall occurrence	Accu(Th) = 73.9%; Sens(Th) = 85.7%; Spec(Th)= 50%; Accu(DL) = 75%; Sens(DL) = 75%; Spec(DL) = 75%
Yang [33](*)	(10 / 19-44)	N\A	N\A	Video recordings from TUG	Accu(gait cycle count) = 100% Accu(segment TUG phases) = 92.23% Accu(spatial–temporal features) = 92%

(*) This study validated a system that extracted features from TUG rather than directly validate the system towards the classification of fall risk.

Seven studies [21,23,24,27–29,32] validated their fall risk assessment systems using data collected from elderly patients, while the remaining 4 manuscripts used data from young subjects [22,30,31,33]. In addition, the number of subjects enrolled in the experimental protocols was usually equal or below 30 subjects [22–24,28,30,31,33]. Only 4 studies [21,27,29,32] included data from more than 30 subjects in their validation process. Saadeh *et al.* [21] was the only study that performed an external validation, i.e., used data collected outside the study's experimental protocol to validate the system. As well as the data collected from 20 subjects (aged between 65 and 70) within their study, these authors also used data from 57 subjects (aged between 20 and 47) from the MobiFall dataset [37]. The remaining studies performed only an internal validation, i.e., validate the system using only data collected within the same study.

Cross-Validation (CV) was the most used validation method using both K-fold [28,30,31] and Leave-one-out [23,24,29]. The Holdout validation method was used in 3 studies [22,27,32]. Saadeh *et al.* [21] did not explicitly mention the validation method used. Lastly, Yang *et al.* [33] performed validation without using an algorithm. Their validation process consisted of comparing the features extracted from their smart insole system during the performance of four environment-adapting TUGs against video ground truth references.

Concerning the references measures for classification, 5 studies [23,24,27–29] used the clinical scale scores obtained at the baseline assessment as the reference measures for comparing the algorithm's classification outcome. The algorithms developed by these 5 studies attempted to estimate the baseline clinical scale scores based on the wearable sensor data collected from the subjects. A group of 4 studies [21,22,30,31] labelled the data based on the activities performed. Thereby, data samples were labelled as fall risk/pre-fall or normal/ADL events and were used as the reference values to compare against the algorithm's outcome. The algorithms developed in these studies attempted to detect if the subject was experiencing a fall risk event and obtain the lead-time values of that detection. Buisseret *et al.* [32] followed a different approach by considering the faller status, i.e., faller or non-faller, associated to each subject based on the prospective occurrence of falls during a follow-up period of 6 months. This faller status served as the reference metric for the algorithm's fall risk outcome. Yang *et al.* [33] used video recordings to obtain reference values. The features extracted by their smart insole systems are compared against these reference values to obtain the system's performance metrics. According to Table 2, the accuracy, sensitivity, and specificity were the most used performance metrics to validate fall risk assessment system's performance. Nevertheless, the mean error is also used by some studies that predicted clinical scale scores [24,28,29]. Generally, studies seem to have reached good performance from the developed fall risk assessment systems.

2.3. Discussion

2.3.1. Which Are the Main Types of Fall Risk Assessment Methods Using Wearable Sensors in Literature Studies?

Concerning the search results, 2 main methods to assess the fall risk were identified. The first and most widely used consisted of the long-term assessment of fall risk and was based on clinical scales. In this method, which was adopted by 9 studies, data from wearable sensors are used to predict subject's fall risk based on clinical scale scores. Thereby, subjects are assigned to either high or low fall risk category. This method will promote the decrease in long-term fall risk by enabling subjects to continuously perform long-term fall risk assessments.

The second method, which was described in 4 studies, comprised a real-time assessment of fall risk by means of the detection of fall risk events. Data from wearable sensors were used to detect pre-fall/unbalanced situations in order to identify fall risk events. This method will promote the decrease in short-term fall risk by allowing subjects to be monitored in real-time on a daily basis, providing subjects feedback as to when a fall risk event is taking place. All the studies within this fall risk assessment method analysed the concept of lead-time. Two different perspectives of lead-time were considered: (i) the time between the detection of the unbalance event and the impact of the fall [21,22,31]; and (ii) the time delay between the onset of the perturbation and the instant when the perturbation was detected [30]. The first definition of lead-time may be particularly interesting, because if the time is high enough, it may enable the trigger of protection systems or alarms to reduce the harmful consequences of a fall [38]. In addition, the second concept of lead-time appears to be oriented to the speed of unbalance event detection rather than time for prevention of a fall. Future work in fall risk assessment should attempt to address both time concepts in order to evaluate not only the time for triggering a system for fall prevention, but also the speed of detection of unbalance events.

Another group of 3 articles, which assessed the risk of falling from other perspectives, was also identified [25,26,34]. Although these studies adopted interesting metrics and approaches to assess the risk of falling, they present some limitations. Selvaraj *et al.* [34] and Parvaneh *et al.* [25] only considered one metric to assess the fall risk and thus their studies did not perform a comprehensive fall risk assessment. Nevertheless, the inclusion of the foot clearance feature in fall risk assessment systems is pertinent, as it may depict the propensity of a subject to trip events [39]. In addition, cardiovascular metrics may also be important, as they can be considered a fall risk factor [40]. The cyber-physical system developed by Annese *et al.* [26] may bring some wearability issues, as users may not be comfortable with using EEG electrodes on a daily basis. In addition, considering that the baseline and environmental factors are constant, the assessment of fall risk based on these factors may not be accurate in all scenarios, as they are subject to change in real-life conditions.

Regarding the search results obtained, it was possible to conclude that the selection of which fall risk assessment method to adopt is strongly linked to the purpose of the assessment. For instance, if it is intended to perform a long-term prediction of the subject's risk of falling, the estimation of clinical scale scores may be the most suitable approach, as it is performed in a single time period and allows direct feedback of fall risk based on the score obtained from the assessment. Further, it is possible to compare clinical scores obtained from the current and previous assessments in order to perceive the effectiveness of the evidence-based treatment interventions applied. On the other hand, if the objective of the assessment is a real-time prediction of the fall risk in the everyday life scenario, the method to detect fall risk events may become the most appropriate. Thereby, it is possible to monitor subjects continuously and alert them when fall risk events are identified.

2.3.2. What Types, Number, and Location of Wearable Sensors Were Adopted in the Literature Studies?

Inertial sensors, especially accelerometers, were used in all the studies that performed fall risk assessment based on clinical scales. As mentioned by Rucco *et al.* [18], the trend for using acceleration sensors may be related to the wide range of these inertial sensors on the market, as well as its low-cost and small size and weight. In addition, accelerometers have a lower power consumption compared to other inertial sensors, such as gyroscopes, which makes them more suitable for continuously monitoring applications [21,41]. In addition, as moderate correlations in scientific literature have been found between accelerometery features and some clinical scales, the use and interest of wearable sensors to assess the risk of falling through clinical-based scales has been growing [27,42]. Although 3 studies [23,27,28] only used accelerometers, 4 studies combined accelerometer with other inertial sensors, namely gyroscope [32,33,35,36] and magnetometer [32,33,36].

The stand-alone use of the described inertial sensors may bring various sources of measurement errors. For instance, in dynamic activities, accelerometers lack the proper estimation of orientation as they measure the motion's external acceleration besides the gravitational acceleration. Additionally, due to gyroscope's cumulative measurement errors, its use for estimating orientation in long-time activities may not be effective. In addition, especially in indoor environments, the geomagnetic field measures from the magnetometer are affected by ferrous structures [43]. Thus, the use of accelerometer, gyroscope, and magnetometer in a single IMU enables their sensing data fusion, which may solve the mentioned drawbacks and provide a reliable orientation estimation [43]. Furthermore, IMUs can be easily attached to subject's clothing, which enhances the wearability of the sensor systems [32,33]. As such, IMUs became a reliable solution for gait analysis and, consequently, the assessment of fall risk. Pressure sensors were also included in 2 studies [24,33] to assess fall risk through clinical scales. Kinetic data collected from these sensors enable the detection of foot–ground contacts due to the pressure increase during specific phases of the gait cycle. This method of phase detection may be more accurate than the methodologies that use IMU sensor data, as contact phases are indirectly detected from inertial data by using foot orientation information [33,44]. Therefore, the use of data collected by pressure sensors in the feet insole may be helpful to enhance the performance of fall risk assessment. As opposed to fall risk assessment based on the detection of fall risk events, no study described the use of EMG sensors in fall risk assessment based on clinical scales.

There was also found to be clear evidence regarding the use of the wearable sensors on the upper body in fall risk assessment through clinical scales. Nevertheless, both studies that included pressure sensors in their systems placed these sensors on the feet [24,33]. According to Rucco *et al.* [18], the upper body placement of sensors is preferred over the lower limbs, as the upper body is preponderant in both static and dynamic stability, and is strongly linked to the upright gait which requires the ability to maintain upper body's balance during walking. The chest and the lower back are the most adopted upper body locations to place the wearable sensors. Rivolta *et al.* [23] focused on the global body stability by placing their single wearable sensor on the chest, which restricts the relative motion between the body and the acceleration sensor. Shahzad *et al.* [28] and Buisseret *et al.* [32] considered the placement of sensors on the lower-back. In fact, the lower back positioning of wearable sensors is relevant in fall risk assessment applications as it is near the Center of Mass of the human body. Therefore, the sensors placed near that location provide signals with information of the whole body movements [28,45]. This evidence allows for wearable sensors to be included in user-friendly systems, e.g., waistbands, which can enhance the compliant use of the sensor systems by the elderly on a daily basis.

On the other hand, EMG sensors were the most used to detect fall risk events in real-time, being adopted in 3 of the 4 studies gathered [22,30,31]. The remaining study [21] used accelerometer data to perform this detection, activating a fall risk alarm whenever a fall event was predicted. As stated by Leone *et al.* [22], most of the studies in the scientific literature use inertial sensors to assess the fall risk. As such, the authors suggested the alternative to assess the unbalance condition by means of muscle contractile EMG data from the lower limb muscles. Concerning the search results, it seems that EMG signals may provide important information towards real-time fall risk assessment. In the 3 studies that used EMG systems to assess the fall risk [22,30,31], it was suggested that using lower limb surface electromyography sensors would promote higher lead-times than using inertial-based sensors, considering that the sudden change of EMG patterns due to an unbalance event is faster than the change of inertial signal patterns. However, the use of conventional EMG sensors may cause discomfort to the users on a daily basis, as they require a proper attachment to the surface of the skin next to the target muscle. This may bring compliance issues with the electrodes' gel considering a long-term use of these kind of wearable devices. To overcome these drawbacks, Leone *et al.* [22] used hybrid polymer electrolytes-based electrodes, instead of the conventional pre-gelled electrodes, incorporated in socks to reduce skin irritation while improving biocompatibility, mechanical properties and signal detection. These novel solutions may increase users' conformity with the use of EMG sensors and enhance its role in fall risk monitoring in free-living context.

Regarding sensor placement, it was observed that all the studies that used EMG sensors [22,30,31] considered its placement on *gastrocnemius* and *tibialis* muscle groups of both legs. These muscles are particularly important due to their role on walking, controlling stability, and maintaining the standing position. They are also relevant to evaluate gait changes related to age, fall risk, and postural deficits [22,31,46,47]. As *gastrocnemius* and *tibialis* are agonist–antagonist muscles, during a normal walk, they are alternatively activated. By detecting simultaneous and persistent activation of these muscles, it is possible to identify an unbalance event [48].

The sampling frequency adopted by each fall risk assessment method was different. While studies that assess fall risk based on clinical scales adopted frequencies below 100 Hz, the real-time detection of fall risk events was performed by acquiring data at a sampling frequency higher than 100 Hz. As the onset of fall risk events happen in fractions of a second, real-time fall risk assessment systems require sensor systems capable of collecting and processing high amounts of data in short periods of time. Therefore, a high sampling frequency is needed [21]. On the other hand, the analysis of long-term fall risk does not need to fulfil such requirements considering that the subject is not in danger of falling during the assessments. In addition, 4 studies [23,27–29] used sampling frequencies equal to or below 50 Hz. The use of lower sampling frequencies in this fall risk assessment method may be based on the fact that human activity frequencies lie between 0 and 20 Hz with 98% of its Fast Fourier Transform (FFT) amplitude contained under 10 Hz [49]. However, as lower sampling frequencies do not capture some useful particularities of the gait pattern, such as the subject's walking style, higher frequencies may still be necessary to further enhance the reliability of metrics extracted for long-term fall risk assessment [50,51].

Regarding both fall risk assessment groups, there was found clear evidence to use the least number of sensors, explained by the fact that most of the studies have developed systems with 4 wearable sensors or less. The technological advances in wearable sensors along with the meaningful data they provide are responsible for enhancing the wearable properties of fall risk assessment systems while maintaining or improving their performance.

Considering the search results, some important advantages are assigned towards the use of wearable sensors for fall risk assessment, as they: (i) increase the objectivity of the evaluation: (a) the assessment is based on objective data collected from sensors; (b) in conventional clinical scale assessments, participants are more aware that they are being evaluated and their behaviour may not be representative of the one in everyday context; and (c) it is removed the bias associated with the inter-operator variability of score assignment of conventional clinical scale assessments; (ii) enable the performance of some clinical standard scales at home, which increases the accessibility of these tests and decreases their related health care costs; and (iii) enable the real-time assessment of fall risk based on data collected during functional tasks performed in the everyday life context, which reflect subject's real fall risk more accurately, and further allow for the timely detection of fall risk events.

Some of the findings in this search are in line with Rucco *et al.* [18], as: (i) the trend to use the upper body sensor placement, particularly of inertial sensors, was identified; (ii) the use of a single accelerometer was the more widespread single-sensor solution; and (iii) the combinations of the accelerometer sensor with either gyroscope or pressure sensors were the most used two-sensor solutions.

2.3.3. Which Tasks or Clinical Scales Were Performed during Experimental Protocols for Data Acquisition?

Considering the activities performed for data acquisition, the majority of studies [23,24,27,32,33,35,36] from the group of fall risk assessment based on clinical scales instructed their participants to perform experimental protocols relative to one or more clinical standard scales. The variety of clinical scales addressed in fall research is depicted by the 6 different scales adopted in the previously mentioned group of studies. According to the search results, the most adopted clinical scales were the TUG [29,32,33,36], the BBS [24,28,35] and the Tinetti test [23,27]. Although TUG is simple to administer in the older population, this test comprises some limitations, mainly due to its simplicity, which leads to the lack of information about gait adaptability that is strongly linked to fall risk [33,52]. This led Yang *et al.* [33] to conduct four environmental adapting TUG tests in order to obtain a more in-depth fall risk assessment. Other clinical scales, such as BBS and Tinetti, involve a more comprehensive group of activities, which may lead to a more representative amount of information on the subject's fall risk [53,54]. Nonetheless, the time, material resources and monitoring from health care providers are more costly, making it less likely to be performed frequently and in the home environment. In order to overcome these issues, Vieira *et al.* [35] developed a gamified application that enables them to safely and autonomously perform the BBS. Nevertheless, as no results have been presented in the paper, there is no actual proof of the usability of the developed method. Despite being only considered in one study, the miniBEST test includes some advantages over the other clinical scales, as it evaluates more components of dynamic stability such as standing on a compliant or inclined surface and reacts to postural perturbations and crossing obstacles [24,55]. Concerning the 6MWT, as it provides relevant information concerning subject's functional capacity, endurance, and systems involved during physical activity while requiring a simple setup, it may be interesting to include this test in fall risk assessment applications [56]. Although 30SCS requires a simple setup requirement, the test only provides the number of stands performed in 30 s as the only quantitative outcome [36,57]. It is noteworthy that 3 studies assessed the risk of fall using more than one clinical-based scale [24,32,36]. This can be particularly useful to gather metrics that are task-specific for each scale, which may enrich the information extracted to assess the fall risk. The decision of which clinical scale to adopt depends not only on the aim of the assessment, but also on the characteristics of the targeted population. Each scale has a specific objective and a preferable target population, both of which should be considered during the clinical scale selection.

On the other hand, a minority of 2 studies [28,29] acquired data outside the clinical scale experimental protocol to predict the clinical scale score. This may be particularly useful if: (i) the activities used to collect data require less time than performing the clinical scale protocol [28]; or (ii) data acquired from free-living conditions could be used to predict a clinical scale score [29]. Therefore, more compliant ways to assess the fall risk can be achieved by decreasing the inconveniences associated with the performance of the whole clinical scale protocols. This should be addressed in future investigations.

The experimental protocol of studies that assessed fall risk based on the detection of fall risk events generally included some common ADLs, ADLs that can be misclassified as falls and fall events in different directions [21,22,30,31]. The inclusion of ADLs that can be misclassified is particularly interesting to test the algorithms' fall positive rate and show its capability in classifying only true fall events. In [21], the conducted experimental protocol was similar to the one used to obtain the MobiFall dataset [37] and, along with the data collected in their study, they used data from that dataset in order to evaluate their system. The other studies from this fall risk assessment method [22,30,31] only included data collected within their experiments, which would limit the reliability of the systems' performance metrics obtained. In addition, Leone *et al.* [22,31] and Rescio *et al.* [30] lack on the variety of ADL and fall events performed and on the number of subjects enrolled in the experimental protocol, in comparison to the study performed by Saadeh *et al.* [21]. Nevertheless, all the activities performed in these 4 studies were conducted in controlled conditions, which will introduce some bias on the data collected regarding real-world ADLs and falls. Future work should attempt to introduce real-world data from both ADL and fall event towards fall risk assessment based on the detection of fall risk events.

2.3.4. Which Algorithms Are Used in the Scientific Literature for the Classification of Fall Risk?

Concerning the analysis of the algorithms used for the classification of fall risk, Machine Learning models were the most used in the fall risk assessment methods identified [21–24,28,29,31]. These models are able to generate more reliable and reproducible results of fall risk classification than simpler algorithms such as threshold-based methods [40]. Aziz *et al.* [58] compared the performance of 5 Machine Learning algorithms against 5 threshold-based algorithms described in the literature to distinguish fall events and non-fall events. Accelerometer data from young adults were collected while performing 8 types of ADLs, 5 types of near-falls, and 7 types of falls in laboratory-controlled conditions. The authors concluded that Machine Learning algorithms had generally greater performance than the threshold-based algorithms by providing higher values of sensitivity and specificity. The use of Machine Learning may be particularly useful in cases where it is complex to define a threshold value to classify data samples. However, if the threshold definition is simple and effective, threshold-based algorithms could be considered. As a matter of fact, Aziz *et al.* [58] found that 2 threshold-based algorithms had a lower false alarm rate than the Machine Learning algorithms. In this regard, the authors suggested that both algorithms could potentially be combined to increase the classification performance.

Nevertheless, Deep Learning algorithms have also been used to assess the fall risk and address some of the drawbacks related to the commonly used Machine Learning methods. Yu *et al.* [59] highlighted that the simple architecture of traditional Machine Learning models consists of only one layer that performs the extraction of a feature space from the raw input signals. However, the information processing mechanisms exhibited by humans indicate a more complex processing of the sensory input information, suggesting that data processing is performed through layered hierarchical structures [59]. Therefore, Deep Learning algorithms may be more appropriate to assess the fall risk, as they extract the most relevant features automatically towards this assessment. Hence, the manual extraction of pre-determined features from the sensor data, needed in traditional Machine Learning methods, is not required [60]. Deep learning models have been compared against traditional Machine Learning algorithms and have been shown to provide greater results, e.g., in gait event detection using accelerometer data [61]. The increasing computational power of micro devices over the recent years may lead to the implementation of more complex and sophisticated AI algorithms in wearable devices, which would enable an enhanced performance of fall risk assessment in a free-living context.

2.3.5. How Was the Validation of Fall Risk Assessment Systems Performed Using Wearable Sensors?

Different approaches were adopted to validate fall risk assessment systems, regarding the 11 studies that performed the validation process [21,22,33,23,24,27–32].

Most studies that performed fall risk assessment based on clinical scales used data from elderly subjects to validate their systems [21,23,24,27–29,32]. However, only one study that performed fall risk event detection used data from elderly participants [21]. Those remaining which used this method collected data from young subjects [22,30,31]. The participation of younger subjects may have been related to the compliance issues of elderly participants, considering the EMG sensor placement, compared to inertial sensors, do not require proper attachment to the skin. Nevertheless, future work on this fall risk assessment method should address the elderly's muscle behaviour towards the detection of fall risk events, as the elderly are the targeted population for fall risk assessment.

Regardless of the fall risk assessment method adopted, the number of subjects enrolled in the experiments was generally reduced. This will directly affect system's performance metrics, as the reduced number of subjects could not be representative of the whole population. Therefore, the algorithm's classification can be biased to the study's participants and not reproduce a reliable fall risk assessment towards subjects outside the study. Thus, researchers should focus on training and testing these algorithms on a larger sample of subjects.

The lack of external validation performed in the selected studies is remarkable. In fact, Saadeh *et al.*'s [21] was the only study which conducted an external validation, which was accomplished by using data from a public dataset, MobiFall [37]. Evaluating the performance of a system with data collected outside the study's experiments would increase the reliability of the classification outcomes by reducing the bias of the system's classification towards data collected within the study. This external validation should be pointed out as one of the main requirements in the design and conception of every fall risk assessment system [42]. The use of public datasets may be an interesting approach to perform external validation, particularly for fall risk assessment based on the detection of fall risk events. Choosing the datasets to perform the external validation must be done carefully and critically. Some recommendations should be followed during the dataset selection process, as pointed out by Casilari *et al.* [62]. By analysing some of the public available datasets, the authors suggested that the performance of a system should be evaluated by more than one dataset, giving the heterogeneity of existing repositories. Therefore, this evaluation would lead to more reliable and reproducible performance results of a system. However, most of the publicly available datasets contain ADLs and falls induced in laboratory controlled conditions rather than in free-living conditions [62]. In this regard, repositories such as FARSEEING contain real-world fall data. Nevertheless, as that dataset is private, the use of the full dataset information is limited to researchers who collaborate with the FARSEEING repository [7]. However, it is important to mention that advances have been performed during the latest years in order to decrease the gap between laboratory-induced and real-world falls [2].

According to the search results, the validation process is mostly achieved either by using CV [23,24,28–31] or Holdout [22,27,32] methods. Despite its simplicity, the Holdout method produces a reduced dataset for algorithms' training and testing, which could lead to a generation of weaker models and a smaller dataset to test its classification performance [42]. CV emerged as an alternative, as it would substantially increase the data available for algorithm training and testing. This validation method became widely used to estimate the generalisation performance of Machine Learning models [42,63]. This is in line with the search results obtained, considering that more than half of the validation methods applied were related to CV [23,24,28–31].

It is noteworthy that none of the studies used the resubstitution method to validate the fall risk assessment systems performance. In this methodology, the model is trained and tested with the same dataset, leading to an obvious overfitting of the model towards the validation dataset and over-optimistic performance results [42]. In fact, Shany *et al.* [42] identified some studies that performed this inefficient validation model. Thus, it is possible to understand that recent work on fall risk assessment systems has been addressing more robust validation methods, disregarding weaker methods such as resubstitution.

Overall, the performance results obtained by fall risk assessment systems were quite promising. Regarding fall risk assessment based on clinical scales, various studies reported high performance from their systems. The Deep Learning model developed by Rivolta *et al.* [27] achieved a sensitivity and a specificity of 86% and 90%, respectively, towards the classification of individuals at high or low fall risk category based on the Tinetti test score attributed at the baseline assessment. In addition, Saporito *et al.* [29] and Shahzad *et al.* [28] obtained a relatively low misclassification error towards the estimation of participants' TUG and BBS clinical scale scores, respectively. The smart insole system developed by Yang *et al.* [33] also showed high values of accuracy in estimating relevant spatio-temporal features from the TUG test that enable the assessment of fall risk. Concerning fall risk assessment based on the detection of fall risk events, Saadeh *et al.* [21] obtained an outstanding performance detecting fall risk events, reporting a sensitivity of 97.8% and a specificity of 99.1%. Leone *et al.* [22,31] also achieved accuracy, sensitivity, and specificity values between 80% and 90%. Nevertheless, as previously mentioned by Shany *et al.* [42], fall risk assessment study results are often over-optimistic considering the reduced number and age of subjects enrolled in the test. In addition, even the pervasively used CV presents some problems given the fact that its statistical properties are not fully understood [42,63]. Furthermore, a remarkable lack of external validation of fall risk assessment systems was observed. These topics should be further addressed and discussed in future studies in order to reliably design and validate fall risk assessment systems while tackling the limitations and gaps found in current studies.

2.4. Future Directions and Work

As the interest in the field of fall risk assessment is growing, it is expected that novel wearable monitoring solutions will emerge and enhance the assessment's performance. That can be enabled by: (i) the advances on the current used sensing technologies; (ii) the used algorithms; or (iii) the introduction of innovative wearable sensors that record meaningful data for this assessment. Regarding this last topic, the advances of sensors that measure biosignals can play an important role by providing meaningful metrics underlying a subject's biomechanical reactions to falls. Future work on the fall risk assessment field may focus on a multifactorial approach to assess the risk of fall, comprising meaningful data provided by wearable kinematic, kinetic, and biosignal sensors [20]. Nevertheless, it is essential to perform a trade-off between the number of sensors used, which should be the lowest number possible, and the system's algorithm performance, that should be as high as possible. Fall risk assessment systems must be user-centred designed so that the user feels compliant with the designed sensor system, in order to be able to use it for long periods of time without any issues [20].

According to the topics previously discussed, a solution to accomplish a comprehensive fall risk assessment may be a system that: (i) monitors the risk of fall in real-time, based on the detection of fall risk events; and (ii) has the option to predict the score of the most suited clinical established scales, in order to conduct a long-term prediction of the individual's fall risk. This long-term evaluation may motivate the subject to decrease its fall risk by being able to compare its current clinical scale index of fall risk with the previous ones obtained. The ideal scenario is that all of this assessment is executed during the everyday life and that the user does not need to go to any medical care centre to perform clinical scales towards fall risk assessment. However, despite the encouraging performance of the real-time fall risk assessment systems towards the timely detection of fall risk events, its applicability to accurately prevent falls in the elderly community remains unclear. The elderly may not be agile enough to react to a fall risk alarm and prevent a fall, considering their level of physical and cognitive decline and how rapidly a fall occurs [1]. In fact, to the authors' knowledge, there are no studies in the scientific literature that address and evaluate the applicability of fall risk assessment systems to actually prevent falls. In this regard, two potential solutions could be used with the fall risk assessment systems in order to enhance the likelihood of balance recovery upon a fall risk event: (i) trigger an assistive system attached to the subject, whenever a fall risk event is detected, in order to help regain balance and thus prevent the fall [64,65]; or (ii) improve subject's reactive stability and fall resisting skills. This can be achieved through conventional training, such as Tai-chi, which has proven effective towards fall prevention by improving balance, muscle strength, endurance, and proprioception [66]. Nevertheless, perturbation-based balance training (PBT), which is a promising new task-specific training, has also been shown to reduce fall incidence [67]. Essentially, PBT consists on the delivery of unexpected destabilising balance perturbations during walking, which match real-life LOB scenarios, in a controlled environment [2,67,68]. The goal of this training scheme is to prepare high fall risk subjects to develop fall resisting skills to counteract real-life loss of balance events. When using an assistive device as a means to prevent a fall, several considerations have to be researched to verify their applicability. Falls happen very fast. Thus, the applicability of a system to prevent a fall must be assessed to guarantee that after the detection of the incoming signal to prevent a fall, there is still enough remaining time to prevent it.

It is also necessary to plan and perform a suitable and reliable validation of the performance of the fall risk assessment systems [42]. Hence, future work should also focus on the identification of gold standard external validation sources, i.e., public datasets, in which systems could be benchmarked. This would provide a reliable comparison between the different literature fall risk assessment systems. In this regard, as these systems are intended to be used by the elderly or subjects with mobility deficits, an effort should be performed to validate the systems with data collected from these target populations.

3. Provoked Falls Review

Human motion data while dealing with gait perturbation exposure is required to test the effectiveness of perturbation detection algorithms. However, despite the higher fall occurrence presented by older individuals (due to their higher fall risk), the average number of falls experienced per year ranges from 0.3 falls in community-dwelling older adults to 3 falls in high fall risk older adults [8]. This low fall incidence of the targeted elderly populations hinders the real-world LOB and fall data collection. In order to answer to this limitation, researchers have been extensively attempting to provoke artificial perturbations in laboratory conditions that mimic the characteristics of real gait disturbances in order to collect data from individuals during LOB events.

The perturbations applied must resemble the most relevant causes preceding fall events in the real-life context. Slips and trips prevail as the most common events that precede falls [4,69]. In that respect, studies that provoke artificial perturbations often rely on the application of these two main kinds of gait perturbations to the participants. Slips occur when the interface between the subject's foot and the floor does not provide sufficient coefficient of friction (COF) [70]. These events take place mostly when the foot is either contacting (heel strike) or leaving (toe-off) the floor, which resemble critical body weight transfer situations between the lower limbs, especially when the heel strikes the floor [70]. Trip events happen when the motion of the swing limb is abruptly interrupted, which can be generally induced by objects while walking [71]. Recent literature has been more focused on addressing slip-related events rather than trips. In fact, slips have been identified as the main contributors to falls with a higher incidence than trips [5,6]. Previous investigations reported that slips accounted for 55% of the falls on the same level, while trips only represented 22% [6].

The perturbations' characteristics and the conditions in which they are applied play a fundamental role to mimic humans' biomechanical reactions to LOB events and thus collect meaningful data to further test perturbation detection algorithms. Previous review studies have addressed the different methods used in the scientific literature to provoke artificial slips and trips. McCrum *et al.* [2], studied the different gait perturbation methods used for PBT to improve healthy older adults' reactive balance recovery and reduce their fall rate. However, the authors applied narrow inclusion criteria regarding age population (mean age of at least 60 years), remaining 8 studies for the analysis. Therefore, review [2] does not analyse the methods used to provoke perturbations from studies that enrolled younger adult participants. Additionally, Karamanidis *et al.* [71] performed a review study that focused on the balance training following slip- and trip-like PBT during treadmill locomotion. Despite including both slips and trips, information about how these LOB events are provoked during overground walking is not provided.

The objective of this state-of-art analysis is to survey the different methods used in the scientific literature to provoke slip- and trip-like perturbations to healthy adults during treadmill and overground walking and identify the key experimental aspects to consider in future related research. Hence, the following research questions were addressed: i) "Which methods and walking conditions are used to provoke slip- and trip-like perturbations?"; ii) "Is it preferable to deliver perturbations during treadmill or overground walking?"; iii) "Is it preferable to use a single-belt or a split-belt treadmill to perturb walking?"; iv) "What procedures are implemented to maintain responses to perturbations unbiased?"; v) "Which limb is generally used to apply the perturbations?"; vi) "Which was the participants' walking speed during the trials?"; vii) "What are the main sensor systems used to collect data during perturbation-based protocols?"; and viii) "Are there benefits to apply both slip- and trip-like perturbations?". This narrative review provides novel literature analysis towards artificial slip and trip perturbations concerning the second, third, fourth, seventh, and eighth research questions since they were not addressed by McCrum *et al.* [2] and Karamanidis *et al.* [71]. Although the first and sixth questions have been analysed in both previously mentioned reviews and that McCrum *et al.* [2] have also considered the fifth question, the work from this manuscript attempted to find if new trends have been adopted in recent literature studies towards these investigation topics. Overall, this state-of-art analysis contributes with the latest knowledge on the best conditions to induce artificial slip and trip perturbations.

3.1. Methods

A comprehensive search was performed in the scientific literature in Pubmed, Web of Science, CINAHL (EBSCO), and Scopus databases. This search was carried out until January 15th of 2021 using the set of keywords: (gait OR walking OR walk OR locomotion) AND (perturb* OR trip* OR slip* OR balance loss OR dynamic stability OR static stability OR waist pull OR provoked falls) AND (training OR exercise OR adaptation OR adaptive OR repeated OR repetition OR rehabilitation OR task OR responses OR adjustments) AND (age OR ageing OR aging OR aged OR elderly OR old OR older OR senior). The keywords used to perform this search were based on the ones used on a previous systematic review [2]. Since in that review paper, the search process was performed at the end of 2015, the present search considered all the articles that were published since 2016 to find updated trends or evidence regarding gait perturbation paradigms.

A total of 3622 articles were gathered from the aforementioned databases and 2288 remained after duplicates removal. Afterwards, the papers obtained were screened based on their title. This process enabled the inclusion of articles that meet the following inclusion criteria: i) perturbations were applied exclusively during walking; ii) perturbations were not visual nor was included a virtual environment on the experimental setup; and iii) the paper was not a review. Reviews were excluded from the search results since the search strategy's purpose was to find studies which described an experimental protocol for slip or trip perturbation delivery. Only studies that included healthy participants were included in order to enable more reliable comparisons across all the studies collected during the search. Also, the participants' age was not used as an exclusion criterion to achieve a comprehensive analysis of a wider range of methods used to deliver slip- and trip-like perturbations. A group of 338 articles resulted from the screening procedure. The article titles in which it was not clear that the conditions stated above were respected were included in the abstract screening. This following selection was based on the careful reading of the abstract of each remaining paper. The eligibility criteria were applied in order to obtain the set of articles that: i) included only slip and/or trip-like perturbations in the experimental protocol; ii) delivered the perturbations unexpectedly; iii) only included healthy subjects; and iv) did not use an assistive robotic device during the experimental trials. Beyond these conditions, the criteria used for title screening were also applied during the abstract's reading. A group of 110 articles was then obtained through the screening procedure. Since it is not possible to ascertain if the papers fulfilled the eligibility criteria previously defined by only reading the title and the abstract, the remaining articles were read and carefully analysed in order to exclude those who did not respect at least one of the above mentioned conditions. After this analysis, a final group of 48 articles was obtained. Figure 4 depicts the PRISMA flowchart concerning the previously described literature search.

From the 48 included studies, slip-like perturbations (40 studies) were more prevalent than trip-like perturbations (15 studies). In addition, 7 studies performed both slip- and trip-like perturbations. We conducted a separate analysis for slip- and trip-like perturbations since they have different characteristics and its critical adverse effects are associated to different phases of gait [70–73]. Table 3 depicts the different methods used in the literature to deliver slip- and trip-like perturbations.

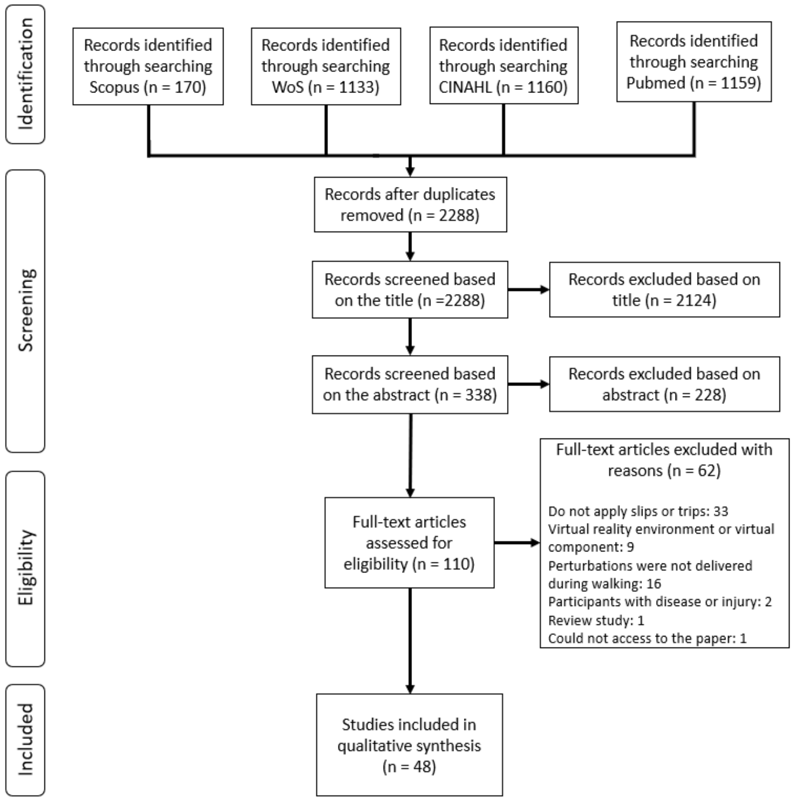

Figure 4. PRISMA flow diagram.

Table 3. Characteristics of perturbations applied in the group of 48 selected articles

Type of perturbation (Number of studies)	Perturbation condition (Number of studies)	Perturbation mechanism	Number of studies	Articles
Slip (40) (*)(**)	Treadmill walking (18)	Changing belt acceleration	18	[10,74,83–90,75–82]
	Overground walking (29)	Movable platforms	19	[76,77,94–102,78,80,81,86,87,91–93]
		Slippery solutions	8	[103–110]
		Novel Robotic Devices	2	[111,112]
Trip (15) (*)	Treadmill walking (6)	Changing belt acceleration	3	[89,90,113]
		Brake-and-release systems	2	[11,114]
		Tripping device	1	[115]
	Overground walking (9)	Obstacle trigger	6	[12,100–102,110,116]
		Manual obstacle placement	2	[117,118]
		Novel robotic devices	1	[112]

(*) some studies conducted both slip and trip perturbations; (**) some studies conducted both types of slip-like perturbations conditions.

3.2. Slip-like perturbations

Slip-like perturbations were issued in 40 studies, 18 and 29 manuscripts during treadmill and overground walking, respectively. Seven of these 40 manuscripts performed slip-like perturbations during both treadmill and overground locomotion. Figure 5 depicts some of the methods used to provoke slips in the selected studies.

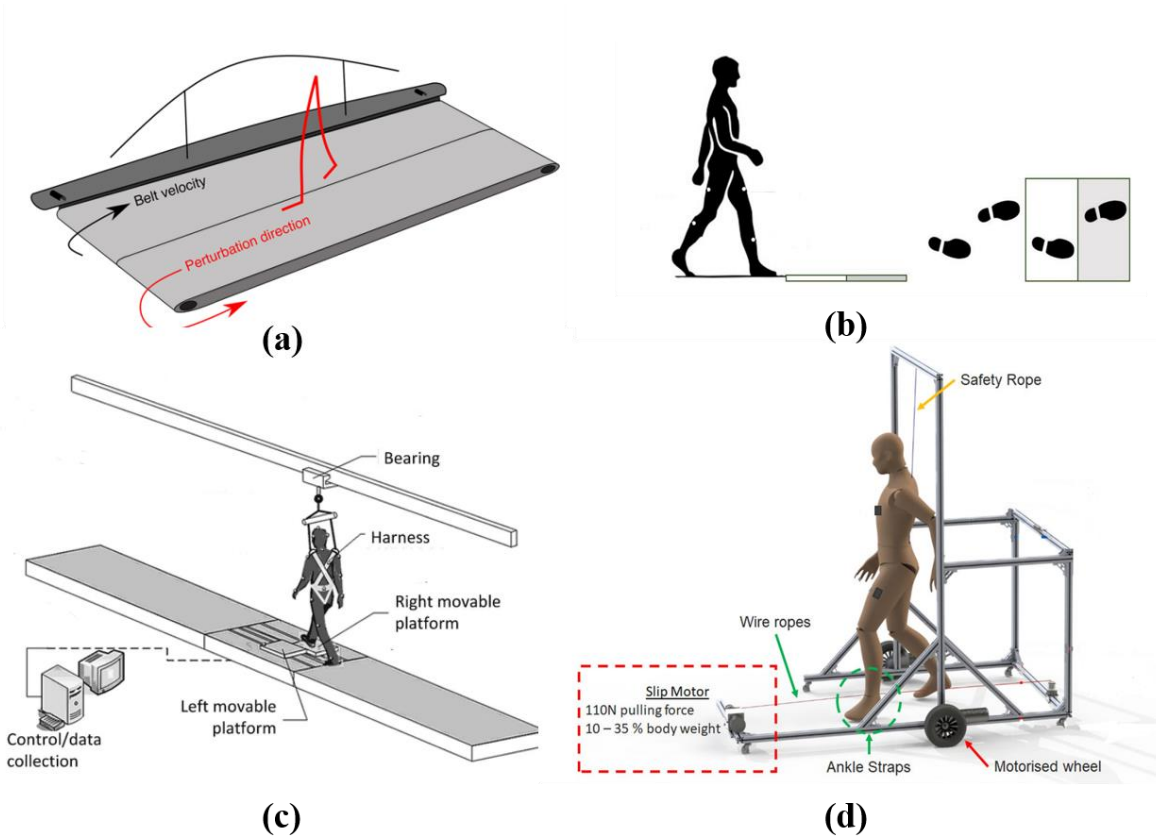

Figure 5. Some slip-like perturbation methods conducted in the selected studies. (a) Changing belt acceleration [75]. (b) Application of a slippery solution (gray surface) [104]. (c) Movable platforms [99]. (d) FIMP robotic system [112].

3.2.1. Treadmill Walking

Table 4 depicts the 18 studies that conducted slip-like perturbations during treadmill locomotion. Ten studies conducted their experiments using only young subjects (aged 40 or younger) [75,79–81,83–85,87,89,90], whereas 6 manuscripts only considered the enrolment of older participants (aged 60 or older) [76–78,82,86,88]. Additionally, 2 studies considered data from both young and older subjects [10,74]. Hereafter, if a study enrolled participants from different age groups, these groups were distinguished within the "Participants" column in the tables. Only 2 studies [78,86] enrolled more than 50 participants during the experimental trials. The sample size ranged from 10 to 152 participants with a median of approximately 28 subjects.

Table 4. Overview of the 18 studies that performed treadmill slip-like perturbations, where: Y = young subjects, Optical MoCap = Optical Motion Capture system, EMG = electromyography sensors and N\A = Not Available

Authors	Participants (Number/Age)	Perturbation method	Gait event	LOB direction	Speed (m/s)	Perturbed leg	Sensor systems
Aprigliano [74]	(10 / 24.4 ± 2.5); (10 / 66.3 ± 5.1)	changing belt acceleration	heel strike	backward	normalised speed calculated for each subject	both legs	Optical MoCap; Force plate
Swart [75]	(30 / 21.6 ± 2.2)	changing belt acceleration	heel strike	backward	1.0	right leg	Force plate
Lee [76]	(45 / 74.5 ± 6.9)	changing belt acceleration	N\A	backward	self-selected speed from 4 speed options (1.2, 1.0, 0.8 or 0.6)	right leg	Optical MoCap; Force plate
Lee [77]	(45 / 74.5 ± 6.9)	changing belt acceleration	N\A	backward	self-selected speed from 4 speed options (1.2, 1.0, 0.8 or 0.6)	right leg	Optical MoCap; Force plate
Wang [78]	(146 / 65≤)	changing belt acceleration	heel strike	backward	self-selected speed from 4 speed options (1.2, 1.0, 0.8 or 0.6)	right leg	Optical MoCap; Force plate
Patel [79]	(10 / 27 ± 4)	changing belt acceleration	N\A	backward	self-selected	N\A	Optical MoCap; fMRI
Lee [80]	(36 / 26.74 ± 4.9)	changing belt acceleration	N\A	backward	1.2	right leg	Optical MoCap; Force plate
Liu [81]	(36 / N\A (Y))	changing belt acceleration	beginning of the single stance phase	backward	1.2	right leg	Optical MoCap; Force plate
Ding [82]	(36 / 71.3 ± 4.7)	changing belt acceleration	foot touchdown	backward	self-selected	N\A	Optical MoCap
Bhatt [83]	(10 / 26.90 ± 4.25)	changing belt acceleration	N\A	backward	self-selected	N\A	fMRI
Debelle [84]	(17 / 25.2 ± 3.7)	changing belt acceleration	heel strike	forward	1.2	right leg	Optical MoCap; Force plate
Hirata [85]	(10 / 21.0 ± 1.0)	changing belt acceleration	heel strike	backward	matched with the beat of a metronome (slow (0.9) and fast (1.6) conditions)	both legs	Optical MoCap; Force plate
Martelli [10]	(8 / 24 ± 2.7); (8 / 65 ± 4.8)	changing belt acceleration	heel strike	backward	normalised speed calculated for each subject	both legs	Optical MoCap; Force plate
Liu [86]	(152 / 65≤)	changing belt acceleration	N\A	backward	self-selected speed from 4 speed options (1.2, 1.0, 0.8 or 0.6)	right leg	Optical MoCap; Force plate
Yang [87]	(43 / N\A (Y))	changing belt acceleration	foot touchdown	backward	1.2	right leg	Optical MoCap
Wang [88]	(25 / 70.2 ± 5.9)	changing belt acceleration	double-stance or single-stance phases	backward	self-selected speed from 4 speed options (1.2, 1.0, 0.8 or 0.6)	N\A	Optical MoCap

Lee [89]	(20 / 23.3 ± 3.3)	changing belt acceleration	initial double limb support	backward	self-selected	non-dominant leg	Optical MoCap; Force plate; EMG
Mueller [90]	(13 / 28 ± 3)	changing belt acceleration	heel strike	backward	1	both legs	EMG; Plantar Pressure Insole

3.2.1.1. Perturbation Methods

All the 18 treadmill studies provoked slips by changing the acceleration of the treadmill belt. This change focuses on the sudden decrease of the belt velocity, and, in some studies, even reverse its direction to cause a slip-like perturbation by inducing an anteriorly displacement of the subjects' Base of Support (BOS) regarding their Centre of Mass (COM) [88]. The belt may reach its maximum reverse velocity in values close to zero speed [10] or crossing the zero speed limit, which resulted in the belt moving in the forward direction [88].

Alternatively, Mueller *et al.* [90] conducted both of these belt speed profile scenarios. After the belt speed peak, belt's velocity would return to steady-state walking velocity [88] or zero velocity [10] depending on each study's experimental protocol. This process mimics overground walking slips that cause a backward LOB. Seventeen studies provoked the slip perturbations to elicit a backward LOB (Table 4). From these studies, Wang *et al.* [88], Martelli *et al.* [10] and Lee *et al.* [89] provoked slip perturbations by sudden accelerating in the forward direction the treadmill belt at an unexpected timing to induce instability to the subjects. Hirata and colleagues [85] applied the perturbations under specific stepping conditions when a subject stepped onto a treadmill mounted on a walkway. If the conditions were met, the belt would accelerate from zero speed to maximum velocity and then decelerated at the same rate to zero speed in order to cause a backward LOB, inducing a slip-like perturbation. In this study, the belt velocity did not reverse its direction to cause the perturbations as the trend identified above, since it was initially stopped before slip onset. On the other hand, study [84] was the only one that considered the application of slip-induced forward LOBs. In this regard, forward falling slips were provoked by suddenly increasing the treadmill's belt velocity in the same the direction as the one in steady walking condition. Therefore, there was no reverse of treadmill's belt velocity as opposed to the studies [10,88,89].

3.2.1.2. Gait Phase Perturbed

Seven out of the 18 studies provoked slip-like perturbations at the heel strike of the leading foot [10,74,75,78,84,85,90]. The other authors applied the slip during the beginning of the single stance phase [81], initial double-limb support [89], both single and double-stance phases [88] or shortly after the foot touchdown [82,87]. These gait events shortly precede or immediately follow the heel strike event. Six studies did not mention the gait event in which the slips were provoked [76,77,79,80,83,86].

3.2.1.3. Gait speed and perturbed leg

Slip perturbations were mostly provoked only on the right or on both legs, with 9 [75,77,78,80,81,84,86,87] and 4 studies [10,74,85,90], respectively.

Furthermore, 50% of these studies instructed their participants to walk at their self-selected speed during the experiments [76–79,82,83,86,88,89]. While studies [79,82,83,89] instructed participants to ambulate at their comfortable self-selected speed, manuscripts [76–78,86,88] required their participants to select a speed from 4 available options (1.2, 1.0, 0.8 or 0.6 m/s). A third of the papers applied a fixed belt speed across all the participants [75,80,81,84,87,90]. Belt speeds of 1.2 and 1.0 m/s were applied in 4 [80,81,84,87] and 2 studies [75,90], respectively. From the 3 remaining manuscripts, 2 applied a belt speed that was normalised for each subject according to their leg length [10,74], whereas the other study [85] matched the speed of the subjects with the beat of a metronome, considering both slow (0.9 m/s) and fast (1.6 m/s) walking conditions.

3.2.1.4. Sensor systems and Data Collection

Most of the studies acquired data from at least an Optical Motion Capture (MoCap) system [74,76–79,82,84,85]. These data were used to compute spatial-temporal gait parameters [74,85], elevation angles of lower limb segments [74], upper limb segment angles [10,89] or stability measures obtained through the computation of COM position and velocity [10,78,80,81,84]. Some authors also collected force data to obtain ground reaction force information [75,80,84–86]. EMG data were collected in 2 studies [89,90]. Also, Patel *et al.* [79] and Bhatt *et al.* [83]collected data from a functional Magnetic Resonance Imaging (fMRI) system. In these studies, subjects were asked to perform mental imagery of slip events after the perturbation trials.

3.2.2. Overground Walking

Table 5 highlights the 29 studies that delivered slip-like perturbations in overground walking conditions. From these studies, 11 conducted their experiments with only young subjects [80,81,112,87,95,101,104,105,109–111], 13 with only older subjects [76,77,98–100,78,86,91–94,96,97], and 3 studies considered both young and older participants [102,103,106]. Additionally, one study allowed the enrolment of young and middle age participants (aged between 40 and 60) [107] while another manuscript considered young, middle age and older subjects [108]. Only studies [78,86,91,92,96–99,108] conducted the experimental trials with more than 50 participants. The number of participants ranged from 6 to 195 with a median of 36 subjects.

Table 5. Overview of the 29 studies that performed overground slip-like perturbations, where: Y = young subjects, O = older subjects, Optical MoCap = Optical Motion Capture system, EMG = electromyography sensors, fMRI = functional Magnetic Ressonance Imaging, N\A = Not Available

Authors	Participants (Number/Age)	Perturbation method	Gait event	LOB direction	Speed (m/s)	Perturbed leg	Sensor systems
Lee [76]	(45 / 74.5 ± 6.9)	Movable platform	heel strike	backward	N\A	right leg	Optical MoCap; Force plate
Lee [77]	(45 / 74.5 ± 6.9)	Movable platform	heel strike	backward	N\A	right leg	Optical MoCap; Force plate
Wang [78]	(146 / 65≤)	Movable platform	heel strike	backward	self-selected	right leg	Optical MoCap; Force plate
Lee [80]	(36 / 26.74 ± 4.9)	Movable platform	heel strike	backward	self-selected	right leg	Optical MoCap; Force plate
Liu [81]	(36 / N\A (Y))	Movable platform	heel strike	backward	N\A	right leg	Optical MoCap; Force plate
Liu [86]	(152 / 65≤)	Movable platform	Step contact	backward	self-selected	right leg	Optical MoCap; Force plate
Yang [87]	(43 / N\A (Y))	Movable platform	Step contact	backward	self-selected	right leg	Optical MoCap
Wang [91]	(195 / 72.3 ± 5.3)	Movable platform	Foot contact	backward	N\A	right leg	Optical MoCap; Force plate
Wang [92]	(195 / 72.3 ± 5.3)	Movable platform	Foot contact	backward	N\A	right leg	Optical MoCap; Force plate
Sawers [93]	(25 / N\A (O))	Movable platform	heel strike	backward	N\A	right leg	Optical MoCap; Force plate; EMG
Sawers [94]	(28 / N\A (O))	Movable platform	heel strike	backward	self-selected	right leg	Optical MoCap; Force plate; EMG
Inkol [95]	(11 / 21.9 ± 0.3)	Movable platform	heel strike	forward, right and left	self-selected	dominant leg	Optical MoCap; Force plate
Liu [96]	(75 / 65≤)	Movable platform	Step contact	backward	self-selected	right leg	Optical MoCap; Force plate
Liu [97]	(131 / 71.8 ± 5.2)	Movable platform	Step contact	backward	self-selected	N\A	Optical MoCap; Force plate
Wang [98]	(114 / 72.5 ± 5.3)	Movable platform	Foot contact	backward	self-selected	right leg	Optical MoCap; Force plate
Wang [99]	(67 / 72.2 ± 5.3)	Movable platform	heel strike	backward	self-selected	right leg	Optical MoCap; Force plate
Merril [103]	(16 / 20-31); (17 / 50-65)	Slippery solution	heel strike	unconstrained	self-selected	left leg	Optical MoCap; Force plate
Nazifi [104]	(20 / 23.6 ± 2.52)	Slippery solution	heel strike	unconstrained	self-selected	left leg	Optical MoCap; Force plate; EMG
Ziaei [105]	(22 / 24.5 ± 3.43)	Slippery solution	N\A	unconstrained	self-selected	right leg	Optical MoCap; Force plate
Soangra [106]	(7 / 22.64 ± 2.56); (7 / 71.14 ± 6.51)	Slippery solution	heel strike	unconstrained	self-selected	dominant leg	Optical MoCap; Force plate; EMG; Inertial Sensors

O'Connel [107]	(24 / 23.75 ± 2.83); (24 / 57.13 ± 2.83)	Slippery solution	heel strike	unconstrained	self-selected	left leg	Optical MoCap; Force plate; EMG
Allin [108]	(108 / 18-66)	Slippery solution	heel strike	unconstrained	self-selected (slightly hurried)	dominant leg	Optical MoCap; Force plate
Kim [109]	(8 / 19–27)	Slippery solution	heel strike	unconstrained	N\A	dominant leg	Optical MoCap; Force plate
Rasmussen [111]	(6 / 23 ± 2.4)	Slippery solution (robotic device)	heel strike, mid-stance and toe-off	unconstrained	self-selected	dominant leg	Optical MoCap
Okubo [100]	(44 / 65-90)	Movable platform	foot contact	backward	matched with the beat of a metronome	both legs	Optical MoCap
Okubo [101]	(10 / 29.1 ± 5.6)	Movable platform	foot contact	backward	matched with the beat of a metronome	both legs	Optical MoCap
Okubo [102]	(10 / 20-40); (10 / 65-90)	Movable platform	foot contact	backward	matched with the beat of a metronome	both legs	Optical MoCap
Arena [110]	(12 / 20.9 ± 2.2)	Slippery solution	heel strike	unconstrained	between 1.45 and 1.60	right leg	Optical MoCap; Inertial Sensors
Er [112]	(7 / 25 ± 0.94)	Motor impulse (robotic device)(*)	early stance phase	backward	self-selected	left leg	Optical MoCap; Inertial Sensors

(*) The impulses were elicited by a robotic device that followed subject's motion.

3.2.2.1. Perturbation methods

As depicted in Table 5, movable platforms were used in 19 studies, whereas slippery contaminant surfaces were the source of instability in 8 other articles. Two additional papers described a novel robotic system that was responsible to apply the perturbations [111,112]. While 19 studies induced slip-induced backward LOBs, 9 papers induced LOBs in an unconstrained direction. Study [95] provoked LOBs in the forward, right and left directions.

Briefly, movable platforms consist of platforms that are assembled to an aluminium track by means of ball bearings and are embedded in a walkway [76,94,97]. In regular walking trials, the platforms are firmly locked. However, when a slip trial is about to be conducted, a trigger mechanism releases the device enabling the participants' leading foot to be exposed to a low-friction surface causing a slip. The trigger mechanism focused on the detection of the heel strike event through force plates embedded beneath the movable platforms [76,97]. In a similar approach, Inkol *et al.* [95] performed a forward translation of the users' entire support surface by means of a robotic movable platform to provoke slip perturbations. Generally, according to the selected studies, movable platforms elicited slip-like perturbations in the anterior-posterior (AP) direction [86,91,97,98]. Liu *et al.* [86,97,119] and Sawers *et al.* [93] mentioned that their platforms could not move in the medial-lateral (MLat) direction. The platforms were generally installed in pairs, i.e., one in the left and one in the right side of the walkway. The platform of the unperturbed foot was automatically released after the activation of the leading/perturbation platform [91]. In [91] and [92], after the perturbed platform's release, the platform of the unperturbed side was released once the recovery foot landed on it.

Another method used to provoke slip perturbations consisted of the application of a slippery surface in a specific location of the walkway. The slippery contaminant solutions were applied to achieve a reduction of the COF, which resembles realistic daily-life slippery conditions. Different contaminant solution compositions were used. Merril *et al.* [103], Nazifi *et al.* [104] and O'Connel *et al.* [107] chose a glycerol and water mixture contaminant while Ziaei *et al.* [105] and Kim *et al.* [109] selected soapy water as the slippery solution. A single study [106] considered a mixture of water and jelly to induce the imbalance event. Vegetable oil was used to create the slippery surface in [108] and [110]. With the exception of Allin *et al.* [108] and Arena *et al.* [110], the contaminant solution was generally applied on the top of a force plate to record ground reaction force data in both slip and non-slip trials [104,106,107].

Furthermore, 2 studies applied slip-like perturbations through robotic devices that were connected to the subject during walking and would unexpectedly provoke slips. Rasmussen *et al.* [111] developed a Wearable Apparatus for Slipping Perturbations (WASP), which consisted of a detachable outsole and a release mechanism controlled via wireless communication. The outsole, worn on subjects' dominant foot, initially presented an adequate friction with the floor but, when wirelessly triggered, could elicit a slip-like perturbation during walking by creating a low-friction surface under the foot. This perturbation mechanism was activated by a wireless command sent by an operator in heel strike, mid-stance, or toe-off phases, which had to be anticipated by the operator due to the delay observed between the trigger signal reception and low friction surface release. The WASP was designed to deliver slip-like perturbations unpredictably and unconstrainably concerning the direction and magnitude of the slip. During the trials, beyond the device on the dominant foot which provoked slip perturbations, another WASP outsole (which did not apply perturbations) was used in the non-dominant foot in order to prevent differences in the length of both limbs and ensure a more natural locomotion. In another study, Er *et al.* [112] developed the Fall Inducing Platform (FIMP), capable of randomly and unexpectedly elicit slip-like perturbations by accelerating subject's left ankle, while providing freedom of movement. The ankle was interfaced with the perturbation mechanism by a wire rope. The FIMP is programmed with a subject follower algorithm that allows it to automatically follow the subject based on camera footage. It also comprises a gait detection phase algorithm that enables the application of the perturbation on the desired gait event based on data collected by IMU sensors placed on the subject's body. There is also a user interface system control that allows the operator to inform the FIMP to trigger a perturbation in the subsequent characteristic gait phase detected, regarding the perturbation chosen to be elicited. In that matter, slips were triggered by forward accelerating the left ankle during the early stance phase by a pull force powered by a DC motor positioned anteriorly to the subject.

3.2.2.2. Gait Phase Perturbed

Sixteen studies provoked the slips at the heel strike, as highlighted in Table 5. In order to ensure that the provoked slips occurred at this gait event and on the intended slipping leg, slippery solution studies included regular walking trials to guarantee that the slipping foot landed on the zone in which the surface would be contaminated [106]. For instance, O'Connell *et al.* [107] varied the start position of the walkway to ensure the correct foot placement of the test subjects. Furthermore, study [111] provoked slips at the heel strike, mid-stance or toe-off phases and study [112] elicited slip-like perturbations during the early stance phase. The other 11 studies (Table 5) did not mention a specific phase and stated that the slip was elicited when the foot step or contact was detected by the force plates. Nevertheless, this foot contact might be resembled by the heel strike event of the slipping foot in most slip scenarios in the studies' experiments.

3.2.2.3. Gait speed and perturbed leg

As depicted in Table 5, most studies (16 in 29) applied slips in the right leg. Four studies only perturbed the left leg, 5 only the subject's dominant leg, and 3 both legs. One study did not mention the perturbed leg. Moreover, 18 manuscripts instructed their participants to ambulate at their self-selected speed, 3 studies matched the speed of the subjects to the beat of a metronome and study [110] instructed participants to maintain their speed between 1.45 and 1.60 m/s. The remaining 7 studies did not mention the speed instructed during the trials.

3.2.2.4. Sensor systems and Data Collection

All the studies used an Optical MoCap for data acquisition (Table 5). Data from these systems were used to compute spatial-temporal gait parameters [106,111], lower limb segment angles [99], joint angles [109,112] and joint moments [92,99] or stability measures obtained through the computation of

COM position and velocity [91,92,95,97,101,102]. Additionally, 22 studies also included force plates to collect ground reaction force data (Table 5). EMG sensors were included in 5 manuscripts [93,94,104,106,107] and 3 studies used wearable inertial sensor systems [106,110,112].

3.3. Trip-like Perturbations

Trip-like perturbations were conducted in 15 studies. From this group, 6 papers described the application of a trip during treadmill walking, whereas the remaining 9 articles concerned its delivery in overground walking conditions. Figure 6 presents some of the methods used to provoke trips in the selected studies.

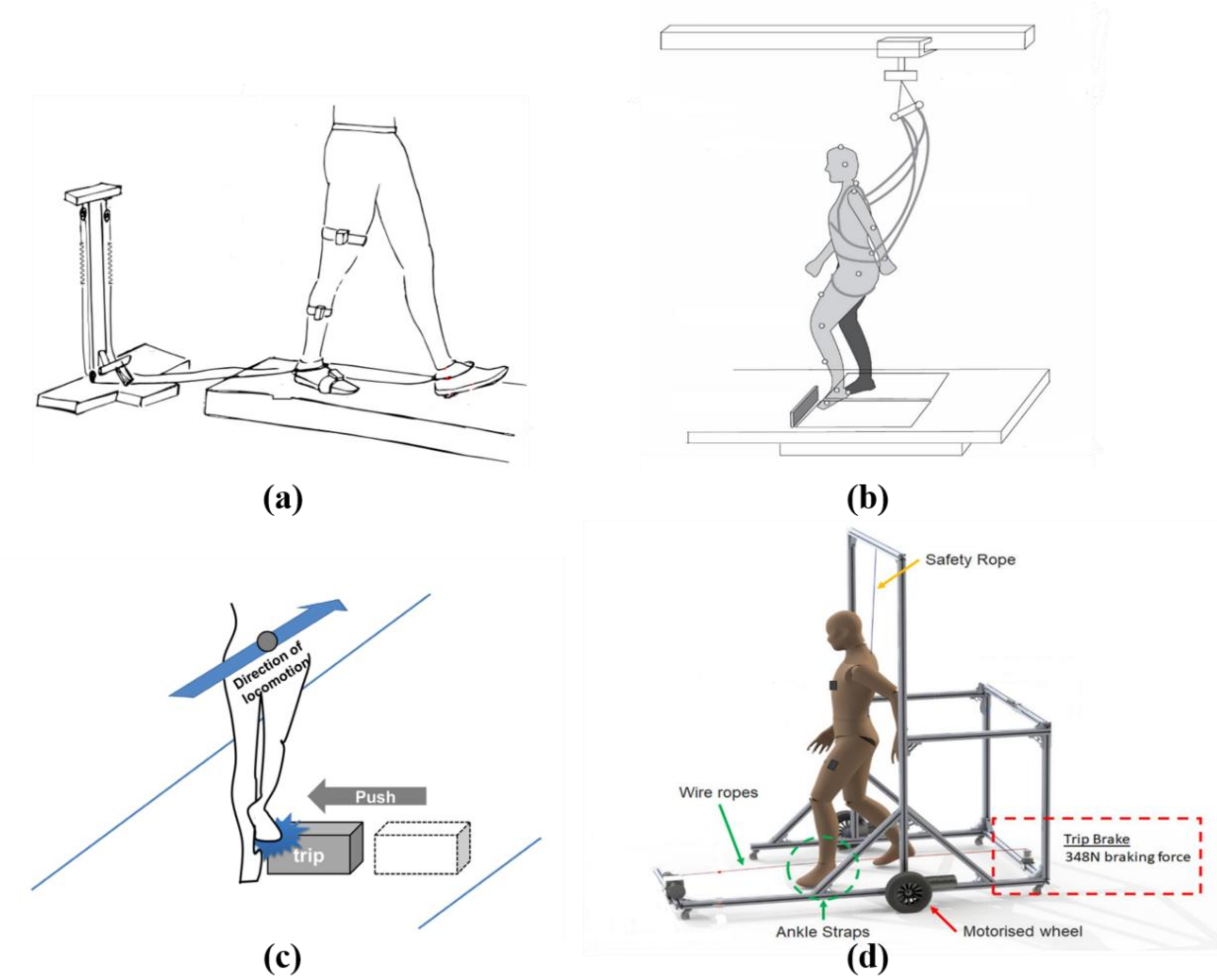

Figure 6. Some trip-like perturbation methods conducted in the selected studies. (a) Brake-and-release system [11]. (b) automatic obstacle trigger [116]. (c) Manual obstacle placement [117]. (d) FIMP robotic system [112].

3.3.1. Treadmill Walking

Table 6 shows the methods applied to induce trip-like perturbations during treadmill walking. Four studies involved young adults [11,89,90,113] and one study included middle age adults [114]. Study [115] enrolled young, middle age, and older adults. All the studies conducted the experiments with less than 25 participants. The sample size ranged from 8 to 24 participants with a mean number of 14 subjects, approximately.

Table 6. Overview of the 6 studies that performed treadmill trip-like perturbations, where: Optical MoCap = Optical Motion Capture system, EMG = electromyography sensors, N\A = Not Available

Authors	Participants (Number/Age)	Perturbation method	Gait event	LOB direction	Speed (m/s)	Perturbed leg	Sensor systems
Lee [113]	(10 / 26.3 ± 4.8)	Changing belt acceleration	initial double-limb support	forward	self-selected	non-dominant leg	Optical MoCap; Force plate
Aprigliano [11]	(8 / 25.9 ± 2.8)	Brake-and-release system	swing phase	forward	1	right leg	Optical MoCap; Inertial sensors
König [114]	(24 / 41-62)	Brake-and-release system	swing phase	forward	1.4	right leg	Optical MoCap; Inertial sensors
Silver [115]	(7 / 24 ± 3.3); (4 / 46 ± 3.0); (3 / 63 ± 3.8)	Tripping device	early swing phase	forward	self-selected	left leg	Optical MoCap
Lee [89]	(20 / 23.3 ± 3.3)	Changing belt acceleration	initial double-limb support	forward	self-selected	non-dominant leg	Optical MoCap; Force plate; EMG
Mueller [90]	(13 / 28 ± 3)	Changing belt acceleration	heel strike	forward	1	both legs	EMG; Plantar Pressure Insole

3.3.1.1. Perturbation methods

Table 6 shows that half of the studies (3 studies) induced trip-like perturbations during treadmill walking by suddenly changing the belt's acceleration. In addition, 2 studies elicited trips using a brake-and-release system connected to the subject's leg. The remaining study used an external device to unexpectedly place a tripping board to perturb subjects' locomotion. All of these studies provoked trip-induced LOBs in the forward direction.

Concerning the studies that provoked trip perturbations by changing the treadmill's belt acceleration, Lee *et al.* [89,113] elicited the trips to the non-dominant leg by the sudden stoppage of the perturbed foot treadmill belt. After the detection of the first heel strike from the unperturbed foot following the perturbation, the belt returned to its pre-perturbation speed, which allowed the subject to recover from the trip-like event by continuing walking. Mueller *et al.* [90] provoked trips to both legs by accelerating the treadmill belt shortly after the heel strike event. This accelerating period was followed by a deceleration phase towards the pre-perturbation speed of 1 m/s.

In a different approach, brake-and-release systems have also been used in 2 studies. These systems unexpectedly apply resistance to the subject's gait and inhibit the foot from going forward, emulating a trip event. In regular walking without perturbations, these systems accompany subject's walking without hindering it [11,114]. König *et al.* [114] applied resistance to the right foot during the swing phase via an ankle strap which was pulled through the brake-and-release system with a Teflon cable [120]. This device was able to generate a force around 55 N with a rise and fall times of the pulling force under 20 ms. During non-perturbation trials, the resistance received by the participants was below 0.1 N, which was considered negligible [114,120]. The cam-based mechanism developed by Aprigliano *et al.* [11] was also able to stop the forward motion of the right foot along with the swing phase. During unperturbed walking, the rope moved according to the foot's movement. A nylon rope was attached to the participants' foot at one side and to the main frame of the brake-and-release system on the other side by a compliant spring with a stiffness of 3 N/m.

The remaining study proposed a tripping device. Silver *et al.* [115] included a device capable of unexpectedly placing an obstacle in front of a subject during single-belt treadmill walking. This tripping system randomly delivered one of two selected objects to the left foot, one closed and one opened, both matching in volume and with a parallelepiped shape. The closed object was used to elicit a perturbation similar to a trip over a solid object placed on the floor while the opened one was used to mimic a trip event where the foot of a subject is "caught" by the open area underneath the obstacle.

3.3.1.2. Gait Phase perturbed

Three studies delivered the trip-like perturbations during the swing phase [11,114,115], 2 at the initial double-limb support phase [89,113], and one at the heel strike [90].

3.3.1.3. Gait speed and perturbed leg

While 3 studies instructed their participants to ambulate at their self-selected speed [89,113,115], the other 3 applied a fixed speed across all the subjects [11,90,114]. Two studies applied the trip-like perturbations to the right leg [11,114], 2 to the subjects' non-dominant leg [89,113], one to the left leg [115], and the remaining one to both legs [90].

3.3.1.4. Sensor systems and Data Collection

As depicted in Table 6, Optical MoCap systems were used to collect data in 5 studies. Data from these systems were used to compute COM position and velocity, as well as upper body segment angles [89,113]. Force data were acquired through force plates embedded on the treadmill in [89,113] or by using a plantar pressure insole in [90]. EMG sensors were used in [89,90]. Wearable inertial sensors were considered in both brake-and-release systems studies [11,114].

3.3.2. Overground Walking

Table 7 presents the 9 studies that conducted trip-like perturbations during overground locomotion. Five studies conducted experiments with only young adults, 2 manuscripts with only older adults and 2 studies with both young and older adults. All the studies conducted the experimental trials with less than 50 participants. The number of subjects ranged from 6 to 44 with a median of 12 participants.

Table 7. Overview of the 9 studies that performed overground trip-like perturbations, where: Optical MoCap = Optical Motion Capture system, EMG = electromyography sensors, N\A = Not Available

Authors	Participants (Number/Age)	Perturbation method	Gait event	LOB direction	Speed (m/s)	Perturbed leg	Sensor systems
Potocanac [12]	(7 / 24.6 ± 3.2)	Obstacle trigger	mid-swing	forward	self-selected	right leg	Optical MoCap; Force plate; EMG
Wang [116]	(40 / 67.9 ± 5.5)	Obstacle trigger	mid-to-late swing phase	forward	N\A	left leg	Optical MoCap; Force plate
Ko [117]	(6 / 21.83 ± 0.75)	Manual obstacle placement	swing phase	forward	N\A	right leg	Optical MoCap
Schulz [118]	(14 / 20-35); (25 / 66-89)	Manual obstacle placement	swing phase	forward	3 speeds: slower than preferred; preferred; and as fast as safely possible	N\A	Optical MoCap
Okubo [100]	(44 / 65-90)	Obstacle trigger	mid-swing	forward	matched with the beat of a metronome	both legs	Optical MoCap
Okubo [101]	(10 / 29.1 ± 5.6)	Obstacle trigger	mid-swing	forward	matched with the beat of a metronome	both legs	Optical MoCap
Okubo [102]	(10 / 20-40); (10 / 65-90)	Obstacle trigger	mid-swing	forward	matched with the beat of a metronome	both legs	Optical MoCap
Arena [110]	(12 / 20.9 ± 2.2)	Obstacle trigger	mid-to-late swing phase	forward	between 1.45 and 1.60	right leg	Optical MoCap; Inertial Sensors

Er [112]	(7 / 25 ± 0.94)	Braking impulse from a novel robotic device (*)	terminal Swing and Mid-swing	forward	self-selected	left leg	Optical MoCap; Inertial Sensors

(*) Impulses were elicited by a robotic device that followed subject's motion.

3.3.2.1. Perturbation methods

Regarding the group of 9 studies that performed trip-like perturbations during overground walking, the triggering of a tripping object was the main source of instability. More specifically, this tripping object was activated in two different ways, either by the automatic spring of the obstacle from the floor (6 studies [12,100–102,110,116]) or by the manual placement of the object in the walkway (2 studies [117,118]). In a different approach, Er *et al.* [112] considered the application of trips by a novel robotic device.

Concerning the studies that described the obstacle triggering, Potocanac *et al.* [12] included a walkway with a layout of 14 hidden obstacles (15 cm height) arranged in a row. During perturbation trials, any of these obstacles could be released from the floor to cause a trip. The released obstacle was selected by a kinematic data-based algorithm while the subject was approaching the obstacles zone [12,121]. In Okubo *et al.* [100], 14 cm height trip boards could suddenly flip up from the walkway to cause a trip. These obstacles were triggered by a foot detection sensor during perturbation trials and were released 50 ms before the foot arrived at the hidden board position. This would lead to the automatic delivery of perturbations in the mid-swing phase. If participants reported increased levels of anxiety or perceived difficulty during the trials, the trip board height was decreased to 7 cm. Wang *et al.* [116] applied an unexpected trip event by releasing an 8 cm height hinged metal plate obstacle in less than 150 ms. This board was locked by the powered electromagnets, but when the unperturbed limb's ground reaction force measured by a force plate (placed before the hidden obstacle) exceed 80% of the subjects' body weight, the electromagnets were turned off and the plate was unlocked to elicit a trip. During baseline non-perturbed walking trials, the starting position of the test subjects was adapted in order to assure that trip-like perturbations were applied during the mid-to-late swing phase [116]. Also, in studies [101,102], 14 cm height tripping boards sprang up from the walkway in order to elicit trip events on the subjects. During the first trials, Okubo *et al.* [102] used a 7 cm height board and further increased the height to 14 cm once the participant became more confident that they could avoid falling. However, in both studies, the obstacle was wirelessly released by a trained tester when the participants leading foot passed beside the location of the hidden trip board, such that the perturbation occurred at the mid-swing phase. Unlike the first 3 mentioned studies [12,100,116], in [101,102] the trip obstacle was manually triggered. Although

Arena *et al.* [110] mentioned that the trip obstacle embedded in the walkway was manually actuated, it is not clear if that activation is performed remotely as in [101] and [102].

Two studies manually placed the obstacles in the walkway. Ko *et al.* [117] and Schulz [118] placed objects in the walkway to induce trip-like perturbations during the unperturbed limb stance and perturbed limb swing phases, respectively. In [118] the obstacles were either visible or hidden. In the visible layout, the obstacles were white coloured placed on a black surface, whereas in the hidden layout both the obstacles and the surface were black.

The remaining study considered the use of FIMP, a robotic device that elicits trip-like perturbations [112]. The device allowed freedom of movement in non-perturbation trials and was able to posteriorly arrest the participant's left ankle with an electromagnetic brake to cause an unexpected trip. Subject's ankle was connected to the FIMP's brake system by wire ropes.

3.3.2.2. Gait phase perturbed

All the studies considered the application of the trip-like perturbations during the swing phase to provoke trip-induced LOBs at the forward direction (Table 7).

3.3.2.3. Gait speed and perturbed leg

Studies instructed the participants to match their speed to the beat of a metronome [100–102], adopt a speed between a range of walking speeds [110] or to walk at their self-selected speed [12,112]. Schulz [118] instructed participants to walk under 3 different speed conditions, namely slower than preferred speed, preferred speed and as fast as safely possible speed. Ko *et al.* [117] did not mention the speed instructed. Three studies perturbed both legs [100–102], 3 perturbed the right leg [12,110,117], and 2 perturbed the left leg [112,116]. Study [118] did not mention which leg was perturbed.

3.3.2.4. Sensor systems and Data Collection

Optical MoCap systems were used for data collection in all of the mentioned studies (Table 7). These systems provided data to compute the COM position and velocity [100,116], spatial-temporal gait parameters [12,116], and upper body segment angles [116]. Force data were acquired in [12,116]. An EMG system was considered in [12] and wearable inertial sensors were used in [110,112].

3.4. Methods used to unbias the perturbations

From the group of 48 selected studies, some strategies have been adopted to mitigate participants' anticipatory behaviours towards the perturbations applied.

Some studies attempted to affect participants' vision in order to reduce the likelihood of them predicting the position of the obstacles and the perturbations' onset. Studies instructed subjects to look straight ahead while walking [82,83,103,107] or to fix their eye sight on an object positioned at eye level [89,109]. Other authors dimmed the lights to prevent visual cues that would allow participants to identify potential slippery areas [103,104,107,108,110] or tripping obstacles [118]. Silver *et al.* [115] and Ko *et al.* [117] attempted to occlude subjects' peripheral visual field with special goggles and eye patches, respectively. Studies also instructed participants to face away from the walkway before each trial to limit their perception about the positioning of the slip or trip perturbation sources [101,103,107,108]. As such, the perturbation sources could be added, removed, or moved to different places along the walkway between trials [100–102,117].

Furthermore, studies did not inform participants about the perturbations' characteristics and provoked perturbations with different: i) intensities [10,74,79]; ii) directions [95]; iii) gait events perturbed [111,112]; and iv) trials' time length [111]. In addition, Okubo *et al.* [100,101]applied slips and trips in a mixed order. Moreover, other studies provoked the perturbations to both legs [10,74,85,90,100–102].

Some authors only applied a single perturbation in order to minimise gait adaptations following repeated perturbation exposure [84,109,110]. Studies also conducted walking trials without perturbations between perturbation trials in order to increase the unpredictability of the perturbation delivery [100,116].

3.5. Discussion

Prevalence of slip-like perturbation studies was higher than trip-like perturbations ones. This is in line with the evidence that slips contribute more to fall events than trips [5,6].

From the group of 48 selected studies, 22 enrolled young subjects, 16 manuscripts included older participants and 6 studies accounted for both young and older subjects. The remaining studies enrolled young, middle age and older adults [108,115], young and middle age participants [107], and middle age adults [114]. The high number of studies that included participants of young and middle age groups has motivated this review to extend the analysis of the review study [2]. Moreover, only 9 out of the 48 selected studies included more than 50 participants during the experimental trials. These search results depict the prevalence of young subjects during the experimental protocols for provoking artificial falls, as well as the low number of participants enrolled. Considering that the elderly entails a substantially higher fall risk than younger adults, an effort should be performed to include older participants in future experiments. Additionally, a higher number of participants should be enrolled in order to enable the generalisation of the study's findings over a higher sample of the population. These efforts would promote a better and wider understanding of the reactions of these high fall risk subjects to slip and trip gait perturbations.

When applicable, the search results obtained from this narrative review will be compared against the evidences found in the review studies conducted by McCrum *et al.* [2] and Karamanidis *et al.* [71].

3.5.1. Which methods and walking conditions are used to provoke slip- and trip-like perturbations?

This review finds a variety of procedures implemented in the scientific literature to elicit slip- and trip-like perturbations.

Slip-like perturbations were applied during both treadmill and overground walking with the latter (29 studies) being more prevalent than the former (18 studies). The application of slips during treadmill walking consisted of the sudden change of the belt's acceleration to induce an anteriorly displacement between the BOS and the COM. This finding is aligned to Karamanidis *et al.* [71]. On the other hand, overground walking slips were delivered by movable platforms, slippery solutions, and novel robotic devices. McCrum *et al.* [2] had also found the prevalent use of movable platforms to provoke slip perturbations.

The slip-like events were generally applied at the instant of the heel strike. This is in line with Lockhart [70] that highlighted this gait event as the most hazardous one towards slip events during walking. During the heel strike, the body weight is being transferred to the limb where the heel strike is taking place (slipping limb). Applying a slip to that limb when this transfer is yet to be concluded would cause a highly unstable situation due to the lack of stable body support provided by the lower limbs. Additionally, Lockhart [70] also pointed out the toe-off event as another critical gait phase for slipping. However, since in this event almost all of the body weight has been transferred from the toe-off limb (slipping limb) to the other one (trailing limb), the likelihood of inducing an hazardous situation is smaller than the slip perturbation at heel strike [70]. This may be the reason why only one study applied slips at the toe-off phase [111].

Although overground walking conditions are more realistic to emulate daily life locomotion, treadmill devices provide continuous collection of gait patterns over longer periods of time. Thereby, slip perturbation's onset timing during treadmill locomotion may be more unpredictable than during overground walking [122]. Regarding real-world slips, treadmill slips may not resemble the whole nature of slips, since treadmill belts can often move in only one direction, generally considered the AP direction [10,74,75,85]. In spite that, study [123] shows that from the total of the instability-induced falls collected during their experimental protocol, only 8.2% were related to the MLat direction. Hence, there is literature evidence that supports the AP direction as the most relevant in slip dynamics, which may provide support to the studies that performed slip-like perturbation during treadmill walking.

Moreover, concerning real-world slips, the slippery solution-based perturbations are more likely to resemble real slippery conditions by reducing COF at the interface between the foot and the floor [70]. Herein, the perturbation direction is not restricted which allows for a more realistic and unpredictable slip dynamics as they happen in real life. However, the slip direction and magnitude unpredictability may hinder the generalisation of specific findings of slip dynamics since the slip conditions are less controlled. When the perturbation is controlled, i.e., its characteristics can be normalised across different experimental trials, specific aspects of the slip dynamics and responses can be studied which can enable a better and more reliable generalisation of the studies' findings [10]. In addition, the slippery solution studies did not automatically deliver the perturbations, which could yield more variability on the onset and the magnitude of the provoked slip. Conversely, slips caused by movable platforms, novel robotic devices and by changing treadmill's belt acceleration were delivered automatically.

Trip-like perturbations were also elicited during treadmill or overground locomotion. Treadmill walking trips were caused by changing the belt's acceleration, using a brake-and-release system or a tripping device. Karamanidis *et al.* [71] verified the same methods except for the tripping device. On the other hand, overground walking trips were caused by triggering an obstacle release, manual placing an object along the walkway, or using a novel robotic device. Trips were mainly applied during the swing phase of gait. This is in line with Karamanidis *et al.* [71], which described trip events as the sudden disruption of the relation between subject's COM and BOS caused by the abrupt interruption of the swing limb motion. The advantages and disadvantages of using treadmill or walkway setups to provoke trips are analogous to the ones mentioned above for the slip-like perturbations. All the treadmill-based setups conceived to apply trip-like perturbations, except study [115], did not use objects to perturb the locomotion. Thereby, the perturbations applied either by changing belt's acceleration or brake-and-release systems may be less likely to resemble real-world trips. Nevertheless, the latter systems are able to interrupt the swing phase of gait by directly pulling the respective foot, which can also accurately depict trip events. While in the manual obstacle placement it was not guaranteed that the trips would occur at a specific phase of gait, studies that triggered an obstacle release had a more automatic and reliable way to perturb participant's gait during their swing phase [12,100–102,116]. Moreover, regarding the tripping obstacles implemented in the selected articles, it was observed the prominent use of boards with height values of 7/8 cm [110,116] and 14/15 cm [12,100–102]. Predictably, an inter-trial variability of the perturbation onset may arise in the obstacle manual trigger. Therefore, it is recommended that researchers consider more automatic approaches to deliver trips. It is noteworthy that from all the trip-like perturbation studies, only Silver *et al.* [115] considered the application of more than one type of obstacle. Future work should follow this approach in order to enable a more comprehensive analysis of the variability of trip events triggered by different types of obstacles.

For both types of perturbations, the selection of the walking condition (treadmill or overground) has to take into consideration the trade-off between the relevance of inducing natural perturbation dynamics and the generalisation of the studies' results. Further, the selection should attend to the available space for the experimental setup and if the perturbations are intended to be delivered: i) automatically or not; and ii) directly from a device connected to the subject or not [11,111,112,114]. Additionally, for slip perturbations, this selection has also to keep in mind whether the perturbations are intended to be delivered in a specific direction or not. For trip perturbations, it is also necessary to consider if one or more types of obstacles are planned to be used to apply the trips.

3.5.2. Is it preferable to deliver perturbations during treadmill or overground walking?

Results showed that there is a prevalence of overground walking perturbations relative to treadmill perturbations in both slip- and trip-like perturbations. The walkway perturbations may be more realistic than the treadmill-based ones since real-life slips and trips occur during overground walking. However, recent research has been attempting to validate the perturbation delivery during treadmill locomotion against overground walking [78,86]. Liu *et al.* [86] compared the retention of fall resisting skills in the follow-up period of 6 months between treadmill and overground walking conditions. Results showed that the group of individuals that received baseline overground walking perturbation training had a lower fall incidence and a higher reactive stability against an overground slip applied 6 months after the perturbation training sessions than the group that underwent the baseline treadmill perturbation training. Therefore, since the treadmill slip training group achieved a lower balance recovery performance than the overground slip training group, the authors could not generalise the delivery of slips during treadmill walking against overground walking. Nevertheless, treadmill perturbation training group had increased stability metrics and lower fall incidence than its control counterpart (treadmill training without perturbations), which depict a long-term relative retention of fall resisting skills from treadmill perturbation training.

Researchers are working towards this topic given all the advantages associated with treadmills to provoke perturbations. Perturbation delivery during treadmill walking provides accurate velocity profile control, which may lead to the reliable delivery of slips [76]. Computer controlled treadmill devices enable the application of different perturbations in a highly precise and standardised manner, which is not observed during overground perturbations studies since the perturbation characteristics entail more variability [88,90]. Additionally, treadmill devices allow researchers to easily modulate the intensity of the perturbation and, therefore, to study subject's adaptation to different perturbations characteristics [88]. Furthermore, the portability of treadmill devices, as well as the reduced space they occupy are also noteworthy [76,81,88]. Treadmills also allow for the collection of multiple and continuous walking patterns over long periods of time [122]. As reported in previous review studies [2,71], this will also lead to an increased difficulty to predict when the perturbation will be delivered, which ensures more realistic reactive balance control strategies adopted by the participants. Concerning all of the above mentioned advantages of treadmill's perturbation delivery, the generalisation of treadmill perturbations application against the ones applied during overground walking becomes essential [81,88].

3.5.3. Is it preferable to use a single-belt or a split-belt treadmill to perturb walking?

Both single and split-belt treadmills have been used to apply treadmill gait perturbations. Single belt treadmills were used in 14 studies [11,76,87,88,114,115,77–83,86], while split-belt treadmills were adopted in 8 manuscripts [10,74,75,84,85,89,90,113]. Compared to single-belt, split-belt treadmills give researchers the opportunity to study kinetic data from both feet independently by integrating force sensors in each of the belts. Additionally, the application of gait perturbations is more standardised and reproducible across different test subjects, allowing to define: i) more accurately the limb that is going to be perturbed; ii) specific velocity profiles for each belt to conduct the perturbation; and iii) automatic onset of the perturbation based on kinetic data from the targeted limb [10,90]. These features turn the split-belt treadmill more suitable to deliver realistic perturbations. However, a comparison study [122] of the walking kinematics between the single- and split-belt treadmill walking, concluded that subjects tend to widen their base of support while walking on a split-belt treadmill to manage the walking gap between the two belts. Despite of this unnatural gait pattern, frontal plane lower limb kinematics were not significantly different between both types of treadmills [122]. With this in mind, it is possible to deliver perturbations on a split-belt treadmill taking advantage of its features compared with the single belt one. Regardless, single-belt treadmills are more accessible to apply gait perturbations [11,79,82,115].

3.5.4. What procedures are implemented to maintain responses to perturbations unbiased?

Different mechanisms were adopted by the authors to reduce the predictability of the perturbation events delivered. Generally, all the studies described that those perturbations were intended to be unexpected and instructed their participants to react naturally and try to recover balance whenever a perturbation was applied. As such, studies did not carry out trials to familiarise subjects with the perturbations to mitigate participants' learning effects and gait adaptation to the perturbations. Previous literature studies suggested that following the first perturbation exposure, subjects alter their gait characteristics to adapt to those perturbation conditions [97,124]. Thus, some authors tripped or slipped their participants only once [83,84,114,96,97,103,104,107–110].

However, 38 studies conducted multiple perturbations on the same subject. Consequently, they included different techniques to enhance the unpredictability of both perturbation's onset and characteristics so as to limit the bias associated with subjects' gait modification following repeated perturbation exposure and increase the reliability of the results obtained. Some authors conducted perturbations with different intensities [10,74,79], directions [95], and on both limbs [10,74,85] to prevent subjects' adaptation to only one type of perturbation. Other sources of variability consisted of changing the gait phase to be perturbed [111,112], trials' duration [111], and the location of obstacles [101]. Overground walking perturbation studies often refer that, between different trials, participants were required to face away from the walkway in order to limit the perception of the perturbations source's placement [101,108,117]. Furthermore, most of these studies included non-perturbation trials between perturbation trials to create more unexpected conditions when perturbations were delivered.

Some authors attempted to somehow control participant's field of view to be less likely for them to perceive the perturbation onset. Studies instructed their subjects to look straight ahead while walking [82,103,107] and focus their sight on an object [109] or a mark [89] in an eye level. Silver *et al.* [115] and Ko *et al.* [117] conducted another approach to limit participants peripheral sight by requiring them to use an eye patch during the trials. In slip-like perturbations through slippery solutions, authors created a dimmed lighting environment so as to reduce the light reflection of the slippery surface and prevent participants to spot its location [103,104,108]. Also, Schulz [118] created a low lighting environment that would reduce subjects' ability to spot the tripping obstacles. However, since these visual constraints introduced do not exist during real-life walking, its application should be avoided to mimic daily-life conditions.

It is also noteworthy that any gait asymmetries provoked by the placement of some constraint on the subject's body during the trials must be compensated to ensure a natural gait. In this regard, despite the perturbations were applied to only one limb, participants in [111] wore the outsole device on both feet and in [11] a rope was attached to each foot.

3.5.5. Which limb is generally used to apply the perturbations?

Studies have applied the perturbations on one or both legs. However, some works did not mention which leg or legs were perturbed [79,82,83,88,97,118]. Most of the studies (35 studies) applied the perturbation to only one leg. From this group of articles, 22 and 8 papers applied the perturbations to the right and left legs, respectively, whereas the 5 remaining studies described the perturbation delivery to the dominant leg. It is also noteworthy that from the 8 studies that only perturbed the left leg, 2 of them described that leg as the participant's non-dominant leg.

There is clear evidence for the application of the perturbations preferably to the right limb instead of the left one. This may be related to the fact that the large majority of individuals present right-side dominance [125]. However, only 7 studies have reported the limb selection according to the side-dominance of individuals: the dominant [95,106,108,109,111] or the non-dominant limb [89,113]. Additionally, Okubo *et al.* [100–102] also considered the side-dominance of the subjects, despite the authors conducted perturbations in both legs. Despite side-dominance is not covered by most of the collected studies (works [92,107] reported this limitation), it should be considered, especially if the study considers PBT, where perturbations are delivered to improve subjects' balance recovery skills. Martelli *et al.* [126] highlighted that the dominant limb is mainly responsible to propel the body forward whereas the main role of the non-dominant limb is to provide body support. A previous work also suggests that there is an increased risk of falling in the situations where the perturbed limb is the non-dominant limb [127]. Therefore, the analysis of the subjects' reactions to perturbations is more comprehensive if the dominance of the leg being perturbed is considered.

Furthermore, 7 studies perturbed participants in both legs [10,74,85,90,100–102]. Although it represents less than 15% of the included studies, the perturbation delivery to both legs play an important role to maintain the natural responses to the perturbations from the participants. As mentioned by Martelli *et al.* [10], Aprigliano *et al.* [74] and Mueller *et al.* [90], although only data from right-sided perturbations were considered for the study's analysis, left-sided perturbations were also randomly delivered to obtain unbiased results by limiting subject's gait pattern adaptation to only right-sided perturbations. The randomisation of the perturbations' side allows to decrease the learning effects to counteract the LOBs induced and the participants' awareness of the perturbations' characteristics in comparison with perturbations provoked always to the same side [85,100–102]. Moreover, the application of perturbations to both sides would enable the study of the differences between subject's reactions to perturbations applied to the dominant and non-dominant limbs. It is also noteworthy that more complex resources are required in order to deliver perturbations to a specific limb. A split-belt treadmill is more suitable to reliably apply perturbations to only one limb during treadmill walking [80]. Yet, these treadmill devices are less available in the market regarding the single-belt treadmill. Similarly, concerning overground walking perturbations, the walkway should be divided into independent segments for each limb so as to enable the reliable and reproducible perturbation delivery towards a specific leg [128].

3.5.6. Which was the participants' walking speed during the trials?

From the forty-one studies that included trials under only one walking condition, either treadmill or overground locomotion, subjects were instructed to walk at self-selected speed on 23 studies, 10 studies applied a fixed walking speed across all participants, 2 studies described the application of a normalised walking speed specific for each subject, and 6 studies did not mention the walking speed adopted. The 7 studies that delivered perturbations during both treadmill and overground walking, reported different velocity paradigms for each walking condition. For instance, Yang *et al.* [87] and Lee *et al.* [80] described the application of 1.2 m/s speed in the treadmill and a self-selected speed while walking along the walkway. The other studies either reported self-selected speed on both walking conditions [78,86] or did not describe the overground walking speed [76,77,81].

Regardless of the walking condition adopted, most of the authors instructed their participants to walk at their self-selected speed. This is in line with the review conducted by McCrum *et al.* [2]. Regarding those 23 manuscripts, subjects selected their own comfortable speed on overground walking studies [12,94,107,111,112,129,95,96,98,99,103–106], while in treadmill walking studies participants were instructed to either ambulate at their own self-selected speed [79,82,83,89,113,115] or were asked to select a speed from 4 available options (1.2, 1.0, 0.8 or 0.6 m/s) [88]. Although walking at that comfortable speed would simulate more realistic walking conditions, it is more difficult to deliver perturbations equally challenging across all the subjects.

Studies [11,75,84,90,114] selected a constant speed throughout all the trials towards mitigating the problem associated with the different velocities from the different participants. In these manuscripts, belt speeds of 1.0 [11,75,90], 1.2 [84], and 1.4 [114] m/s were applied. The constant speed condition is easier to perform in the treadmill than in overground since a constant belt speed can be employed. However, some overground walking perturbation studies adopted strategies to overcome that limitation. Arena *et al.* [110] initially instructed their participants to walk naturally while monitoring their gait speed using Optical MoCap data. Afterwards, participants were told to increase or decrease their speed to keep it between 1.45 and 1.6 m/s. In addition, Okubo *et al.* [100–102] regulated participants' speed using a metronome such they stepped in the tiles positioned along the walkway according to the metronome's beat. These tiles were configured according to subject's cadence and normal step length. Hirata *et al.* [85] also matched the speed of the subjects with the beat of a metronome, considering both slow (0.9 m/s) and fast (1.6 m/s) walking conditions. However, in this constant walking speed condition, subjects' normal walking is partially disconsidered and the velocities in which perturbations are delivered may not still be equally challenging for subjects with different anthropometric characteristics [84]. In order to answer this limitation, Martelli *et al.* [10] and Aprigliano *et al.* [74] calculated a velocity that was specific for each participant according to the leg length. This procedure is in line with McCrum *et al.* [130], who claimed that the walking speed should be adapted to each subject to induce a similar margin of stability across all the participants along the trials. This procedure enables to create an equally challenging environment of perturbation delivery regardless of the subjects' characteristics.

3.5.7. What are the main sensor systems used to collect data during perturbation-based protocols?

The Optical MoCap devices were the most used sensor systems (45 out of 48 studies). The use of reflexive markers to acquire subject's motion data enables the extraction of relevant kinematic and angular information of subjects' motion in laboratory conditions. This may be particularly important to find parameters that relate to the biomechanical reactions to falls, which could be employed in the development of fall prevention strategies for individuals with increased risk of falling, as shown in [10,98,99]. Data from these systems were used to compute subject's stability through the computation the COM position and velocity [10,78,81,84,89,92,95,97,101,116] and for the analysis of spatial-temporal gait parameters [12,74,85,106,116], upper limb segment angles [10,89,116], lower limb segment angles [74,99], joint angles [109], and joint moments [92,99].

Force data were acquired in 32 studies. These data were mainly collected by force plates either installed beneath treadmill's belts [10,85] or embedded in some position along a walkway [92,106]. The main purpose for using the force plates was to provide ground reaction force information to detect the reliable timing of perturbation application rather than to collect data for further analysis [10,90,91,116].

Five studies equipped participants with wearable inertial sensors with different purposes. Arena *et al.* [110] placed an IMU on the forehead to acquire meaningful information from head motion during slip and trip events. Aprigliano *et al.* [11] collected inertial data to compute several limb elevation angles during normal and perturbed walking trials. Additionally, Er *et al.* [112] used data provided by inertial sensors to feed a gait event detection algorithm that led to a precise application of the gait perturbations.

Lastly, EMG sensors were considered in 8 studies. They were the only type of biosensor used among the 48 studies collected. EMG data may provide useful information about muscles activated during imminent fall risk situations [131]. Accordingly, Sawers *et al.* [93,94] and Nazifi *et al.* [104] explored muscle synergies, which represent groups of muscles that coactivate to produce a biomechanical function that is required to perform a certain motor task [132], during perturbation trials. The study of the synergies underlying gait perturbation recovery could be promising to better understand which muscles are not being properly activated in fall risk individuals. In addition, it can also promote an evidence-based fall prevention treatment. Moreover, during human imbalance condition, a sudden EMG pattern alteration due to a reactive neuromuscular response may be generated faster than the modification of inertial signal patterns [22]. Accordingly, Marigold & Patla [133] and Pijnappels *et al.* [134] showed that rapid lower limb muscle activation was elicited following slip- and trip-like events, respectively. Thereby, future studies should consider the use of EMG sensors concerning the relevant information they provide towards the better understanding and faster detection of human's reactions to perturbation events.

Although load cells were used in some studies, these sensors did not provide meaningful data regarding the subject's reactions to the provoked perturbations since their main purpose was to label the experimental trials as fall or non-fall/recovery [76,97,101].

3.5.8. Are there benefits to apply both slip- and trip-like perturbations?

Among the included studies, 6 studies delivered both types of perturbations to each participant [89,90,100–102,112]. The application of both types of perturbations may be more suitable than the single type of perturbation if the purpose of the study regards to PBT [89,90,101,102]. Okubo *et al.* [101] pointed out that the application of only slip-like perturbations may lead individuals to learn recovery strategies related to the predictive adaptation of anterior shifting the COM, which may in turn increase the risk of tripping. Thus, to adapt individuals to real-life perturbations these COM predictive alterations must be mitigated by the mixed application of both slips and trips. Furthermore, study [102] applied slips and trips in a mixed order to mimic more realistic perturbation conditions. This would ensure more natural reactions to the gait perturbations applied, similar to the real-life context. Nevertheless, the inclusion of both types of perturbations may yield a more complex experimental protocol.

4. Slip-related Fall Prevention Strategy Proposal

The fall prevention strategy concept is divided in 2 major modules: i) the actuation strategy; and ii) the detection strategy. Requirements were drawn for each strategy in order to promote the effective performance from the detection of slip-induced LOBs to the successful corrective actuation of the assistive device. Considering that the slip fall prevention is aimed at real-world conditions, the sensors used for data acquisition were considered to be wearable devices or implemented on the assistive device.

Concerning the actuation strategy definition, a literature investigation was conducted on studies that analysed the human biomechanical reactions to slip perturbations. Only slips induced at the heel strike were analysed for the current strategy, considering that this gait event was found to be the most prominent and prevalent to onset slip perturbations during walking [70]. In fact, the state-of-art literature research on Provoked Falls (Chapter 3), highlighted that almost all the studies considered this gait event as the slip onset. Considering the prominent role of the perturbed (leading) and unperturbed (trailing) legs to counteract slip-induced LOBs, the ideal scenario would include the assistive torque supply to all the lower limb joints from both legs upon a slip. However, such an approach would increase the complexity of the fall prevention strategy, in both computational and mechanical aspects, which could lead to an ineffective fall prevention. Therefore, only the leg and joint found to be the most relevant to counteract the slip-induced LOBs will be provided with assistive actuation. Actually, Trkov *et al.* [65] and Mioskowska *et al.* [135] assisted only one joint with their slip fall prevention system. Hence, the current search was aimed at understanding: i) 'Which leg has a more prominent role to counteract slip-induced LOBs?'; ii) 'Which lower limb joint has a more determinant role to counteract slip-induced LOBs?'; and iii) 'Which should be the joint moment characteristics applied towards the actuation joint?'. The first question considers the selection of the most suitable leg to actuate upon a slip-induced LOB. The second question allows to define the actuation joint for the slip-related fall prevention strategy. The third question allows to understand the joint moment characteristics that should be applied towards the actuation joint upon a slip-induced LOB. The answers given to these questions allowed to define the assistive device for the fall prevention strategy.

The detection strategy definition relies on the use of biological-inspired controllers, which are able to learn and adapt its output to almost periodic signals. As such, these controllers are well-adapted to monitor human locomotion variables and present advantages, which are further highlighted, in comparison with other training-based algorithms. In the presence of a gait perturbation, the signal predicted by the biological-inspired controller will deviate from the actual motion signal. Thus, threshold-based algorithms were used to detect the gait perturbations based on these induced deviations. Nevertheless, it is necessary to objectively select the variables which will be monitored towards the detection of slip-induced LOBs. Therefore, important human motion variables were considered based on the previous literature reviewed and further criteria was applied to them in order to select the most suitable variables to be monitored by the biological-inspired controllers.

Following these procedures, the timings assigned to the slip-related fall prevention strategy, namely the times attributed to the detection and actuation stages, were determined according to literature evidence on biomechanical reactions to slip perturbations.

4.1. Introduction

4.1.1. Biomechanics of the Slip event

Slips have been identified as the main contributors to falls [5,6]. In addition, occupational fall mortality rates are substantially higher for elderly aged 65 and above in comparison with other age groups [6]. Hence, researchers have been studying the biomechanics of slips to better understand the human responses to these events and reduce their harmful consequences. Slips occur when the interface between the subject's foot and the floor does not provide sufficient COF [70]. As such, the environmental conditions play an important role in the likelihood of slipping. These events take place mostly when the foot is either contacting or leaving the floor, which resemble critical body weight transfer situations between the lower limbs, especially when the heel strikes the floor [70]. For instance, if at the end of the swing phase the heel is not sufficiently decelerated, an increased heel velocity will take place at the heel strike, which increases the possibility of slip initiation, whenever slippery conditions are presented [136]. Slips initiated at the heel strike deviate subject's COM relative to the BOS causing a backward LOB. Upon the detection of this abnormal deviation by human sensory systems, information is sent through afferent nerves to the motor control regions of the Central Nervous System (CNS). The CNS processes the information received and further sends efferent signals towards targeted skeletal muscles to compensate the LOB suffered by properly contracting to maintain the body position within the BOS. The coactivity of the activated lower limb muscles counteracts the displacement of the perturbed foot and promotes slip recovery [70]. The slip perturbation direction is often referred as the direction of motion, i.e., the AP direction. In fact, Wang *et al.* [123] has shown that from all the instability-induced falls provoked during their experiments, only 8.2% were related to the MLat direction.

A previous study performed by Cham & Redfern [9] investigated the corrective strategies to prevent falls adopted during a slip event based on the lower limb joint moment profiles from the leading leg. The authors found that the primary response to counteract the LOB induced by a slip at the heel strike consisted on the increase of both knee flexion and hip extensor moments at the leading leg, which is also corroborated by Moyer *et al.* [137]. This allows to counteract the sliding motion of the perturbed foot to bring it back closer to the COM and minimise the body's vertical descent. These increased moments, which are produced in the leading limb joints between 25% and 45% of the stance phase, comprise the dominant corrective response to slip events. Despite only addressing the recovery biomechanics from the leading limb, Cham & Redfern [9] also acknowledged the possible assistive role of the trailing leg during a slip. In this regard, Moyer *et al.* [137] underlined the lack of study of the trailing leg kinematics and emphasised its importance towards the human biomechanical reaction to slips. These researchers distinguished 4 responses of the trailing leg towards slips provoked at the heel strike, which were recruited based on the slip severity (measured by the peak heel horizontal velocity of the leading foot) and were evoked after the onset of the leading limb's corrective responses. As in Marigold & Patla [133], Moyer *et al.* [137] observed that the higher was the slip severity, the faster the swing phase of the trailing foot was interrupted by lowering the foot to the ground, by means of a corrective hip extension, and reestablish a stable BOS to increase the chances of recovery. The increase in slip severity also induces a more posterior landing of the trailing foot on the ground and with a smaller contact area. The time taken to reverse the swing motion direction following a slip before landing the foot on the ground plays an important role towards the slip recovery [10]. If the slip was minimally disturbing to the user, the trailing leg behaved similarly to normal walking conditions and its swing phase was not interrupted [137].

Moyer *et al.* [137] also found evidence on interlimb coordination while recovering from slip events, since the magnitude of the trailing leg's response was associated with the knee moment exerted in the leading leg following the slip. As such, the successful recovery after a slip event is achieved by the interlimb coordination of both lower limbs. An increase of the flexion moment applied at the knee is accompanied with an increase in the hip extension moment in order to decelerate the sliding motion of the slipping leg and bring it back closer to the COM [9]. In parallel, the trailing leg's response is also characterised with the application of increased moments at the hip and knee joints [137]. The hip response is characterised by an increased extension moment in order to lower the foot onto the ground to interrupt the swing phase and reestablish a stable BOS. A corrective flexion moment is also provided at the knee to: i) decelerate the forward swing motion of the trailing limb; ii) absorb the energy produced by the hip extensors; and iii) allow to perform the trailing leg's foot clearance during swing despite the slip [137]. These corrective responses promptly applied to the leading and trailing legs are derived from different muscle synergies, which may crucially represent the neural control during a slip event [104].

Muscle synergies constitute groups of muscles that coactivate in order to produce a biomechanical function that is required to perform a certain motor task [132]. The 3rd and 4th muscle synergies highlighted in the study conducted by Nazifi *et al.* [104] depict the previously highlighted corrective actions adopted by the leading and trailing legs, respectively, upon a slip event. These findings further corroborate the interlimb coordination achieved in both lower limbs to counteract the slip perturbations. Moyer *et al.* [137] also found that intralimb coordination was also implied on the trailing leg, since the corrective moments generated at its knee and hip were also correlated. To sum up the literature evidence found, Figure 7 depicts the main human biomechanical reactions adopted upon a slip event.

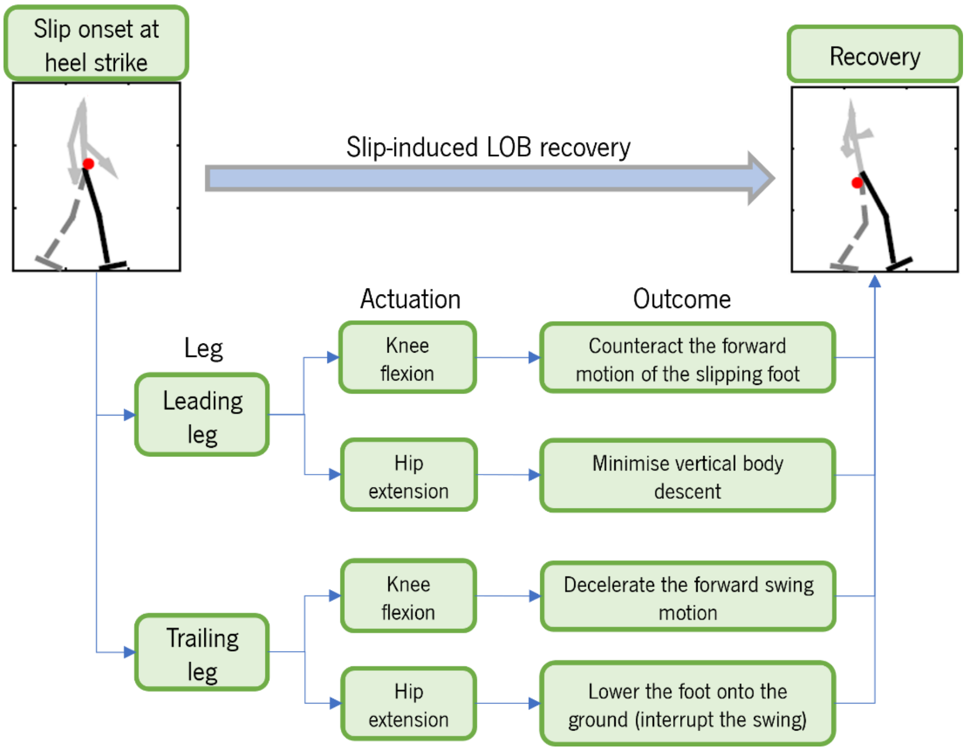

Figure 7. Human biomechanical reactions adopted upon a slip event. The human stick diagrams were extracted from study [10]. The red dot represents the extrapolated COM.

Wang *et al.* [99] presented a schematic diagram illustrative of all possible slip outcomes (Figure 8), i.e., the consequences a slip has on an individual. According to Figure 8, the slip outcome is firstly classified into LOB or no-LOB. In the presence of a slip, if the body COM state, which is described by the relationship between the COM position and the COM velocity relative to BOS [97], remains within the limits of stability without the need of stepping or grasping actions, the outcome is a no-LOB. In this scenario, the trailing leg proceeds with the forward motion progression, as in regular walking, by landing in line with the slipping foot or in front of it. The no-LOB can be further classified into skate over and walkover outcomes. A walkover takes place when the sliding motion of the leading foot is minimised or completely neutralised. Nevertheless, if the sliding motion is mitigated, but not eliminated, the outcome is a skate over. However, if the body COM state is moved outside the limits of stability, a LOB occurs. In this condition, the forward progression of the trailing leg is interrupted to immediately provide a stable BOS to counteract the perturbation [137]. As such, the trailing leg lands behind the slipping foot, as a backward stepping action is necessary. Upon a slip-induced LOB, a fall takes places when an individual fails to restore stability, i.e., bring back the COM state within the limits of stability, or is unable to produce sufficient vertical limb support. However, in the non-fall outcome, individuals regain stability by effectively taking a recovery step with the trailing leg, which will end up providing enough vertical limb support to slow down or reverse the hip descent and consequently avoid falling [138].

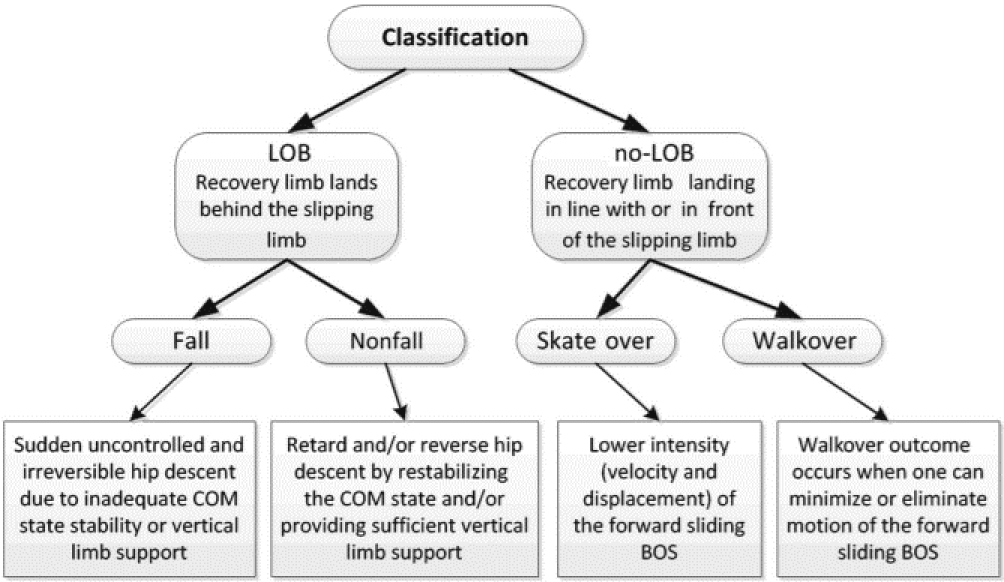

Figure 8. Schematic diagram depicting the possible slip outcomes [99] .

4.1.2. Literature Slip-related Fall Prevention Strategies

High fall risk individuals are constantly threatened by the unpredictability of the occurrence of gait perturbations, which can happen in a wide range of scenarios during the everyday living. Although these subjects are able to produce reactive responses to counteract the LOBs, they are generally not agile and strong enough to avoid falling [64]. According to the overwhelming prevalence and harmful consequences associated with the occurrence of slips, recent literature has attempted to implement slip-related fall prevention strategies.

Monaco *et al.* [64] developed a wearable robotic device which consists of an Active Pelvis Orthosis (APO) to assist balance recovery following unannounced slip perturbations. The authors grounded their approach considering that a stiffness increase at the hip joints could help subjects to recover from treadmill slip-like perturbations. The APO operated either in the zero-torque mode (Z-mode), in which no assistance torque was applied to the participants, or in the assistive mode (A-mode), where the system supplied assistive torques at the hip joints. Herein, the APO assistance consists of the synchronous extensor and flexor torques towards the leading and trailing limbs, respectively, in the sagittal plane. Monaco *et al.* [64] adopted some assumptions towards the APO's assistive actuation since they claimed that no previous study had closed the loop from the LOB detection to the assistive support provided by a wearable robot: i) the assistive torque duration was chosen as 0.25 s, considering that a fall happens within 0.7 and 1 s [139] and the APO's LOB detection time is between 0.3 and 0.4 s; and ii) Since the subject's inertia affects the reactive response, APO's assistive torque was proportional to the sum weight of participant and exoskeleton by the ratio of 0.2 Nm/kg. Perturbations were detected based on the real-time comparison between the actual APO's hip angles and the hip angles predicted by a group of adaptive oscillators. An adaptive-threshold algorithm monitored the difference between the actual hip angle and the one predicted by a pool of adaptive Hopf oscillators [13]. Whenever this difference or error value exceeded the computed threshold, a LOB was detected. Then, the system switched from the passive Z-mode to the active A-mode in order to provide assistive torques so as to counteract the downward COM displacement. The adaptive threshold algorithm was able to detect a LOB situation in about 350 ms. Furthermore, it was concluded that the APO did not significantly alter gait characteristics, which makes it transparent to subject's steady gait.

Mioskowska *et al.* [135] presented a wearable knee assistive device that aims to prevent slip related falls. The system was designed to actively extend the trailing leg's knee by means of a knee brace once a slip perturbation has been detected. This leg would immediately restore contact with the ground under perturbation conditions and thus extend subject’s BOS to help achieve balance recovery and regain stability. The system contains a lightweight cable-driven knee brace and a backpack, which stores the actuator and electronic components of the system. The system's actuation is powered by means of an air cylinder and a small cartridge with CO_2 compressed gas. The system contains one cartridge, which must be replaced for each slip assistance. Upon pressure release into the air cylinder, its piston pulls the Bowden cable connected to the knee brace around a circular hub, which provides torque to pull the device straight and perform knee extension. The hub was placed on the outer side of the knee to mitigate potential walking constraints. Unlike the previous system, these authors did not test the system's LOB detection performance since this study focused on the actuation strategy to prevent slip-induced falls. Firstly, the authors performed benchtop testing by actuating the system from 90 to 0 and 60 to 0 degrees.

Afterwards, 3 human subject tests were conducted to test the system's knee extension during: i) sitting; ii) standing; and iii) walking. Results showed that the system is promising to be used in slip experiments due to its demonstrated capability of performing fast knee extension during gait. Benchtop testing results demonstrated an average actuation time for device extension was 0.082 and 0.072 seconds from the initial 90 to 0 degrees and 60 to 0 degrees, respectively. In addition, the device was shown to extend a human knee more than 30 degrees within the short period of 0.4 seconds. The authors also concluded that the device caused minimal deviations on subject's walking.

Trkov *et al.* [65] developed a Robotic Knee Assistive Device (ROKAD) capable of providing assistive knee torque to the leading limb during slip events. The system's design requirements rely on the comparison of the computed knee angular velocities and torques during normal walking and walking with slip perturbation exposure. ROKAD operates with an impedance and torque feedback control. The desired torque magnitude is determined based on the linear feedback between the actual and desired knee angle positions and velocities. The electric motor that powers the ROKAD, as well as the battery, actuators and other embedded systems is dislocated from the knee in order to ensure subjects' natural gait by lessening the external weight on the knee. Similar to Mioskowska *et al.* [135], the authors focused on the actuation strategy to prevent slips rather than testing the system's LOB detection performance. Nevertheless, Trkov *et al.* [65] mentioned that a slip detection algorithm that uses data from wearable IMUs is integrated into the ROKAD. The authors conducted benchtop and human subject testing. The former allowed for the device's characterisation. The latter tests consisted of performing sit-to-stand task with a 90 degrees motion range and fast squat motions. The human subject testing allowed to ascertain if the participants took advantage of the external torque assistance to perform the tasks. Furthermore, the sudden knee flexion and extension performed during the squat motion can mimic those from slip events and allowed to test the device's response under the impedance controller. Benchtop test results show that ROKAD is able to properly track the knee angle profile. It was also suggested that the ROKAD device did not hinder subject's gait. ROKAD was also capable of generating torques up to 40Nm in less than 0.2 sec. According to human testing results, it was found that subjects stood up faster in both tasks with the torque assistance compared with no torque assistance. Thus, subjects positively used the ROKAD torque assistance to perform the experimental tasks. Hence, these results suggested that ROKAD could effectively provide torque assistance during slip events.

Figure 9 depicts a general overview of the actuation system from the 3 previously described studies. Monaco *et al.* [64] sought to provide assistive torque to the hip of both leading and trailing limbs, whereas

Mioskowska *et al.* [135] and Trkov *et al.* [65] applied this torque to the trailing and leading knee, respectively. Some of the most relevant characteristics from these systems are summarised in Table 8.

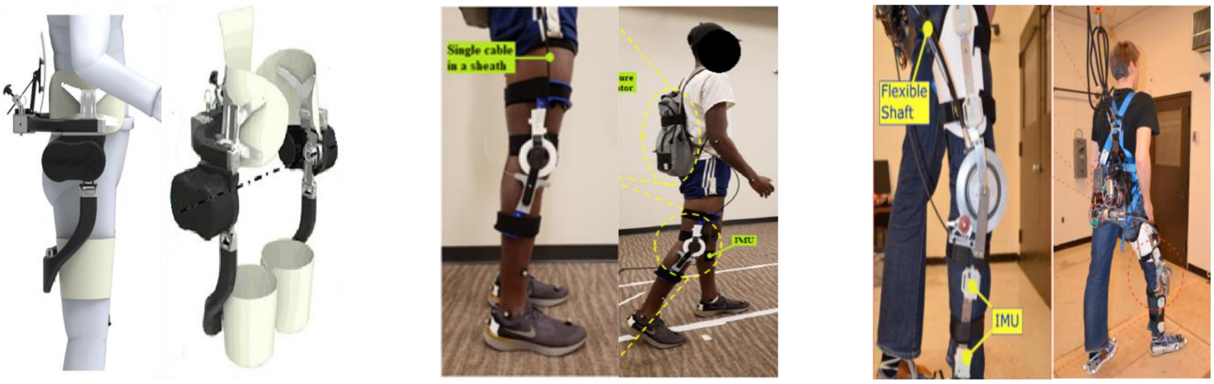

(a) (b) (c)

Figure 9. Literature slip-related fall prevention actuation systems. (a) Monaco *et al.* [64]. (b) Mioskowska *et al.* [135]. (c) Trkov *et al.* [65].

Table 8. Overview of the literature slip-related fall prevention systems

Authors	Actuation location	Embedded slip detection?	Actuation Strategy	Usage	Slip Onset	Torque Magnitude	System tested during slip-like experiments?
Monaco (2017) [64]	hip (both legs)	yes	extend perturbed leg and flex unperturbed leg	continuous	after heel strike	0.2 Nm/kg	yes
Mioskowska (2020) [135]	knee (trailing leg)	no	extend the unperturbed leg knee	Single usage (replace CO_2 cartridge)	after heel strike	25 Nm	no
Trkov (2017) [65]	knee (leading leg)	yes	apply the desired torque on the perturbed knee based on the linear feedback between its actual and desired angular positions and velocity	continuous	after heel strike	0.45 Nm/kg	yes

4.2. Actuation

Successful fall prevention requires the comprehensive definition of the assistive actuation characteristics. Thereby, it is important to reliably ascertain which leg and joint present the most relevant reactive response to counteract a slip-induced LOB, considering that only one joint will be provided with assistive actuation. Once a joint has been identified, the assistive actuation characteristics and the assistive device, which will provide the actuation, were determined. Figure 10 provides the assistive actuation characteristics proposed for the current slip-related fall prevention strategy. This selection was based on the literature evidence collected, which is further described.

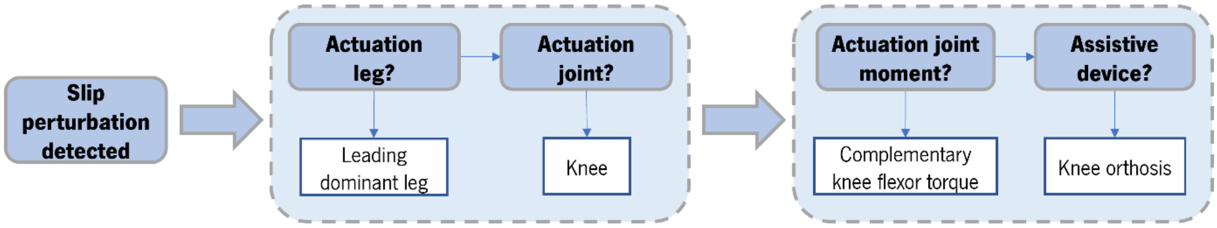

Figure 10. Assistive actuation strategy characteristics.

4.2.1. Which leg has a more prominent role to counteract slip-induced LOBs?

Concerning the selection of the actuation leg, two criteria that must be considered: i) the leg which is perturbed; and ii) the subject's side-dominance. For the first criteria, one should consider the actuation of the system in either the leading or the trailing legs. For the second criteria, the decision concerns to the actuation on the dominant or non-dominant legs.

Previous research has underlined the crucial response of both the leading [9] and the trailing [137] legs towards balance recovery after a slip perturbation at the heel strike. The leading leg's function essentially consists on bringing the anteriorly displaced BOS, as result of the sliding motion of the foot, closer to the COM [9]. The trailing leg's role consists on interrupting the swing phase by lowering the swing limb onto the ground in order to provide support and prevent the body from collapse, in case of a more severe slip [137]. Despite the importance given to the individual action of each leg, previous literature studies have suggested that the overall recovery response to slip perturbations results from the interlimb coordination between the corrective responses of both legs [94,104,137,140]. However, the leading leg's corrective reactions are believed to be the most relevant. This is depicted by the higher amount of studies that consider the leading leg's corrective responses in comparison with the ones that address the trailing leg's responses [9,137,141]. In fact, the primary corrective response to a slip is attributed to the leading leg [9]. Yang *et al.* [142] found that slip outcomes, i.e., fall or non-fall, were critically determined by the leading leg before the recovery touchdown of the trailing limb, which suggests that by individually controlling the leading leg it is possible to prevent slip-induced falls [99]. Indeed, an increased knee flexion angle elicited in the leading leg can result in a reduction in the demand of the braking impulse needed to counteract the sliding motion of the leading foot after the slip perturbation [143]. Hence, the timely actuation on the leading leg following a slip may reduce the further efforts needed from the trailing leg to restore the stability. Thereby, the actuation on the leading leg may tackle the slip in its origin by decreasing the displacement between the COM and the BOS, which directly reduces the slip severity. Despite the crucial role of the trailing leg towards slip fall prevention, this leg is not able to directly counteract the sliding motion of the slipping foot and thus reduce the severity of the slip. The trailing leg only allows to produce a compensatory response to the slip that has already happened. This corrective response mainly consists of the interruption of trailing leg's swing phase motion to reestablish a stable BOS, if the slip is severe enough. Therefore, the leading leg was chosen as the actuation leg.

Nevertheless, since the leading leg can be the right or the left leg, it still remains in open discussion which should be the actuation leg. In this regard, the side-dominance or laterality, i.e., the preference exhibited for one side of the body over the other, should be considered. Previous research has hypothesised that the asymmetrical behaviour during healthy locomotion between the two lower limbs potentially mirrors natural functional differences between the dominant and non-dominant limbs [144]. Despite the foundation of these bilateral asymmetries during healthy gait is still unclear, the "functional asymmetry" hypothesis suggests that these asymmetries may relate to the task discrepancy between both lower limbs. This theory postulates that the dominant lower limb is more responsible to propel the body forward, whereas the non-dominant lower limb provides more support function [145]. The laterality has been found to produce gait asymmetries, which increase fall risk when the non-dominant leg was perturbed [127]. Thereby, the laterality may influence the reactions adopted to both standing [146] and walking [126] corrective reactions towards perturbations. Martelli *et al.* [126] observed an asymmetric interlimb coordination behaviour, which was depicted by the different coupled body segments to perform the balance recovery, concerning the side in which the perturbation was delivered. According to the above mentioned, the non-dominant leg is more used to and prepared to provide the body support function in comparison with the dominant leg. Therefore, in the presence of a slip perturbation during walking, it seems more appropriate to provide the assistive actuation to the dominant leg, considering that the leading leg was selected as the actuation leg. In this regard, the danger associated with the slip is lessened compared to the supply of the assistive actuation to the non-dominant leg as the leading leg, since in this scenario the body support would have to rely on the less prepared dominant leg. Therefore, the strategy will hereafter consider the dominant leg as the perturbed limb and thus the actuation leg. Hence, as a preliminary approach, the actuation strategy herein conceived only considered slips delivered to the dominant leg.

4.2.2. Which lower limb joint has a more determinant role to counteract slip-induced LOBs?

Sawers *et al.* [94] found that during slip trials, subjects who fell exhibited a delayed knee muscle activity onset time in the leading leg, when compared with subjects that recovered. These findings suggested that the capability to timely coordinate muscle activity around the knee may play a crucial role in avoiding slip-induced falls. Sawers & Bhatt [93] also showed that participants who recovered from slips had increased diversity and complexity of neuromuscular control, which is grounded on the coordination of the knee muscle activity in the perturbed and unperturbed legs. In fact, the overall muscle strength among adults can be depicted by the knee muscle strength [147]. Additionally, the crucial function of knee joints in arresting slip-induced falls has been empirically [9] and analytically [142] proven. These evidences led Ding *et al.* [82], to build predictive models that calculate the probability of falling based on the flexor and extensor knee joint strength (joint torque in isometric condition) and computed optimal threshold knee strength values to classify fallers and non-fallers for both knee extensor and flexor torques.

Additionally, Cham & Redfern [9] found that increased knee flexion and hip extensor moments were the corrective reactions adopted by the leading leg in order to recover from a slip. In fact, the knee and hip moments in slip trials differed from dry trials, which depicts their crucial role on the recovery biomechanics during slip events. Conversely, this difference was not observed in the ankle joint as it was found to act as a passive joint with no net moment during the recovery attempts in slip trials.

In addition, Liu & Lockhart [148] showed that the major actuators for balance recovery following a slip perturbation were the ankle and the knee. The larger moments actively produced by these joints revealed to be crucial in controlling and correcting the sagittal plane motion perturbation. Conversely, the hip joint function was to increase its frontal joint moment to passively maintain and stabilise the upright upper body posture.

Furthermore, Moyer *et al.* [137] showed that the corrective response produced by the hip of both leading and trailing legs did not scale with slip severity. Nevertheless, the knee response of both legs was modulated according to the slip severity which shows that the knee joint has a more versatile role in counteracting slip-induced LOBs since it can adapt its response concerning the severity of the slip. In addition, the authors also found that the corrective moments generated by the ankle joint were reduced in severe slips when compared to the knee and hip moments.

Moreover, Beschorner & Cham [136] examined the association between the heel acceleration, which is an important fall risk factor according to slip biomechanics [70], in the motion direction at the heel strike from the leading foot with fall risk and studied the main joint torque contributors to heel acceleration. In fact, this study revealed that subjects who recovered from a slip contacted the floor with a significantly greater heel deceleration in comparison with subjects who fell. Despite the ankle, knee and hip strongly correlate with the heel deceleration at the heel strike with increasing plantar flexion, flexion and extension moments, respectively, 76% of the heel acceleration variability was explained by the knee torque alone compared to the 38% from the ankle joint and the 56% from the hip joint. Furthermore, the combined contribution of any 2 or all 3 joint torques explained heel acceleration variability no more than 1%, i.e., 77%, above the knee torque contribution alone. Hence, since the heel acceleration at the heel strike, is mostly controlled by the moment exerted at the knee joint from the leading leg, the actuation on the knee joint will provide control on this important factor in order to reduce the likelihood of slip-induced falls. As such, walking with an increased knee flexion at the heel strike results in an increased heel deceleration and therefore reduce the risk of slipping.

Considering the above mentioned, the knee appears to be the major lower limb joint to counteract slip-induced LOBs. Hence, the fall prevention strategy conceptualised in this dissertation will highlight the knee joint as the actuation joint towards slip fall prevention.

4.2.3. Which should be the joint moment characteristics applied towards the actuation joint?

According to the decision taken towards the actuation leg and actuation joint, the next concern resides on the joint moment that should be applied in order to prevent slip-induced falls. As previously mentioned, literature studies have underlined the importance of the knee flexion response in order to act against slips at the heel strike. In fact, the primary response to counteract slip-induced LOBs includes the increase of the knee flexion moment, which magnitude is related to the slip severity [9,104,137]. Upon a slip, this joint moment increase allows to retard the sliding motion of the slipping foot and reduce its anterior displacement to bring it closer to the COM. As such, according to literature evidence, the torque exerted to flex the knee allows to control important variables for slip-induced fall prevention, namely the heel acceleration [136] and the shank-to-ground angle, i.e., the angle formed by the shank segment relative to the ground [99].

As mentioned above, the heel acceleration in the motion direction at heel strike is considered a crucial predictor of slip occurrence [70,136]. In fact, experimental studies have considered heel kinematic metrics to quantify the severity of slips [137,148]. Beschorner *et al.* [136] concluded that the heel acceleration at the heel strike was mainly determined by the torque exerted by the knee from the leading leg with 76% of the heel acceleration variability being explained by the knee torque alone.

Additionally, Wang *et al.* [99] found that the shank-to-ground angle, in the sagittal plane of motion, from the leading leg was associated with the forward displacement of the BOS induced by slips and was the most crucial determinant towards LOB prevention. The authors claimed that, upon the heel strike on a slippery surface, if the shank-to-ground angle was above 90°, i.e., the ankle was anterior to knee, an external knee extensor moment would be exerted on the shank due to gravity. This additional moment would cause the propulsion of the leading foot forward, which would increase the likelihood of a LOB. Conversely, if the angle is below 90°, i.e., the ankle was posterior to knee, an external knee flexor moment would be added to the shank due to gravity, which would retard the forward propulsion of the leading foot, reducing the LOB likelihood.

Therefore, the heel acceleration and the shank-to-ground angle can be decreased in the presence of slip perturbations by properly controlling the flexion moment of the leading leg's knee. As such, the flexion of the leading leg's knee arises as an important action to counteract slip-induced LOBs. It is necessary to consider that despite high fall risk subjects are generally not agile and strong enough to avoid falling from slip-induced LOBs, they are still capable of producing some actions to counteract these gait perturbations [64]. As such, the torque values exerted from the assistive device must be context-dependent by considering the reactive torque produced by the subject upon the gait perturbation to compute the additional torque needed to successfully recover from the slip-induced LOB. Hence, only a complementary 'delta' torque would be applied on the actuation joint. In this regard, the assistive robotic system would only assist as needed and when needed the subject, which promotes a symbiotic interaction between the human and the robotic system [64].

In order to provide the assistive torque needed, an orthotic system would be worn on the knee. Previous research regarding human knee reflexes, has shown that it is safe to provide short and rapid knee torque assistance during gait, which supports the use of the knee orthosis to provide assistive torque to the knee [149].

4.2.4. Assistive device

A knee orthosis was considered as the assistive device for the slip-related fall prevention strategy conceived. A Powered Knee Orthosis (PKO) is integrated in the SmartOs system, which was developed by a research team in BiRD Lab. SmartOs is a smart and modular wearable active lower limb orthotic system that provides repetitive and user-oriented gait training in impaired gait while assessing human motor condition using kinematic and muscular gait metrics. Currently, SmartOs's framework integrates 2 active orthoses, the ankle and knee right-side modules of the lower-limb H2-exoskeleton (Technaid S.L., Spain).

The PKO assists gait in the sagittal plane of motion for gait speed between 0.5 and 1.6 km/h. It also comprises the following embedded sensors: i) an angle position sensor, which consists of a precision potentiometer with a resolution of 0.5°; ii) a user-PKO interaction torque sensor comprised by strain gauges (4 strain gauges connected in a full Wheatstone bridge) with a resolution of 1 Nm; and iii) a hall effect sensor, which measures the motor's angular speed (rpm), current and torque.

The PKO's actuation system comprises an electrical actuator (flat brushless DC motor EC60-100 W, Maxon) coupled to a gearbox (CSD20-160-2A strain wave gear, Harmonic Drive), with a ratio of 160:1, which provides an average torque of 35 Nm and peak torques of 180 Nm. The PKO's mechanical structure is made of type 7005 aluminium and stainless steel and incorporates a 4-strap system with 2 lower straps on the shank and 2 upper straps on the tight, as depicted in Figure 11. More details on the PKO can be observed in [150]. Considering the herein conceived fall prevention strategy, the PKO will assist subjects with an assistive torque, whenever a slip-like perturbation is detected.

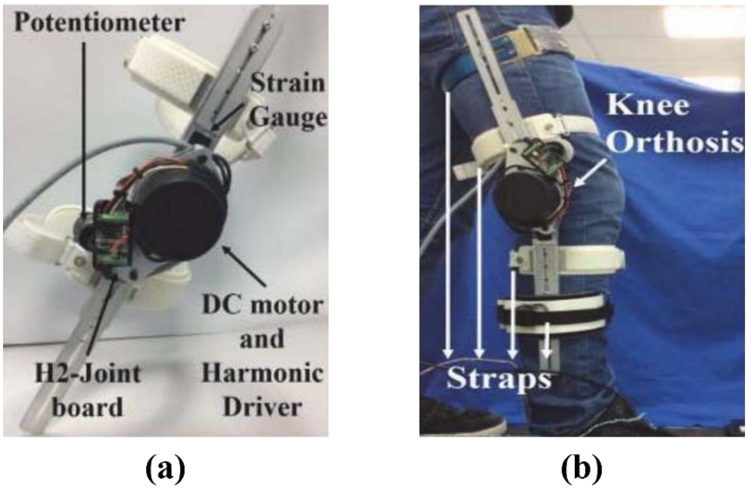

Figure 11. PKO device. (a) Device's elements. (b) Mounted in one subject. The images were extracted from study [150].

4.2.5. Additional Actuation Requirements

The actuation stage of the fall prevention strategy must fulfil some requirements related to the assistive system's operation and to the interaction between the subject and the system. Previous literature studies proposed and attempted to fulfil some requirements, which the fall prevention system should satisfy. The fall prevention system requirements found to be the most adopted were: i) easy customisation between different users [64]; ii) assisting when needed behaviour [64,151]; iii) no (or very limited) disturbance to the subjects, which can be depicted by: a) lightweight and comfortable to wear during walking [64,65,135]; b) compact design [65]; c) mechanical compliance between the subject and the exoskeleton [151]; and d) position heavy parts of the device away from the actuation joint [65,135,151]; iv) high torque development in a short time [65,135]; and v) continuously adapt to the mechanical demands of subject's motion and intentions [151]. The fulfilment of these demands allows the system to ensure a natural gait under no-assistance circumstances and fast assistive torque supply to counteract the LOB events in assistance conditions. In addition, in the case of the fall prevention strategy herein conceived, the actuation of the assistive system must be completed under the actuation time period further defined (100 ms).

4.3. Detection

The timely and successful detection of slip-induced LOBs requires a comprehensive selection of the perturbation detection algorithm and the motion variables which it will monitor. Figure 12 presents the characteristics of the detection strategy conceived. Candidate motion variables were selected from literature studies. Then, these variables underwent through objective criteria to ensure that the final monitoring variables selected highlight visible changes upon a slip without requiring costly computation. A slip-like perturbation protocol (described in Chapter 5) was designed and conducted to collect data from the selected monitoring variables, which were further used to test the perturbation detection algorithm. The proposed detection algorithm presents: i) a CPG controller, which monitors and predicts the selected variables' signals; and ii) a threshold-based algorithm that monitors the prediction error signal to detect the slip perturbations. A perturbation was detected whenever the error signal surpassed a threshold value.

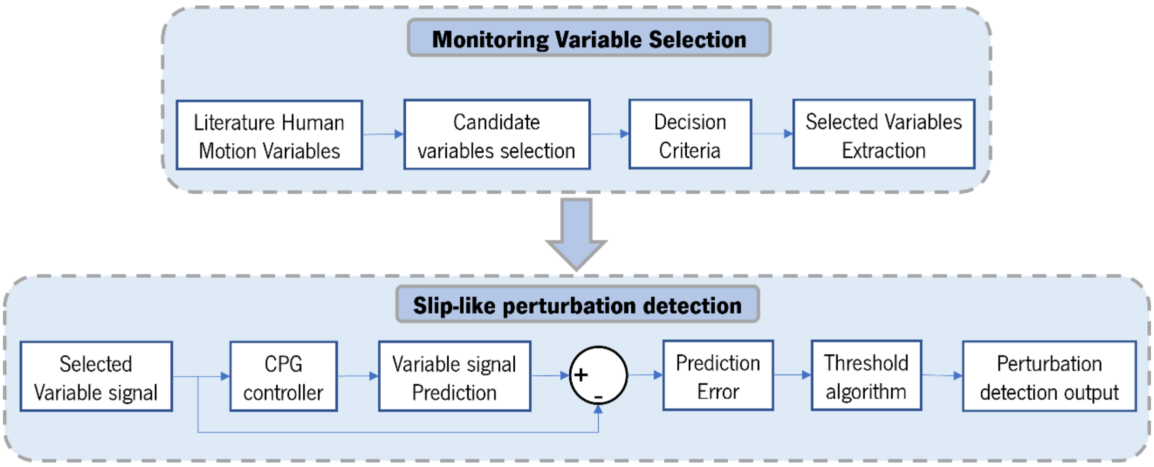

Figure 12. Detection strategy characteristics.

4.3.1. Selection of monitoring variables

Literature studies highlight several motion variables to assess the human biomechanical reactions to slip perturbations. Therefore, there is the need to comprehensively identify the most suitable motion variables, which the CPG algorithm will monitor, towards the gait perturbation detection. The variable selection process adopted is hereafter described.

4.3.1.1. Candidate variables

Concerning the biomechanics of the slip event, some of the important variables previously highlighted may potentially be relevant towards the detection of slip-induced LOBs. The human motion variable selection herein developed only included kinematic variables, considering that the slip-related fall prevention strategies analysed [64,65,135], as well as the majority of literature studies that address the human biomechanical responses to slip events [9,137] only considered the study of kinematic parameters.

Beyond the evident influence the slip perturbation elicits on the perturbed leg's motion, the unperturbed leg kinematics may also be promptly altered upon a slip, considering the interlimb coordination observed during the human reactive responses [137]. Therefore, the variables selected towards the detection of slip-induced LOBs were analysed for both the perturbed and unperturbed legs. This allowed to understand the alterations induced by slips to the kinematics of both legs and enable the identification of which data from which leg provides a more effective detection of perturbation occurrence.

From the previously reviewed literature, the **heel acceleration**, the **shank-to-ground angle**, as well as the **hip angle** were highlighted as important kinematic variables. Additionally, other variables were further included to widen the amount of potentially relevant kinematic parameters and perform a more comprehensive selection. As such, the variables of **knee angle** and the **shank angular velocity** were also considered. Considering the critical contribution that the knee joint presents to the slip recovery dynamics, the study of the knee angle may become pertinent towards the slip perturbation detection [9,137,148]. In addition, the external knee torque applied in the fall prevention system presented by Trkov *et al.* [65] is directly associated with the linear feedback between the actual and desired knee angle values. Concerning the shank angular velocity variable, Aprigliano *et al.* [11] suggested that the perturbed shank angle could be potentially used to detect slip perturbations, since it had a good performance in detecting trip perturbations. As such, alterations in the shank angular velocity, which is a variable widely used for gait analysis and event detection [152–154], may also be relevant to detect slip-induced LOBs.

4.3.1.2. Criteria for variable selection

An objective selection of the most relevant monitoring variables was attempted with the criteria defined. As such, most of the criteria were aimed at describing technical aspects of the variables including: i) the simplicity of the data processing needed to obtain the variable in real-time from sensor data (Criterion 1); ii) the ability of the variable's signal to effectively perform gait event detection, based on the scientific literature (Criterion 2); iii) the number of sensors needed to compute the variable, the simplicity of the sensor placement, and if additional instrumentation beyond the assistive device is needed to obtain the variable (Criterion 3); and iv) bibliography evidence of the use of the variable or its respective body segment (e.g. knee) to study human biomechanical reactions to slips and/or to detect these perturbations (Criterion 4). In addition, some videos recorded during the perturbation trials from the slip-like perturbation protocol were visually inspected in order to perceive visual alterations of the human body segments upon a slip-like perturbation. This allowed to obtain visual cues about the alterations provoked by the gait perturbations on the variable signal's time evolution (Criterion 5). Moreover, it was also included an innovation criterion in order to account to whether the variable was previously addressed in a fall prevention strategy in the scientific literature, to the best of the author's knowledge (Criterion 6).

Afterwards, these criteria were sorted according to their priority. As such, since the objective is to ensure the functional performance of the slip-induced LOB detection rather than to produce an innovative approach, priorities were given to each criterion as shown in Table 9.

In this regard, criterion 4, which relates to the bibliography support, was chosen as the most important criteria, since it underlines the direct influence a slip has on a variable, which ensures its feasibility in the detection process.

Criteria 1 and 2 were considered equally important, since both of these criteria play a key role towards the functional detection of the slip-induced LOBs. Criterion 1 regards to the real-time computation of the variable, which has a critical role regarding the computational resource demands of the system and thus on the slip detection latency. Concerning criterion 2, if the variable is suitable for performing gait event detection, it is possible to acknowledge whether the LOB detected took place around the heel strike event, which would increase the reliability of the slip detection.

Equal priority was also given to criteria 5 and 6, considering that both introduce a somewhat subjective analysis. Criterion 5 depicts the video-based evidence (based on the videos recorded during the experimental protocol trials) that the variable’s characteristics are altered upon a slip-like perturbation. This criterion was chosen given that it could provide additional visual information beyond the bibliography consulted. In addition, criterion 6 highlights the innovative characteristics of the variable regarding the ones used in the literature to perform slip detection. The use of innovative variables can expand the knowledge on the human corrective behaviours upon slip events and potentially lead to an accurate detection of slip-induced LOBs.

Lastly, criterion 3 mainly represents the number of sensors needed to obtain a variable. Thereby, it benefits the variables whose computation require the least number of wearable sensors. This criterion was considered the least important, considering that the conceptualised fall prevention strategy gave more importance to the functionality of the system rather than the constraints associated to the number of sensors.

Table 9 represents the priorities and weights ascribed to all the criteria. Relative priority was assigned to each criterion, such that the higher the number, the least relevant is the criterion. As such, from the most to least relevant, criteria were ordered as: 4, 2, 1, 5, 6, 3. Then, weights were attributed to each criterion according to their relative priority in order to depict their weighted contribution towards the decision process. The higher was the relative priority, the higher was the weight assigned to the criterion. The weight attribution to each criterion and the further variable selection process were determined by all the investigation team members.

Table 9. Criteria priority established

Criteria	Relative Priority	Weight attributed
1. Real-time computation	2	1.75
2. Gait event detection	2	1.75
3. Subject instrumentation	4	1
4. Bibliography support	1	2
5. Video-based evidence	3	1.5
6. Innovation	3	1.5

4.3.1.3. Variable Decision Process

Thus, according to the above mentioned, the Decision Table (Table 10) was built. For each criterion, a classification between 1 and 3 was attributed. A classification of 1 was assigned when the variable minimally respected the criterion, while a classification of 3 was attributed if the variable fully met the criterion. Then, the final score of each variable resulted from the weighted sum of the scores attributed to each criterion (concerning the weights assigned in Table 9). In light of the fall prevention strategy defined, it is noteworthy that these kinematic variables are either obtained from wearable IMUs or from sensors coupled to the knee orthosis device.

Table 10. Decision table established

Criteria \ Variable	Knee angle	Heel acceleration	Shank-to-ground angle	Shank angular velocity	Hip angle
1. Real-time computation	3(*)	3	1	2	1
2. Gait event detection	2	1	2	3	2
3. Subject instrumentation	3	1	3	3	3
4. Bibliography support	3	3	2	2	3
5. Video-based evidence	2	2	2	2	3
6. Innovation	3	3	3	3	1
Total score	25.25	21.5	19.75	23.25	20.25

(*) considering the orthosis' encoder will provide the Knee angle information directly.

According to the Decision Table 10, the knee angle and the shank angular velocity appear to be the most suitable variables in order to perform the detection of slip-induced LOBs, in light of the decision criteria applied.

Despite the importance given to the heel acceleration towards the slip biomechanics [136], two main factors contributed to the disregard of this variable: i) the difficulty of properly placing and using wearable sensors attached to heel; and ii) the impact of the foot on the floor introduces a substantial amount of noise in the heel acceleration signal, which hinders its use and its ability to detect gait events. In fact, Beschorner *et al.* [136] collected the heel acceleration signals using reflexive marker recordings from an Optical MoCap, which solved the noise issue. However, that solution presupposes a non-wearable monitor system, which goes against the fall prevention strategy premise.

The hip angle and the shank-to-ground angle variables were also disregarded mainly due the need to integrate the respective angular velocity signal in real time to obtain the angle signal. The integration process constraints would increase the time needed to obtain the variable, the computational costs of the system, and introduce drift errors, which would have to be properly compensated [155]. In addition, since the hip angle has already been analysed to detect slip-induced LOBs, the total score assigned to this variable was further reduced [13,64].

Considering the fall prevention strategy conceived, it is noteworthy that the knee angle variable would be provided by the encoder from the knee orthosis. As such, the extraction of this variable would not need any integration and therefore would not bring any drift problems. Accordingly, the detection of slip-induced LOBs proceeded considering the monitoring of the **knee angle** and the **shank angular velocity** variables.

4.3.2. Central Pattern Generators controllers

Human locomotion as well as their crucial vegetative functions are known to be repetitive and cyclic tasks. Despite the important role played by neuromuscular dynamics and sensory feedback in modulating these rhythmic functions, the foundation of the cyclic activity patterns generation is attributed to the functional activity of the neuronal circuits located in the spinal cord, i.e., Central Pattern Generators or CPGs [14,15]. The term "Central" implies that the peripheral nervous system and its sensory feedback are not recruited towards the rhythm generation [156]. Thereby, the implementation of biomimetic or biological-inspired CPG controller systems to monitor and control variables of human locomotion becomes attractive, since such motion is very likely controlled by spinal oscillators, i.e., biological CPGs [16,17]. The artificial CPG is thereby presumed to synchronise along with the biological one, which plays a fundamental role towards rhythmic movement assistance [16,157]. From the rehabilitation point of view, the artificial CPG would feedback an assistive torque to the controlled joint, whenever necessary, that would allow to compensate the deficits of biological CPGs, for instance due to a neural injury, towards an healthy locomotion [16].

Furthermore, a system capable of accurately and real-time monitor the main rhythmic features of steady human locomotion fosters the detection of sudden and unexpected gait perturbations, whereupon these rhythmic features are momentarily lost [13]. In this regard, CPG controllers based on nonlinear Adaptive Frequency Oscillators (AFO) arise as a reliable solution to assist this detection. An AFO is a mathematical tool capable of synchronising its output to a frequency component of a periodic or quasi-periodic input signal, while learning its relevant characteristics, such as amplitude and phase. In turn, a network of AFOs, i.e., a CPG controller, can continuously synchronise with and provide an estimate of a periodic or quasi-periodic input signal [13,157,158]. The occurrence of an unexpected perturbation during steady walking would introduce abnormal variations to the input signal and lead the AFOs to seek for new signal patterns associated with distinct frequencies. This would quickly deviate the input signal from the trajectory expected by the CPG, i.e., the predicted or estimated signal, which would allow to early and effectively detect an unexpected gait perturbation [13]. In fact, this controller architecture has been previously employed to detect gait perturbations due to its interesting properties [13,64]. From the fall prevention point of view, the artificial CPG would trigger a robotic assistive system to provide a timely assistive torque at the controlled joints to counteract the LOB and promote an efficient balance recovery, whenever a perturbation was detected [64]. Since the biped locomotion exhibited by humans consists of a periodic or quasi-periodic motor task, it can be thereby decomposed into the sum of periodic or quasi-periodic signals [159]. As such, a prior knowledge of the periodicity of human locomotion can be performed by making use of the ability of nonlinear oscillators to generate stable rhythmic patterns, i.e., limit cycle behaviour, which is useful for decomposing the respective signals into a sum of sinusoidal waves that can be learned by a network of oscillators [157,158].

The application of artificial CPG controllers, regardless of its rehabilitation or fall prevention purposes, allows for the contribution effort of both the therapeutic system and the patient to produce a stable locomotion and overcome gait perturbations. Hence, the parallel intervention of both artificial and biological CPGs may have an important key role on the stimulation of the human nervous system plasticity [160]. This cooperation could be especially beneficial for elderly people according to their increasingly reduced cognitive, physical and sensory status [1]. Also, robots based on CPG controllers stand out from traditional robots, as they are agile and more adaptable for real-world environments [161].

According to the model architecture presented in Righetti & Ijspeert [162], each CPG is modelled by a group of coupled nonlinear Hopf AFOs. Generally, a fixed parameter controls an oscillator intrinsic frequency. Nevertheless, the Hopf oscillators used by these authors are modified in order to be able to constantly adapt their intrinsic frequency to one main frequency component, i.e., frequencies with more power in the frequency spectrum, from a periodic or quasi-periodic input signal, as long as the CPG is receiving the input signal. Righetti *et al.* [163] described this modification of the Hopf AFOs. The CPG controller must contain as many AFOs as the number of main frequencies components needed to successfully describe the input signal, i.e., the learning signal. If the number of oscillators is insufficient to account for all the relevant frequency components of the input signal, the oscillator network will only learn and adapt to the frequency components with more power [162]. Thereby, the learned signal provided at the CPG output will be a relatively rough approximation to the input signal. Contrariwise, according to Righetti *et al.* [162], if the number of oscillators is higher than the number of frequency components to learn from the input signal, two cases can happen: i) either some oscillators will not converge towards any frequency and therefore they will have a null contribution to the learned signal; or ii) more than a single oscillator will code the same frequency component and the sum of their corresponding amplitudes will match the amplitude of the respective frequency component. During the AFO's frequency adaptation, the amplitude of the correspondent frequency component, α, is also learned as well as the phase relationship between the different AFOs, ϕ, within the CPG to ensure their phase coupling. This coupling is also important to guarantee the phase synchronisation between different CPGs, in cases where more than 1 CPG is considered, such as for distributed implementation applications [156,160]. This phase coupling ensures that, upon the input signal removal, the rhythmic pattern is still maintained at the CPG's output. The CPG learning process does not require any pre-processing of the input signal or any optimisation algorithms or external regression, since the learning process is fully embedded into the dynamical system [162].

Ijspeert *et al.* [160], Tropea *et al.* [13] and Santos *et al.* [156] pointed out several interesting characteristics that make CPG controllers suitable for the monitoring of human locomotion concerning other alternative methods: i) the CPG controllers can generate stable limit cycles, which are robust against perturbations. More specifically, if the rhythmic pattern is perturbed, the controller promptly returns to its previous cyclic behaviour; ii) different CPGs can be used to individually control different segments or modules within the same system. The different CPGs can be coupled together through phase relationship. This makes CPG model architecture well appropriate for distributed implementation [156]; iii) CPG controllers have few control parameters, which allow to modulate the locomotion, according to changes in direction and speed. This property allows CPGs to properly perform online trajectory generation with smooth modulations even when there is an abrupt change of the control parameters; iv) CPGs allow for the mutual entrainment between the mechanical system and the CPG, since these controllers are ideally appropriate for the integration of sensory feedback; v) CPG controllers do not require any training before being implemented, which happens for other algorithms that require a prior training stage, since the algorithm's learning process is included in the network dynamics; vi) CPG controllers do not have high computational costs as it not required any demanding signal or algorithmic processing; and vii) once the frequency bandwidth of the controlled signals is known, the CPG can be tuned to only monitor these signals (all the higher frequency components can be associated to LOB reactions). Hence, unlike training-based algorithms, the tuning of the CPG does not require the use of signals recorded during complex unexpected gait perturbation protocols, as only steady-state walking parameters are used to tune the algorithm.

4.3.2.1. Hopf AFO

The traditional Hopf oscillator dynamics is represented by the differential equations below. The oscillator state variables are depicted by (x, y), and the oscillator's intrinsic frequency is defined by ω and r = $\sqrt{x^2 + y^2}$. In the traditional Hopf oscillator, ω is constant and always equal to its initial value. The variable γ dictates the convergence speed to the limit cycle and μ, which is positive, controls the steady-state amplitude of the oscillations. As previously mentioned, these nonlinear oscillators exhibit limit cycle behaviour, i.e., they produce closed loop trajectories in the state space $x - y$, limit cycles, which specify that the system is periodic in time. During a stable steady-state locomotion, the state variables oscillate rhythmically throughout time [164].

$$\dot{x} = \gamma(\mu - r^2)x - \omega y$$

$$\dot{y} = \gamma(\mu - r^2)y + \omega x$$

As previously mentioned, Righetti *et al.* [162,163] modified the traditional Hopf oscillator, creating the Hopf AFO based on the following differential equations.

$$\dot{x} = \gamma(\mu - r^2)x - \omega y + \varepsilon \mathrm{F}(\mathrm{t})$$

$$\dot{y} = \gamma(\mu - r^2)y + \omega x$$

$$\dot{\omega} = -\varepsilon \mathrm{F}(\mathrm{t})\frac{y}{r}$$

The variable $F(t)$ corresponds to the periodic input signal. The oscillator intrinsic frequency, ω, will adapt to one main frequency component from $F(t)$, as opposed to the fixed ω from the traditional Hopf oscillator. Nevertheless, this adaptation depends on the ω attributed to the oscillator as the initial intrinsic frequency. The latter equation represents the learning rule, which allows ω to converge into the $F(t)$ frequency, if the signal only has one frequency component, or to one of the $F(t)$ frequencies if the signal has more than one frequency component. In the multi-frequency case, the oscillator often converges towards the main frequency component of $F(t)$ that is closer to the initial ω. The higher is the intensity, i.e., amplitude in the frequency spectrum, of a frequency component from the input signal and the less is its distance to an AFO intrinsic frequency, the higher is the attraction of that frequency component to the oscillator [163]. Essentially, CPG controllers generate a dynamic Fourier series representation of the input signal, with each oscillator encoding a single main frequency component of the input signal [162]. The oscillator is coupled with the input signal with a coupling strength of ε. When ε is null, the system will not learn from the input signal and will oscillate at a frequency of ω rad/s. Thereby, the modified Hopf oscillator equations will essentially match the ones from the traditional Hopf oscillator. However, when ε is positive, the oscillator will be coupled to $F(t)$ with a positive coupling strength, which allows for its adaptive frequency adaptation [163]. The variable ε controls the convergence rate, considering that the learning process is faster if the ε is higher. Nevertheless, a faster learning promotes a higher error of adaptation from the oscillator [163].

4.3.2.2. Coupling of multiple Hopf AFOs

Within the CPG, the first oscillator, i.e., oscillator 0, provides a phase reference measure for the remaining AFOs from the oscillator network. As such, the i^{th} AFO has a scaled phase difference of ϕ from the oscillator 0. Oscillator 0 transmits the respective phase difference to each oscillator by sending them its state variables. This allows for all the AFOs within the same CPG to be phase coupled. The use of a coupled oscillator architecture allows for the CPG to keep the phase relations between the oscillators and to encode the periodic signal within the system as a stable limit cycle, even when the input signal is removed from the system or in the presence of other temporary perturbations. In order to account for this coupling, a single generic CPG formed by N AFOs is characterised by the following equations, where the i^{th} AFO is represented by x_i, $y_i$and ω_i.

$$\dot{x}_i = \gamma(\mu - r_i^2)x_i - \omega_i y_i + \varepsilon F(t) + \tau \sin(\theta_i - \phi_i)$$

$$\dot{y}_i = \gamma(\mu - r_i^2)y_i + \omega_i x_i$$

$$\dot{\omega}_i = -\varepsilon F(t)\frac{y_i}{r_i}$$

$$\dot{\alpha}_i = \eta x_i F(t)$$

$$\dot{\phi}_i = \sin\left(\frac{\omega_i}{\omega_0}\theta_0 - \theta_i - \phi_i\right)$$

$$\theta_i = \operatorname{sgn}(x_i)\cos^{-1}\left(-\frac{y_i}{r_i}\right)$$

$$i \in 0, \dots, N$$

While ε determines the coupling strength between each AFO and the input signal, τ determines the coupling strength between each AFO and the oscillator 0 to maintain the correct phase difference between oscillators. The coefficient η corresponds to a learning constant. These 3 variables control the learning rate of the oscillator [163]. The phase difference between oscillator i and oscillator 0, ϕ_i, converges to the difference between θ_0, scaled at frequency ω_i, and θ_i, which resemble the instantaneous phase of oscillator 0 and i, respectively.

Considering the operating basis of the above stated equation, the generic CPG network is depicted in Figure 13. The signal already learned by the oscillator network, *learnedS*, is computed as the sum of all outputs from all the oscillators, x, weighted by their respective amplitude, α, and accounting for the learned phase relations among them, ϕ. Then, *learnedS* is subtracted to the signal intended to be learned, *learningS*, in the negative feedback loop, which results in the learning signal, $F(t)$. Afterwards, $F(t)$ is provided to all oscillators to proceed with their frequency adaptation to $F(t)$. As soon as an AFO has completely adapted to a main frequency from the signal to be learned, *learningS*, that frequency component is generated by the correspondent AFO at the CPG output, *learnedS*, and is thus removed in the negative feedback loop. In addition, the evolution of the amplitude of each oscillator, α_i, is firmly related to the evolution of its frequency, ω_i. As ω_i is converging towards one main frequency component of $F(t)$, α_i increases. When the oscillator completely converges to the targeted frequency, this frequency component is removed from $F(t)$ in the negative feedback loop and α_i stagnates. As such, the signal $F(t)$ will only contain the frequency components from *learningS* that were still not learned by the oscillator network. The learned frequencies will stay encoded in the respective oscillators as stable limit cycles. Therefore, the negative feedback loop allows for the dynamic learning of the oscillator network.

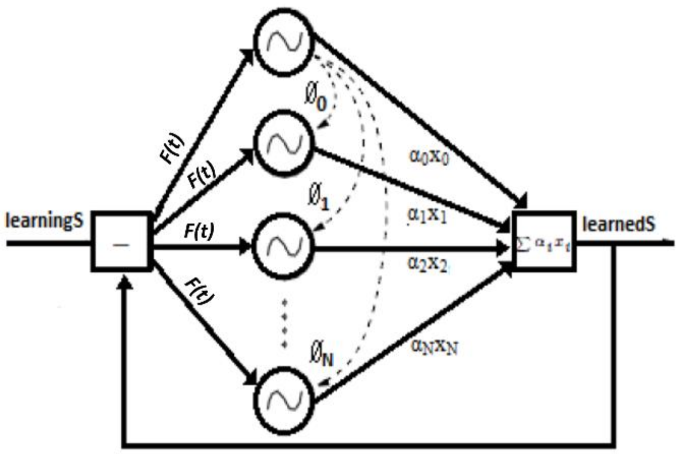

Figure 13. Generic CPG network of modified Hopf oscillators [158,162].

In cases where more than one CPG is used, the coupling between different CPGs is achieved by the transmission of the state variables from the oscillator 0 from the designated first CPG to the oscillators 0 from the other CPGs. Thereby, the phase differences among the different CPGs are ensured. Although the work performed in this dissertation only considers the use of a single CPG, more details from the use of a multiple CPG network can be found in [156].

4.3.2.3. Multi-frequency periodic input learning

Subsequently, one example of the learning dynamics of the CPG system is given, which depicts the adaptation behaviour of the CPG system towards a multi-frequency periodic input signal. Following the example used by Righetti *et al.* [158], the CPG controller will receive as input the multi-frequency signal described by $F(t) = 0.8sin(15t) + cos(30t) - 1.4sin(45t) - 0.5cos(60t)$. All the AFOs are configured with $\mu = 1$, $\gamma = 8$, $\varepsilon = 1$, $\tau = 0.03$ and $\eta = 0.5$. The initial frequencies were set to be uniformly distributed between 6 and 70 rad/s [158]. As such, $w_1(0) = 6\, rad/s$, $w_2(0) = 27\, rad/s$, $w_3(0) = 48\, rad/s$, and $w_4(0) = 70\, rad/s$. The initial amplitudes $\alpha(0)$ and phases $\phi(0)$ are set to 0. In addition, $r(0) = 1$. Considering that each AFO adapts to one main frequency component of the input signal and that the $F(t)$ signal spectrum is limited to 4 frequency components, the CPG system will be formed by 4 Hopf AFOs. All 4 AFOs are phase coupled.

The *Matlab Simulink* software was used to conduct simulations of the CPG learning of multi-frequency component signal. The learning process outcomes are depicted in the Figures below. Figure 15 depicts the frequency evolution of each of the oscillators' intrinsic frequencies. Figure 14 shows the evolution of the global CPG output in comparison with the input signal $F(t)$.

According to Figure 14, it is possible to acknowledge that each AFO within the CPG controller converged into one main frequency component of $F(t)$. As expected, each AFO's intrinsic frequency converged towards the closest frequency component of F(t). Once an AFO achieves this convergence and stabilises, its output amplitude becomes equivalent to the weighted amplitude of the input signal $F(t)$ relative to the converged frequency. Upon the convergence of all the AFOs, the input signal is completely learned by the CPG controller.

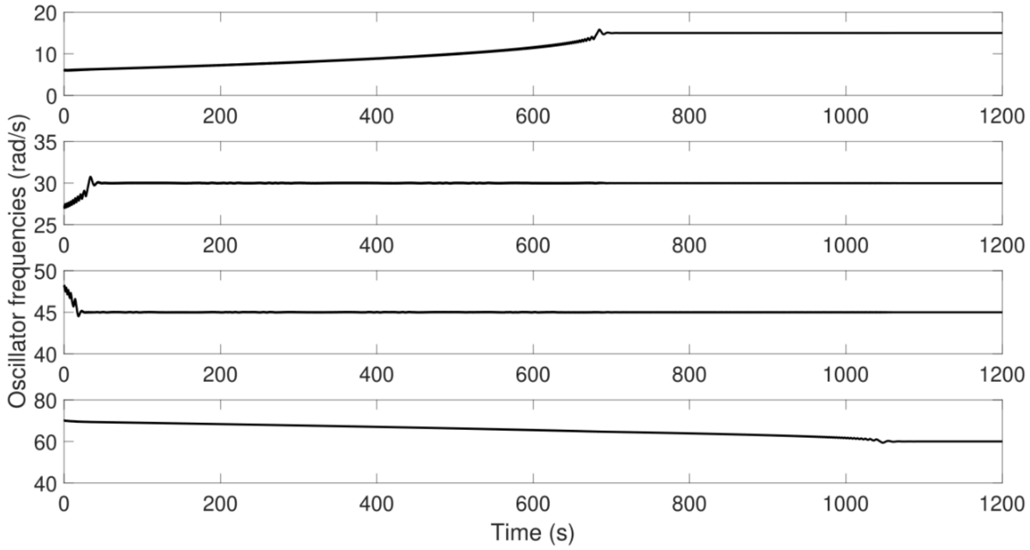

Figure 14. Simulation time course of the 4 oscillator frequencies. From top to bottom: $\omega 1$, $\omega 2$, $\omega 3$ and $\omega 4$.

Figure 15 depicts the CPG dynamic learning process throughout different stages. The top-left graphic presents the moment when the CPG started learning the input signal. For that reason, the error signal between the CPG output and $F(t)$ is very noticeable. At the time of the top-central graphic, some adaptation of CPG output signal towards the input signal has already been performed due to the convergence of some AFOs to the desired frequencies. Consequently, the error is reduced comparing to the start of the learning. On the top-right graphic, all the AFOs are already correctly phase-coupled, the CPG output matches the input signal, and the error produced between them converges to 0.

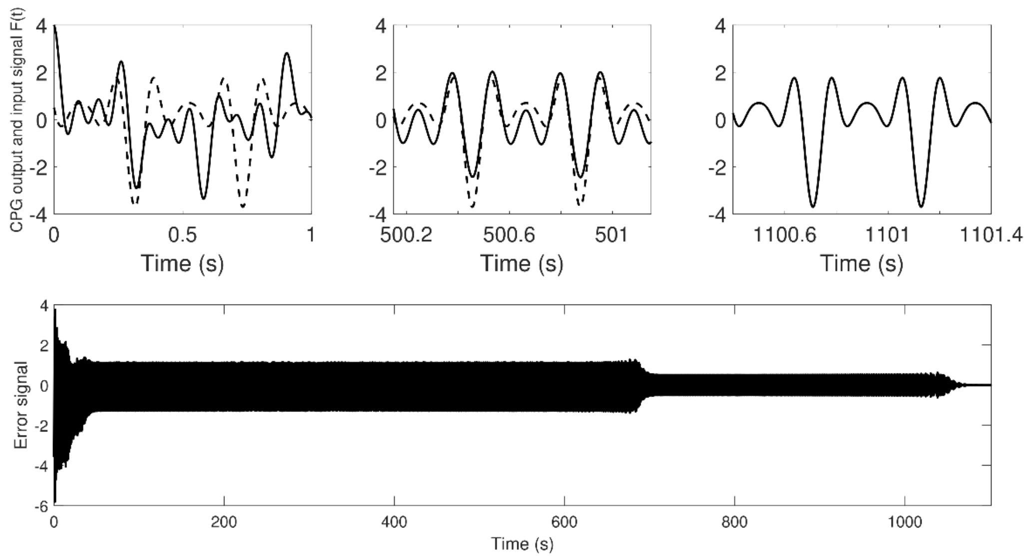

Figure 15. CPG learning dynamics simulation. Top: Simulation time course of the sum of the outputs from all the Hopf oscillators (solid line) in addition to the input signal (dashed line). The learning onset (left graphic), its middle (central graphic) and the total learning (right graphic) of the input signal F(t) are presented. Bottom: Simulation time course of the error between the CPG output and F(t).

As expected, the initial conditions applied to the oscillators will influence its adaptation towards a main frequency component of the input signal. This adaptation is as fast as the closer is the initial frequency parameter to one targeted frequency of the input signal. The knowledge of the frequency spectrum of the controlled signal becomes important in order to determine appropriate initial conditions and allow the prediction of the oscillators behaviour [156,163]. In the case where the nominal trajectory is not known, the frequency spectrum information of the controlled signal, which contains the corresponding amplitudes, is extracted by performing a static spectral analysis [156]. From the spectral analysis, the frequency components with more power or amplitude, i.e., the frequencies more important to describe the signal, are depicted and it is thus possible to use a limited number of frequencies from the controlled signal to manually reproduce it with a good approximation. Thereby, by considering only the frequencies of higher power, it is possible to verify the minimal number of oscillators necessary to generate a sufficiently good approximation between the learned and the controlled signals. This optimisation of the number of oscillators within the network avoids higher computational costs due to a broaden number of oscillators. In that sense, for each different input signal analysed, it should be performed its Fourier Frequency Decomposition to not only determine the initial frequencies of the oscillators, but also to determine the minimal number of main frequency components needed to properly describe the input signal. In order to identify these main frequencies, one has to examine the frequencies of the input signal that have the highest amplitude among the frequency spectrum [163]. This analysis will reduce the time taken by the CPG to properly adapt to the input signal.

4.3.3. Threshold-based algorithms

The gait perturbations were detected using threshold algorithms based on the work developed by Tropea *et al.* [13], as show in Figure 16. A simple threshold-based algorithm was proven effective and generalisable to detect slip-like perturbations based on the error produced between the actual kinematics and the kinematics predicted by a network of oscillators [13]. In the presence of a perturbation, the error signal promptly increases and surpasses the established threshold values, allowing to timely and effectively detect the postural disturbances. This timely detection would allow to promptly trigger a powered orthosis worn by the subject to provide mechanical assistance in order to mitigate the fall risk [13,64]. In this respect, it was studied the ability of a simple threshold algorithm and an adaptive threshold algorithm towards this detection. The performances obtained for both types of threshold algorithms are further compared.

For the simple threshold approach, which is depicted in Figure 16(a), it was firstly verified if the current sample, i, of the error signal was between the defined fixed threshold values. $T1$ and $T2$ represent the upper and lower threshold values, respectively. If the error value surpassed one of the thresholds, which depicts an abnormal situation, a warning was raised and a counter variable, c, was incremented. Otherwise, c was reseted. Secondly, it was verified if the number of consecutive warnings exceeded the number of acceptable warnings, r. The variable r was applied in order to provide a more consistent perturbation detection by minimising the number of false alarms detected, which could arise from individual samples that surpassed a threshold but were not perturbations. If c was lower than r, the algorithm proceeds towards the evaluation of the next sample, i.e., $i + 1$. Contrarily, a perturbation was detected by the algorithm if c was equal or greater than r. Further, in order to ascertain the correct detection of the perturbation, the detection time (DT) was calculated. DT was obtained as the time difference between the actual onset of the perturbation, given by $pert\_sample$, and the perturbation onset detected by the algorithm. The $time$ variable provided the timestamp information for each sample. If the perturbation was detected before its onset or was detected later than 1 second after its occurrence, the detection was considered a false alarm. However, if the perturbation was detected within the 1 second interval following its onset, the perturbation was considered successfully detected. This time period was selected as a reference, since previous research mentioned that falls occur in a maximum time of 1 second [64,139].

The adaptive threshold algorithm, which is shown in Figure 16(b), follows a similar method in comparison with the fixed threshold. However, unlike the fixed threshold approach, the adaptive threshold allowed to consider contextual information about previous samples in the definition of the threshold values. In this regard, the mean, μ, and standard deviation, σ of the m-sized window preceding the current sample i were obtained in order to compute the dynamic thresholds adapted to each sample. The thresholds were also calculated according to the coefficients a and b assigned to each subject in order to enhance the performance of the subject-specific perturbation detection. The coefficients a and b depict the influence that the standard deviation, σ, has on the calculation of the upper and lower thresholds, respectively. Once the thresholds were calculated, the principle of perturbation detection was similar to the fixed threshold methodology.

The threshold and window size parameters applied in these algorithms were determined for each subject and are described in Chapter 6. The variable r was assigned with the value 3 in order to only detect a perturbation if 3 or more samples consecutively surpass one of the threshold values. Since both threshold-based algorithms do not use information from future samples, these algorithms are considered to perform an online perturbation detection, which is adapted to the real-world settings.

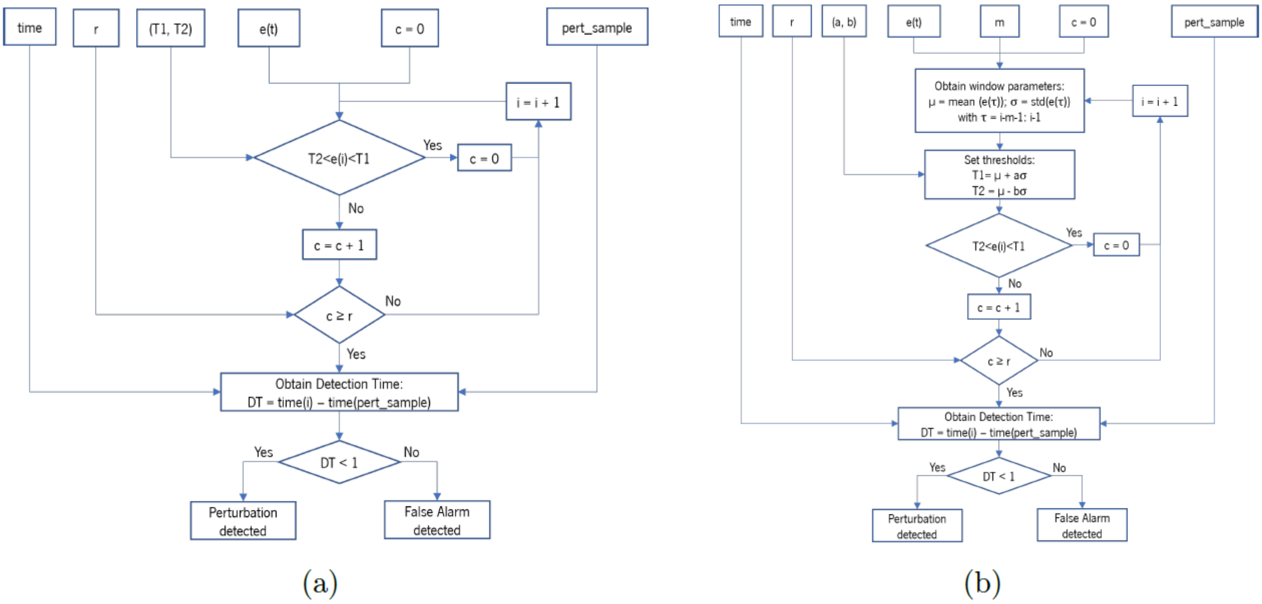

Figure 16. Perturbation detection algorithm based on (a) fixed threshold and (b) adaptive threshold.

4.3.4. Additional Detection Requirements

Despite few studies describe the detection of slip-induced LOBs [64], some requirements were defined for the detection stage of the fall prevention strategy in order to validate the perturbation detection performance: i) the detection accuracy of real perturbations must be above 75%; ii) the mean detection time (MDT) of the real perturbations must be inferior to the detection time further defined for the fall prevention strategy (360 ms); and iii) the number of false perturbations detected must be inferior to the number of correct perturbations detected, i.e., less than one false perturbation must be detected for each correct perturbation identified. Considering that this dissertation addresses a fall prevention strategy in its preliminary stage, the current goal of this work is to ascertain whether the perturbation detection algorithm can achieve an acceptable rather than an optimal performance. Hence, the fulfilment of the above defined requirements would prove an acceptable performance of the perturbation detection algorithm and pave the way for the future optimisation of the detection process.

4.4. Fall Prevention Strategy Timings

As previously mentioned, the trailing leg has a prominent role to counteract slip-induced LOBs. Upon a slip perturbation of sufficient intensity, a successful response is characterised by promptly interrupting the forward swing motion of the trailing limb after its lift-off, reverse its direction and land the trailing foot posteriorly, i.e., behind, to the leading foot to compensate for the backward LOB [137].

As such, the time taken by the subjects to reverse the trailing leg's swing motion direction may be related to the time needed to detect that a slip perturbation is happening. Martelli *et al.* [10] named this variable as the "Reverse time" (RT) and associated it with the time required by the subjects to select the most suitable biomechanical response. The spatial-temporal parameters of the backward swing motion in response to the slip were similar between the elderly and young age groups. However, these authors also observed that the elderly participants (0.36 ± 0.01 s) revealed a higher RT in comparison with the younger subjects (0.32 ± 0.01 s). The age-related modification of the periphery nervous system, which causes the reduction of the speed of sensory information processing, may be the foundation of this delayed reaction shown by the elderly and their consequent less efficient reactive response to the perturbations [10,165]. As such, according to the results presented and considering that the strategy is targeted to the elderly subjects, 360 ms was defined as the maximum time period needed to detect the perturbations. Since the objective of this strategy is to provide assistance to counteract the perturbation, the system is required to detect the occurrence of the perturbation before the subject, i.e., in a maximum mean time period of 360 ms after the perturbation onset [10]. This timely detection of the perturbation would allow to provide early and appropriate mechanical support to help subjects recover their balance before they are even aware that the perturbation is taking place.

Furthermore, it is also necessary to address the actuation time, i.e., the maximum time needed to complete the assistive actuation, from the instant of the perturbation detection. Martelli *et al.* [166] observed that the compensatory cycle induced by a slip perturbation, which ranged from the instant of the perturbation onset to the instant of the trailing foot's landing on the ground, lasted for 0.46 ± 0.07 s. Therefore, the time required for subjects to recover from a slip perturbation was defined as 460 ms. Since this duration already includes the mean time needed by the subjects to detect the perturbation occurrence, i.e., 360 ms [10], the actuation time was defined as the time period between the instant of subjects' perturbation detection and the instant of the trailing foot landing on the ground. Hence, the actuation time was determined as 100 ms long. Thus, the strategy herein conceived purposes to detect slip perturbations within 360 ms following the slip onset and complete the assistive actuation under 100 ms following the perturbation detection. Overall, the timings purposed suggest that the time duration between the slip initiation and the completion of the assistive torque supply must be under 460 ms.

Additionally, Lockhart [70] mentioned that dangerous slips that lead to falls are most expected to happen between 70 and 120 ms after the heel strike. Therefore, the detection and actuation times are applied after this time period. The fall prevention strategy timings defined are summarised in Figure 17.

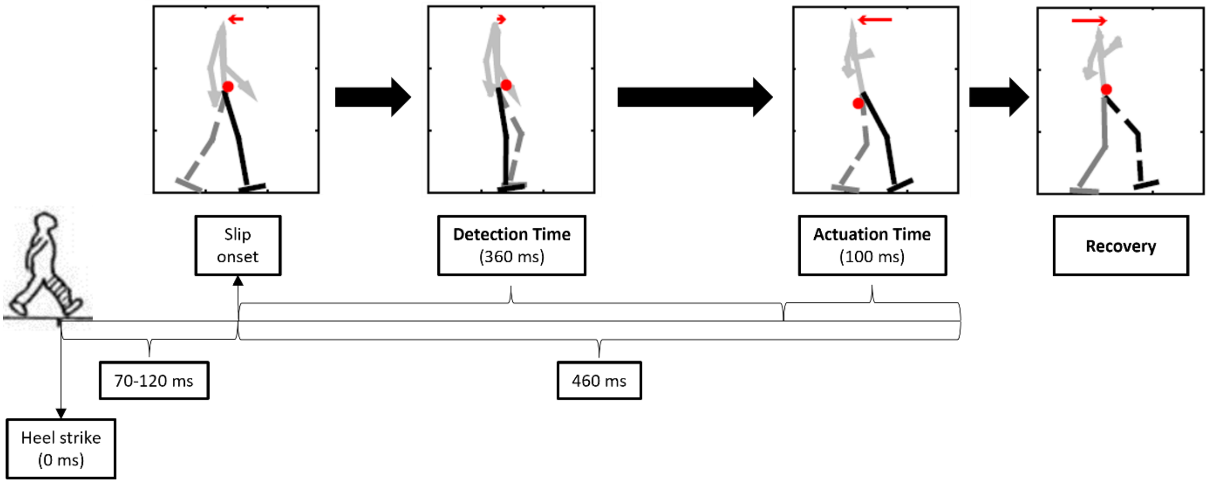

Figure 17. Proposed fall prevention strategy timings. The time durations are not to scale. The human stick diagrams were extracted from study [10]. The continuous and dashed line legs depict the perturbed and trailing legs, respectively. The red dot represents the extrapolated COM. The red arrows depict the backward Margin of Stability in the direction of motion (AP direction). It represents the difference between the extrapolated COM position and the position of the posterior boundary of the BOS ($BOSMin$), i.e., the foot that last finished the swing phase to the ground. The Margin of Stability assumes positive values (rightward arrow) when the extrapolated COM is in front of the $BOSMin$ and vice-versa.

Table 11 depicts the comparison between the timings proposed for the current slip-related fall prevention strategy and the timings already obtained by the fall prevention strategies previously addressed.

Table 11. Comparison between the timings proposed and the ones obtained for the literature fall prevention strategies analysed, where N\A = not available

Study	Detection time (ms)	Actuation time (ms)
Monaco [64]	350	250
Mioskowska [135]	100*	N\A
Trkov [65]	90**	N\A
Current proposal	360	100

(*) the detection time is based on a previous study [167]. (**) the detection time is based on a previous study [168].

The detection times obtained in studies [65,135] were considerably lower than the detection time attributed in the fall prevention herein conceived. Nevertheless, although those studies developed a real-time slip perturbation detection algorithm, the approach was only tested under offline conditions. Thereby, Mioskowska *et al.* [135] and Trkov *et al.* [65] studies did not close the loop from the slip-induced LOB detection to the assistive support provided by a wearable robot. Conversely, Monaco *et al.* closed this loop [64] by performing the real-time detection and prevention of slip-induced LOBs during their experimental protocol, which confers more reliability to the detection time attributed in this particular fall prevention strategy. Hence, considering the comparison between the fall prevention strategy herein conceived and the other strategies developed, it was given an higher importance to the detection time obtained by Monaco *et al.* [64] in comparison with the detection times reported by the remaining authors [65,135].

In addition, Mioskowska *et al.* [135] and Trkov *et al.* [65] did not specifically mention the actuation times defined for their devices. During bench tests, Mioskowska *et al.* [135] mentioned that their assistive system was capable of performing the transition of the knee angle from 90° and 60° to 0° in the average times of 82 and 72 ms, respectively. Despite the authors reported that the device could assist human subjects with more than 30° of knee extension in under 150 ms during standing, no information was given about the time taken by the device to perform the knee extension during walking. Furthermore, Trkov *et al.* [65] only mentioned that their assistive device could produce up to 40 Nm torque values with rise times under 200 ms during the bench tests. Contrarily, Monaco *et al.* [64] defined the fixed duration of 250 ms to supply the assistive torque during experimental slip-like perturbation trials. This actuation time is greatly higher than the 100 ms defined for the proposed fall prevention strategy. However, 100 ms were determined as the actuation time considering previous literature evidence on the biomechanical reactions to slip perturbations [10,166].

Since this dissertation describes the preliminary steps of the slip-related fall prevention strategy, the actuation requirements conceived were not tested. Conversely, the slip perturbation detection algorithm was further tested and validated according to the detection requirements stipulated. However, it is necessary to collect meaningful data from individuals while dealing with slips to test the algorithm. Chapter 5 describes the experimental protocol designed and conducted for data collection.

5. Materials and Methods

The collection of meaningful human motion data while dealing with gait perturbations is essential to reliable define and test gait perturbation detection algorithms. In this regard, a slip-like perturbation protocol was designed and conducted to extract the selected monitoring variables, i.e., knee angle and shank angular velocity in the motion direction, during normal and perturbed walking. Considering that this dissertation comprises a preliminary stage of the slip-related fall prevention strategy, older subjects were not enrolled and the PKO was not worn by the subjects during the experiments. As a preliminary approach, it is firstly required to ascertain whether the perturbation detection algorithm developed presents an acceptable perturbation detection performance using healthy steady-state gait data, according to the detection requirements previously defined.

Regarding to the improvement opportunities identified in Chapter 3 for experimental protocols that provoke artificial falls, the protocol designed attempted to tackle some limitations: i) data from slip-like perturbations provoked to both legs was collected in order to account for individuals' side-dominance; ii) one of the walking speeds adopted during the trials was adapted for each subject. This allowed to simulate similar dynamic conditions among participants while dealing with the slip-like perturbations; and iii) data acquisition was performed from multiple different sensors, including not only kinematic data, but also biosignal data. This allowed to build a dataset with vast sensor information to be further used to comprehensively study the motion alterations induced by slip-like perturbations.

In addition, the slip-like perturbations were provoked by anteriorly pulling the participant's ankle at the heel strike or posteriorly pulling the ankle at the toe-off using a rope. The heel strike and toe-off were chosen as the slip onset events, considering that slip-induced LOBs are mainly initiated in these gait events. An experienced operator manually performed the rope pulling.

5.1. Participants and Equipment

Eleven healthy young subjects (age: 24.55 ± 2.15; height: 1.70 ± 0.09 m; weight: 63.25 ± 7.11 kg; males = 6; females = 5) were enrolled in the experimental protocol. Subjects were selected if they presented: i) healthy locomotion; ii) total postural balance; iii) more than 18 years; and iv) body mass lower than 135 kg. Subjects were excluded if they: i) presented a disease or deficit that affects locomotion; and ii) were recently subjected to surgical procedures that affect mobility. All participants provided written informed consent and voluntarily accepted to participate in the experimental trials. Each participant performed the qualitative assessment of the preferred foot by completing the Waterloo Footedness Questionnaire [169].

In order to better understand the changes that slip perturbations introduce to human motion, data were collected from a wide range of sensor systems so as to provide a vast dataset with kinematic and biosignal data during both normal and perturbed walking. Xsens MVN Awinda (Enschede, The Netherlands) and Optitrack V120 Trio (Corvallis, OR, USA) systems provide information about any potential changes in motion kinematic parameters towards LOB situations provoked by slip-like events. The remaining sensor systems provide biosignal data and, therefore, information about their change in the presence of slip-like perturbations. Delsys Trigno (Natick, MA, USA) provides muscles' electrical activity data, RespiBAN (Lisbon, Portugal) collects subject's respiration data and Shimmer (Dublin, Ireland) Galvanic Skin Response (GSR) provides information from subject's galvanic skin response and heart frequency rate. Furthermore, Kinect v2.0 camera (Redmond, WA, USA) offers video support to the labelling of events in the data samples.

Subjects were firstly equipped with 8 Delsys Trigno wearable sensors, which collected EMG data at approximately 1111 Hz. The sensors were placed in some lower body muscles, namely the *rectus femoris*, *biceps femoris*, *tibialis anterior* and *gastrocnemius lateralis* from both legs (Figure 18). Three trials of Maximum Voluntary Contraction (MVC) were performed for each muscle for further normalisation of EMG envelope. Further, participants were equipped with the full body configuration of Xsens MVN Awinda wearable inertial system that collected data at 60 Hz, which is composed by 17 IMUs placed in the following body landmarks: i) head; ii) sternum; iii) pelvis; iv) right and left shoulders; v) right and left upper arms; vi) right and left forearms; vii) right and left hands; viii) right and left upper legs; ix) right and left lower legs; and x) right and left feet. Following the sensor placement, participants underwent the N-Pose calibration of the system. Afterwards, reflexive markers were placed in the following body landmarks (based on a previous study [170]): i) head; ii) sternum; iii) midtrunk; iv) right and left shoulders; v) right and left elbows; vi) right and left wrists; vii) right and left hips; viii) right and left knees; ix) right and left heels; and x) right and left feet. These markers were tracked at 120 Hz by an Optitrack V120 Trio camera bar. Any existing shiny surface from subjects' clothing was removed in order to reduce the noise on the Optitrack cameras while tracking the reflexive markers. Kinect camera was used to provide video recordings from the experimental trials at 30 frames per second. Lastly, participants also worn the RespiBAN system on the upper trunk, between the sternum and the Xiphoid process, and the Shimmer GSR device on the dominant forearm with the electrodes placed on the index and middle fingers. These devices collected data at 1000 Hz and 100.21 Hz, respectively. The reflexive marker and IMU placements are depicted in Figure 19.

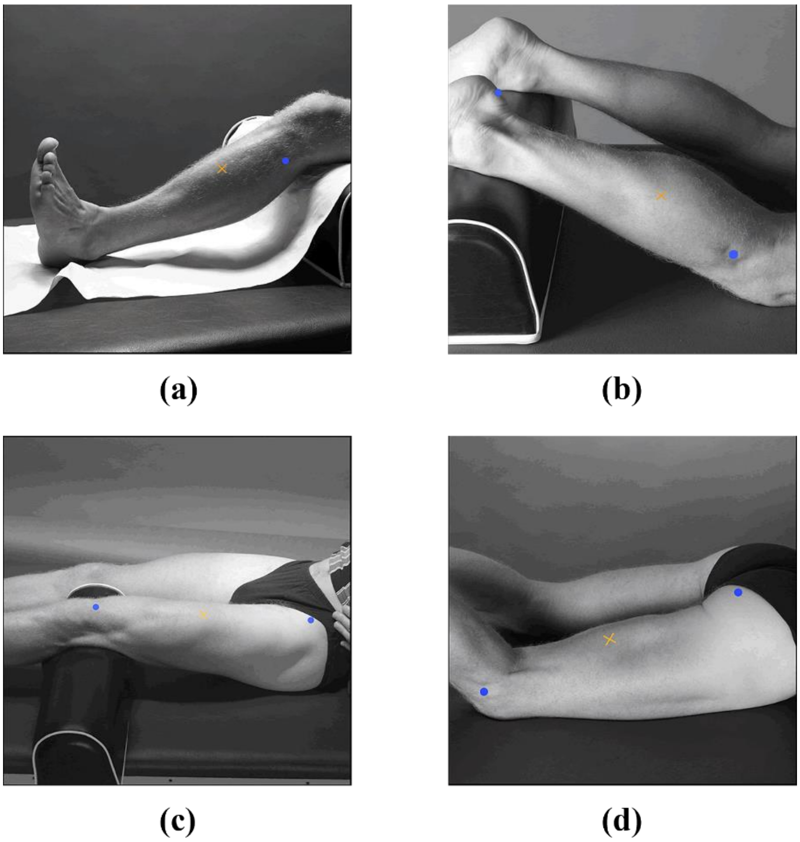

Figure 18. Muscles monitored by the EMG sensors, which were placed on the "x"marks highlighted in each of the 4 subfigures. (a) Tibialis anterior. (b) Gastrocnemius lateralis. (c) Rectus femoris. (d) Biceps femoris. The images were extracted from [171].

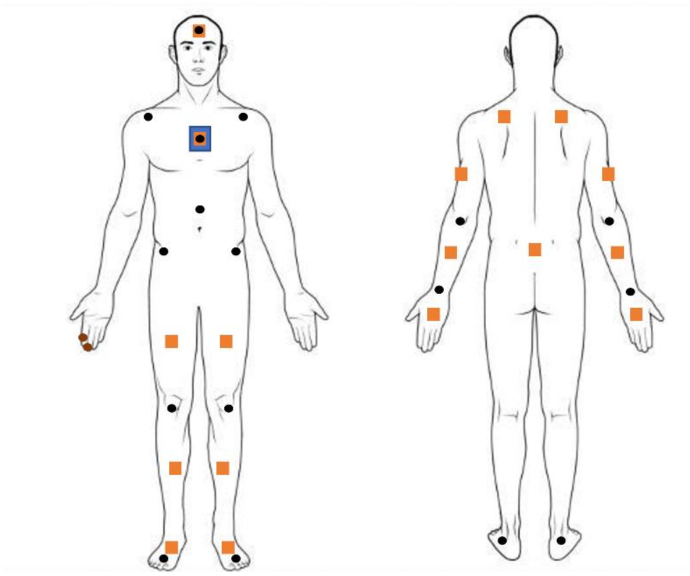

Figure 19. Reflexive marker (black dots), IMU (orange squares), RespiBAN device (blue square) and Shimmer electrodes (brown dots) placement.

Afterwards, subjects worn a safety harness system in the case an irreversible slip-induced LOB took placed. The harness system consisted in a vest that was attached to a structure in the ceiling through a rope. The length of the harness rope was adjusted in order to register a minimum of 15cm between the knees and the treadmill belt. This procedure was accomplished by asking participants to raise their feet, which led to the application of all the body weight into the harness system [100].

In order achieve synchronous data acquisition from all the sensor systems, Sync Lab Desktop App was used. This team-developed desktop application for Windows OS is capable of synchronously start and stop data collection from the above mentioned systems and save the collected data in the computer that runs the app. The trigger signals sent by the Desktop application are electronic or wireless pulses. The former are either sent via Syncbox, which is a team-developed hardware interface that connects to the Xsens and Delsys systems or by direct USB communication, which is used to connect to both Kinect and Optitrack cameras. The wireless communication with the RespiBAN and Shimmer GSR systems is performed directly from the computer running the app. Figure 20 summarises the experimental setup prepared for the data collection. It is noteworthy that the Optitrack cameras were tilted in order to capture all the reflexive markers placed on the subject's body.

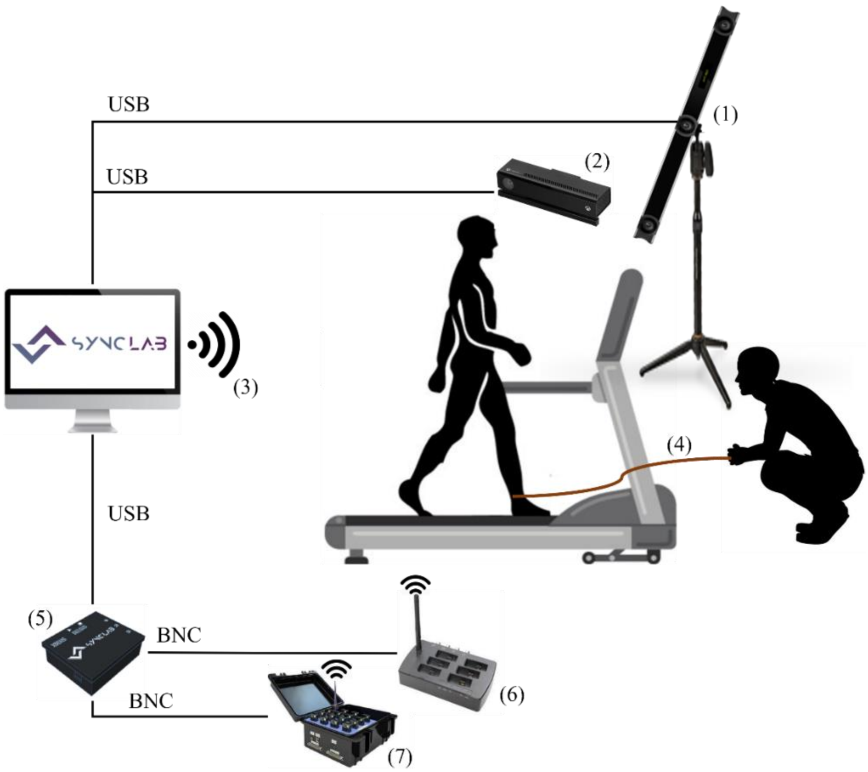

Figure 20. Experimental setup used for slip-like perturbation data collection. (1) Optitrack V120 Trio cameras. (2) Kinect v2.0 camera. (3) wireless communication between the computer running the app and RespiBAN and Shimmer systems. (4) Rope attached to the participant's ankle, which is pulled by the operator to cause the perturbation. (5) Sync Box. (6) Xsens Awinda station, which establishes wireless communication with the Xsens IMUs. (7) Delsys Trigno Workstation, which establishes wireless communication with the Delsys sensors. The safety harness system connected to the subject was not included for simplification. Some of the content from this image was extracted from a previous study [172].

5.2. Slip-like perturbation protocol

During the experimental protocol, participants were asked to manage unexpected slip-like perturbations during locomotion on a treadmill. All subjects were blind to the protocol to not introduce any prior bias on their response to the slip-like perturbations. Thus, subjects did not know when, how and how many times they were going to be perturbed. Firstly, subjects performed a familiarisation trial by walking in the treadmill without slip-like perturbations exposure while using the entire sensor setup. Subjects were instructed to fix their gaze on a point at eye level while walking so as not to foresee the onset of a potential perturbation.

During perturbation trials, a trained operator pulled a rope attached to the subjects' ankle at some heel strike events, i.e., when the subject's heel strikes the floor, performed by the subjects during their gait, which ended up provoking an instability similar to a slip event. In other perturbations trials, slips were induced at the toe-off gait event, i.e., when the subject's toe is raised from the floor to start the swing phase. In these perturbations, the operator pulled the rope in some of the toe-off events performed by the subjects. The rope was always attached to one of the participant's feet throughout all the trials. Thereby, participants did not know if there was going to be a perturbation or not.

Each subject underwent 8 trials, which depicted all the combinations between perturbed leg (right or left), perturbed gait event (heel strike or toe-off) and treadmill belt inclination (0 and 10%). Table 12 exhibits each trial's order and characteristics.

Table 12. Trial's order organisation during the experimental protocol for data acquisition

Trial Number	Perturbed leg	Perturbed gait event	Treadmill inclination (%)
1	Right	Heel strike	0
2	Right	Heel strike	10
3	Right	Toe-off	0
4	Right	Toe-off	10
5	Left	Heel strike	0
6	Left	Heel strike	10
7	Left	Toe-off	0
8	Left	Toe-off	10

Within each trial, 6 sub-trials were performed. Subjects walked at 3 different speeds (1.8 km/h (slow speed), 5.4 km/h (fast speed), and a normalised speed that was calculated through a formula, according to the subject's leg length, in order to simulate similar dynamic conditions across all the participants) and in 2 different conditions (perturbation or non-perturbation). Slow and fast gait speed were defined according to the literature [173–175]. The normalised speed (v) for each subject was calculated in accordance with the principle of dynamic similarity, which is expressed by the equation below.

$$v(m/s) = \sqrt{F_r g L}$$

F_r is the Froude number (0.15); g is the gravity accelerations (9.81 m/s²); and L is the leg length from the prominence of the greater trochanter external surface to the lateral malleolus) [166].

Table 13 depicts the characteristics from each of the 6 sub-trials. These sub-trials were conducted in a randomised order to make the perturbations delivered more unpredictable. During perturbation trials, the operator applied 3 perturbations in random moments of the trial. Non-perturbation trials had a mean duration of 30 seconds, whereas perturbation trials had a more variable duration, which was generally between 30 seconds and 1 minute.

Table 13. Characteristics of the 6 sub-trials performed within each trial

Velocity	**Perturbation?**
1.8 km/h	Yes
1.8 km/h	No
Velocity adapted to subject's leg length	Yes
Velocity adapted to subject's leg length	No
5.4 km/h	Yes
5.4 km/h	No

5.2.1. Discussion

Considering the procedures performed during the experimental protocol, some topics should be addressed. First, the perturbations delivered to the subjects were non-standardised. Since the operator manually pulled the participants ankle, a variability on the timing and the magnitude of the perturbation application was created. More specifically, the perturbations were not applied consistently at the heel strike instant and the strength of rope pull was not fixed. For instance, if a perturbation was applied shortly after the heel strike, the subject would already have more height supported by the perturbed limb. Therefore, the perturbation would not be as perturbing to the participant. In this regard, some perturbations were not considered during the labelling process since they were not considered sufficiently destabilising. This caused the reduction of the number of perturbations available for the further analysis. However, the operator was experienced with the perturbation delivery and was not changed throughout all the trials in order to mitigate the perturbation variability. Secondly, although participants were instructed to fix their gaze on a point at eye level during the trials, their peripheral vision of the operator could potentially have allowed cues to predict the onset of a perturbation. Nonetheless, the operator was almost totally occluded from the participants' vision by the treadmill velocity panel. Thirdly, since all the perturbation trials accounted for 3 perturbations, participants may at some point of the trials have adapted their gait towards the perturbation received. Nevertheless, participants were instructed to always maintain their normal walking pattern and reminded that if any irrecoverable LOB took place, they would be arrested by the harness, which was securely attached to the ceiling and provided unconditional safety. In addition, the time of the perturbation trials was varied in order to enhance the unpredictability of the perturbation delivery and stimulate subjects to walk naturally.

5.3. Data Processing

Once data has been collected, it was further processed using *Matlab* software to convert data from all the sensors into *Matlab* table format. However, some sensor data had to be previously processed using other software before being processed in *Matlab*. This is depicted in the Software processing stage from Figure 21. For instance, each subject's EMG data collected from the Delsys sensors had to be previously normalised with their MVC information using *EMG Analysis* software. Optitrack reflexive markers were labelled for each trial using *Motive* software. Only some of the markers were labelled since some markers suffered constant occlusions, i.e., markers disappeared from the video recordings because they were occluded by some obstacle, during the treadmill gait. Therefore, the labelled markers were: i) head; ii) sternum; iii) midtrunk; iv) right and left shoulders; and v) right and left hips. The frames provided by the Kinect camera were aligned together using *Adobe Premiere Software* in order to produce a video for each trial.

Once these steps were concluded, all data were ready to be processed in *Matlab* in the *Matlab* data processing stage. Since the sampling frequencies among the sensor systems were different and the system which had the lower sampling frequency was Xsens with 60 Hz, all data were downsampled to 60 Hz. The downsampling of RespiBAN data had to be performed second by second, since the device's sampling frequency was variable throughout the data collection. Further, data from each sensor were organised into mat tables with each column depicting one feature extracted from the sensors. For each trial, the number of Xsens data samples served as reference. Therefore, the excess data samples acquired from the other sensors were excluded and empty samples were added if there was a lack of data samples. Data samples from the different systems were temporally aligned according to the timestamps of start and stop data recording provided by the Sync Lab Desktop App. This was particularly useful in RespiBAN and Shimmer GSR devices, which often did not start and stop data collection at the same time as the other sensor systems. Thereby, all the data collected from the different sensors were aligned and had the same number of samples for each trial. Sensor data tables from the same trials were then concatenated in order to generate a single data table for each trial.

Once this process was concluded, it was proceeded to the labelling of events for each trial. The events of interest are: i) start of a sub-trial: marked in the frame of the first heel strike of the foot being perturbed (with the rope) since the subject achieved steady walking during the sub-trial; ii) end of a sub-trial: marked in the frame of the last heel strike of the foot being perturbed in steady walking during the sub-trial; iii) perturbation onset: marked in the frame where the operator starts to pull the rope to perturb the participant's gait; and iv) end of the perturbation: marked in the frame of the first heel strike of the perturbed foot after the participant has recovered from the perturbation and regained steady walking. To this end, videos generated from the Kinect frames for each trial were uploaded to *Djv* software to facilitate the labelling process. This software allowed to identify Kinect frame numbers in which an event occurred. Since Sync Lab Desktop App provided the timestamp associated with each Kinect frame, it was possible to correlate the identified frame timestamps with data table timestamps from the same trial in order to mark events. The number of the frames of interest were introduced in a *Matlab* script in order to label the data samples from each trial table with the respective event. Thereby 2 columns were added to each trial data table from this labelling process. One column indicates the type of sub-trial of the data samples and the other indicates if the data samples correspond to a perturbation or not. It is noteworthy that only the perturbations that were found to disturb subject's gait and balance based on video evidence were labelled. Once the labelling process was concluded, each trial data table was divided into their individual sub-trials for the further test of the perturbation detection algorithm.

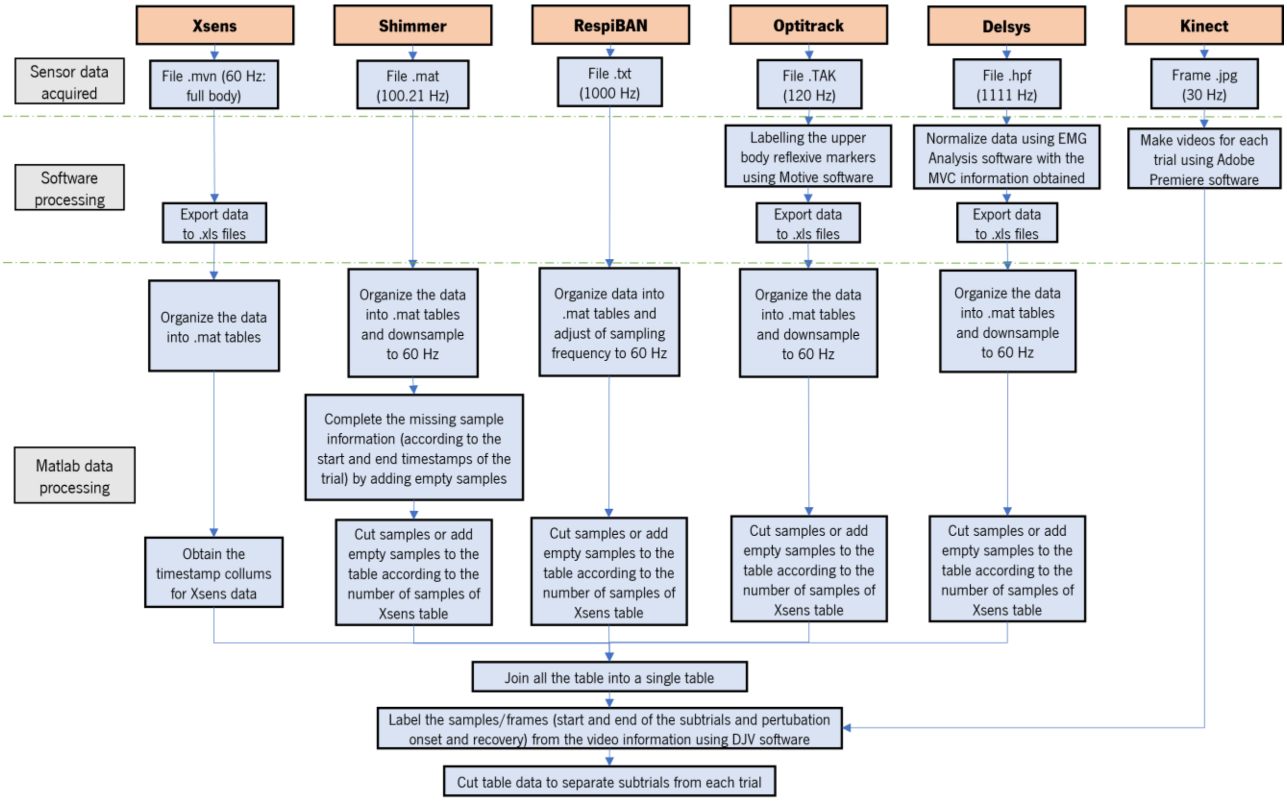

Figure 21. Experimental Protocol data processing flowchart.

6. Slip-like perturbation Detection Validation

The validation strategy proposal for slip-like perturbation detection was conducted considering data from the 2 selected variables, the knee angle and the shank angular velocity. The validation scheme is depicted in Figure 22. For each selected variable, the perturbation detection algorithm was tested using perturbation data from the perturbed and the unperturbed legs. The validation strategy was employed using the data collected from normal walking trials and perturbation delivery trials, while subjects were ambulating on the treadmill with 0% inclination at a normalised speed previously calculated for each subject. The locomotion conditions considered for this analysis depict a level-ground walking scenario and a velocity that is likely to be adopted by the subjects during their daily-life. Hence, data from these conditions were considered for analysis, since these conditions are the most likely to precede the occurrence of a real-life slip perturbation for the enrolled participants [5,6]. Also, according to the literature reviewed, only perturbation trials where the slips were provoked during the heel strike were considered, since this gait event is the most prominent for the onset of real-world slips [70]. As such, for each subject, there were data from 6 trials: i) 4 normal walking trials, i.e., without perturbation; and ii) 2 perturbation trials. However, data from 2 subjects were unable to be used due to data loss. From the total of perturbation trials included, there were 23 valid slip-like perturbations from 9 participants (according to the perturbation labelling process described in Chapter 5), which were further used to test the performance of the perturbation detection algorithm.

Initially, the data collected from each selected variable from all 6 trials were jointly normalised within the interval between 0 and 1. The normalisation was performed in order to scale the amplitude variations of the kinematic signals to a shorter and equal interval while respecting and maintaining the differences among data from the different trials.

From the 4 normal walking trials, data from 3 trials were chosen to tune the oscillators within the CPG, i.e., normal walking tuning data. Data from the remaining trial were used to further test the tuned CPG, i.e., normal walking testing data. For each subject, 2 CPGs were tuned and tested, one with knee angle data and the other with shank angular velocity data. A Fourier frequency spectral decomposition of the tuning data was performed to obtain the frequency, amplitude and phase values associated to each relevant frequency component. Once these parameters were obtained, their mean was determined for each relevant frequency component. The mean parameters of frequency and their respective amplitudes and phases were used to tune the initial conditions of the CPG's oscillators specifically for each subject. Then, normal walking testing data were augmented, i.e., replicated, by a factor of 200 and used as input to the tuned CPG. This allowed to test the subject-specific tuned CPG to track the steady-state walking profile of the selected variables (Normal Walking Testing). The selection of this high augmentation factor allowed to perceive and study the CPG's adaptation to the input signals for longer time periods. The Normal Walking Testing performance was evaluated between the selected variables, according to the mean error metrics (Mean error and root mean square error (RMSE) values) obtained across all the participants.

After the Normal Walking Testing, the perturbation labelled data were extracted from the perturbation trials' data. As such, knee angle and shank angular velocity data from the 23 valid slip-like perturbations were obtained. For each selected variable, data from each perturbation was individually processed and further concatenated between normal walking data from the respective subject. This concatenation process allowed to obtain, for each valid perturbation, steady-state walking data before and after the slip-like perturbation occurrence. Then, these concatenated data were provided as input to the CPG tuned for the respective subject with data from the respective motion variable, i.e., knee angle or shank angular velocity. As previously mentioned, the CPGs were subject-specifically tuned during the Normal Walking Testing. This allowed to obtain simulation data from the CPG's signal prediction upon the occurrence of a slip-like perturbation during steady walking. In this regard, an error signal between the CPG output and the actual kinematic signal was produced for each perturbation, which was further used by threshold-based algorithms to detect the perturbation onset (Perturbed Walking Testing). The MDT, the detection accuracy of real perturbations (the 23 valid slip-like perturbations), the mean number of false perturbations detected per each real perturbation identified, and the mean number of samples per false perturbation detected (false alarms) were used to evaluate the perturbation detection performance of the threshold-based algorithms. All the data processing previously described was performed using the *Matlab* software, while the simulation data were obtained using the *Simulink* software.

Nonetheless, before conducting the proposed validation strategy, it was necessary to perform the study of the most suited number of oscillators within the CPG to monitor the selected variables. For the purpose of this master dissertation, this Chapter will address 3 main study topics for each selected variable: i) ascertain the most suited number of oscillators within the CPG for monitoring purposes; ii) perform the Normal Walking Testing; and iii) perform the Perturbed Walking Testing.

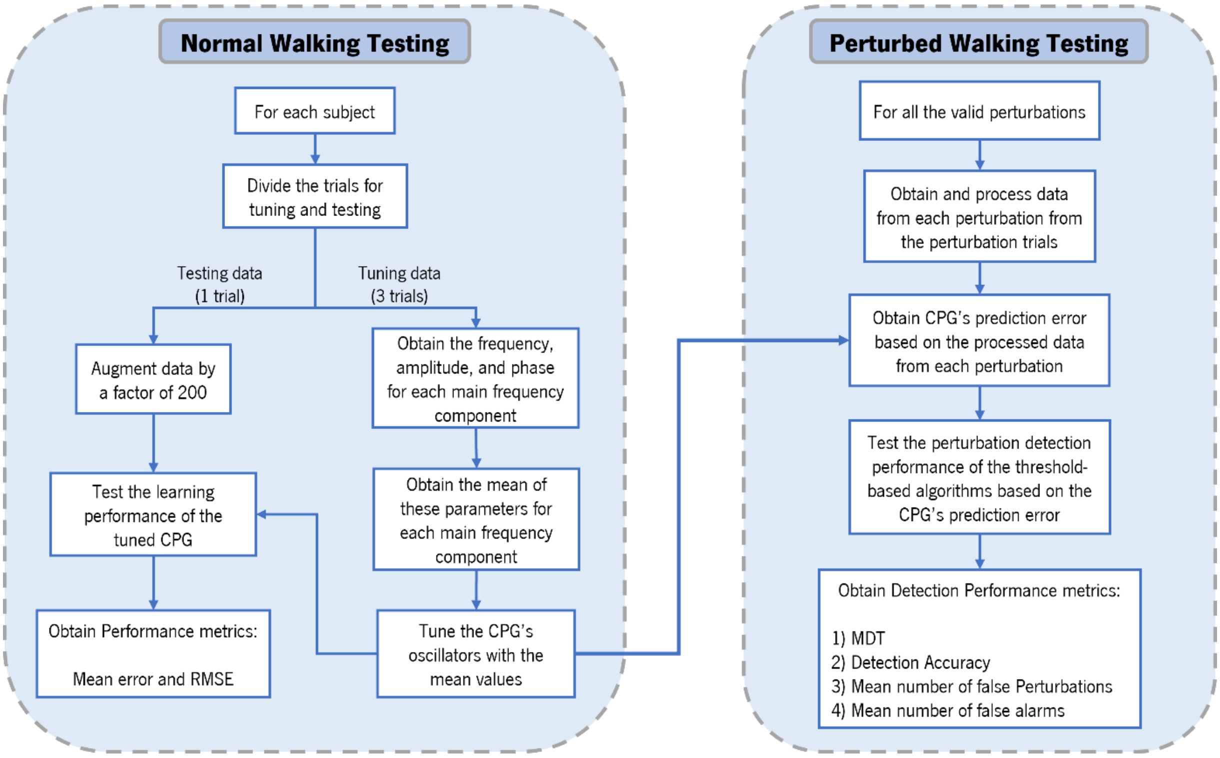

Figure 22. Validation strategy proposal for slip-like perturbation detection.

6.1. Study of the number of oscillators within the CPG

In order to tune the oscillator network according to the selected variables (knee angle and shank angular velocity), the number of oscillators within the respective CPG must be chosen. The analysis of the number of main frequency components needed to properly describe the selected variables' signals allows to optimise the number of oscillators to track each variable. This avoids unnecessary computational costs due to the use of an excessive number of oscillators. The selection process of the most suited number of oscillators was carried out for each variable and is summarised in Figure 23.

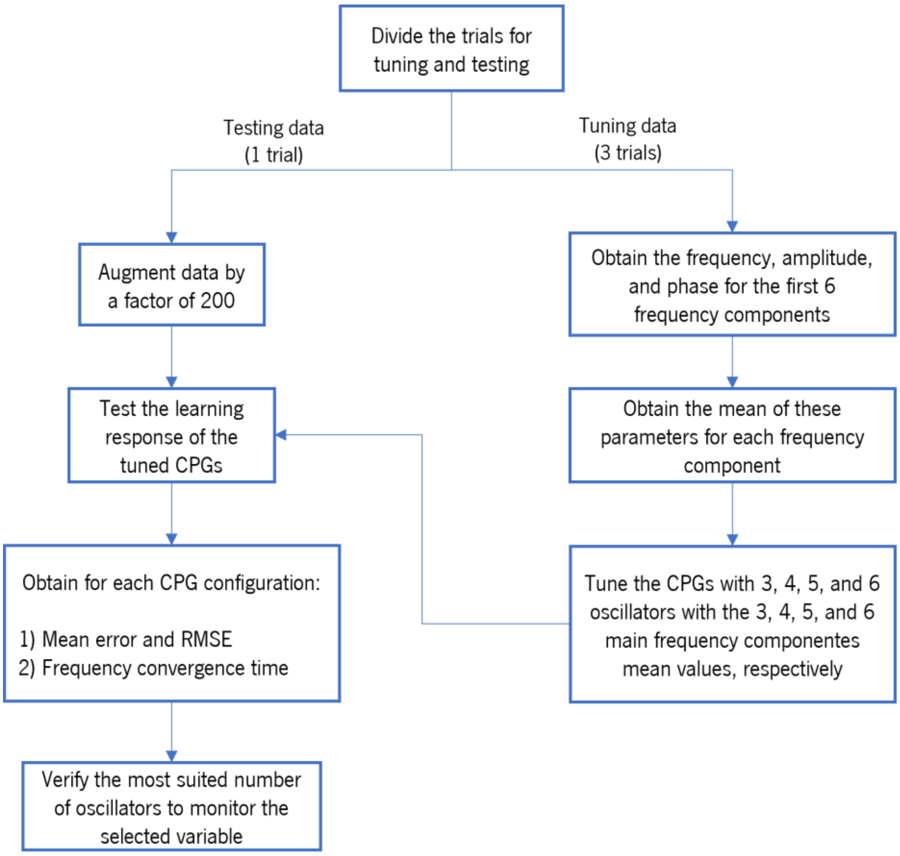

Figure 23. Selection process of the number of oscillators.

A spectral analysis was firstly performed to perceive the most relevant frequency components from each variable signals. This analysis was carried out using data from only one subject, since the signals' profile was considered similar among subjects, considering that all of them were healthy and belonged to the same age group. From the 4 normal walking trials of the chosen subject, data from 3 trials were used to parameterise the initial conditions of frequency, amplitude, and phase of each oscillator. For each of these 3 trials' data, the FFT was performed in order to decompose the signal in its frequency components. In this process, the amplitude and phase spectra were calculated with a resolution of 0.001 [176]. Figures 24 and 25 depict examples of regular knee angle and shank angular velocity signals, respectively, during steady-state walking, and their corresponding frequency spectrum.

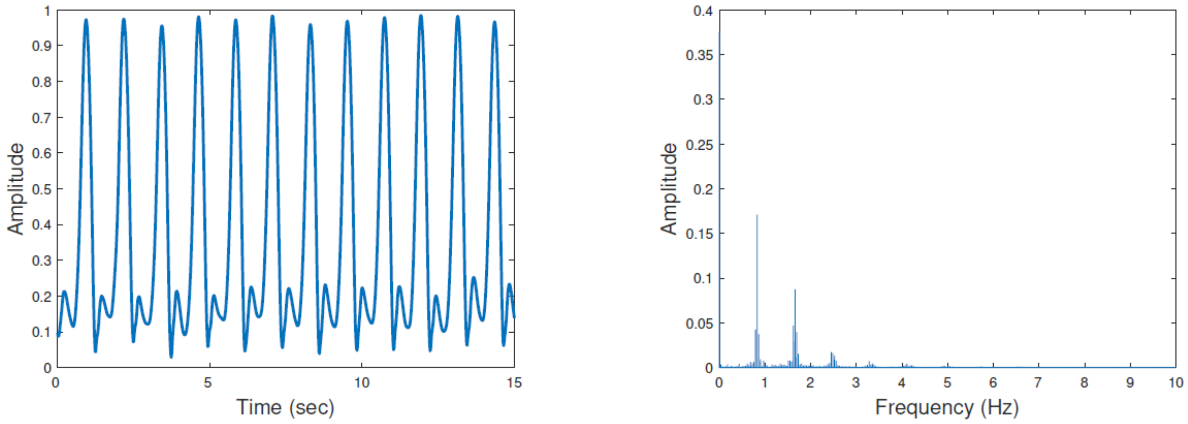

(a) (b)

Figure 24. Knee angle (a) time-course amplitude; and (b) frequency amplitude spectrum.

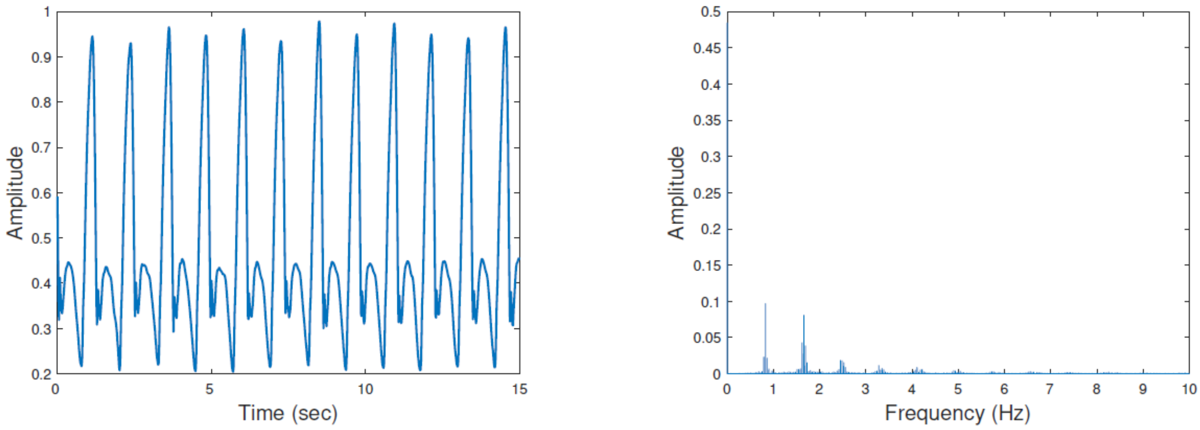

(a) (b)

Figure 25. Shank angular velocity (a) time-course amplitude; and (b) frequency amplitude spectrum.

As depicted in Figures 24(a) and 25(a), although it is observed a clear pattern in both knee angle and shank angular velocity signals, there is some variability among the different gait cycles, which underlines the quasi-periodic property of human gait. This variability will, in turn, result in the attribution of considerable amplitude values not only to the main frequency components, but also to the frequencies surrounding them (Figures 24(b) and 25(b)). However, the main frequency components of both signals are still noticeable and depicted by the frequencies corresponding to the peak amplitude values in the amplitude spectrum. These main frequency components are sorted in ascending order according to their frequency value. As such, considering Figures 24(b) and 25(b), the first main frequency component, which is the one with the lowest frequency value, corresponds to the 0 Hz frequency and the second main frequency component is assigned to the frequency associated with a peak amplitude just below 1 Hz. According to these frequency spectra, it was possible to acknowledge the existence of more visible and less perceptible amplitude peaks. This is related to the importance of a frequency to describe the signal, which is as high as the amplitude it has the frequency spectrum [163]. Since there is no prior knowledge of the minimum number of frequency components needed to accurately reproduce the knee angle signal, 6 peaks were considered for further analysis.

6.1.1. Knee angle

Table 14 highlights the frequency, amplitude, and phase values for the first 6 frequency components of the knee angle signal obtained from the 3 normal walking tunning trials.

Table 14. Values of frequency, amplitude, and phase of the first 6 frequency components of the knee angle variable (3 normal walking tuning trials)

Trial 1			Trial 2			Trial 3		
Frequency (Hz)	**Amplitude**	**Phase (º)**	**Frequency (Hz)**	**Amplitude**	**Phase (º)**	**Frequency (Hz)**	**Amplitude**	**Phase (º)**
0	0.3678	0	0	0.3548	0	0	0.3882	0
0.8224	0.1668	-42.3826	0.7731	0.1613	127.3497	0.8541	0.1692	108.8388
1.6448	0.0905	-84.1338	1.5462	0.0914	-102.7192	1.7082	0.0913	-137.4449
2.4329	0.0184	13.8409	2.3193	0.0177	-28.0031	2.5623	0.0176	-72.9138
3.2553	0.0070	-162.6813	3.1353	0.0048	-61.3806	3.4164	0.0056	-101.0342
4.0777	0.0047	97.5756	3.9084	0.0045	-10.0613	4.2705	0.0025	-51.3716

Then, the mean of the frequency, amplitude, and phase values for each main frequency component was determined, i.e., it was performed the mean of the values within the same row, which have the same frequency component order. According to the oscillator model input format on the *Simulink* software, the mean frequencies were converted from Hz to radians per second (rad/s), the amplitude values were powered by a factor of 2 and the phase values were converted to radians (rad). The mean values obtained for each frequency component are highlighted in Table 15.

Table 15. Mean values of frequency, amplitude, and phase for the first 6 frequency components from the knee angle signal

Mean Frequency (rad/s)	Mean Powered Amplitude	Mean Phase (rad)
0	0.137105	0
5.130428	0.027485	1.127517
10.260863	0.008293	-1.886689
15.319455	0.000321	-0.506588
20.539733	0.000034	-1.891332
25.670161	0.000016	0.526089

The values presented in Table 15 will thereafter be used to assign initial frequency, amplitude, and phase for each oscillator. As an example, the intrinsic frequency of the first AFO, as well as its initial amplitude and phase are depicted by the values from the first row of Table 15. The other AFO parameters were attributed according to Santos *et al.* [156] with the exception of ε, which was maintained similar among all the oscillators. Thus, all the oscillators were parameterised with $\gamma = 8$, $\varepsilon = 1$, $\tau = 0.03$ and $\eta = 0.5$. Once the AFOs were tuned with their respective initial parameters, their number within the CPG was varied across different simulations in order to ascertain the most suitable number of oscillators to track the knee angle signal. In this regard, knee angle data from the remaining normal walking trial (the only one that was not used to compute the initial parameters of the oscillators) were used to verify the CPG's ability to adapt to this signal. According to the knee angle frequency spectrum amplitudes presented in Figure 24(a), the first 3 frequency components seem to contain crucial information to describe the knee angle signal. Thereby, a minimum of 3 oscillators was considered in the CPG controller. In addition, considering the frequency component information previously extracted from the knee angle signal, the highest number of oscillators within the CPG was 6. Thus, there were performed simulations considering the CPG configurations with 6, 5, 4 and 3 oscillators, which will adapt to the 6, 5, 4 and 3 main frequencies of the knee angle signal, respectively.

In order to allow all the oscillators to have time to adapt to a frequency component and to study their behaviour after achieving frequency convergence, the knee angle signal from the remaining normal walking trial was augmented 200 times. This augmented signal was used as input for the oscillator network. Considering that these data refer to steady-state walking conditions and that the data samples start and stop at the same gait event, i.e., the heel strike of the foot being perturbed (as previously depicted in the Chapter 5), it was possible to properly replicate the knee angle signal without introducing abnormal variations during the data augmentation process. The simulation time was defined as the time duration of the augmented knee angle signal, considering the sampling frequency of 60 Hz of the kinematic data from Xsens. The simulation results are depicted from Figures A1 to A4 (Appendix I).

The relationship between the error metrics obtained during the simulations (mean error and RMSE) and the time taken for the last oscillator's frequency to converge (convergence time) were studied to select the most suitable number of oscillators to track the knee angle signal. The error produced regards to the difference between the CPG's prediction output and the input knee angle signal. The CPG was assumed to achieve convergence (and thus be adapted to all main frequency components from the input signal) from the point when the frequency values from all oscillators did not vary more than 1 rad/s for the rest of the simulation time. The outcomes are presented in Table 16.

Table 16. Performance results of knee angle monitoring for all the tested CPG configurations

Number of oscillators	Mean error (RMSE)	Convergence time (s)
3	0.0482 (0.0659)	instantaneous
4	0.0459 (0.0656)	1868
5	0.0407 (0.0607)	2506
6	0.0413 (0.0635)	5912

According to Table 16, it is possible to depict that a higher number of oscillators is generally accompanied with a decrease in the error values. However, the error obtained with the CPG with 5 oscillators was lower than the one observed with the CPG with 6 oscillators. The increase in the number of AFOs, which accounts for the inclusion of more frequency components from the knee angle signal, was expected to produce a better approximation of the CPG output to the input signal and thus reduce the error obtained. The CPG with 3 oscillators was associated with the highest error values. Nevertheless, the error difference between all the CPG configurations was not very noticeable, as the increase in the number of oscillators does not substantially reduce the error produced. In fact, the RMSE difference between the highest (0.0659) and lowest (0.0607) error values obtained was only around 7.9%. According to Figure 24(a), the amplitudes of the fourth, fifth and sixth frequency components of the knee angle signal are significantly lower than the ones from the first 3 components. Thereby, it was expected that the information added to the CPG output by the fourth, fifth and sixth oscillators would not be significant enough to considerably reduce the error.

The increase in the amount of AFOs also leads to a higher global frequency convergence time for the CPG. Despite the initial frequencies attributed to the oscillators being relatively close to the main frequency components of the input signal, regarding to the initial parameterisation performed (Table 15), the amplitudes of the higher frequencies are considerably lower than the amplitudes observed for the first frequency components (Figure 24(b)). As such, the attraction between the AFOs and the higher frequency components will be lower [163]. This justifies the larger amount of time taken by the oscillators to converge to higher frequency components. As such, a noticeable difference was observed between the convergence times obtained for the CPG with 3 oscillators and the other CPG configurations. Indeed, the high frequency convergence times obtained for the networks with 4, 5 and 6 oscillators hinder the use of these CPG configurations in daily-life scenarios, considering the high number of gait cycles needed to achieve frequency convergence. Conversely, the convergence time of the CPG with 3 oscillators was considered instantaneous, since the intrinsic frequencies of the different oscillators seem to instantaneously adapt and converge to a frequency component, as the frequency values from each of the 3 oscillators did not vary more than 1 rad/s since the start of the simulation (Figure A4, Appendix I). Considering that the first 3 frequency components from the knee angle signal present a significant amplitude (Figure 24(b)), their attraction to their respective oscillators will be more intense and thus the convergence time will be substantially lowered [163]. In order to better understand the frequency time course from each of the 3 oscillators, Figure 26 depicts an expanded version of Figure A4 (Appendix I).

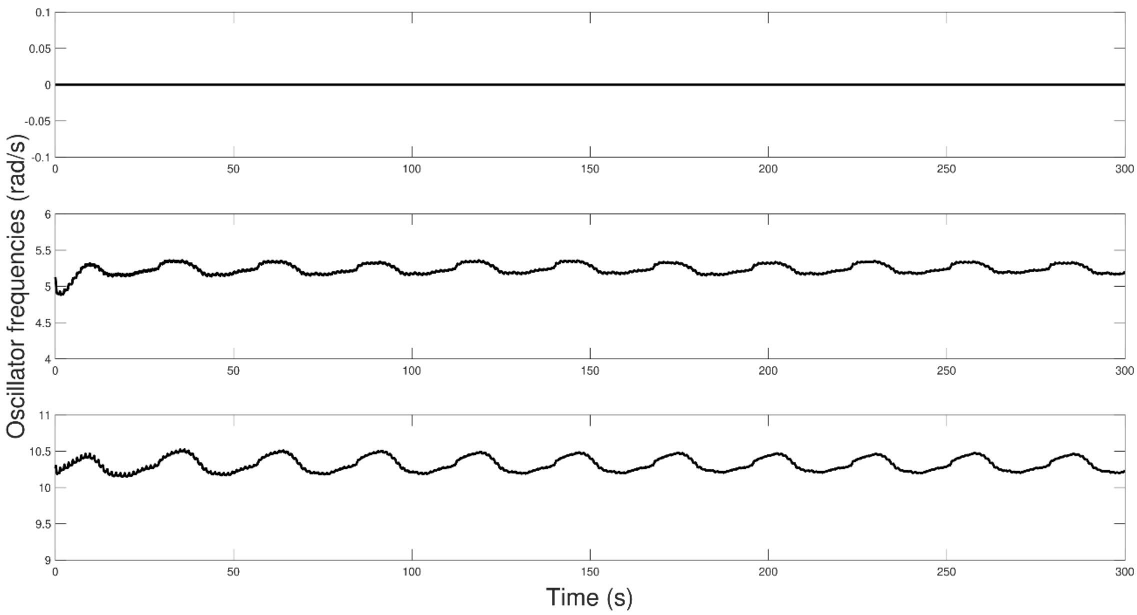

Figure 26. Expanded frequency evolution of the CPG with 3 oscillators throughout the simulation time course (knee angle). From top to bottom: $\omega 1$, $\omega 2$ and $\omega 3$.

While the variations of the first oscillator frequency are imperceptible, the second and third oscillators seemed to have almost immediately produced nearly stable oscillations around a central frequency. These low amplitude oscillations, with peak-to-peak amplitudes less than 0.5 rad/s, depict the quasi-periodic nature of human gait, considering that the kinematic differences observed among different gait cycles may reflect variations of the frequency values from the main frequency components. This results in the cyclical adaptation to a central main frequency, which is observed in the graphics of the second and third oscillators from Figure 26. In the fourth, fifth and sixth oscillators from the CPG configurations with 4 oscillators or more (Figures A1 to A3, Appendix I), the frequency values changed considerably before reaching a cyclical adaptation to a central main frequency.

Therefore, among all the CPG configurations considered, it is possible to understand that the CPG with 3 oscillators has the best relationship between the mean error produced and the time taken for the oscillators' frequencies to converge. Thereby, the detection of gait perturbations using knee angle data considered a CPG with 3 oscillators.

6.1.2. Shank angular velocity

Table 17 depicts the frequency, amplitude, and phase values for the first 6 frequency components of the shank angular velocity signal obtained from the 3 normal walking tuning trials.

Table 17. Values of frequency, amplitude, and phase of the first 6 frequency components of the shank angular velocity variable (3 normal walking tuning trials)

Trial 1			Trial 2			Trial 3		
Frequency (Hz)	**Amplitude**	**Phase (º)**	**Frequency (Hz)**	**Amplitude**	**Phase (º)**	**Frequency (Hz)**	**Amplitude**	**Phase (º)**
0	0.5120	0	0	0.4787	0	0	0.5146	0
0.8224	0.0927	-101.1107	0.7731	0.0755	67.5162	0.8541	0.0998	51.6990
1.6448	0.0826	-164.8690	1.5462	0.0696	177.5450	1.7082	0.0903	140.7318
2.4329	0.0162	-75.6084	2.3193	0.0137	-100.700	2.5623	0.0208	-159.1366
3.2553	0.0144	102.3050	3.1353	0.0067	-157.6629	3.4164	0.0112	163.8546
4.0777	0.0099	16.1080	3.9084	0.0052	-68.2749	4.2705	0.0064	-128.7854

Afterwards, for each frequency component, the frequency, amplitude, and phase values were averaged similarly to the knee angle variable. The values obtained for each frequency component are highlighted in Table 18.

Table 18. Mean values of frequency, amplitude, and phase for the first 6 frequency components from the shank angular velocity signal

Mean Frequency (rad/s)	Mean Powered Amplitude	Mean Phase (rad)
0	0.251751	0
5.130428	0.007980	0.105328
10.260863	0.006535	0.892490
15.319455	0.000286	-1.951540
20.539733	0.000116	0.631208
25.670161	0.000051	-1.052738

The values presented in Table 18 will be assigned to the different AFOs within the CPG. The remaining parameters (γ, ε, τ, and η) attributed to each oscillator were similar to the knee angle variable. The shank angular velocity data from the remaining trial were augmented by a factor of 200 and were used as input to the CPG in order to ascertain its ability to adapt to this signal. The shank angular velocity frequency spectrum shown in Figure 25(a) suggests that the first 3 frequency components entail the most important signal information. Thereby, a minimum of 3 AFOs were considered within the CPG. Once more, the number of oscillators within the CPG network was varied from 3 to 6 during the different simulations. The simulation results are presented from Figures A5 to A8 (Appendix I).

For each of the 4 simulations, the mean error, the RMSE, and the frequency convergence times were obtained. The outcomes obtained are depicted in Table 19.

Table 19. Performance results of shank angular velocity monitoring for all the tested CPG Configurations

Number of oscillators	Mean error (RMSE)	Convergence time (s)
3	0.0615 (0.0869)	instantaneous
4	0.0486 (0.0733)	instantaneous
5	0.0491 (0.0735)	did not converge
6	0.0451 (0.0685)	5453

Considering Table 19, the CPG configurations with 3 and 6 oscillators obtained the highest and lowest error values, respectively. However, the increase in the number of oscillators did not imply the decrease in the error values produced, since the CPG with 4 oscillators obtained smaller error values than the CPG with 5 oscillators. In fact, the error difference between the CPG configurations with 4, 5 and 6 oscillators were not very noticeable, which showed that the increase in the number of AFOs did not substantially reduce the error produced. The RMSE values obtained for the CPG with 4 oscillators

(0.0733) and the CPG with 6 oscillators (0.0685) differed in only around 6.5%. Nonetheless, the RMSE difference between the CPG configurations with 3 and 4 oscillators was more perceptible, being 15.7% higher for the CPG with 3 oscillators. Results suggest the lack of additional relevant information provided by the fifth and sixth frequency components, regarding to their considerably lower amplitudes in comparison with the amplitudes from the first 3 frequency components, which is depicted in Figure 25(b).

Additionally, the CPG with 6 AFOs presented the highest frequency convergence time. Despite the network with 5 oscillators seemed to have achieved convergence at around 644 seconds, the frequency values decrease considerably later in the simulation (Figure A6, Appendix I). This implied that the respective oscillator was not yet stably adapted to a frequency component of the input signal. The CPG configurations with 3 and 4 AFOs were considered to have achieved an instantaneous frequency convergence, since all of their oscillators' frequency values did not vary more than 1 rad/s since the start of the simulation. Therefore, the increase in the number of oscillators led to higher frequency convergence times. Although the initial parameterisation of each oscillator (Table 18) allowed them to be closer to one main frequency component of the input signal, the lower amplitude of the higher frequency components led to a decrease of the attraction intensity between these frequency components and the respective oscillators [163]. This caused longer time periods for the oscillators to converge towards the high frequency components. Figure 27 provides an expanded version of Figure A7 (Appendix I) to better understand the frequency time-course of the 4 oscillators.

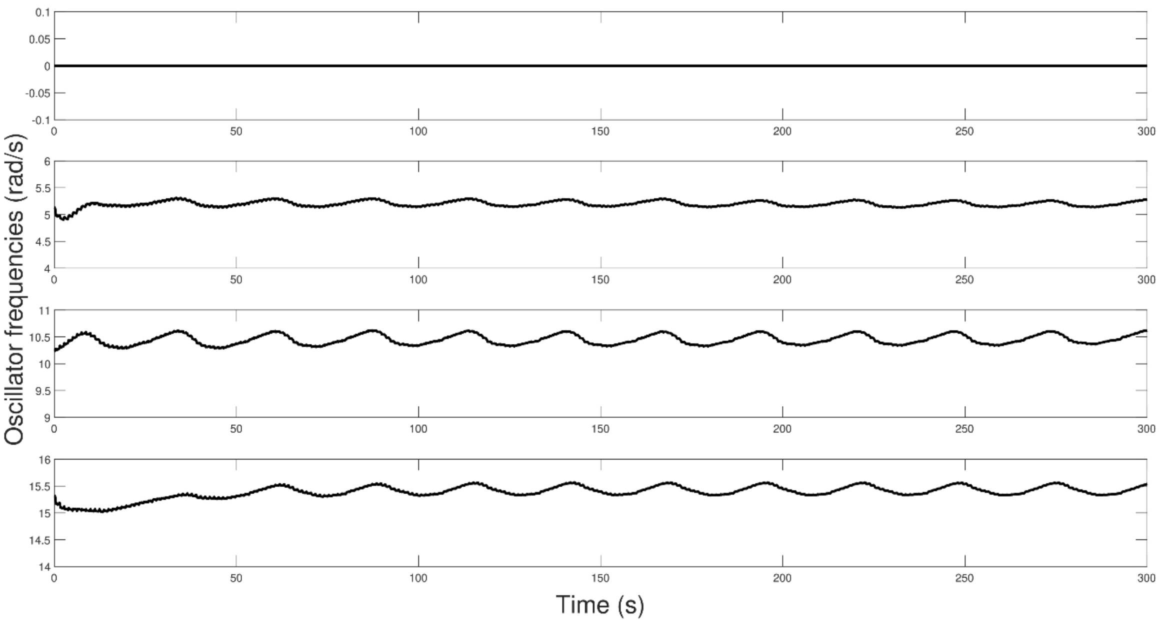

Figure 27. Expanded frequency evolution of the CPG with 4 oscillators throughout the simulation time course (shank angular velocity). From top to bottom: $\omega 1$, $\omega 2$, $\omega 3$, and $\omega 4$.

As depicted in Figure 27, the first oscillator frequency appears stable on the 0 rad/s throughout the simulation time. The second and third AFOs rapidly produced nearly stable oscillations around a central frequency. These oscillations were characterised by a low peak-to-peak amplitude of less than 0.5 rad/s. The foundation of this oscillatory behaviour may rely on the quasi-periodic nature of human gait, as depicted for the knee angle variable. The fourth AFO also reached this cyclical adaptation, despite needing an additional time to achieve it. Conversely, in the fifth and sixth oscillators from the CPG configurations with 5 and 6 oscillators, the frequency values changed considerably before achieving a cyclical adaptation towards a central frequency (Figure A5 and A6, Appendix I).

Hence, considering all the CPG configurations analysed, the CPG with 4 oscillators appears to be the most suitable option to monitor the shank angular velocity variable, as it provides the best relationship between the error metrics produced and the frequency convergence time. As such, the detection of gait perturbations using shank angular velocity data will proceed using a CPG with 4 oscillators.

6.2. Normal Walking Testing

Before providing the CPG algorithm with perturbation data, it was firstly tested with normal walking data to perceive the adaptation of the CPG's output to the normal walking knee angle and shank angular velocity signals (Figure 22). Two CPGs were specifically tuned and tested for each subject using their normal walking data (one tuned with knee angle data and the other tuned with shank angular velocity data). According to the previous analysis, the CPGs that monitor the knee angle and shank angular velocity variables were composed by 3 and 4 oscillators, respectively. The parameterisation of the intrinsic frequency of each oscillator, as well as their respective amplitude and phase, was similar to the CPG tuning process described to obtain the most suited number of oscillators for each variable. Also, all the oscillators were parameterised with $\gamma = 8$, $\varepsilon = 1$, $\tau = 0.03$, and $\eta = 0.5$, which were similar to the previous analysis. Once more, the normal walking data used to test the tuned CPGs were augmented by a factor of 200 to allow the study of the error signal's evolution for longer time periods of steady-state walking. Figures 28 and 29 present 3 different stages of the CPG's output adaptation to steady-state knee angle and shank angular velocity signals, respectively.

Considering both signals, some time is required for the CPG to adapt its amplitude to the input signal. However, it is possible to acknowledge that the CPG output rapidly adopts a signal pattern similar to the input signal. According to the simulation outcomes, there are some visible phase deviations, even after a long period of simulation. This is due to the quasi-period property of human gait, which is reflected by the differences observed among different gait cycles and the consequent variable frequency values of the main frequency components. Therefore, the non-static main frequency components from the actual signal will lead to the constantly adaptation of the CPG to this change, which inherently justifies the foundation of the deviations between the CPG output and the actual signals. Some amplitude deviations between the predicted and actual signals were also observed. This may be due to the learning dynamics of the oscillator network, which take longer to adapt to the input signal's amplitude, according to their initial parameter definition. As shown in Figure 29, it is also noteworthy that the CPG output prediction of the shank angular velocity data does not account for the small peak that follows the highest peak from the actual signal profile. The frequency component complexity required to describe this small peak may be the reason why none of the 4 oscillators was capable to produce it at the CPG output. Nevertheless, since the heel strike is marked by the derivative signal change of the shank angular velocity signal following the highest signal peak [152], this event may however be still timely detected. Considering that the knee angle profile (Figure 28) entails less complexity than the previous signal, the knee angle signal prediction from the CPG fully respects the morphology of the actual knee angle signal.

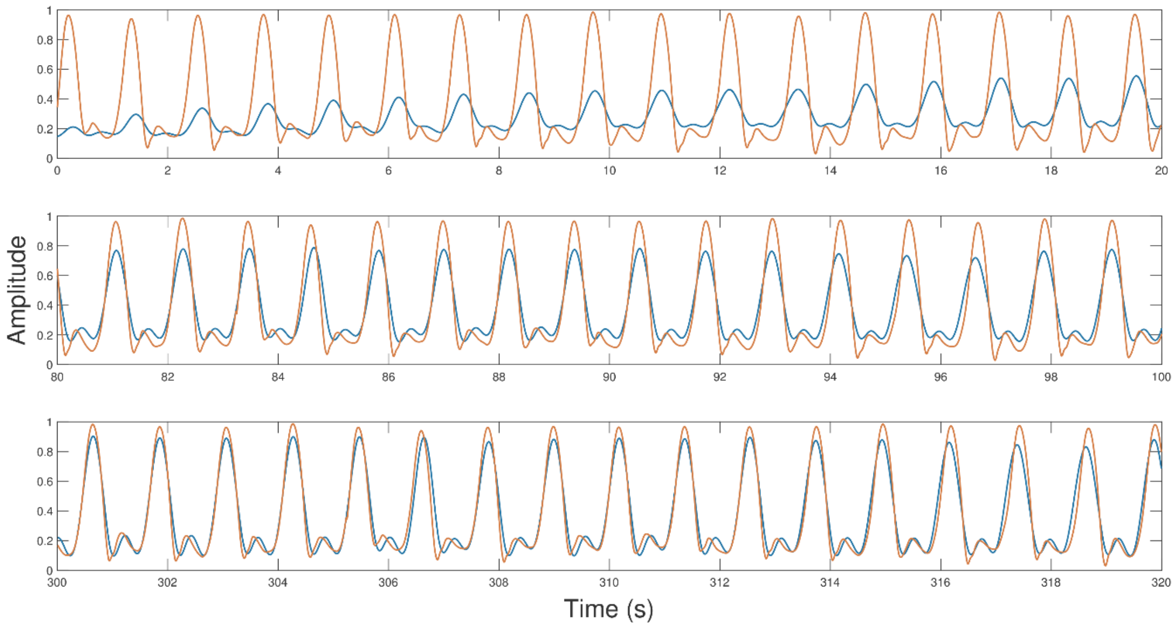

Figure 28. Three different stages of the CPG's output signal (blue) adaptation to the steady-state knee angle signal (orange).

Overall, the CPG output signals' morphologies and amplitudes were identical and in phase to the input signal. Once the CPG output starts to stabilise according to the steady-state walking input signal data, the error produced between both signals was considered irrelevant. Thus, the error signal would adopt considerable values only when the steady-state gait is disrupted, for e.g., in the presence of a gait perturbation. In these situations, larger deviations between the CPG output and the actual signal would be caused. Considering the similarities between the predicted and actual signals, it is possible to perform an accurate detection of gait events based on the signals predicted by the CPG. For instance, the recognition of the heel strike, which is the most critical and common gait event associated with a slip during walking [70], shortly before or upon a perturbation detection would increase the reliability of the slip detection. The detection of this gait event would be based on the identification of derivative change of the steady-state CPG output signal following the highest peak for both the knee angle [177] and the shank angular velocity [152] variables.

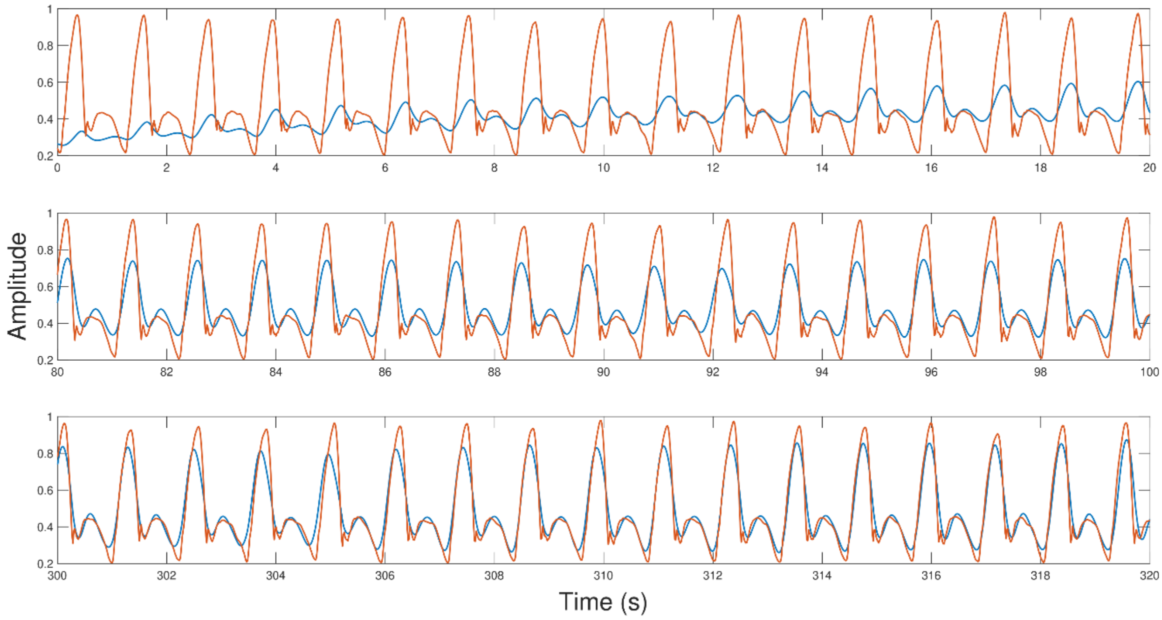

Figure 29. Three different stages of the CPG's output signal (blue) adaptation to the steady-state shank angular velocity signal (orange).

Once the simulations have been performed, it was computed the mean error and the RMSE values of the error signal obtained for each subject. Then, the mean error values obtained from all subjects were averaged in order to compare the tracking performance obtained for the knee angle and shank angular velocity variables. The error values obtained using the knee angle and shank angular velocity variables are depicted in Table 20. Only 9 subjects were considered since data collected for 2 subjects were unable to be used. Overall, although both variables produced a similar mean RMSE, the average mean error was marginally shorter for the shank angular velocity. This suggests that the CPG output achieved a slightly better approximation to the shank angular velocity rather than to the knee angle.

Table 20. Mean Error and RMSE values obtained during the Normal Walking Testing using knee angle and shank angular velocity data

Subject	Knee angle		Shank angular velocity	
	Mean error	RMSE	Mean error	RMSE
1	0.0485	0.0664	0.0494	0.0746
2	0.0531	0.0714	0.0488	0.0716
3	0.0505	0.0676	0.0448	0.0676
4	0.0456	0.0605	0.0374	0.0587
5	0.0593	0.0853	0.0430	0.0617
6	0.0493	0.0639	0.0480	0.0718
7	0.0630	0.0909	0.0395	0.0591
8	0.0458	0.0657	0.0583	0.0908
9	0.0523	0.0721	0.0553	0.0873
Mean	0.0519	0.0715	0.0472	0.0715

6.3. Perturbed Walking Testing

6.3.1. Gait perturbation influence

In order to understand the influence of the slip-like perturbations applied to the selected variables (knee angle and shank angular velocity), one perturbation from a perturbation trial was considered. Figure 30 depicts the various stages of the application of one slip-like perturbation during the experimental protocol. Figures 31 and 32 represent the respective influence of this perturbation on the knee angle and shank angular velocity signals, respectively, from both legs. For both the knee angle and shank angular velocity variables, the heel strike events are marked by the derivative change of the signals following the highest signal peaks [152,177].

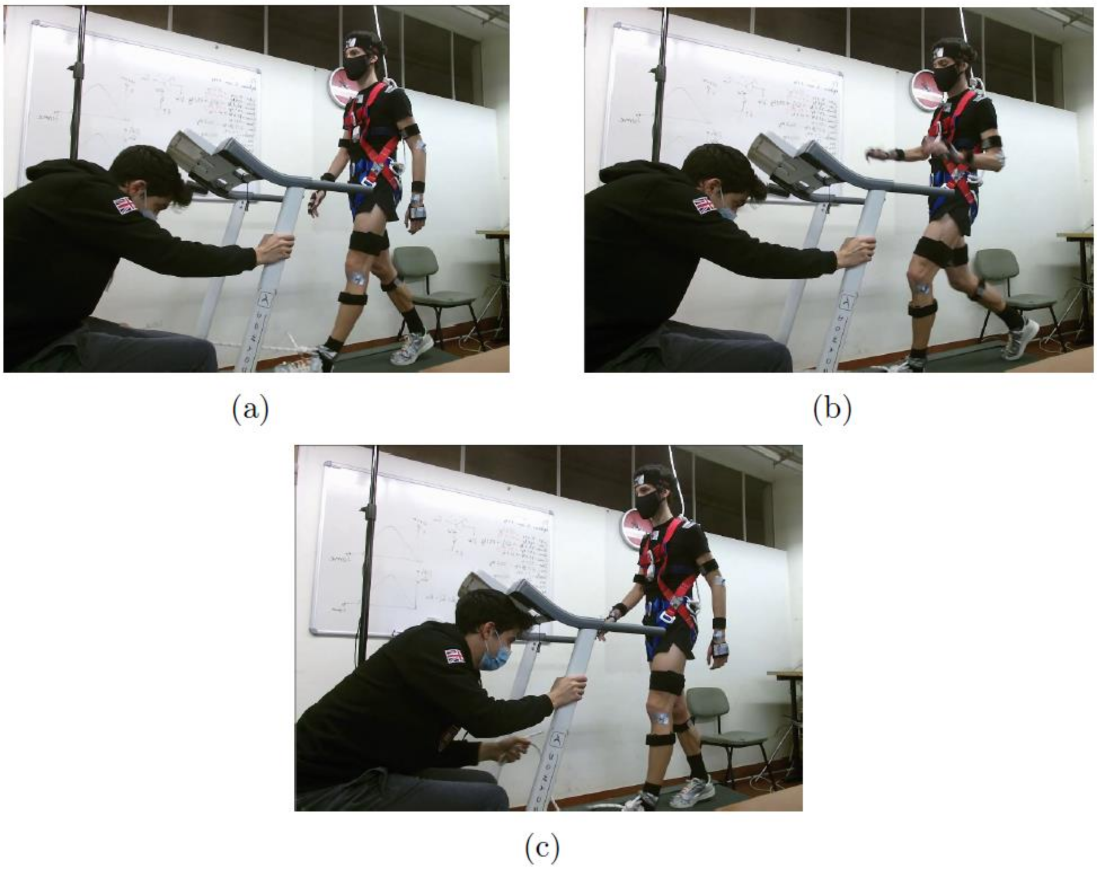

Figure 30. Slip-like perturbation application: (a) the operator pulls the rope attached to the participant's ankle when he performs the heel strike; (b) the participant is perturbed by the rope pull; and (c) the participant recovered the balance.

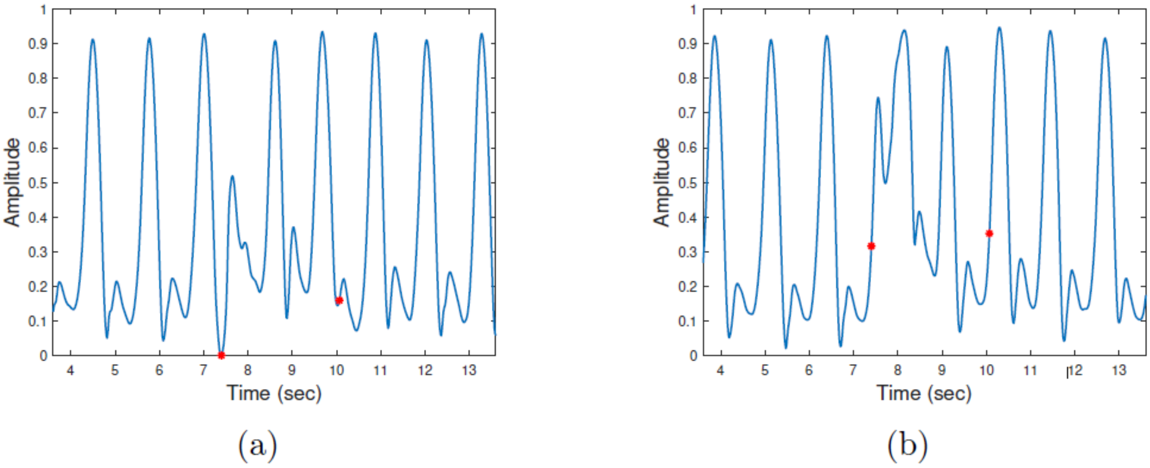

Figure 31. Knee angle signal from: (a) the perturbed limb; and (b) the unperturbed limb. These signals were collected during steady-state gait affected by the application of a slip-like perturbation. The red marks in the graphics depict the first and the last samples labelled as perturbation.

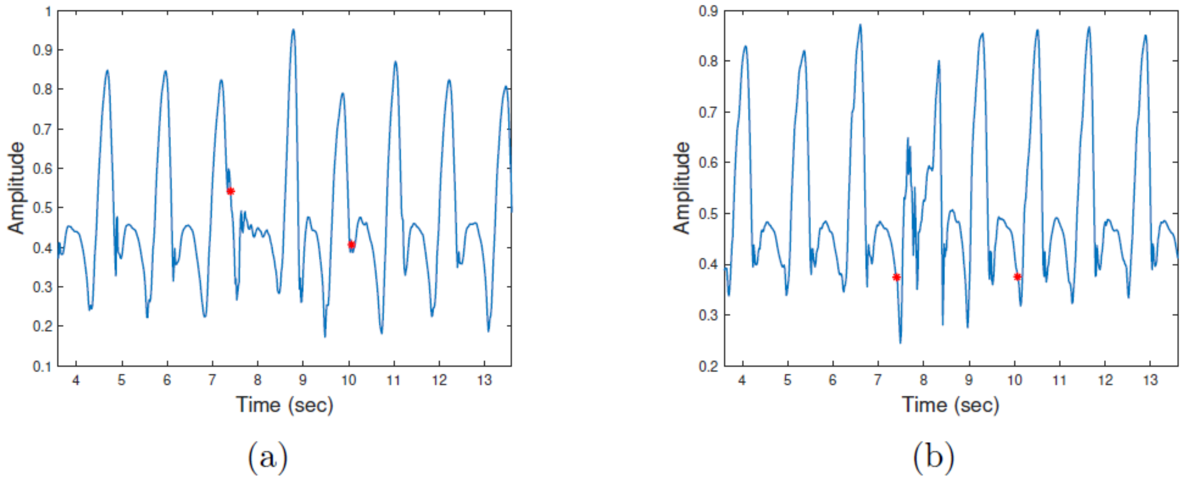

Figure 32. Shank angular velocity signal from: (a) the perturbed limb; and (b) the unperturbed limb. These signals were collected during steady-state gait affected by the application of a slip-like perturbation. The red marks in the graphics depict the first and the last samples labelled as perturbation.

The knee angle is composed by 2 main signal peaks within each gait cycle, one with a higher amplitude, which corresponds to the knee angle variation during the swing phase, and a smaller peak, characterised by the knee angle variation during the stance phase. As depicted in Figure 31(a), upon a slip perturbation with sufficient intensity at the heel strike, the stance peak amplitude from the perturbed limb's knee angle remarkably increases due to the pull provoked by the operator, which caused the knee to abnormally extend and thus increase its angle. The perturbation applied also affected the unperturbed knee angle signal, specifically during its swing phase. Figure 31(b) highlights the visible deviations produced at the swing peak of the unperturbed knee angle provoked by the slip. Both the perturbed and unperturbed knee angle signals seemed to be evidently affected by the slip-like perturbation.

The shank angular velocity is characterised by 3 main peaks within each gait cycle. The highest one describes the shank angular velocity variation during the swing phase, while the shorter peak following the swing and its subsequent peak are associated with the stance phase. According to Figure 32(a), the delivery of a slip perturbation at the heel strike causes the 2 peaks from the stance phase to merge and slightly increase the stance phase time duration in the perturbed shank angular velocity signal. The swing phase of the unperturbed limb was also affected by the slip-like perturbation applied. In fact, Figure 32(b) clearly depicts the alterations provoked to the swing signal peak. Considering the shank angular velocity signal, it appears that the unperturbed leg's signal is more affected by the slip-like perturbation than the perturbed leg's signal.

6.3.2. Perturbed walking data processing

As previously mentioned, 2 perturbation trials were considered for each subject, one for perturbations delivered to the right leg and the other one to the left leg. However, due to data loss, data from 2 subjects were unable to be used and for some subjects only data from one perturbation trial were available. Furthermore, it is noteworthy that although perturbation trials accounted for 3 perturbations given to each participant, some were excluded during the labelling process, as they were not considered to perturb the subject's motion. As such, data from a total of 23 slip-like perturbations from 9 different subjects were available for the further perturbation detection analysis. Since the perturbation trials presented few gait cycles, according to their limited time, and that they accounted for more than one perturbation, data relating to each perturbation were extracted individually from the perturbation trials. Data from both the perturbed and unperturbed legs were considered. Then, in order to simulate a single perturbation delivery during steady-state walking for the perturbation detection algorithm, data from each extracted perturbation were concatenated between normal walking data from the non-perturbation trials of the respective subject and leg. Thus, the data obtained for each perturbation accounted for steady walking before the perturbation, the following perturbation occurrence and steady walking after the recovery. For each subject, the normal walking data used in this concatenation were the data used for their respective Normal Walking Testing. These data were augmented by a factor of 20 in order to guarantee sufficient time for the CPG to achieve a steady-state output before the perturbation onset.

Since both normal walking and perturbation labelled data start and end in the same gait event, i.e., the heel strike of the perturbed foot, and that both data were collected during the same speed and at steady walking conditions, it was possible to perform this concatenation. As such, considering data from a perturbation, the first perturbation sample is concatenated to the last sample of the augmented normal walking data and the last sample of perturbation is concatenated to the start of another augmented normal walking data. However, to assure that the concatenation was properly performed, especially considering that the heel strike labelling could have not been optimal across all the trials, a manual correction was performed for each concatenated perturbation. Figure 33 clarifies the importance of the manual correction.

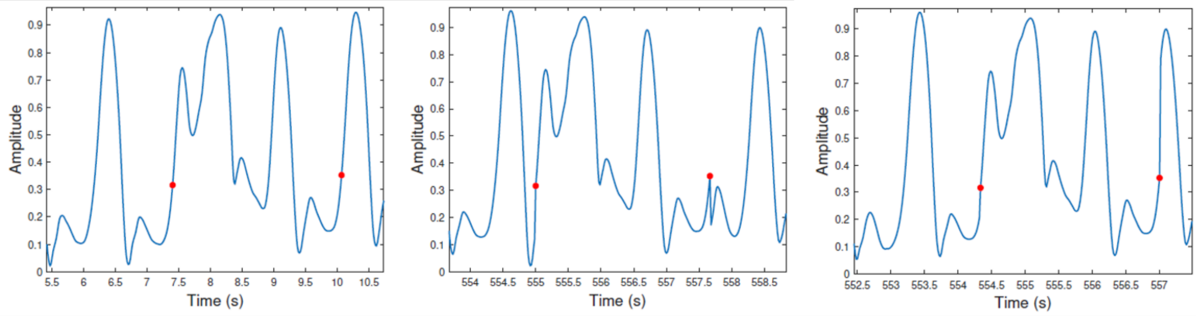

(a) (b) (c)

Figure 33. Concatenation of knee angle data from one perturbation between normal walking knee angle data. The red marks in the graphics depict the first and the last samples labelled as perturbation from: (a) original perturbation data from the perturbation trial; (b) the perturbation data concatenated between the normal walking data without the manual corrections; and (c) the perturbation data concatenated between the normal walking data after the manual corrections.

According to Figure 33(b), it is possible to acknowledge that the perturbation data were not correctly concatenated to the normal walking data without the manual corrections. This is depicted by the noticeable difference between the perturbation data within the perturbation trial (Figure 33(a)) and the same perturbation data concatenated between augmented normal walking data (Figure 33(b)). Conversely, after performing the manual corrections by adjusting the normal walking data to both ends of the perturbation samples, it was possible to obtain a graphic similar to original perturbation trial data, as shown in Figure 33(c). The manual corrections were therefore necessary and used to enhance the reliability of the concatenation process in order to accurately depict the kinematic changes provoked by the perturbations.

Afterwards, the manually corrected concatenated data was provided to the CPG algorithm as input. This allowed to obtain the CPG's signal prediction of the manually corrected concatenated data and the respective prediction error (perturbed walking simulation data). This process of obtaining perturbed walking simulation data is summarised in the flowchart from Figure 34(a). As previously suggested, the perturbation detection algorithm will detect the perturbation onset based on the error signal acquired. A detailed description of the steps taken to perform the CPG simulations is provided in Figure 34(b). For each subject, it was initially considered the first perturbation trial. From this trial, it was firstly performed the CPG simulation using data from its first perturbation and data from the right leg. Once the simulation was concluded, the simulations signals, namely the CPG prediction of the input signal and the error generated between this prediction and the actual signal, were saved. In addition, some relevant information regarding to the timestamp of the perturbation onset was extracted from each perturbed walking simulation. This information was important to localise the perturbation timestamp on the simulation data for the further detection of perturbations. This process was repeated to the left leg's data and posteriorly to the second perturbation trial's data. Regarding subjects that presented data from only the first or second trials, the simulation data extraction was only performed for the respective trial. When all the simulations were performed for one subject, the simulation data extraction process proceeded to the next subject.

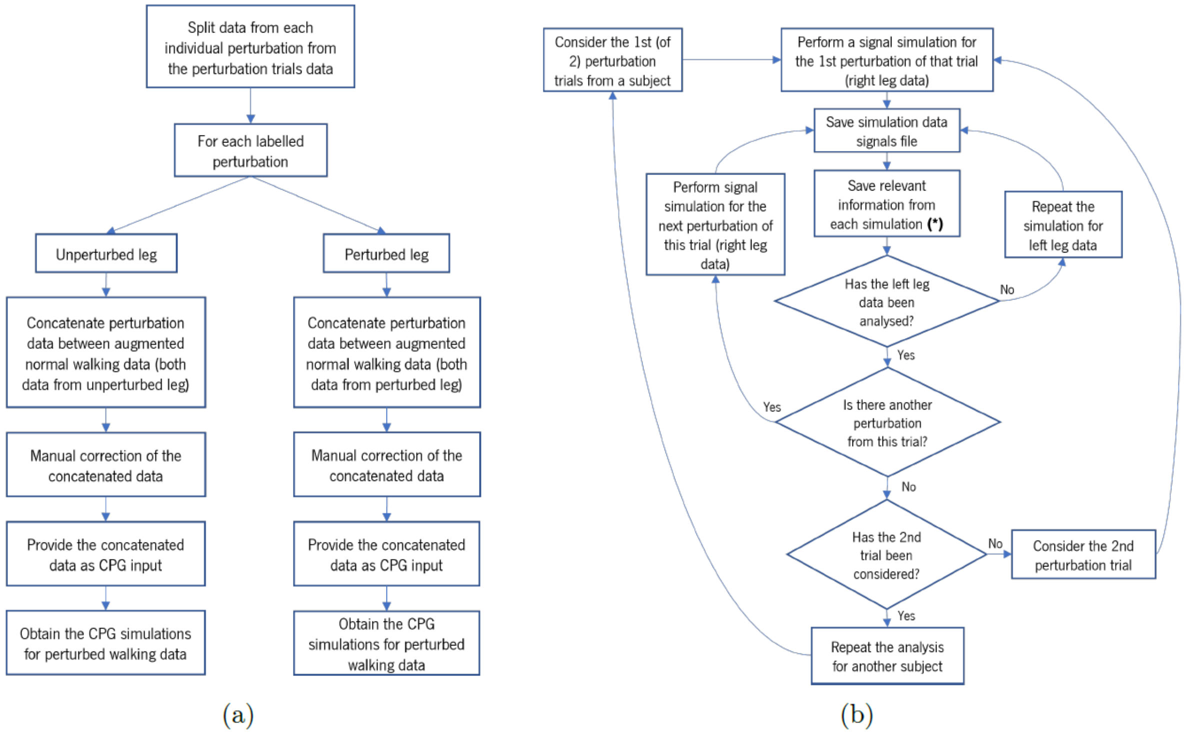

Figure 34. (a) Perturbed walking simulation data extraction. (b) Description of the steps taken to perform the CPG simulations. (*) Information relating to the perturbation onset timestamp.

6.3.3. Threshold Algorithm Parameters Definition

Since the goal of this detection was to be subject-specific, the criterion for threshold definition was based on the analysis of the gait signals from each subject individually. As such, thresholds were empirically determined for each participant based on the CPG's prediction error signal produced during the simulation using normal walking data. To this end, data from a normal walking trial were augmented by a factor of 50 (to allow sufficient time for the error signal to stabilise) and provided as input to the CPG. Based on the time-course evolution of the respective error signal produced, different threshold values were tested in order to ascertain their respective false perturbation detection. The thresholds were applied 80 seconds after the start of the simulation since the error signal started to stabilise around this timestamp across all the subjects. It is noteworthy that although the frequencies were considered to achieve convergence instantaneously, as previously mentioned, the amplitude of the CPG output took longer to adjust to the input signal and consequently achieve steady-state error values.

Then, a pair of upper and lower threshold values were obtained, in which no false perturbations were detected. These threshold values were relatively close to the error signal with some margin to account for subtle deviations and thus were selected for the further perturbation detection algorithm. Essentially, considering that the threshold parameters defined are adapted to the normal gait of each subject, a significant deviation of the normal gait, which can be induced by a perturbation, would cause the error signal to surpass one of the threshold values and thus detect a perturbation.

For the fixed threshold algorithm, the upper and lower threshold values were varied from 0.2 with increments of 0.01 and from -0.2 with increments of -0.01, respectively. When the first pair of fixed thresholds with no false perturbations detected was obtained, a tolerance absolute value of 0.05 was added to both thresholds. Figure 35 presents the threshold values selected for one subject, considering the knee angle variable, according to the criteria previously defined. In this case, the upper and lower threshold values were defined as 0.3 and -0.35. Note that the perturbation detection signal, which is the black signal in the graphic, was maintained at 0, since no false perturbations were detected.

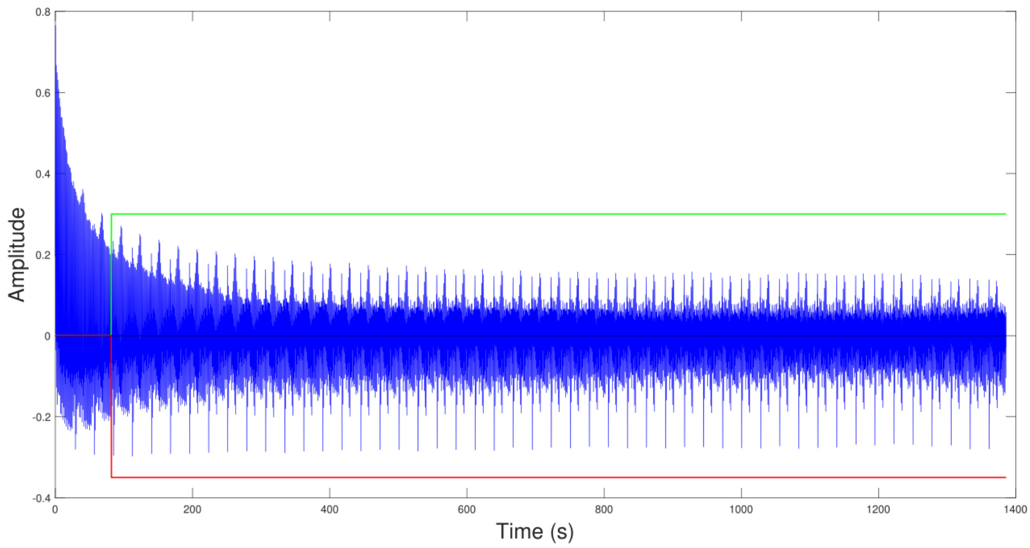

Figure 35. Fixed threshold definition based on the error signal between the CPG output and the actual normal walking signal (blue). The green and red signals represent the upper and lower threshold, respectively. The black signal depicts the perturbation detection signal, which is 0 when no perturbation is detected and 1 upon a perturbation detection.

The adaptive threshold definition was based on the variation of the standard deviation's (σ) multiplier factor. As such, for each subject, the multiplier factors associated to the upper (a) and lower (b) adaptive thresholds were varied from 2 with increments of 0.1 and from -2 with increments of -0.1, respectively. When the first pair of adaptive thresholds with no false perturbations detected was obtained, a tolerance absolute value of 0.1 was added to both a and b multiplier factors. In addition, for the adaptive threshold, it was also necessary to define the number of samples from the window preceding the current sample (window size) to compute the μ and σ threshold parameters. The number of samples chosen influenced the threshold calculated and was tested initially with 100 samples, as it was the minimum number of samples tested in [13], with increments of 50 samples. Considering the knee angle signal, 200 samples were empirically chosen for the most part of the participants. A window size of 400 samples was selected for the shank angular velocity variable across all the participants.

Figure 36 depicts the adaptive threshold values selected for one subject, considering the knee angle variable, and according to the criteria previously defined. In this case, the upper and lower threshold values were defined as $\mu + 3\sigma$ and $\mu - 4.1\sigma$, respectively. Similarly to the fixed threshold, the perturbation detection signal, which is the black signal on the graphic, was maintained at 0, since no false perturbations were detected.

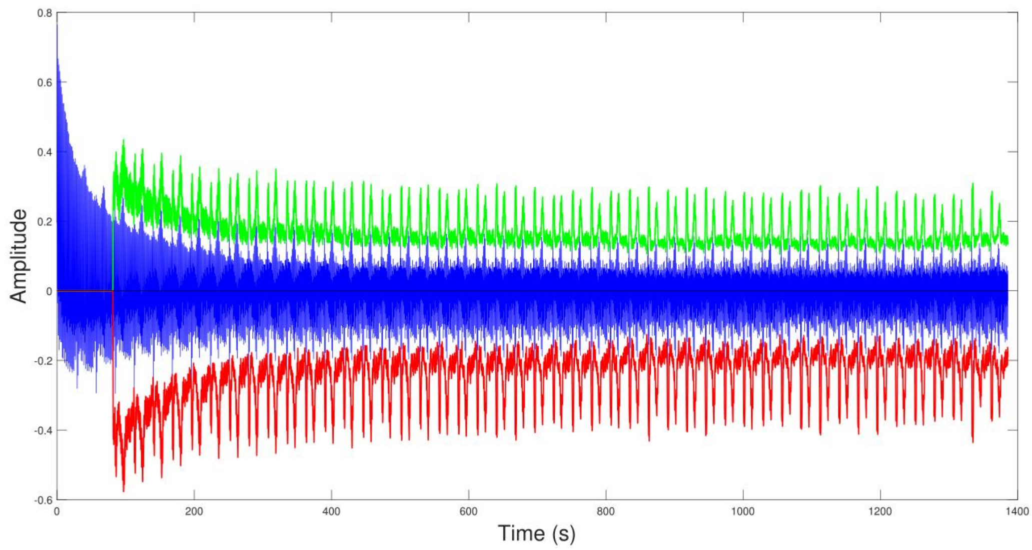

Figure 36. Adaptive threshold definition based on the error signal between the CPG output and the actual normal walking signal (blue). The green and red signals represent the upper and lower threshold, respectively. The black signal depicts the perturbation detection signal, which is 0 when no perturbation is detected and 1 upon a perturbation detection.

The selection of the threshold parameters for the shank angular velocity variable was similar to the process adopted for the knee angle. The fixed and adaptive thresholds defined for each subject based on the knee angle and shank angular velocity normal walking data are presented in Table 21.

Table 21. Knee angle and shank angular velocity threshold parameters attributed to all the subjects

Subject	Knee angle					Shank angular velocity				
	Fixed threshold		Adaptive threshold			Fixed threshold		Adaptive threshold		
	Upper	Lower	Upper (μ + aσ)	Lower (μ - bσ)	Window size	Upper	Lower	Upper (μ + aσ)	Lower (μ - bσ)	Window size
1	0.3	-0.35	$\mu + 3\sigma$	$\mu - 4.1\sigma$	200	0.35	-0.27	$\mu + 4.4\sigma$	$\mu - 4.8\sigma$	400
2	0.25	-0.25	$\mu + 2.8\sigma$	$\mu - 3.2\sigma$	200	0.27	-0.27	$\mu + 3.6\sigma$	$\mu - 4.8\sigma$	400
3	0.25	-0.25	$\mu + 3\sigma$	$\mu - 3.7\sigma$	200	0.3	-0.25	$\mu + 4.8\sigma$	$\mu - 4.2\sigma$	400
4	0.25	-0.25	$\mu + 3\sigma$	$\mu - 3.5\sigma$	200	0.25	-0.25	$\mu + 4.1\sigma$	$\mu - 4.2\sigma$	400
5	0.3	-0.25	$\mu + 3\sigma$	$\mu - 3.5\sigma$	250	0.35	-0.25	$\mu + 4.5\sigma$	$\mu - 4.6\sigma$	400
6	0.3	-0.25	$\mu + 3.6\sigma$	$\mu - 3.8\sigma$	200	0.33	-0.3	$\mu + 4.5\sigma$	$\mu - 4.9\sigma$	400
7	0.3	-0.35	$\mu + 3.7\sigma$	$\mu - 4.1\sigma$	200	0.3	-0.3	$\mu + 4.3\sigma$	$\mu - 4.1\sigma$	400
8	0.2	-0.2	$\mu + 2.8\sigma$	$\mu - 3.3\sigma$	200	0.3	-0.3	$\mu + 4.2\sigma$	$\mu - 5.5\sigma$	400
9	0.3	-0.35	$\mu + 3.1\sigma$	$\mu - 4.4\sigma$	200	0.33	-0.4	$\mu + 4\sigma$	$\mu - 4.9\sigma$	400

Comparisons between the threshold parameters present in Table 21 suggest that higher absolute threshold values and window sizes were adopted for the shank angular velocity signal rather than the knee angle variable. This may be related to the fact that the shank angular velocity signal is more complex than the knee angle signal. The shank angular velocity signal (Figure 25) values within one gait cycle entail more variability than one gait cycle from the knee angle signal (Figure 24). As such, this increased complexity of the shank angular velocity variable may have increased its respective error between the actual signal and the respective CPG prediction during the simulations. In fact, to obtain similar RMSE values during the Normal Walking Testing simulations (Table 20), the shank angular velocity variable needed an additional oscillator in relation to the knee angle variable. Thus, the higher error values produced by the shank angular velocity signal required increased threshold values towards the perturbation detection in order to mitigate the false perturbation detection. Additionally, a higher window size was demanded for the shank angular velocity to account for the higher complexity and variability of the signal during the threshold parameters computation.

6.3.4. Online Perturbation Detection

Figure 37 presents the variation of the real and the CPG output signals, upon the occurrence of a slip-like perturbation. Before the perturbation occurrence, the CPG output was similar to the actual signal. However, when the perturbation was provoked, the real knee angle signal pattern was altered, which caused its consequent deviation from the CPG output. Since the CPG oscillators did not recognise the new frequency components and signal patterns introduced by the perturbation, the network output entered a transient state to try to adapt to the perturbation signal. Nevertheless, since the subject rapidly recovered from the perturbation and promptly regained the normal gait, the perturbation pattern was removed from the signal as the real knee angle signal returned to its steady-state. This caused the CPG output to quickly re-adapt to its previous learned state.

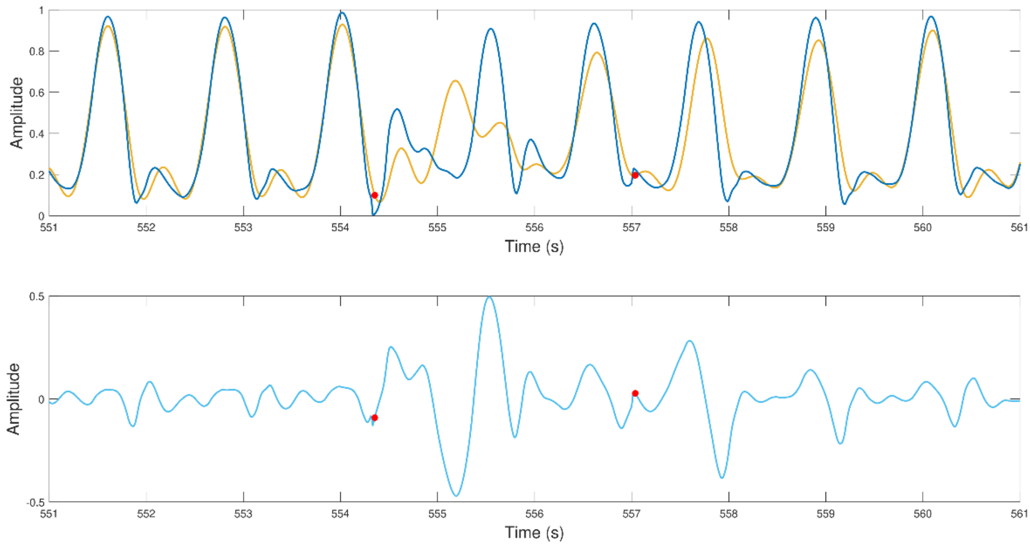

Figure 37. Variation of the CPG output upon the occurrence of a slip-like perturbation. Top: the real (blue) and CPG output (yellow) knee angle signals. Bottom: the error produced between the real and CPG output knee angle signal. The red dots in both top and bottom graphics depict the samples from the start and end of the perturbation.

Considering the same perturbation, Figure 38 highlights the use of the fixed threshold algorithm to detect the slip-like perturbation onset. Herein, the algorithm detected the perturbation 0.7537 seconds following its onset. Since the detection time was below 1 second, it was possible to acknowledge that the perturbation was successfully detected. However, the algorithm also detected 2 false perturbations, accounting for a total of 23 misclassified samples (false alarms). These were considered false perturbations since they were detected either: i) before the perturbation occurrence; or ii) more than 1 second after its onset. Conversely, as shown in Figure 39, the adaptive threshold algorithm was able to detect the perturbation in a shorter time, 0.1392 seconds, and without any false perturbation detected. In this case, the contextual information provided by the adaptive thresholds allowed the algorithm to avoid the misclassification of perturbations. This is due to the fact that the thresholds computed accounted for the variability of previous samples from the error signal. As such, the error signal peaks following the perturbation peak were associated with higher absolute threshold values and thus were not misclassified.

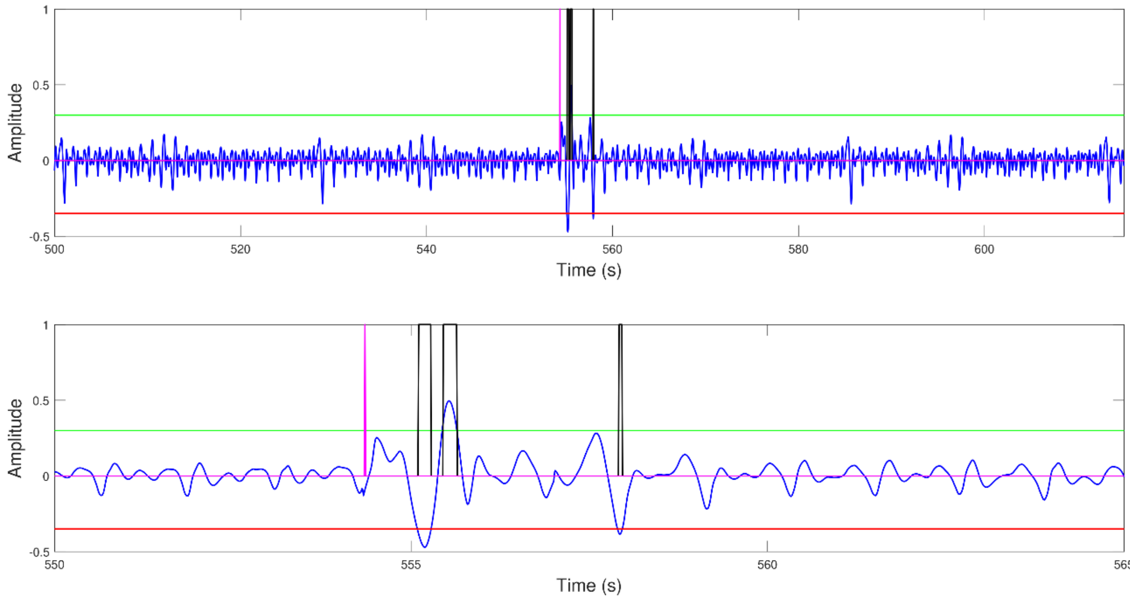

Figure 38. Detection of the perturbation onset based on the fixed threshold algorithm. The top panel is expanded into the bottom panel to simplify the graphical interpretation. The fixed upper (green) and lower (red) thresholds are used to classify the error signal (blue). If 3 or more consecutive samples of the error signal surpass one threshold, a perturbation is detected (black signal changes from 0 to 1). The lilac signal's peak represents the onset timestamp of the perturbation.

Then, the detection performance of both threshold-based algorithms was also tested using data from the remaining perturbations in order to obtain the global MDT and mean number of False Perturbations. From the 23 perturbed walking simulations obtained from the group of 9 subjects, the detection performance of both fixed and adaptive threshold algorithms was tested. In addition, it was also ascertained the ability of the knee angle and shank angular velocity variables to perform the perturbation detection, regarding each threshold algorithm individually. The performance of the perturbation detection was obtained considering: i) MDT, which is the mean time taken by the algorithm to detect the perturbation occurrence in relation to the real perturbation onset timestamp; ii) Detection accuracy, i.e., the number of real perturbations successfully detected by the algorithm among all the 23 real perturbations; iii) Mean number of false perturbations detected per perturbed walking simulation data and the respective mean number of samples (false alarms) associated with each false perturbation detected.

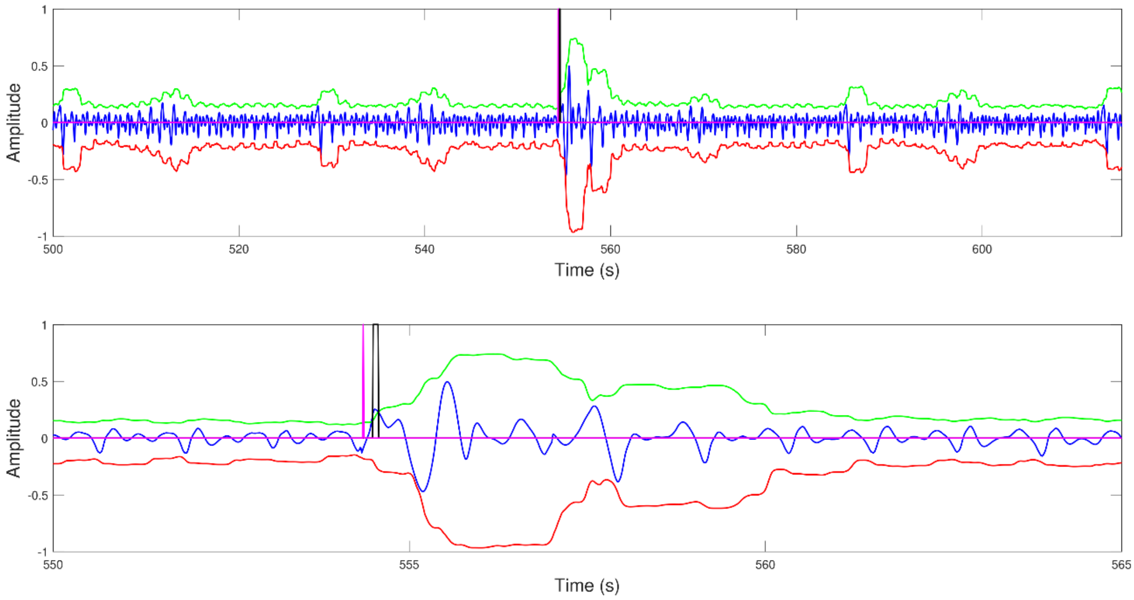

Figure 39. Detection of the perturbation onset based on the adaptive threshold algorithm. The top panel is expanded into the bottom panel to simplify the graphical interpretation. The adaptive upper (green) and lower (red) thresholds are used to classify the error signal (blue). If 3 or more consecutive samples of the error signal surpass one threshold, a perturbation is detected (black signal changes from 0 to 1). The lilac signal's peak represents the onset timestamp of the perturbation.

6.3.4.1. Knee angle

Regarding to the use of knee angle data to detect the perturbations, Table 22 depicts the performances obtained for the fixed and adaptive threshold algorithms. Both threshold algorithms achieved a successful detection of the real perturbations with accuracy values above 80%. However, for each real perturbation successfully identified, a mean of 1.78 and 1.608 false perturbations were detected for the fixed and adaptive thresholds, respectively. Although for some perturbed walking simulation data no false perturbation was detected, some had an increased false perturbation detection rate, which in turn increased the global mean of false perturbations. The fixed threshold obtained a considerable higher MDT in comparison to the adaptive threshold, with a difference of 180 ms. In addition, the accuracy of the detection was slightly higher for the adaptive threshold, by around 4%. Furthermore, even though the mean number of false perturbations was slightly higher for the fixed threshold, the mean number of samples of each false perturbation detected by the adaptive threshold algorithm (2.946) was considerably smaller than the one detected by the fixed threshold algorithm (9.293). This suggests that once a false perturbation was detected by the adaptive threshold algorithm, it rapidly stopped detecting that perturbation, within a mean lower than 3 samples. Overall, the adaptive threshold algorithm had a considerable better perturbation detection performance than the fixed threshold algorithm.

Table 22. Knee angle detection performance based on the type of threshold algorithm

Type of threshold	MDT (s)	Detection accuracy (%)	False perturbations detected (Mean)	False alarms per false perturbation (Mean)
Fixed	0.521	80.435	1.780	9.293
Adaptive	0.341	84.783	1.608	2.946

Nonetheless, the individual detection performance of the perturbed and unperturbed knee angle data was also evaluated for each type of threshold algorithm, which is depicted in Table 23. This allowed to ascertain which leg's data had a more prominent detection role.

For the fixed threshold, there were observed few differences between the use of perturbed and unperturbed knee angle data. The perturbed knee angle data achieved a smaller MDT (by a mean difference of 25 ms) and a slightly smaller mean number of both false perturbations detected and their respective false alarms. However, a marginally higher accuracy was obtained for the unperturbed knee angle data (82.609%) in comparison with the perturbed knee angle data (78.261%).

According to the results obtained for the adaptive threshold, a substantial difference was observed between the MDT values obtained. For the perturbed leg data, a mean duration 250 ms was needed to detect the perturbation onset, whereas for the unperturbed leg data a MDT of 419 ms was observed. Additionally, the mean number of false perturbations detected was considerably inferior using perturbed leg data. In fact, less than one false perturbation in average (0.652) was detected per each real perturbation identified, which contrast with the mean 2.565 false perturbations detected using data from the unperturbed leg. Furthermore, the mean number of samples associated with each false perturbation detected (false alarms) was lower for the perturbed leg data (2.6) than for the unperturbed leg data (3.034). However, the accuracy of 91.304% achieved with the unperturbed leg data was superior to the 78.261% obtained using the perturbed leg data.

Table 23. Knee angle detection performance based on the type of leg and type of threshold algorithm

Type of threshold	Leg	MDT (s)	Detection accuracy (%)	False perturbations detected (Mean)	False alarms per false perturbation (Mean)
Fixed	Perturbed	0.508	78.261	1.696	8.513
	Unperturbed	0.533	82.609	1.870	10.000
Adaptive	Perturbed	0.250	78.261	0.652	2.600
	Unperturbed	0.419	91.304	2.565	3.034

Considering the results presented above, the adaptive threshold showed a general better perturbation detection performance than the fixed threshold. In addition, the perturbed knee angle data presented an overall higher perturbation detection performance in comparison to the unperturbed leg data. Despite the detection accuracy obtained for the former was lower, the perturbed leg data presented smaller MDT values, lower mean of false perturbations detected and fewer samples for each false perturbation detected. Therefore, considering the knee angle variable, monitoring data from the perturbed leg using an adaptive threshold algorithm seems to be the most reliable option.

6.3.4.2. Shank angular velocity

Table 24 highlights the perturbation detection performance obtained for the fixed and adaptive threshold algorithms using shank angular velocity data. The detection accuracy of the real perturbations obtained for both threshold algorithms were below 80%. Although the fixed threshold achieved an overall accuracy of 78.261%, the adaptive threshold obtained a considerable smaller accuracy of 56.522%. Nevertheless, for each real perturbation successfully detected, a mean of 5.28 and 3.935 false perturbations were identified for the fixed and adaptive thresholds, respectively. Despite no false perturbations being detected for some perturbed walking simulation data, some of these data had a higher false perturbation detection rate, which caused the overall increase in the mean of false perturbations detected. The fixed threshold algorithm was associated with a substantial higher MDT in relation to the adaptive threshold, with a mean time difference of 192 ms. Moreover, the fixed threshold algorithm detected a considerable higher mean of both false perturbations and their false alarms, comparing to the adaptive threshold algorithm. This implied that once a false perturbation was detected by the adaptive threshold algorithm, it rapidly stopped detecting that perturbation, within a mean of around 3 samples.

Table 24. Shank angular velocity detection performance based on the type of threshold algorithm

Type of threshold	MDT (s)	Detection accuracy (%)	False perturbations detected (Mean)	False alarms per false perturbation (Mean)
Fixed	0.534	78.261	5.280	6.914
Adaptive	0.342	56.522	3.935	3.155

Additionally, the perturbation detection performance was compared between the perturbed and unperturbed shank angular velocity data. Table 25 presents the performance results obtained for the perturbed and unperturbed shank angular velocity data using the fixed and adaptive threshold algorithms.

For the fixed threshold algorithm, it was possible to acknowledge that the unperturbed leg data achieved a better detection performance with a remarkably lower MDT, a considerable higher accuracy, and a lower mean number of false perturbations identified per real perturbation detected. Nevertheless, the mean number of false alarms per false perturbation was slightly lower for the perturbed leg.

Considering the results from the adaptive threshold algorithm, the unperturbed leg data obtained the best performance. This is depicted by the lower MDT (266 ms) and the significantly higher accuracy (73.913%) achieved in comparison to the MDT (486 ms) and the accuracy (39.13%) of the adaptive threshold. Nonetheless, the use of the unperturbed leg data was associated with a higher number of false perturbations detected and with a slightly higher number of false alarms per false perturbation.

Table 25. Shank angular velocity detection performance based on the type of leg and type of threshold algorithm

Type of threshold	Leg	MDT (s)	Detection accuracy (%)	False perturbations detected (Mean)	False alarms per false perturbation (Mean)
Fixed	Perturbed	0.795	73.913	5.870	6.067
	Unperturbed	0.301	82.609	4.696	7.972
Adaptive	Perturbed	0.486	39.130	2.696	2.724
	Unperturbed	0.266	73.913	5.174	3.420

Regarding to the results obtained using the shank angular velocity data, the adaptive threshold algorithm led to the decrease of MDT and to an overall decrease of the number of false perturbations and their respective number of false alarms. However, the accuracy achieved with the adaptive threshold algorithm was considerably lower in comparison with the fixed threshold. The unperturbed leg shank angular velocity data presented an overall better detection performance in comparison to the perturbed leg data. Although the former detected a generally higher number of false perturbations and false alarms per false perturbation, their MDT and accuracy results were considerably better than for the perturbed leg data. Thus, for the shank angular velocity variable, the most reliable option seems to be the monitoring of the unperturbed leg. However, the use of both fixed and adaptive threshold algorithms appeared to have their advantages and disadvantages. While the fixed threshold allowed for a higher accuracy and lower mean number of false perturbations detected, the adaptive threshold provided a lower MDT and a lower number of false alarms per false perturbation. As such, it is necessary to perform a trade-off between the detection accuracy, the time taken to perform the detection and the number of false detections towards the selection of the most suitable type of threshold algorithm for the shank angular velocity data. Nonetheless, the mean number of false alarms obtained per false perturbation for the fixed threshold algorithm was considered exceedingly high with a mean of almost 8 false alarms per each false perturbation detected, which contrasts with the mean of 3.420 false alarms obtained for the adaptive threshold. This reveals that the fixed threshold approach is less capable of recognising that a false perturbation has been detected. Therefore, the contextual information provided by the adaptive threshold algorithm may play a crucial role towards the reliability of the perturbation detection. Despite the accuracy achieved with the adaptive threshold (73.913%) being lower than the one obtained for the fixed threshold (82.609%), according to the previously mentioned trade-off, the adaptive threshold algorithm seems to be the most reliable option to perform the perturbation detection using shank angular velocity data.

6.3.4.3. Comparative detection performance between the variables

Concerning the results obtained, it is possible to acknowledge that the adaptive threshold was responsible to generally lower the false detection rate, by considerably decreasing the mean number of false perturbations detected and their respective number of false alarms. Despite the adaptive threshold not always increasing the accuracy in comparison with the fixed threshold, the former algorithm was also able to substantially decrease the MDT. For instance, although the knee angle data from the perturbed leg obtained similar accuracies for both types of threshold algorithms (Table 23), the adaptive threshold led to a lower MDT, mean number of false perturbations detected, and mean number of false alarms per false perturbation. Thus, the adaptive threshold algorithm achieved a generally better performance than the fixed threshold algorithm, which may be mostly due to the contextual information it provides about previous samples during the threshold definition.

While data from the perturbed leg allowed to obtain a better performance for the knee angle variable, the shank angular velocity achieved a greater performance with the unperturbed leg information. According to these findings, it is highlighted the need to initially consider data from both legs in order to select the leg that should be monitored for each selected variable. In fact, data from one leg may achieve a considerably better perturbation detection performance than data from the other one (Table 25). While the primary response to a slip perturbation is attributed to the perturbed leg [9], the unperturbed leg has a strong role to counteract the LOB induced by the slip event and should be included in the perturbation detection analysis [137].

Table 26 presents the best detection performances obtained for both the knee angle and the shank angular velocity variables. For both variables, the adaptive threshold algorithm was considered the most suitable to perform the perturbation detection. Both MDT values reported were similar, with a difference of around 16 ms and the accuracies obtained differed with a percentage shortly above 4%. However, a substantial difference was observed between the mean number of false perturbations detected. While for each correctly detected perturbation the shank angular velocity from the unperturbed leg detected a mean of 5 false perturbations, the knee angle from the perturbed leg detected less than one false perturbation (0.652). Moreover, the mean number of false alarms detected for each false perturbation was slightly lower for the knee angle variable. Hence, from the study conducted, monitoring the knee angle from the perturbed leg using an adaptive threshold algorithm, appears to be the best option towards the detection of slip perturbations during walking.

Table 26. Best detection performances obtained for the knee angle and shank angular velocity variables

Variable	Type of threshold	Leg	MDT (s)	Detection accuracy (%)	False perturbations detected (Mean)	False alarms per false perturbation (Mean)
Knee angle	Adaptive	Perturbed	0.250	78.261	0.652	2.600
Shank angular velocity	Adaptive	Unperturbed	0.266	73.913	5.174	3.420

Although the false detection rate obtained with the adaptive threshold algorithm using perturbed knee angle data was the lowest, future work must be performed to lower the mean number of false perturbations detected. As such, the algorithm must be further optimised in order to only account for the detection of the real perturbations.

6.3.4.4. Comparative detection performance with the detection requirements stipulated

Considering that the practical work performed in this dissertation was aimed at performing the detection of slip-like perturbations and did not address the actuation stage of the fall prevention strategy, only the fulfilment of the detection requirements was addressed.

According to the fall prevention strategy conceived, a maximum time period of 360 ms after the perturbation onset was required for the perturbation detection. Considering that the MDT values associated with the overall best performances obtained for the knee angle and shank angular velocity variables were 250 ms and 266 ms, respectively, it was possible to acknowledge that the perturbations were on average timely detected. In fact, the perturbations were detected on average 100 ms earlier than the detection time stipulated on the strategy. This timely detection allows an additional lead-time to actuate the potential assistive device, which would be triggered upon the perturbation detection to early assist the subjects and help them to promptly recover the balance.

The best overall performance obtained using the knee angle variable also achieved a detection accuracy of real perturbations above the requirement of 75% (78.261%). Indeed, the monitoring of the knee angle from the perturbed leg using an adaptive threshold algorithm allowed to roughly detect 8 out of 10 slip-induced LOBs. Conversely, the overall best performance obtained for the shank angular velocity variable was below 75%, although by close margin (73.913%).

The knee angle's best performance was also characterised by the lowest mean number of false perturbations detected (0.652) and mean number of false alarms per false perturbation (2.6). Hence, the false perturbation detection requirement was also fulfilled, since less than one false perturbation was detected per correct perturbation identified. In fact, according to the results, for each 10 correct perturbations detected, only an estimated number of 6 false perturbation are identified. However, the best overall performance obtained using the shank angular velocity data comprised the mean of 5.174 false perturbations identified per correct perturbation detected, which was far from fulfilling the false perturbation detection requirement.

Considering that the best overall performance obtained for the knee angle variable was able to fulfil all the slip perturbation detection requirements, the perturbation detection performance was considered acceptable. The achievement of this goal proves the effectiveness of simple adaptive threshold-based algorithms to perform a timely and subject-specific detection of slip perturbations based on human kinematic data and paves the way towards the optimisation of this algorithm to achieve optimal performances. For instance, in order for the algorithm to be able to accurately monitor the occurrence of slip perturbations in real-life, the number of false perturbations detected must be lowered. Future work must focus on optimising the adaptive threshold algorithm to mitigate the false perturbation detection and attempt to increase the detection accuracy of real perturbations.

7. Conclusions

Falls are one of the leading causes of unintentional injury deaths worldwide. These harmful events mostly affect the elderly, which entail the highest fall risk due to the cognitive, physical, and sensory deficits associated with the ageing process. Slip-like perturbations have been widely addressed in the scientific literature as they were shown to be the main precursors to fall events. Hence, wearable sensors and assistive robotic devices may be coupled to allow the timely detection of these gait perturbations and provide effective mechanical countermeasures to help the subject regain balance, respectively.

In this regard, this dissertation developed a proof-of-concept slip-related fall prevention strategy based on the human biomechanical responses to these gait perturbations highlighted in the scientific literature. This strategy was divided into detection and actuation stages. The detection of slip perturbations was achieved with an adaptive threshold algorithm that analyse the error produced between a kinematic signal and the same kinematic signal predicted by a biological-inspired CPG controller.

A state-of-art of fall risk assessment systems was firstly conducted in order to identify the main methods used to assess the fall risk, since, to the best of the author's knowledge, no study has previously addressed this issue. Most of the studies assessed the fall risk based on clinical scales by collecting kinematic or kinetic data from inertial and pressure sensors, respectively, generally placed in the upper body. Other studies performed fall risk assessment based on the detection of fall risk events by using EMG sensors on lower limb muscles. Machine Learning models were preferably adopted to classify the subject’s risk of fall. Considering that almost all studies performed internal validation of the developed fall risk assessment systems, a lack of external validation was remarkably noticed. This highlights the need for establishing an open access gold standard by which different fall risk assessment systems could be benchmarked.

Considering that previous literature studies underlined slips and trips as the main gait perturbations preceding falls, a subsequent state-of-art analysis was performed to survey the different methods and key experimental aspects to mimic these perturbations in laboratory conditions. Slip and trip perturbations were mostly provoked during overground walking conditions. However, the perturbation application during treadmill locomotion entails several advantages due to its ability to collect continuous walking patterns over long periods of time and deliver more unexpected perturbations. Studies attempted to mitigate the participant's prediction towards the perturbations' onset. Most studies perturbed only the right leg during the experimental trials and did not consider the laterality of the subjects. Despite most studies instructed participants to ambulate at their self-selected speed, literature evidence suggested that the walking speed should be adapted to each subject in order to create an equally challenging environment of perturbation delivery across all subjects.

The investigations concerning the human biomechanical responses to slip perturbations suggest the prominent role of both leading and trailing legs to counteract the slip perturbation. However, despite the considerable number of manuscripts that studied the slip event and its consequences on the human motion, there are still few slip-related fall prevention strategies developed.

Considering the limitations and evidence found in the scientific literature, a slip-related fall prevention strategy was proposed. The actuation stage considered the assistive torque supply on a single leg using a single assistive device, an orthosis, in order to reduce the complexity of the actuation to only the main joint that counteracts slip-induced LOBs. The strategy highlighted the need to provide a knee flexion moment to the leading leg, considering it to be the dominant leg, upon the occurrence of a slip-induced LOB provoked at the heel strike. The magnitude of the assistive knee flexor torque must be complementary to the torque generated by the subject's knee to counteract the slip. The detection stage considered the attractive properties associated with biological-inspired CPG controllers to monitor the quasi-periodic variables of the human locomotion and to help to timely detect gait perturbations. The occurrence of a perturbation rapidly increases the error produced between the monitoring signal and the signal predicted by the CPG, since CPGs do not recognise the abnormal patterns introduced by the disturbance. Simple threshold-based algorithms are then able to early detect the perturbation onset based on the error signal increase. The knee angle and shank angular velocity variables were selected as the most suitable kinematic variables to perform the detection of slip-induced LOBs, in light of the decision criteria applied. Furthermore, the definition of timings and requirements to be fulfilled for both stages based on the scientific literature allowed to conceptualise a fall prevention strategy that timely and effectively prevents slip-initiated falls.

Considering the literature evidence found, an experimental protocol was designed in order to collect data from healthy young subjects while dealing with unexpected slip-like perturbations during treadmill walking. This allowed to obtain a vast dataset with kinematic and physiological information concerning subjects' reactions to slip-induced LOB events. Some kinematic features obtained were used for the further perturbation detection algorithm analysis.

According to the trade-off analysis between the frequency convergence times and the mean error values produced during the simulations, CPGs with 3 and 4 oscillators were attributed to the knee angle and shank angular velocity variables, respectively. Overall, the CPG configurations chosen on the previous analysis were shown to accurately produce output signals with similar morphology and in phase to the signals from the selected kinematic variables. Concerning the perturbation detection, the performance was evaluated by considering the different combinations of the 2 kinematic variables selected, i.e., knee angle and shank angular velocity, 2 lower limbs (perturbed and unperturbed) and 2 types of threshold algorithms (fixed and adaptive threshold algorithms). Generally, a higher performance was obtained using the adaptive threshold rather the the fixed threshold algorithm. The best overall performance was achieved with the monitoring of the perturbed leg's knee angle using the adaptive threshold algorithm. This combination achieved a detection accuracy of real perturbations close to 80% (78.261%), a MDT of 250 ms and a mean number of 0.652 false perturbations detected for each correct perturbation detected. These results allowed to fulfil the detection requirements previously stipulated, which proves an acceptable performance of the perturbation detection algorithm implemented. However, in order to achieve an optimal performance, the mean number of false perturbations detected must be further reduced.

The work developed allowed to answer the RQs specified in Chapter 1:

- **RQ1:** What are the main fall risk assessment methods implemented in the scientific literature?

Chapter 2 answered this RQ. Concerning the literature search results, 2 main fall risk assessment methods were identified. The most widely adopted was the long-term assessment of fall risk and was based on clinical scales. This method consisted of the data collection from wearable sensors to predict subject's fall risk based on clinical scale scores. Thereby, subjects are allocated to either high or low fall risk category. This method will promote the decrease in long-term fall risk by enabling subjects to continuously carry out long-term fall risk assessments. The second method comprised a real-time fall risk assessment by means of the detection of fall risk events. Data from wearable sensors were used to detect unbalance situations and further identify fall risk events. This method will promote the decrease in short-term fall risk by enabling the real-time monitoring of subjects on a daily basis, providing subjects feedback as to when a fall risk event is taking place.

- **RQ2:** What are the key experimental methods implemented in the scientific literature to provoke artificial slip and trip perturbations?

Chapter 3 answered this RQ. The current state-of-the-art on provoking artificial slip and trip perturbations suggested that these perturbations are provoked during either treadmill or overground walking conditions. Slip perturbations were provoked during treadmill locomotion by changing the belt's acceleration or during overground walking by using: i) a movable platform; ii) a slippery solution; or iii) novel robotic devices. Treadmill trips were elicited by means of: i) changing belt acceleration; ii) using a brake-and-release-system; or iii) using a tripping device. Trips were provoked during overground locomotion by: i) triggering an obstacle; ii) manually placing an obstacle along the walking path; or iii) using a novel robotic device.

- **RQ3:** Which are the main aspects that a fall prevention strategy should include in terms of detection of slip perturbations and actuation upon slip-induced LOB events?

Chapter 4 answered this RQ. According to literature studies that address the human biomechanical responses to slip perturbations, a maximum detection and actuation times of 360 ms and 100 ms were delineated, respectively. Upon a slip perturbation at the heel strike, a knee orthosis would provide an assistive flexor moment to the perturbed limb, considering it to be the dominant limb. The flexor moment exerted would allow to bring the anteriorly displaced BOS back near the COM. The flexor moment magnitude must be complementary with respect to the torque generated at the subject's knee to counteract the slip. The slips were considered to be initiated at the heel strike, since previous research showed that this gait event is the most prominent event that onsets slips. The application of the assistive knee torque was considered to the perturbed leg in order to tackle the slip-induced LOB at its genesis and directly reduce its severity. The assistive actuation was provided to the dominant leg, considering it as the perturbed leg, since the non-dominant leg is already more used to provide the body support function in comparison with the dominant leg. Therefore, the hazard associated with the slip will be lessened if the assistive actuation was provided to the dominant leg.

- **RQ4:** Are the biological-inspired CPG controllers and the threshold-based algorithms able to effectively track human motion variables and timely detect slip perturbation occurrences, respectively?

Chapter 6 answered this RQ. According to the results obtained, the CPG algorithms were able to successfully produce an acceptable estimation of the monitoring signals. These biological-inspired controllers generated output signals with similar morphology and in phase with the knee angle and shank angular velocity variables, which is depicted by the relatively low mean error values obtained during the simulations. Furthermore, the adaptive threshold algorithm effectively detected the slip-induced LOBs. The best overall performance was obtained with the monitoring of the perturbed leg's knee angle using the adaptive threshold algorithm, which achieved a detection accuracy of real perturbations near 80% (78.261%), a MDT of 250 ms and a mean number of 0.652 false perturbations detected for each correct perturbation detected. These results suggest an acceptable performance of the perturbation detection algorithm implemented in light of the detection requirements previously specified.

7.1. Future work

Several improvement opportunities were identified along this dissertation, which should be addressed in future work.

Firstly, despite the low false detection rate achieved with the adaptive threshold algorithm using perturbed limb's knee angle data, the mean number of false perturbations detected must be further lowered. Hence, future work should focus on the optimisation of the adaptive threshold algorithm to improve the reliability of the perturbation detection towards the algorithm's adaptation to the real-world settings. In addition, artificial intelligence algorithms should be tested to understand their possible application and performance towards the slip-like perturbation detection.

Secondly, although the knee angle and shank angular velocity variables were selected based on decision criteria, more kinematic and biosignal-based variables should be addressed for perturbation detection. In fact, previous studies suggested that lower limb surface EMG data would provide a faster LOB detection than using kinematic data, considering that the sudden change of EMG patterns provoked by an unbalance event is faster than the change of inertial signal patterns [22,30,31,131].

Thirdly, since the threshold and the window size parameters were empirically determined, the optimal conditions may have not been addressed for each subject. As such, future work should attempt to find more objective and automatic procedures to compute optimal parameters. This would potentially increase the perturbation detection performance and pave the way for a future perturbation detection algorithm that would not be affected by the inter-subject variability. Although the goal of this dissertation was to develop a proof-of-concept subject-specific perturbation detection, future work should also consider the development of an inter-subject perturbation detection approach. In addition, although the number of acceptable warnings, r, was defined based on a previous study, its value was not optimised. Hence, future work should test different values of r and select its optimal value based on the trade-off between the false detection rate, the MDT and the accuracy values obtained.

Furthermore, although some of the initial conditions attributed to the adaptive oscillators, such as the γ, τ and η parameters, were equal among all the oscillators (based on a previous study [156]), future work should consider the test of new values of these initial conditions. This may allow to improve the quality of the CPG prediction of the monitoring signals.

Although, slip-like perturbations were delivered under various conditions of gait event onset, treadmill inclination and gait speed, only slips at the heel strike during normalised speed and level ground, i.e., 0% inclination, walking conditions were considered for perturbation detection. These walking conditions were chosen as they depict the most likely scenario for participants to experience a slip perturbation during their daily-life [5,6,70]. However, future work could address the detection of slip perturbation under other walking conditions.

In addition, considering that the elderly are the targeted population of the fall prevention strategy conceived, normal and perturbed walking data from these subjects should be collected in the future in order to tune and test the oscillator networks. In addition, the data collection should also consider subjects ambulating while wearing the assistive device, since the gait alterations it provokes must be accounted by the algorithms towards perturbation detection.

Moreover, it is possible to not only increase the reliability of slip event detection, but also to detect other types of perturbations by performing the gait event detection. For instance: i) a slip would be identified if the heel strike or toe-off events of the leading leg were detected upon the detection of a perturbation; and ii) a trip would be identified in the cases where a perturbation was detected while the leading leg was identified to be in the swing phase. Although the objective of this dissertation was to only perform the detection of slip perturbations, future work should broaden the fall prevention strategy to consider different types of gait perturbations, taking advantage of the gait event detection.

Considering the actuation stage, further tests should be conducted with a powered knee orthosis in order to ascertain the capability of the assistive device to be triggered and provide the assistive knee flexor torque under the actuation time defined in the fall prevention strategy (100 ms).

Finally, future work should integrate the CPG controller algorithm into an electronic development board and connect it to the knee orthosis system. This would allow to: i) close the loop from the real-time detection of slip-induced LOBs to the actuation of the orthosis' flexor moments; and further ii) validate the fall prevention strategy conceived.

References

1. WHO. Falls [Internet]. 2021. Available from: https://www.who.int/news-room/fact-sheets/detail/falls
2. McCrum C, Gerards MHG, Karamanidis K, Zijlstra W, Meijer K. A systematic review of gait perturbation paradigms for improving reactive stepping responses and falls risk among healthy older adults. Eur Rev Aging Phys Act [Internet]. 2017;14(1). Available from: https://www.scopus.com/inward/record.uri?eid=2-s2.0-85014356079&doi=10.1186%2Fs11556-017-0173-7&partnerID=40&md5=f1c091b05aec0ea76dee040e95ddd9af
3. Boyé NDA, Mattace-Raso FUS, Van der Velde N, Van Lieshout EMM, De Vries OJ, Hartholt KA, et al. Circumstances leading to injurious falls in older men and women in the Netherlands. Injury. 2014 Aug;45(8):1224–30.
4. Berg WP, Alessio HM, Mills EM, Tong C. Circumstances and consequences of falls in independent community-dwelling older adults. Age Ageing. 1997 Jul;26(4):261–8.
5. Chang W-R, Leclercq S, Lockhart TE, Haslam R. State of science: occupational slips, trips and falls on the same level. Ergonomics. 2016 Jul;59(7):861–83.
6. Courtney TK, Sorock GS, Manning DP, Collins JW, Holbein-Jenny MA. Occupational slip, trip, and fall-related injuries–can the contribution of slipperiness be isolated? Ergonomics. 2001 Oct;44(13):1118–37.
7. Klenk J, Schwickert L, Palmerini L, Mellone S, Bourke A, Ihlen EAF, et al. The FARSEEING real-world fall repository: a large-scale collaborative database to collect and share sensor signals from real-world falls. Eur Rev aging Phys Act Off J Eur Gr Res into Elder Phys Act. 2016;13:8.
8. Rubenstein LZ. Falls in older people: epidemiology, risk factors and strategies for prevention. Age Ageing. 2006 Sep;35 Suppl 2:ii37–41.
9. Cham R, Redfern MS. Lower extremity corrective reactions to slip events. J Biomech [Internet]. 2001;34(11):1439–45. Available from: https://www.sciencedirect.com/science/article/pii/S0021929001001166
10. Martelli D, Aprigliano F, Tropea P, Pasquini G, Micera S, Monaco V. Stability against backward balance loss: Age-related modifications following slip-like perturbations of multiple amplitudes. Gait Posture [Internet]. 2017;53:207–14. Available from: https://www.scopus.com/inward/record.uri?eid=2-s2.0-85012298574&doi=10.1016%2Fj.gaitpost.2017.02.002&partnerID=40&md5=aa156a9b9c7602f0d2f7878e397236a0
11. Aprigliano F, Micera S, Monaco V. Pre-Impact Detection Algorithm to Identify Tripping Events Using Wearable Sensors. SENSORS. 2019;19(17).
12. Potocanac Z, Pijnappels M, Verschueren S, van Dieen J, Duysens J. Two-stage muscle activity responses in decisions about leg movement adjustments during trip recovery. J Neurophysiol. 2016 Jan;115(1):143–56.
13. Tropea P, Vitiello N, Martelli D, Aprigliano F, Micera S, Monaco V. Detecting Slipping-Like Perturbations by Using Adaptive Oscillators. Ann Biomed Eng. 2015;43(2):416–26.
14. Bucher D. Central Pattern Generators. In: Squire LR, editor. Encyclopedia of Neuroscience [Internet]. Oxford: Academic Press; 2009. p. 691–700. Available from: https://www.sciencedirect.com/science/article/pii/B9780080450469019446
15. Dietz V. Spinal cord pattern generators for locomotion. Clin Neurophysiol Off J Int Fed Clin Neurophysiol. 2003 Aug;114(8):1379–89.
16. Ronsse R, Vitiello N, Lenzi T, van den Kieboom J, Chiara Carrozza M, Ijspeert AJ. Adaptive

oscillators with human-in-the-loop: Proof of concept for assistance and rehabilitation. In: 2010 3rd IEEE RAS EMBS International Conference on Biomedical Robotics and Biomechatronics. 2010. p. 668–74.

17. Frigon A, Rossignol S. Experiments and models of sensorimotor interactions during locomotion. Biol Cybern. 2006 Dec;95(6):607–27.
18. Rucco R, Sorriso A, Liparoti M, Ferraioli G, Sorrentino P, Ambrosanio M, et al. Type and Location of Wearable Sensors for Monitoring Falls during Static and Dynamic Tasks in Healthy Elderly: A Review. SENSORS. 2018;18(5).
19. Montesinos L, Castaldo R, Pecchia L. Wearable inertial sensors for fall risk assessment and prediction in older adults: A systematic review and meta-analysis. IEEE Trans Neural Syst Rehabil Eng. 2018;26(3):573–82.
20. Rajagopalan R, Litvan I, Jung T-P. Fall Prediction and Prevention Systems: Recent Trends, Challenges, and Future Research Directions. SENSORS. 2017 Nov;17(11).
21. Saadeh W, Butt SA, Altaf MAB. A Patient-specific single sensor iot-based wearable fall prediction and detection system. IEEE Trans Neural Syst Rehabil Eng. 2019;27(5):995–1003.
22. Leone A, Rescio G, Giampetruzzi L, Siciliano P. Smart EMG-based Socks for Leg Muscles Contraction Assessment. In: 2019 IEEE International Symposium on Measurements Networking (M N). 2019. p. 1–6.
23. Rivolta MW, Aktaruzzaman M, Rizzo G, Lafortuna CL, Ferrarin M, Bovi G, et al. Automatic vs. clinical assessment of fall risk in older individuals: A proof of concept. In: 2015 37th Annual International Conference of the IEEE Engineering in Medicine and Biology Society (EMBC). 2015. p. 6935–8.
24. Tang W, Fulk G, Zeigler S, Zhang T, Sazonov E. Estimating Berg Balance Scale and Mini Balance Evaluation System Test Scores by Using Wearable Shoe Sensors. In: 2019 IEEE EMBS International Conference on Biomedical Health Informatics (BHI). 2019. p. 1–4.
25. Parvaneh S, Najafi B, Toosizadeh N, Riaz IB, Mohler J. Is there any association between ventricular ectopy and falls in community-dwelling older adults? In: 2016 Computing in Cardiology Conference (CinC). 2016. p. 433–6.
26. Annese VF, De Venuto D. FPGA based architecture for fall-risk assessment during gait monitoring by synchronous EEG/EMG. In: 2015 6th International Workshop on Advances in Sensors and Interfaces (IWASI). 2015. p. 116–21.
27. Rivolta MW, Aktaruzzaman M, Rizzo G, Lafortuna CL, Ferrarin M, Bovi G, et al. Evaluation of the Tinetti score and fall risk assessment via accelerometry-based movement analysis. Artif Intell Med. 2019;95:38–47.
28. Shahzad A, Ko S, Lee S, Lee J, Kim K. Quantitative Assessment of Balance Impairment for Fall-Risk Estimation Using Wearable Triaxial Accelerometer. IEEE Sens J. 2017;17(20):6743–51.
29. Saporito S, Brodie MA, Delbaere K, Hoogland J, Nijboer H, Rispens SM, et al. Remote timed up and go evaluation from activities of daily living reveals changing mobility after surgery. Physiol Meas. 2019 Mar;40(3).
30. Rescio G, Leone A, Caroppo A, Siciliano P. A preliminary study on fall risk evaluation through electromiography systems. In: 2015 International Conference on Interactive Mobile Communication Technologies and Learning (IMCL). 2015. p. 219–21.
31. Leone A, Rescio G, Siciliano P. Fall risk evaluation by surface electromyography technology. In: 2017 International Conference on Engineering, Technology and Innovation (ICE/ITMC). 2017. p. 1092–5.
32. Buisseret F, Catinus L, Grenard R, Jojczyk L, Fievez D, Barvaux V, et al. Timed Up and Go and Six-Minute Walking Tests with Wearable Inertial Sensor: One Step Further for the Prediction of the Risk of Fall in Elderly Nursing Home People. Sensors (Basel). 2020 Jun;20(11).

33. Yang Z, Song C, Lin F, Langan J, Xu W. A Smart Environment-Adapting Timed-Up-and-Go System Powered by Sensor-Embedded Insoles. IEEE INTERNET THINGS J. 2019;6(2):1298–305.
34. Selvaraj M, Baltzopoulos V, Shaw A, Maganaris CN, Cullen J, Obrien T, et al. Stair fall risk detection using wearable sensors. In: Proceedings - International Conference on Developments in eSystems Engineering, DeSE [Internet]. 2019. p. 108–12. Available from: https://www.scopus.com/inward/record.uri?eid=2-s2.0-85063141174&doi=10.1109%2FDeSE.2018.00023&partnerID=40&md5=b6682e72143279b30eb2d4309d0f8531
35. Vieira B, Pereira L, Freitas R, Terroso M, Simoes R. A gamified application for assessment of balance and fall prevention. In: 2015 10th Iberian Conference on Information Systems and Technologies (CISTI). 2015. p. 1–6.
36. Dzhagaryan A, Milenkovic A, Jovanov E, Milosevic M. Smart Button: A wearable system for assessing mobility in elderly. In: 2015 17th International Conference on E-health Networking, Application Services (HealthCom). 2015. p. 416–21.
37. Vavoulas G, Pediaditis M, Chatzaki C, Spanakis E, Tsiknakis M. The MobiFall Dataset:: Fall Detection and Classification with a Smartphone. Int J Monit Surveill Technol Res. 2016;2:44–56.
38. Yao M, Zhang Q, Li M, Li H, Ning Y, Xie G, et al. A wearable pre-impact fall early warning and protection system based on MEMS inertial sensor and GPRS communication. In: 2015 IEEE 12th International Conference on Wearable and Implantable Body Sensor Networks (BSN). 2015. p. 1–6.
39. Begg R, Best R, Dell'Oro L, Taylor S. Minimum foot clearance during walking: strategies for the minimisation of trip-related falls. Gait Posture. 2007 Feb;25(2):191–8.
40. Hemmatpour M, Ferrero R, Montrucchio B, Rebaudengo M. A review on fall prediction and prevention system for personal devices: Evaluation and experimental results. Adv Human-Computer Interact. 2019;2019.
41. Abbate S, Avvenuti M, Cola G, Corsini P, Light J, Vecchio A. Recognition of false alarms in fall detection systems. In: 2011 IEEE Consumer Communications and Networking Conference (CCNC). 2011. p. 23–8.
42. Shany T, Wang K, Liu Y, Lovell NH, Redmond SJ. Review: Are we stumbling in our quest to find the best predictor? Over-optimism in sensor-based models for predicting falls in older adults. Healthc Technol Lett. 2015;2(4):79–88.
43. Nazarahari M, Rouhani H. 40 years of sensor fusion for orientation tracking via magnetic and inertial measurement units: Methods, lessons learned, and future challenges. Inf Fusion [Internet]. 2021;68:67–84. Available from: https://www.sciencedirect.com/science/article/pii/S1566253520303997
44. Mariani B, Rouhani H, Crevoisier X, Aminian K. Quantitative estimation of foot-flat and stance phase of gait using foot-worn inertial sensors. Gait Posture. 2013 Feb;37(2):229–34.
45. Mathie MJ, Coster ACF, Lovell NH, Celler BG. Accelerometry: providing an integrated, practical method for long-term, ambulatory monitoring of human movement. Physiol Meas. 2004 Apr;25(2):R1-20.
46. Cheng J, Chen X, Shen M. A Framework for Daily Activity Monitoring and Fall Detection Based on Surface Electromyography and Accelerometer Signals. IEEE J Biomed Heal Informatics. 2013;17(1):38–45.
47. Lee D, Kim Y, Yun J, Jung M, Lee G. A comparative study of the electromyographic activities of lower extremity muscles during level walking and Pedalo riding. J Phys Ther Sci. 2016 May;28(5):1478–81.
48. Annese VF, De Venuto D. Gait analysis for fall prediction using EMG triggered movement related

potentials. In: 2015 10th International Conference on Design Technology of Integrated Systems in Nanoscale Era (DTIS). 2015. p. 1–6.
49. Antonsson EK, Mann RW. The frequency content of gait. J Biomech [Internet]. 1985;18(1):39–47. Available from: https://www.sciencedirect.com/science/article/pii/0021929085900430
50. Martínez-Solís F, Claudio-Sánchez A, Rodríguez-Lelis JM, Vergara-Limon S, Olivares-Peregrino V, Vargas-Treviño M. A portable system with sample rate of 250 Hz for characterization of knee and hip angles in the sagittal plane during gait. Biomed Eng Online. 2014 Mar;13(1):34.
51. Winter DA. Biomechanics and Motor Control of Human Movement: Fourth Edition. Biomechanics and Motor Control of Human Movement: Fourth Edition. 2009. 1–370 p.
52. Podsiadlo D, Richardson S. The timed "Up & Go": a test of basic functional mobility for frail elderly persons. J Am Geriatr Soc. 1991 Feb;39(2):142–8.
53. Berg KO, Wood-Dauphinee SL, Williams JI, Maki B. Measuring balance in the elderly: validation of an instrument. Can J Public Health. 1992;83 Suppl 2:S7-11.
54. Tinetti ME, Williams TF, Mayewski R. Fall risk index for elderly patients based on number of chronic disabilities. Am J Med. 1986 Mar;80(3):429–34.
55. Franchignoni F, Horak F, Godi M, Nardone A, Giordano A. Using psychometric techniques to improve the Balance Evaluation Systems Test: the mini-BESTest. J Rehabil Med. 2010 Apr;42(4):323–31.
56. Crapo RO, Casaburi R, Coates AL, Enright PL, MacIntyre NR, McKay RT, et al. ATS statement: guidelines for the six-minute walk test. Am J Respir Crit Care Med. 2002 Jul;166(1):111–7.
57. Jones CJ, Rikli RE, Beam WC. A 30-s chair-stand test as a measure of lower body strength in community-residing older adults. Res Q Exerc Sport. 1999 Jun;70(2):113–9.
58. Aziz O, Musngi M, Park E, Mori G, Robinovitch S. A comparison of accuracy of fall detection algorithms (threshold-based vs. machine learning) using waist-mounted tri-axial accelerometer signals from a comprehensive set of falls and non-fall trials. Med Biol Eng Comput. 2016;55.
59. Yu D, Deng L. Deep Learning and Its Applications to Signal and Information Processing [Exploratory DSP]. IEEE Signal Process Mag. 2011;28(1):145–54.
60. Meyer BM, Tulipani LJ, Gurchiek RD, Allen DA, Adamowicz L, Larie D, et al. Wearables and Deep Learning Classify Fall Risk From Gait in Multiple Sclerosis. IEEE J Biomed Heal Informatics. 2021;25(5):1824–31.
61. Tan H, Aung N, Tian J, Chua M, Ou Yang Y. Time series classification using a modified LSTM approach from accelerometer-based data: A comparative study for gait cycle detection. Gait Posture. 2019;74.
62. Casilari E, Santoyo-Ramón J-A, Cano-García J-M. Analysis of Public Datasets for Wearable Fall Detection Systems. Sensors [Internet]. 2017;17(7). Available from: https://www.mdpi.com/1424-8220/17/7/1513
63. Arlot S, Celisse A. A Survey of Cross Validation Procedures for Model Selection. Stat Surv. 2009;4.
64. Monaco V, Tropea P, Aprigliano F, Martelli D, Parri A, Cortese M, et al. An ecologically-controlled exoskeleton can improve balance recovery after slippage. Sci Rep. 2017;7.
65. Trkov M, Wu S, Chen K, Yi J, Liu T, Zhao Q. Design of a Robotic Knee Assistive Device (ROKAD) for Slip-Induced Fall Prevention during Walking. IFAC-PapersOnLine [Internet]. 2017;50(1):9802–7. Available from: https://doi.org/10.1016/j.ifacol.2017.08.887
66. Huang Z-G, Feng Y-H, Li Y-H, Lv C-S. Systematic review and meta-analysis: Tai Chi for preventing falls in older adults. BMJ Open. 2017 Feb;7(2):e013661.
67. Gerards MHG, McCrum C, Mansfield A, Meijer K. Perturbation-based balance training for falls reduction among older adults: Current evidence and implications for clinical practice. Geriatr Gerontol Int. 2017 Dec;17(12):2294–303.

68. Granacher U, Muehlbauer T, Zahner L, Gollhofer A, Kressig RW. Comparison of traditional and recent approaches in the promotion of balance and strength in older adults. Sports Med. 2011 May;41(5):377–400.
69. Gabell A, Simons MA, Nayak US. Falls in the healthy elderly: predisposing causes. Ergonomics. 1985 Jul;28(7):965–75.
70. Lockhart T. Biomechanics of Human Gait – Slip and Fall Analysis. In: Encyclopedia of Forensic Sciences. 2013. p. 466–76.
71. Karamanidis K, Epro G, McCrum C, König M. Improving Trip- and Slip-Resisting Skills in Older People: Perturbation Dose Matters. Exerc Sport Sci Rev. 2020 Jan;48(1):40–7.
72. Eng JJ, Winter DA, Patla AE. Strategies for recovery from a trip in early and late swing during human walking. Exp brain Res. 1994;102(2):339–49.
73. Shirota C, Simon A, Kuiken T. Trip recovery strategies following perturbations of variable duration. J Biomech. 2014;47.
74. Aprigliano F, Martelli D, Tropea P, Pasquini G, Micera S, Monaco V. Aging does not affect the intralimb coordination elicited by slip-like perturbation of different intensities. J Neurophysiol. 2017 Sep;118(3):1739–48.
75. Swart SB, den Otter R, Lamoth CJC. Anticipatory control of human gait following simulated slip exposure. Sci Rep. 2020 Jun;10(1).
76. Lee A, Bhatt T, Liu X, Wang Y, Pai Y-C. Can higher training practice dosage with treadmill slip-perturbation necessarily reduce risk of falls following overground slip? Gait Posture. 2018 Mar;61:387–92.
77. Lee A, Bhatt T, Liu X, Wang Y, Wang S, Pai Y-C (Clive). Can Treadmill Slip-Perturbation Training Reduce Longer-Term Fall Risk Upon Overground Slip Exposure? J Appl Biomech. 2020;36(5):298–306.
78. Wang Y, Bhatt T, Liu X, Wang S, Lee A, Wang E, et al. Can treadmill-slip perturbation training reduce immediate risk of over-ground-slip induced fall among community-dwelling older adults? J Biomech. 2019 Feb;84:58–66.
79. Patel PJ, Bhatt T, DelDonno SR, Langenecker SA, Dusane S. Examining Neural Plasticity for Slip-Perturbation Training: An fMRI Study. Front Neurol. 2018;9:1181.
80. Lee A, Bhatt T, Pai Y-C. Generalization of treadmill perturbation to overground slip during gait: Effect of different perturbation distances on slip recovery. J Biomech. 2016 Jan;49(2):149–54.
81. Liu X, Bhatt T, Pai YC. Intensity and generalization of treadmill slip training: High or low, progressive increase or decrease? J Biomech. 2016 Jan 25;49(2):135–40.
82. Ding L, Yang F. Muscle weakness is related to slip-initiated falls among community-dwelling older adults. J Biomech. 2016 Jan;49(2):238–43.
83. Bhatt T, Patel P, Dusane S, DelDonno SR, Langenecker SA. Neural Mechanisms Involved in Mental Imagery of Slip-Perturbation While Walking: A Preliminary fMRI Study. Front Behav Neurosci. 2018;12.
84. Debelle H, Harkness-Armstrong C, Hadwin K, Maganaris CN, O'Brien TD. Recovery From a Forward Falling Slip: Measurement of Dynamic Stability and Strength Requirements Using a Split-Belt Instrumented Treadmill. Front Sport Act living. 2020;2:82.
85. Hirata K, Kokubun T, Miyazawa T, Hanawa H, Kubota K, Sonoo M, et al. Relationship Between the Walking Velocity Relative to the Slip Velocity and the Corrective Response. J Med Biol Eng. 2020;
86. Liu X, Bhatt T, Wang Y, Wang S, Lee A, Pai Y-C. The retention of fall-resisting behavior derived from treadmill slip-perturbation training in community-dwelling older adults. GeroScience. 2021 Apr;43(2):913–26.
87. Yang F, Cereceres P, Qiao M. Treadmill-based gait-slip training with reduced training volume

could still prevent slip-related falls. Gait Posture. 2018;66:160–5.
88. Wang Y, Wang S, Lee A, Pai Y-C, Bhatt T. Treadmill-gait slip training in community-dwelling older adults: mechanisms of immediate adaptation for a progressive ascending-mixed-intensity protocol. Exp brain Res. 2019 Sep;237(9):2305–17.
89. Lee B-C, Kim C-S, Seo K-H. The Body's Compensatory Responses to Unpredictable Trip and Slip Perturbations Induced by a Programmable Split-Belt Treadmill. IEEE Trans NEURAL Syst Rehabil Eng. 2019 Jul;27(7):1389–96.
90. Mueller J, Engel T, Mueller S, Kopinski S, Baur H, Mayer F. Neuromuscular response of the trunk to sudden gait disturbances: Forward vs. backward perturbation. J Electromyogr Kinesiol. 2016;30:168–76.
91. Wang S, Liu X, Lee A, Pai Y-C. Can Recovery Foot Placement Affect Older Adults' Slip-Fall Severity? Ann Biomed Eng [Internet]. 2017;45(8):1941–8. Available from: https://www.scopus.com/inward/record.uri?eid=2-s2.0-85018726524&doi=10.1007%2Fs10439-017-1834-4&partnerID=40&md5=40c115a81c2da09999b64f5150baf85b
92. Wang S, Pai Y-C, Bhatt T. Is There an Optimal Recovery Step Landing Zone Against Slip-Induced Backward Falls During Walking? Ann Biomed Eng. 2020 Jun;48(6):1768–78.
93. Sawers A, Bhatt T. Neuromuscular determinants of slip-induced falls and recoveries in older adults. J Neurophysiol. 2018 Oct;120(4):1534–46.
94. Sawers A, Pai Y-CC, Bhatt T, Ting LH. Neuromuscular responses differ between slip-induced falls and recoveries in older adults. J Neurophysiol. 2017 Feb;117(2):509–22.
95. Inkol KA, Huntley AH, Vallis LA. Repeated Exposure to Forward Support-Surface Perturbation During Overground Walking Alters Upper-Body Kinematics and Step Parameters. J Mot Behav. 2019;51(3):318–30.
96. Liu X, Bhatt T, Wang S, Yang F, Pai Y-CC. Retention of the "first-trial effect" in gait-slip among community-living older adults. GeroScience. 2017 Feb;39(1):93–102.
97. Liu X, Reschechtko S, Wang S, Pai Y-CC. The recovery response to a novel unannounced laboratory-induced slip: The "first trial effect" in older adults. Clin Biomech (Bristol, Avon). 2017 Oct;48:9–14.
98. Wang S, Bhatt T, Liu X, Pai Y-C. The Role of Recovery Lower Limb Segments in Post-Slip Determination of Falls Due to Instability or Limb Collapse. Ann Biomed Eng. 2020 Jan;48(1):192–202.
99. Wang S, Wang Y, Pai Y-C (Clive), Wang E, Bhatt T. Which Are the Key Kinematic and Kinetic Components to Distinguish Recovery Strategies for Overground Slips Among Community-Dwelling Older Adults? J Appl Biomech. 2020;36(4):217–27.
100. Okubo Y, Sturnieks DL, Brodie MA, Duran L, Lord SR. Effect of Reactive Balance Training Involving Repeated Slips and Trips on Balance Recovery Among Older Adults: A Blinded Randomized Controlled Trial. JOURNALS Gerontol Ser A-BIOLOGICAL Sci Med Sci. 2019;74(9):1489–96.
101. Okubo Y, Brodie MA, Sturnieks DL, Hicks C, Carter H, Toson B, et al. Exposure to trips and slips with increasing unpredictability while walking can improve balance recovery responses with minimum predictive gait alterations. PLoS One. 2018;13(9).
102. Okubo Y, Brodie MA, Sturnieks DL, Hicks C, Lord SR. A pilot study of reactive balance training using trips and slips with increasing unpredictability in young and older adults: Biomechanical mechanisms, falls and clinical feasibility. Clin Biomech (Bristol, Avon). 2019 Jul;67:171–9.
103. Merrill Z, Chambers AJ, Cham R. Arm reactions in response to an unexpected slip—Impact of aging. J Biomech [Internet]. 2017;58:21–6. Available from: https://www.scopus.com/inward/record.uri?eid=2-s2.0-

85018991861&doi=10.1016%2Fj.jbiomech.2017.04.011&partnerID=40&md5=7346510a3d26b4d84a497911358490c3
104. Nazifi MM, Beschorner KE, Hur P. Association between Slip Severity and Muscle Synergies of Slipping. Front Hum Neurosci. 2017 Nov;11.
105. Ziaei M, Mokhtarinia H, Tabatabai Ghomshe F, Maghsoudipour M. Coefficient of friction, walking speed and cadence on slippery and dry surfaces: shoes with different groove depths. Int J Occup Saf Ergon. 2019 Dec;25(4):524–9.
106. Soangra R, Lockhart TE. Dual-Task Does Not Increase Slip and Fall Risk in Healthy Young and Older Adults during Walking. Appl bionics Biomech. 2017;2017:1014784.
107. O'Connell C, Chambers A, Mahboobin A, Cham R. Effects of slip severity on muscle activation of the trailing leg during an unexpected slip. J Electromyogr Kinesiol Off J Int Soc Electrophysiol Kinesiol. 2016 Jun;28:61–6.
108. Allin LJ, Nussbaum MA, Madigan ML. Feet kinematics upon slipping discriminate between recoveries and three types of slip-induced falls. Ergonomics. 2018 Jun;61(6):866–76.
109. Kim S, Joo K-S, Liu J, Sohn J-H. Lower extremity kinematics during forward heel-slip. Technol Heal care Off J Eur Soc Eng Med. 2019;27(S1):345–56.
110. Arena SL, Davis JL, Grant JW, Madigan ML. Tripping Elicits Earlier and Larger Deviations in Linear Head Acceleration Compared to Slipping. PLoS One. 2016 Nov;11(11).
111. Rasmussen CM, Hunt NH. A novel wearable device to deliver unconstrained, unpredictable slip perturbations during gait. J Neuroeng Rehabil. 2019 Oct;16(1):118.
112. Er JK, Donnelly CJW, Wee SK, Ang WT. Fall inducing movable platform (FIMP) for overground trips and slips. J Neuroeng Rehabil. 2020;17(1).
113. Lee B-C, Martin BJ, Thrasher TA, Layne CS. A new fall-inducing technology platform: development and assessment of a programmable split-belt treadmill. In: 2017 39th Annual International Conference Of The Ieee Engineering In Medicine And Biology Society (Embc). 2017. p. 3777–80.
114. König M, Epro G, Seeley J, Catala-Lehnen P, Potthast W, Karamanidis K. Retention of improvement in gait stability over 14 weeks due to trip-perturbation training is dependent on perturbation dose. J Biomech. 2018;84.
115. Silver TA, Mokha GM, Peacock CA. Exploring fall training adaptations while walking. Work. 2016 Jun;54(3):699–707.
116. Wang Y, Wang S, Bolton R, Kaur T, Bhatt T. Effects of task-specific obstacle-induced trip-perturbation training: proactive and reactive adaptation to reduce fall-risk in community-dwelling older adults. Aging Clin Exp Res. 2020 May;32(5):893–905.
117. Ko Y-C, Ryew C-C, Hyun S-H. Relationship among the variables of kinematic and tilt angle of whole body according to the foot trip during gait. J Exerc Rehabil. 2017;13(1):117–21.
118. Schulz BW. A new measure of trip risk integrating minimum foot clearance and dynamic stability across the swing phase of gait. J Biomech. 2017;55:107–12.
119. Liu X, Bhatt T, Wang S, Yang F, Pai Y-C (Clive). Retention of the "first-trial effect" in gait-slip among community-living older adults. GEROSCIENCE. 2017;39(1):93–102.
120. Epro G, McCrum C, Mierau A, Leyendecker M, Brüggemann G-P, Karamanidis K. Effects of triceps surae muscle strength and tendon stiffness on the reactive dynamic stability and adaptability of older female adults during perturbed walking. J Appl Physiol. 2018 Jun;124(6):1541–9.
121. Potocanac Z, de Bruin J, van der Veen S, Verschueren S, van Dieën J, Duysens J, et al. Fast online corrections of tripping responses. Exp brain Res. 2014 Nov;232(11):3579–90.
122. Altman AR, Reisman DS, Higginson JS, Davis IS. Kinematic comparison of split-belt and single-belt treadmill walking and the effects of accommodation. Gait Posture. 2012 Feb;35(2):287–

91.
123. Wang S, Liu X, Pai Y-C. Limb Collapse or Instability? Assessment on Cause of Falls. Ann Biomed Eng. 2019 Mar;47(3):767–77.
124. Wright RL, Peters DM, Robinson PD, Watt TN, Hollands MA. Older adults who have previously fallen due to a trip walk differently than those who have fallen due to a slip. Gait Posture. 2015 Jan;41(1):164–9.
125. Side-Dominant Science: Are You Left- or Right-Sided? - Scientific American [Internet]. [cited 2022 Mar 17]. Available from: https://www.scientificamerican.com/article/bring-science-home-dominant-side/
126. Martelli D, Luciani LB, Micera S, Member S. Angular Momentum During Unexpected Multidirectional Perturbations Delivered While Walking. IEEE Trans Biomed Eng. 2013;60(7):1785–95.
127. Nagano H, Begg RK, Sparrow WA, Taylor S. Ageing and limb dominance effects on foot-ground clearance during treadmill and overground walking. Clin Biomech (Bristol, Avon). 2011 Nov;26(9):962–8.
128. Bassi Luciani L, Genovese V, Monaco V, Odetti L, Cattin E, Micera S. Design and Evaluation of a new mechatronic platform for assessment and prevention of fall risks. J Neuroeng Rehabil. 2012;9(1):1–13.
129. Allin LJ, Wu X, Nussbaum MA, Madigan ML. Falls resulting from a laboratory-induced slip occur at a higher rate among individuals who are obese. J Biomech. 2016 Mar;49(5):678–83.
130. McCrum C, Willems P, Karamanidis K, Meijer K. Stability-normalised walking speed: A new approach for human gait perturbation research. J Biomech [Internet]. 2019;87:48–53. Available from: https://www.scopus.com/inward/record.uri?eid=2-s2.0-85062059483&doi=10.1016%2Fj.jbiomech.2019.02.016&partnerID=40&md5=c11ca52e966b7dfddc67cda7fa065e97
131. Ferreira RN, Ribeiro NF, Santos CP. Fall Risk Assessment Using Wearable Sensors: A Narrative Review. Sensors [Internet]. 2022;22(3). Available from: https://www.mdpi.com/1424-8220/22/3/984
132. Chvatal SA, Macpherson JM, Torres-Oviedo G, Ting LH. Absence of postural muscle synergies for balance after spinal cord transection. J Neurophysiol. 2013 Sep;110(6):1301–10.
133. Marigold DS, Patla AE. Strategies for dynamic stability during locomotion on a slippery surface: effects of prior experience and knowledge. J Neurophysiol. 2002 Jul;88(1):339–53.
134. Pijnappels M, Bobbert MF, van Dieën JH. How early reactions in the support limb contribute to balance recovery after tripping. J Biomech. 2005 Mar;38(3):627–34.
135. Mioskowska M, Stevenson D, Onu M, Trkov M. Compressed gas actuated knee assistive exoskeleton for slip-induced fall prevention during human walking. IEEE/ASME Int Conf Adv Intell Mechatronics, AIM. 2020;2020-July:735–40.
136. Beschorner K, Cham R. Impact of joint torques on heel acceleration at heel contact, a contributor to slips and falls. Ergonomics. 2008 Dec;51(12):1799–813.
137. Moyer BE, Redfern MS, Cham R. Biomechanics of trailing leg response to slipping - evidence of interlimb and intralimb coordination. Gait Posture. 2009 Jun;29(4):565–70.
138. Yang F, Bhatt T, Pai Y-C. Role of stability and limb support in recovery against a fall following a novel slip induced in different daily activities. J Biomech [Internet]. 2009;42(12):1903–8. Available from: https://www.sciencedirect.com/science/article/pii/S0021929009002747
139. Aprigliano F, Martelli D, Micera S, Monaco V. Intersegmental coordination elicited by unexpected multidirectional slippinglike perturbations resembles that adopted during steady locomotion. J Neurophysiol. 2016;115(2):728–40.
140. Tang PF, Woollacott MH, Chong RK. Control of reactive balance adjustments in perturbed

human walking: roles of proximal and distal postural muscle activity. Exp brain Res. 1998 Mar;119(2):141–52.
141. Wilson S, Donahue PT, Williams C, Hill C, Simpson J, Waddell D, et al. Differences in Falls and Recovery from a Slip Based on an Individual's Lower Extremity Corrective Response. Int J Kinesiol Sport Sci. 2019;7:34.
142. Yang F, Pai Y-C. Role of individual lower limb joints in reactive stability control following a novel slip in gait. J Biomech. 2010 Feb;43(3):397–404.
143. Bhatt T, Wening JD, Pai Y-C. Adaptive control of gait stability in reducing slip-related backward loss of balance. Exp brain Res. 2006 Mar;170(1):61–73.
144. Sadeghi H, Allard P, Prince F, Labelle H. Symmetry and limb dominance in able-bodied gait: a review. Gait Posture. 2000 Sep;12(1):34–45.
145. Seeley MK, Umberger BR, Shapiro R. A test of the functional asymmetry hypothesis in walking. Gait Posture. 2008 Jul;28(1):24–8.
146. Young PM, Whitall J, Bair W-N, Rogers MW. Leg preference associated with protective stepping responses in older adults. Clin Biomech (Bristol, Avon). 2013 Oct;28(8):927–32.
147. Bohannon R. Is it Legitimate to Characterize Muscle Strength Using a Limited Number of Measures? J Strength Cond Res. 2008;22:166–73.
148. Liu J, Lockhart TE. Age-related joint moment characteristics during normal gait and successful reactive-recovery from unexpected slip perturbations. Gait Posture. 2009 Oct;30(3):276–81.
149. Mrachacz-Kersting N, Lavoie BA, Andersen JB, Sinkjaer T. Characterisation of the quadriceps stretch reflex during the transition from swing to stance phase of human walking. Exp brain Res. 2004 Nov;159(1):108–22.
150. Félix P, Figueiredo J, Santos CP, Moreno JC. Electronic design and validation of Powered Knee Orthosis system embedded with wearable sensors. In: 2017 IEEE International Conference on Autonomous Robot Systems and Competitions (ICARSC). 2017. p. 110–5.
151. Zhang T, Tran M, Huang H. Design and Experimental Verification of Hip Exoskeleton With Balance Capacities for Walking Assistance. IEEE/ASME Trans Mechatronics. 2018;23(1):274–85.
152. Gouwanda D, Gopalai AA. A robust real-time gait event detection using wireless gyroscope and its application on normal and altered gaits. Med Eng Phys [Internet]. 2015;37(2):219–25. Available from: https://www.sciencedirect.com/science/article/pii/S1350453315000028
153. Chia Bejarano N, Ambrosini E, Pedrocchi A, Ferrigno G, Monticone M, Ferrante S. A Novel Adaptive, Real-Time Algorithm to Detect Gait Events From Wearable Sensors. IEEE Trans Neural Syst Rehabil Eng. 2015;23(3):413–22.
154. Alshehri YS, Liu W, Mullen S, Phadnis M, Sharma NK, dos Santos M. Inertial sensors identified asymmetries in shank angular velocity at different gait speeds in individuals with anterior cruciate ligament reconstruction. Gait Posture [Internet]. 2020;80:302–7. Available from: https://www.sciencedirect.com/science/article/pii/S096663622030165X
155. Abyarjoo F, Barreto A, Cofino J, Ortega F. Implementing a Sensor Fusion Algorithm for 3D Orientation Detection with Inertial/Magnetic Sensors. In 2012.
156. Santos CP, Alves N, Moreno JC. Biped Locomotion Control through a Biomimetic CPG-based Controller. J Intell Robot Syst Theory Appl [Internet]. 2017;85(1):47–70. Available from: http://dx.doi.org/10.1007/s10846-016-0407-3
157. Ronsse R, Lenzi T, Vitiello N, Koopman B, van Asseldonk E, De Rossi SMM, et al. Oscillator-based assistance of cyclical movements: model-based and model-free approaches. Med Biol Eng Comput. 2011 Oct;49(10):1173–85.
158. Righetti L, Buchli J, Ijspeert AJ. From Dynamic Hebbian Learning for Oscillators to Adaptive Central Pattern Generators. 2005;

159. Whittington BR, Thelen DG. A simple mass-spring model with roller feet can induce the ground reactions observed in human walking. J Biomech Eng. 2009 Jan;131(1):11013.
160. Ijspeert AJ. Central pattern generators for locomotion control in animals and robots: A review. Neural Networks [Internet]. 2008;21(4):642–53. Available from: https://www.sciencedirect.com/science/article/pii/S0893608008000804
161. Ayers J, Davis JL, Rudolph A. Neurotechnology for Biomimetic Robots. Cambridge, MA, USA: MIT Press; 2002.
162. Righetti L, Ijspeert AJ. Programmable central pattern generators: an application to biped locomotion control. In: Proceedings 2006 IEEE International Conference on Robotics and Automation, 2006 ICRA 2006. 2006. p. 1585–90.
163. Righetti L, Buchli J, Ijspeert AJ. Dynamic Hebbian learning in adaptive frequency oscillators. Phys D Nonlinear Phenom [Internet]. 2006;216(2):269–81. Available from: https://www.sciencedirect.com/science/article/pii/S0167278906000819
164. Full RJ, Kubow T, Schmitt J, Holmes P, Koditschek D. Quantifying dynamic stability and maneuverability in legged locomotion. Integr Comp Biol. 2002 Feb;42(1):149–57.
165. Lockhart TE. An integrated approach towards identifying age-related mechanisms of slip initiated falls. J Electromyogr Kinesiol Off J Int Soc Electrophysiol Kinesiol. 2008 Apr;18(2):205–17.
166. Martelli D, Monaco V, Bassi Luciani L, Micera S. Angular momentum during unexpected multidirectional perturbations delivered while walking. IEEE Trans Biomed Eng. 2013 Jul;60(7):1785–95.
167. Trkov M, Chen K, Yi J, Liu T. Inertial Sensor-Based Slip Detection in Human Walking. IEEE Trans Autom Sci Eng. 2019;16(3):1399–411.
168. Trkov M, Yi J, Liu T. Slip detection and prediction in human walking using only wearable inertial measurement units (IMUs). In 2015. p. 854–9.
169. Elias LJ, Bryden MP, Bulman-Fleming MB. Footedness is a better predictor than is handedness of emotional lateralization. Neuropsychologia. 1998;36(1):37–43.
170. Pellikaan P, Giarmatzis G, Vander Sloten J, Verschueren S, Jonkers I. Ranking of osteogenic potential of physical exercises in postmenopausal women based on femoral neck strains. PLoS One [Internet]. 2018;13(4):1–18. Available from: https://doi.org/10.1371/journal.pone.0195463
171. SENIAM. Welcome at Seniam.org [Internet]. [cited 2022 Feb 25]. Available from: http://www.seniam.org/
172. Abdulatif S, Aziz F, Armanious K, Kleiner B, Yang B, Schneider U. Person Identification and Body Mass Index: A Deep Learning-Based Study on Micro-Dopplers. 2018.
173. Klemetti R, Moilanen P, Avela J, Timonen J. Effects of gait speed on stability of walking revealed by simulated response to tripping perturbation. Gait Posture [Internet]. 2014;39(1):534–9. Available from: http://dx.doi.org/10.1016/j.gaitpost.2013.09.006
174. Quach L, M. Galica A, N.jones R, Procter-Gray E. The Non-linear Relationship between Gait Speed and Falls:The Mobilize Boston Study. J Am Geriatr Soc. 2012;59(6):1069–73.
175. Kyrdalen IL, Thingstad P, Sandvik L, Ormstad H. Associations between gait speed and well-known fall risk factors among community-dwelling older adults. Physiother Res Int. 2019;24(1):1–6.
176. Aghayan A, Jaiswal P, Siahkoohi HR. Seismic denoising using the redundant lifting scheme. In 2016. p. 4679–84.
177. Ahn J, Hogan N. Walking Is Not Like Reaching: Evidence from Periodic Mechanical Perturbations. PLoS One. 2012;7:e31767.

Appendix I - Study of the number of oscillators within the CPG

Figures A1 to A4 represent the results of the oscillators' intrinsic frequency adaptation to the knee angle signal throughout the simulation time from the CPG configurations with 6, 5, 4 and 3 oscillators, respectively.

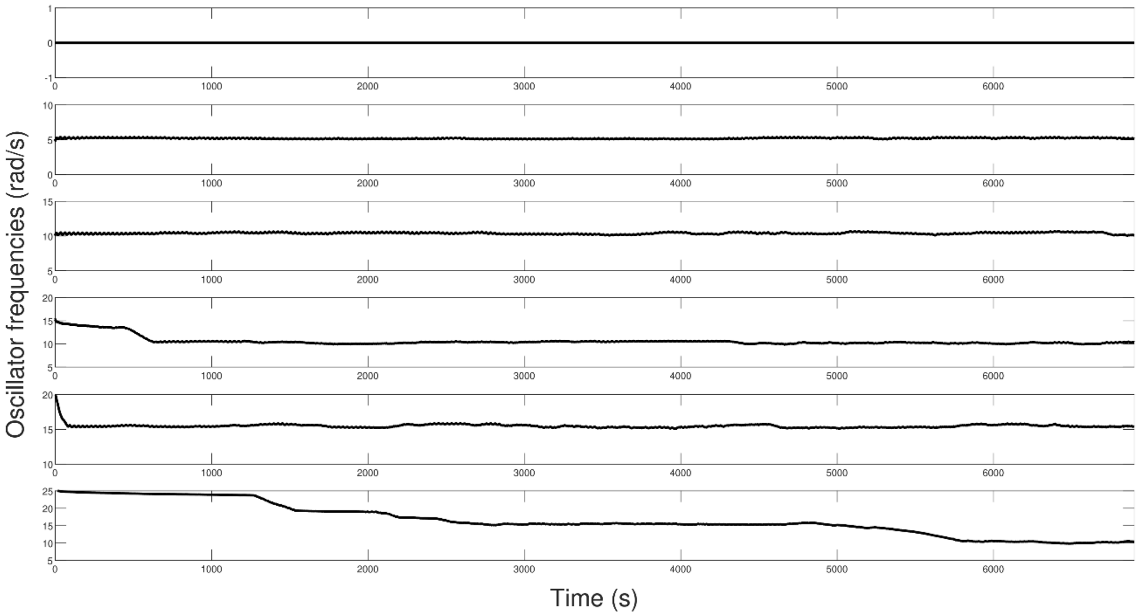

Figure A9. Frequency evolution of the CPG with 6 oscillators throughout the simulation time course (knee angle). From top to bottom: $\omega 1$, $\omega 2$, $\omega 3$, $\omega 4$, $\omega 5$ and $\omega 6$.

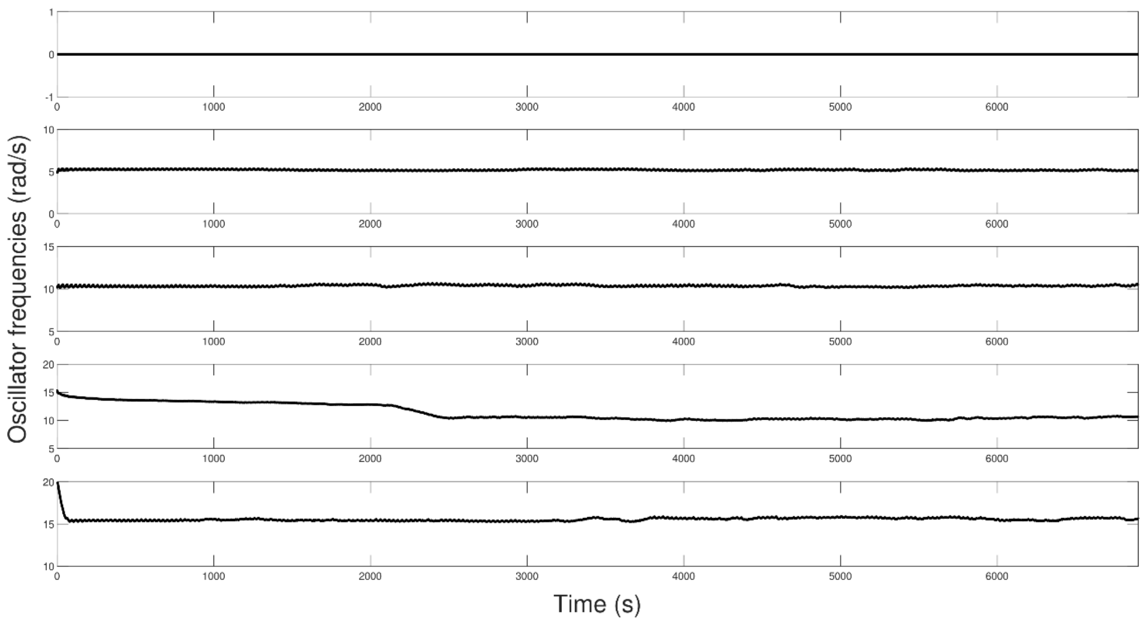

Figure A10. Frequency evolution of the CPG with 5 oscillators throughout the simulation time course (knee angle). From top to bottom: $\omega 1$, $\omega 2$, $\omega 3$, $\omega 4$ and $\omega 5$.

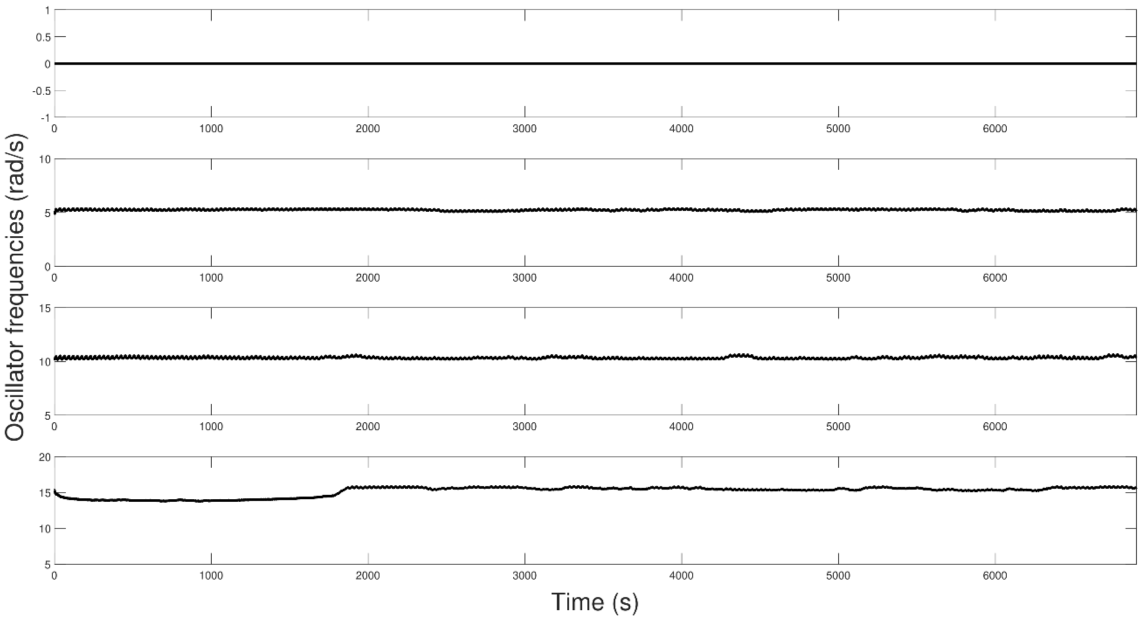

Figure A11. Frequency evolution of the CPG with 4 oscillators throughout the simulation time course (knee angle). From top to bottom: $\omega 1$, $\omega 2$, $\omega 3$ and $\omega 4$.

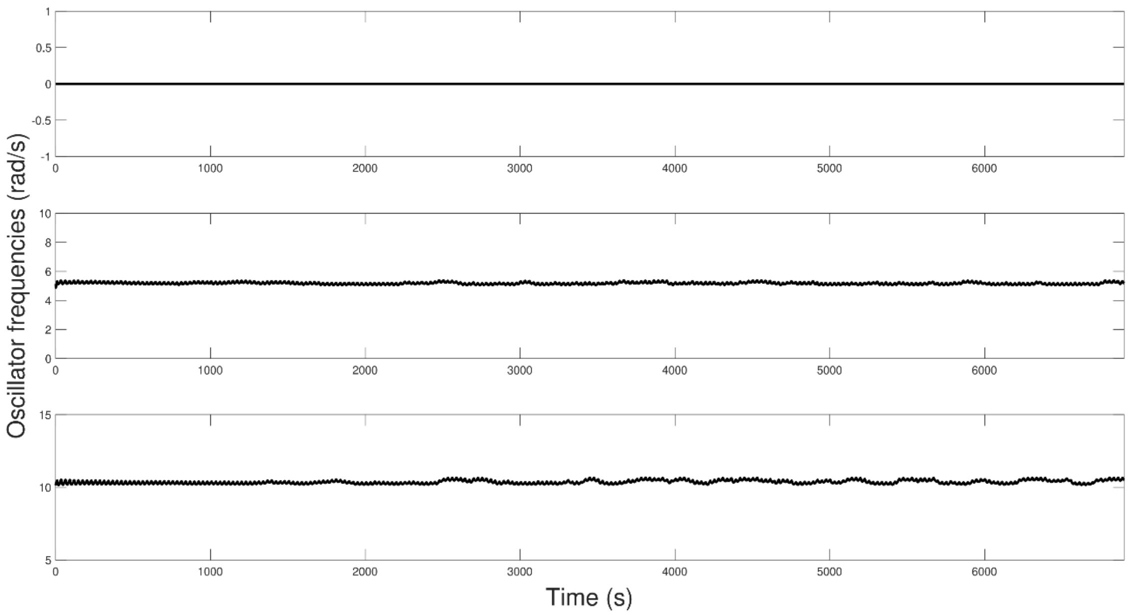

Figure A12. Frequency evolution of the CPG with 3 oscillators throughout the simulation time course (knee angle). From top to bottom: $\omega 1$, $\omega 2$ and $\omega 3$.

Figures A5 to A8 present the results of the oscillators' intrinsic frequency adaptation to the shank angular velocity signal throughout the simulation time from the CPG configurations with 6, 5, 4 and 3 oscillators, respectively.

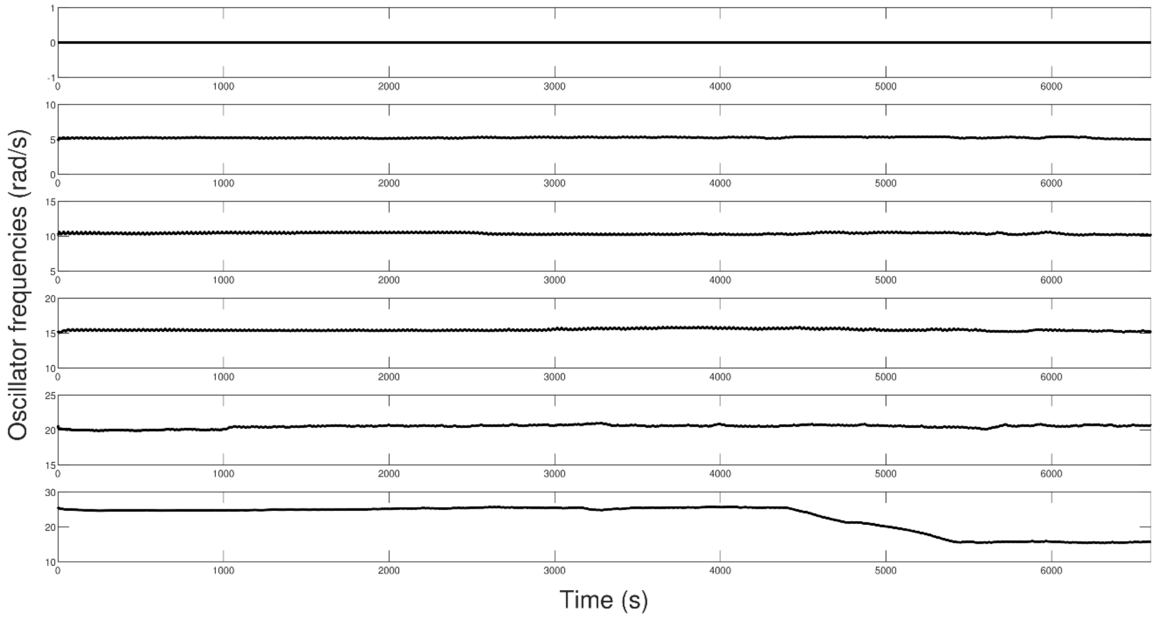

Figure A13. Frequency evolution of the CPG with 6 oscillators throughout the simulation time course (shank angular velocity). From top to bottom: $\omega1$, $\omega2$, $\omega3$, $\omega4$, $\omega5$ and $\omega6$.

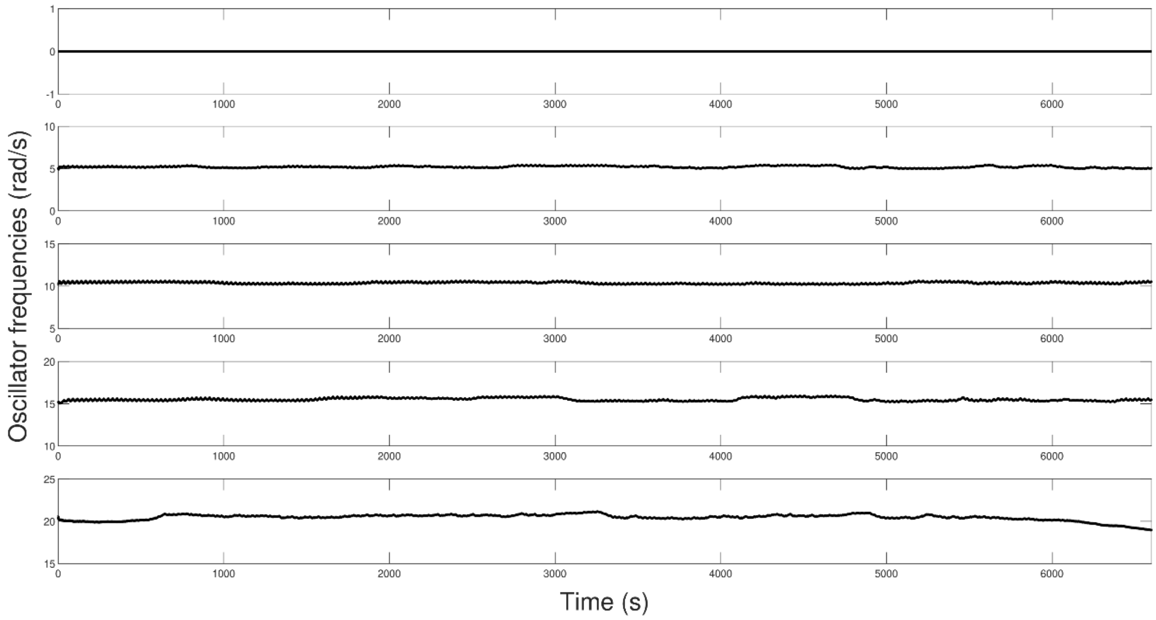

Figure A14. Frequency evolution of the CPG with 5 oscillators throughout the simulation time course (shank angular velocity). From top to bottom: $\omega1$, $\omega2$, $\omega3$, $\omega4$ and $\omega5$.

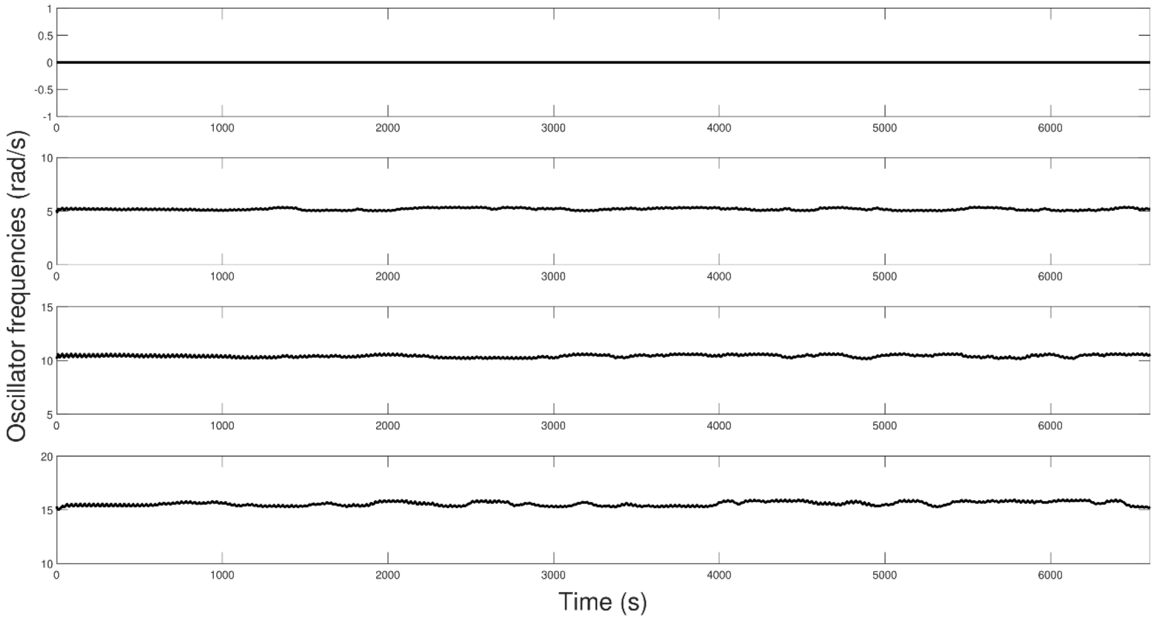

Figure A15. Frequency evolution of the CPG with 4 oscillators throughout the simulation time course (shank angular velocity). From top to bottom: $\omega 1$, $\omega 2$, $\omega 3$ and $\omega 4$.

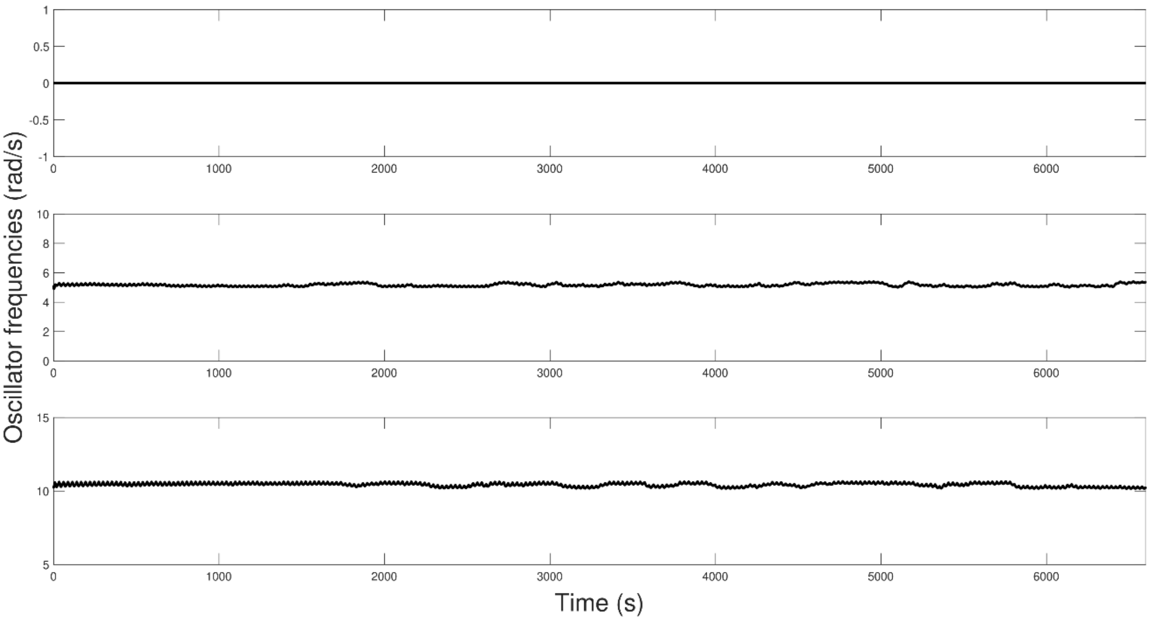

Figure A16. Frequency evolution of the CPG with 3 oscillators throughout the simulation time course (shank angular velocity). From top to bottom: $\omega 1$, $\omega 2$ and $\omega 3$.